NUREG/CR-5586
SAND90-1102

Mitigation of Direct Containment Heating and Hydrogen Combustion Events in Ice Condenser Plants

Analyses with the CONTAIN Code and NUREG-1150 PRA Methodology

Prepared by D. C. Williams, T. J. Gregory

Sandia National Laboratories

Prepared for
U.S. Nuclear Regulatory Commission

AVAILABILITY NOTICE

Availability of Reference Materials Cited in NRC Publications

Most documents cited in NRC publications will be available from one of the following sources:

1. The NRC Public Document Room, 2120 L Street, NW, Lower Level, Washington, DC 20555

2. The Superintendent of Documents, U.S. Government Printing Office, P.O. Box 37082, Washington, DC 20013-7082

3. The National Technical Information Service, Springfield, VA 22161

Although the listing that follows represents the majority of documents cited in NRC publications, it is not intended to be exhaustive.

Referenced documents available for inspection and copying for a fee from the NRC Public Document Room include NRC correspondence and internal NRC memoranda; NRC Office of Inspection and Enforcement bulletins, circulars, information notices, inspection and investigation notices; Licensee Event Reports; vendor reports and correspondence; Commission papers; and applicant and licensee documents and correspondence.

The following documents in the NUREG series are available for purchase from the GPO Sales Program: formal NRC staff and contractor reports, NRC-sponsored conference proceedings, and NRC booklets and brochures. Also available are Regulatory Guides, NRC regulations in the *Code of Federal Regulations*, and *Nuclear Regulatory Commission Issuances*.

Documents available from the National Technical Information Service include NUREG series reports and technical reports prepared by other federal agencies and reports prepared by the Atomic Energy Commission, forerunner agency to the Nuclear Regulatory Commission.

Documents available from public and special technical libraries include all open literature items, such as books, journal and periodical articles, and transactions. *Federal Register* notices, federal and state legislation, and congressional reports can usually be obtained from these libraries.

Documents such as theses, dissertations, foreign reports and translations, and non-NRC conference proceedings are available for purchase from the organization sponsoring the publication cited.

Single copies of NRC draft reports are available free, to the extent of supply, upon written request to the Office of Information Resources Management, Distribution Section, U.S. Nuclear Regulatory Commission, Washington, DC 20555.

Copies of industry codes and standards used in a substantive manner in the NRC regulatory process are maintained at the NRC Library, 7920 Norfolk Avenue, Bethesda, Maryland, and are available there for reference use by the public. Codes and standards are usually copyrighted and may be purchased from the originating organization or, if they are American National Standards, from the American National Standards Institute, 1430 Broadway, New York, NY 10018.

DISCLAIMER NOTICE

NUREG/CR-5586
SAND90-1102
R1, R4, UL, XA,
1A, 1F, RG

Mitigation of Direct Containment Heating and Hydrogen Combustion Events in Ice Condenser Plants

Analyses with the CONTAIN Code and NUREG-1150 PRA Methodology

Manuscript Completed: August 1990
Date Published: October 1990

Prepared by
D. C. Williams, J. J. Gregory

Sandia National Laboratories
Albuquerque, NM 87185

Prepared for
Division of Safety Issue Resolution
Office of Nuclear Regulatory Research
U.S. Nuclear Regulatory Commission
Washington, DC 20555
NRC FIN A1838

ABSTRACT

Using Sequoyah as a representative plant, the CONTAIN severe accident analysis code has been used to evaluate the ability of several proposed containment improvements to reduce the threat to containment integrity associated with direct containment heating (DCH) and hydrogen combustion in ice condenser plants. Calculations were performed using 4-cell, 6-cell, and 26-cell representations of the containment. Potential improvements considered include containment venting, improved igniter systems, containment inerting, subatmospheric containment, reduced ice condenser bypass, independent power supplies for the air return fans, and intentional depressurization of the reactor coolant system (RCS).

In station blackout accidents with the primary system remaining highly pressurized, most of the improvements considered offer at best moderate reductions in DCH loads. These reductions were probably insufficient to substantially alter the contribution of DCH to risk in PRAs such as NUREG-1150. The one exception was containment inerting, which yielded considerably greater mitigation. However, it is not clear that inerting is feasible due to operational considerations.

The effectiveness of mitigating DCH threats by intentionally opening the PORVS in order to partially depressurize the primary system was analyzed. In station blackout accidents, this strategy was found to be effective if and only if independent power supplies were provided to operate the igniter systems. Given operational igniters, partial depressurization significantly reduced (but did not eliminate) the threat to containment integrity associated with DCH and hydrogen deflagrations.

With or without partial depressurization, calculations with the 26-cell deck indicated that, in station blackout accidents, highly detonable gas mixtures were likely to form in the ice condenser region. Providing dedicated power supplies for the existing igniter system does not appear to completely solve the problem. Providing power for the air return fans offers some additional reduction in the detonation threat, but still may not totally eliminate it. It should be noted that the present work did not assess the consequences of a detonation occurring in the ice condenser; it is not known whether such a detonation could actually fail the containment.

Sensitivity studies were performed using the NUREG-1150 PRA methodology and models to estimate the potential impact of the improvements considered upon the overall Sequoyah risk profiles for early fatality and latent cancer fatality potentials. Depressurization combined with hydrogen control offered an approximately three-fold reduction in the contribution to the mean risk potentials associated with scenarios involving early containment failure due to severe accident phenomena; other improvements considered were less effective. However, containment bypass accidents are also important risk contributors at Sequoyah, and these sequences are largely unaffected by the containment improvements considered here. Hence, reductions in the total mean risk potentials were about 30% to 40% at best.

TABLE OF CONTENTS

Table of Contents (Continued)

Table of Contents (Continued)

LIST OF FIGURES

List of Figures (Continued)

List of Figures (Continued)

List of Figures (Continued)

List of Figures (Continued

LIST OF TABLES

PREFACE

The purpose of the present work is to provide information as to the degree to which various proposed improvements to ice condenser containments can mitigate containment loads associated with direct containment heating (DCH) and/or hydrogen combustion events. One major analytical tool used in this work was a developmental version of the CONTAIN 1.1 code which incorporates models for DCH phenomena. In addition, some of the methodologies and models developed for the NUREG-1150 effort were applied.

It must be acknowledged that there are substantial phenomenological uncertainties that affect the accuracy of the analyses of the accident scenarios considered here. Some of these uncertainties involve uncertainties in the phenomena that are modeled in the containment analyses performed for this work. In addition, there are substantial uncertainties in the in-vessel accident progression analyses that provide inputs important to the containment analyses. Given these uncertainties, a considerable degree of engineering judgment was required in selecting input values and modeling choices for the various computer code calculations that were performed. Additional details concerning some of the more important uncertainties are discussed in the text of this report.

In assessing the impact of these uncertainties, it should be remembered that the present work does not, in itself, attempt to determine the likelihood of containment failure for the scenarios considered. Hence, a comprehensive, quantitative uncertainty study was not considered necessary (nor would it have been possible, in view of the large number of containment improvement strategies that were considered). The assessment of the various mitigation strategies considered was generally based upon comparisons of containment loads calculated with and without implementation of the proposed strategy. In most cases, these comparisons were less sensitive to the various uncertainties involved than were the absolute magnitudes of the loads themselves. Although careful consideration of the uncertainties in this work is certainly warranted, it is not believed likely that the major conclusions offered here, properly interpreted, will be invalidated by the uncertainties involved.

ACKNOWLEDGMENTS

It is a pleasure to acknowledge the support of the CONTAIN code development staff, without whose frequent and timely assistance this work could not have been performed. The assistance of D. W. Golden and his colleagues at the Idaho National Engineering Laboratory, who provided the SCDAP/RELAP calculational results utilized in this work, is gratefully acknowledged. Special thanks are also due John Lane of the U.S. Nuclear Regulatory Commission for his understanding support and encouragement of this work.

FOREWORD

In SECY-88-147, dated May 25, 1988, the NRC staff presented to the Commission a program plan to evaluate generic severe accident containment vulnerabilities via the Containment Performance Improvement (CPI) program. This effort was based on the presumption that there are generic severe accident challenges for each light water reactor containment type. These challenges should be addressed to determine the possible need for additional regulatory guidance or requirements related to containment features. The ability of containments to survive successfully some severe accident challenges is uncertain, as indicated in draft NUREG-1150. The CPI effort is extended to focus on evaluation of hardware and procedural issues related to generic containment challenges.

This report documents the results of work performed under NRC sponsorship that could indicate ways that containment performance could potentially be improved. The purpose of this report is to provide PWR Ice Condenser owners with information they may find useful in assessing their plants as part of their Individual Plant Examination (IPE) program. No requirements are contained in this report, and it is being provided for information only. Specific guidance to the industry on the use of this report, and similar reports, has been given to Generic Letter 88-20, Supplement 3, dated July 6, 1990.

EXECUTIVE SUMMARY

Overview of Major Findings

Calculations were performed using the CONTAIN code to assess the benefits associated with a variety of potential containment improvements designed to reduce the likelihood of early containment failure in ice condenser plants during station blackout accidents. Sequoyah was selected as a representative plant for detailed study. The principal threats involved are direct containment heating (DCH) and/or hydrogen combustion events, including detonations. Hence, a developmental version of the CONTAIN 1.1 code that incorporates DCH modeling was used in this work.

Mitigation strategies considered included independent power and other improvements for the igniter systems, containment venting, containment inerting, subatmospheric containment, reduced ice condenser bypass flows, independent power for the air return fans, and RCS depressurization by intentionally opening the PORVs. Combinations of improvements were assessed when significant additional benefits appeared possible. In addition, the impact of some of these improvements upon the Sequoyah risk profile was assessed by performing sensitivity studies using the NUREG-1150 methodology and modeling. Major conclusions drawn from this work include the following:

- If the reactor coolant system remains fully pressurized up until the time of vessel breach (VB), DCH loads are difficult to mitigate. Results for specific mitigation strategies include:
  - Of all the strategies considered, only containment inerting appeared to promise substantial reductions in the probability of early containment failure.
  - Dedicated power for igniter systems, containment venting, and operating the containment at subatmospheric pressures offered small to moderate benefits; on the other hand, operating the air return fans appeared to enhance DCH loads somewhat.
  - Some additional reduction in DCH loads could be obtained by combining selected containment improvements. The optimum combination (inerting excluded) appeared to be independent power for igniters combined with containment venting; the total reduction in DCH loads was still not large.
  - The reactor cavity region, below the vessel, was calculated to pressurize severely during a DCH event. Possible implications of this pressurization should be considered.
- Depressurization of the RCS by opening the PORVs was assessed, under the assumption that the RCS pressure would still be at 1.5 MPa at VB and that there would be a residual DCH threat in addition to hydrogen combustion threats at and prior to VB.
  - Depressurization without hydrogen control offers no advantages over the scenario with fully-pressurized RCS.

- Depressurization combined with dedicated power supplies for existing igniters offered substantial reductions in maximum pressures. Operating the air return fans yielded no additional reductions.

- Given operating igniters, hydrogen deflagrations before vessel breach never resulted in containment pressures that would threaten failure.

- Phenomenological uncertainties preclude giving an absolute assurance that depressurization to 1.5 MPa, combined with igniters, would totally eliminate DCH threats; however, substantial reductions in containment failure probabilities would be expected.

- The potential for detonation hazards to develop was assessed by comparing calculated gas compositions with available information on sensitivity to detonation as a function of gas composition.

  - In the station blackout accident with either the fully-pressurized RCS or the depressurized RCS, there was a strong tendency for highly detonable gas mixtures to develop in the ice condenser.

  - Independent power for the existing igniter systems might not eliminate the detonation threat. Operating the air return fans in addition to the igniters would improve the situation, but development of detonable gas compositions under adverse circumstances still could not be ruled out.

- Sensitivity studies using the NUREG-1150 containment event trees and related modeling showed that no containment improvements of the type considered here could yield large reductions in mean risk because none of the improvements addressed containment bypass accidents. Substantial reductions in the risk-significance of early containment failure could be achieved, however.

  - RCS depressurization combined with operating the existing igniters and air return fans yielded the largest benefits. Depressurization alone offered little benefit, while depressurization combined with igniter operation gave intermediate results.

  - Increasing the median failure pressure from 0.54 to 1.14 MPa (the latter corresponds to that of the Watts Bar plant) resulted in large reductions in risks associated with early containment failure; thus, the importance of the class of event studied in this work can be quite plant-specific.

Background

The Containment Performance Improvements (CPI) program is a project sponsored by the Office of Research - Division of Safety Issue Resolution of the U.S. Nuclear Regulatory Commission to review existing information on threats to containment integrity and to perform additional analyses as needed in order to determine what, if any, improvements might be made to these containments which could reduce the probability and/or consequences of containment failure. The present report describes work performed at SNL in support of the CPI evaluation of ice condenser containments. The Sequoyah plant is the representative plant which has been selected for detailed study, in order to make use of the large amount of information available on this plant through the NUREG-1150 program and other studies.

One major analytical technique employed was use of the CONTAIN-DCH code to assess threats in the unmodified plant and to determine the effectiveness of possible improvements. CONTAIN-DCH is a developmental version of the CONTAIN 1.1 code which includes a combination of mechanistic and parametric models for direct containment heating (DCH) phenomena. In addition, sensitivity studies using the NUREG-1150 event tree and related modeling were employed to determine how various possible improvements would affect the overall risk profile for the plant. The present report describes these studies and offers some conclusions that may be drawn from the results.

Interpretation of the Results of CONTAIN Analyses. If a given containment improvement is to be judged effective, it must yield a substantial mitigation of the threat it is intended to address. Some care is required in the evaluation of mitigation schemes when there are important uncertainties in the analysis (either uncertainties in the input parameters or in the modeling), as is known to be the case in the present study. Clearly, it will be difficult to justify an improvement which is effective given one specific scenario description (or modeling assumption), but which becomes ineffective given another, equally plausible, description. In order to be justifiable, the improvement should be effective throughout most, if not all, of the parameter space spanned by the uncertainty ranges of the dominant parameters.

Performing a detailed uncertainty study for even some of the rather numerous mitigation strategies that were considered here would be a major task and was not attempted in this work, although a limited number of sensitivity studies were performed. One method used to acknowledge the potential importance of the uncertainties was that, in a number of cases, input parameters and modeling assumptions were intentionally selected to be moderately but not excessively conservative; e.g., between the 50th and 90th percentiles of their uncertainty distributions. However, the calculations cannot be considered to be conservative in all respects, as some hypothetical phenomena which could increase containment loading were not included. In addition, some modeling assumptions are "conservative" for one set of conditions but "nonconservative" for others.

Problem Description for the CONTAIN Calculations

The recent NUREG-1150 risk assessment study indicated that risk to the public at the Sequoyah plant is dominated by two categories of events: containment bypass accidents, and station blackout accidents with early containment failure due to direct containment heating (DCH) and/or hydrogen combustion events. The present work addresses only the second category, since the former category is governed primarily by issues which do not involve containment phenomenology and which cannot be mitigated by improvements to the containment of the type considered here. Other approaches would be required to reduce the risk-significance of that category of accidents.

Accident Scenarios Analyzed Using the CONTAIN Code. All CONTAIN code analyses have been restricted to assessing one version or another of the station blackout accident. In these scenarios, no engineered safety features (ESFs) other than the ice condenser itself are available in the Sequoyah plant as it currently exists. Two major variations of the station blackout have been considered:

1. The classic TMLB' sequence, in which auxiliary feedwater is lost at accident initiation. Core melt and vessel breach (VB) occurs within a few hours of accident initiation, with the primary system fully pressurized, i.e., at the PORV set point (about 16 MPa).

2. A station blackout sequence in which it is assumed that the primary system is intentionally depressurized by opening the PORVs and the head vents. In the in-vessel analysis employed here (see below), depressurization delayed VB to about 9 hours after accident initiation, and vessel pressure was about 1.5 MPa at VB.

Because the CONTAIN code does not model in-vessel processes, sources of primary system water, steam, and hydrogen to the containment prior to VB had to be taken from available analyses of the in-vessel melt progression. Appropriate calculations for Sequoyah were not available, and the primary system sources were therefore based upon calculations that had been performed for the Surry plant. For the fully-pressurized case, a MARCH code analysis performed at Battelle Columbus was employed, while SCDAP/RELAP analyses performed at INEL were used for the intentionally depressurized case. Steam and water sources from these Surry analyses were scaled up to the Sequoyah plant using the ratio of the primary system volumes, while the ratio of the zirconium inventories was used to scale up the hydrogen sources. The magnitude of the additional uncertainties resulting from this procedure is not known, but it is believed to be less than the uncertainties associated with the in-vessel melt progression analysis.

Calculations were performed for this work assuming that 25%, 50%, and 75% of the total corium mass could participate in DCH. The 50% corium participation fraction corresponds approximately to the 85th percentile of the NUREG-1150 distribution for this parameter. In-vessel Zr oxidation and associated hydrogen production were taken directly from the calculations used to supply primary system sources; they were equivalent to about 50% and 72% zircalloy oxidation for the high-pressure and the depressurized accident sequences, respectively.

Containment Nodalizations. Three different CONTAIN input nodalizations describing the Sequoyah containment have been used in this work: a 4-cell deck, a 6-cell deck, and a 26-cell deck. The 4-cell deck included cells representing the cavity region (including instrument tunnel keyway), the lower containment, the ice condenser, and the upper containment. In the 6-cell deck, two cells were added to represent the lower and upper plena of the ice condenser. The nodalization of the 26-cell deck included four cells representing the lower plenum, four more representing the ice condenser, and two cells representing the upper plenum. Only the latter deck was sufficiently detailed to be useful in analyzing the gas distributions that govern detonation threats. Since this deck was rather expensive to run, DCH loads (that is, quasi-static pressurization due to DCH and associated hydrogen deflagrations) were generally analyzed using the simpler decks when possible. Comparison with the results obtained using the 26-cell deck generally supported this usage of the simpler decks, especially in the case of the 6-cell deck.

Uncertainties and Their Implications. In both the fully pressurized and the depressurized case, the containment analysis can be strongly affected by large uncertainties which exist in the analyses of the in-vessel melt progression. There are additional important uncertainties in the modeling of the containment phenomenology itself. Taken together, it must be acknowledged that these uncertainties result in large uncertainties in the absolute magnitudes of the containment loads which were calculated in this work.

The principal purpose of the present work, however, was not to evaluate the absolute magnitude of the threat to containment integrity in a specific accident sequence, but to gain understanding as to the degree to which this threat might be

reduced by various possible containment improvements. The principal method used was to compare calculations for the unimproved plant with otherwise-similar calculations for the plant with the various improvements in place. It is not believed that the uncertainties involved are likely to invalidate these comparisons, although careful consideration of these uncertainties is still warranted and they are therefore discussed in more detail in the main text of this report.

Before making a definite decision to implement a particular containment improvement strategy, it would still be desirable to perform a more detailed study of that specific improvement than was possible here. For example, a quantitative estimate of the reduction in containment failure probability might be desired. It would then be necessary to perform a detailed uncertainty study for both the unmodified and the improved plant. This uncertainty study would have to include assessment of the effects of phenomenological uncertainties and related modeling uncertainties in the analytical tools employed.

Results for DCH Events with Fully Pressurized RCS

CONTAIN-DCH analyses were performed for a number of potential containment improvements in order to assess the degree to which they could mitigate DCH events in which the RCS remains fully pressurized up until the time of vessel breach. Potential improvements considered include containment venting, independent power for igniters, augmentation of the existing igniter systems, containment inerting, operation of the containment at subatmospheric pressures, reduction of flow paths bypassing the ice condenser, and independent power supplies for the fans. Where meaningful, the improvements were also considered in combination with igniter operation. Any additional combinations of these improvements that might be promising were also considered.

The response of an ice condenser containment to a DCH event is quite complex, and the calculations performed for this work have provided substantial insights as to the governing phenomena. From a practical point of view, however, the most important conclusion is simple to state: DCH events with the RCS at system pressure are difficult to mitigate. Of all the strategies considered, only containment inerting offers much possibility of bringing about a substantial reduction in the probability of containment failure as it would be estimated in a PRA similar to NUREG-1150 (i.e., a PRA including assessment of phenomenological uncertainties).

The other mitigation schemes offer at best moderate reductions in the combined threat presented by DCH and hydrogen combustion following vessel breach. This conclusion holds even when combinations of improvements (not involving inerting) are considered. Improved igniters, containment venting, and a subatmospheric containment all offered some improvement, while reduced ice condenser bypass had little effect. Operating the air return fans appeared to increase the maximum pressures calculated somewhat. One possible reason is that fan operation enhances ice melting. The optimum combination considered was improved igniters together with containment venting; in the scenario with a 50% corium participation fraction, this combination reduced the maximum pressures from about 0.7 MPa to about 0.55 MPa, based upon calculations using the 26-cell deck.

The reason for the limited benefits associated with the various improvements assessed is that an important contributor to the containment pressurization is the large amount of hydrogen calculated to be generated within a few seconds by metal-steam reactions, combined with the transport of significant amounts of this hydrogen to the

oxygen-rich regions of the containment and its subsequent combustion. It is likely that only improvements which either prevent the generation of this hydrogen or prevent its subsequent combustion can offer much hope of substantial mitigation. Of the improvements considered here, only inerting meets this criterion.

Comparisons between the 4-cell, 6-cell, and 26-cell calculations indicated that the maximum pressures calculated by the 6-cell and 26-cell decks agreed to within 10%, while the 4-cell results showed somewhat larger differences. With some qualifications, the comparisons support the use of the 6-cell deck for evaluating maximum pressures during a DCH event. One important finding of the 26-cell calculations was that ice melt was quite unevenly distributed in the ice condenser. This effect may reduce somewhat the ability of the ice condenser to mitigate a DCH event, although this impaired performance has not been rigorously demonstrated.

CONTAIN-DCH calculations in Sequoyah, as well as in several other plants, have indicated that extreme pressurization of the cavity may develop, with cavity pressures 1 to 4 MPa higher than in adjacent portions of the containment often being calculated. Although certain limitations of the CONTAIN-DCH modeling may exaggerate this effect somewhat, the limitations of the model are not large enough to invalidate the conclusion that the cavity region may pressurize severely during a DCH event. No mitigation scheme considered in this work significantly affects the degree of cavity pressurization. The potential implications of cavity pressurization (structural failures, vessel lifting, effects of altered flow paths on DCH pressurization) require more study.

The calculations performed here were carried out only far enough to assess the maximum pressures following vessel breach. At the time the calculations were terminated, there was typically a large amount of unburned hydrogen (of the order of 1000 kg) in the ice condenser and the lower containment, while substantial unreacted oxygen remained available in the upper containment. The potential for additional large-scale combustion events therefore still exists. Detailed assessment of whether and under what conditions such events might occur would be a complex task which is beyond the scope of the present work. Some information illustrating the nature of the problem and the types of analysis required is given, however.

Mitigation Strategies Including RCS Depressurization

Partial depressurization of the RCS (to 1.5 MPa in the present analyses) can reduce the DCH threat in two ways. The first is that corium dispersal from the cavity may be reduced or possibly even eliminated, and the second is that the reduced steam supply reduces the amount of debris-atmosphere thermal and chemical interaction which can take place. In the calculations considered here, no credit was taken for the first of these effects and a 50% corium fraction was still assumed. Hence the calculations of the residual DCH threat in this scenario may be quite conservative, more so than in the analyses for a fully pressurized RCS.

In the NUREG-1150 study, it was judged quite likely that various thermally-induced failures of the RCS boundary would result in at least partial RCS depressurization even in the absence of any deliberate depressurization strategy. Qualitatively, the present analysis is applicable to these scenarios also.

Results showed that depressurizing the RCS was of no benefit if measures were not taken to control hydrogen. Even in the absence of any DCH phenomenology at all, hydrogen burns could present a severe threat to containment integrity if the large amounts of hydrogen released prior to VB were allowed to accumulate.

If power is supplied to the existing igniter system, RCS depressurization does confer substantial benefits. Maximum pressures are reduced from 0.65-0.7 MPa in the fully-pressurized case to 0.4-0.5 MPa in the depressurized case with igniters, assuming a 50% corium participation fraction in both cases. Installing additional igniters (e.g., in the ice condenser) does not yield substantial additional reductions in the maximum pressures, nor does operating the air return fans. With igniters operating, hydrogen burns prior to VB present no significant threat to the containment in the cases analyzed.

Ice depletion prior to vessel breach was substantially larger in this scenario than in the fully-pressurized scenario; as in the latter, the distribution of ice melting was calculated to be very uneven when the 26-cell deck was used. With the air return fans operating, ice was totally depleted well before vessel breach.

Flows through small leakage paths that bypass the ice condenser could have substantial effects upon containment conditions prior to VB. In one case, modifying these leakage paths appeared to have a beneficial effect upon the pressurization occurring after VB. The behavior was sensitive to details of the calculation that were quite uncertain, however, and no firm conclusions can be drawn concerning the potential benefits of modifying the bypass flows.

Although the benefits of depressurization combined with power for the igniters are substantial, containment-threatening loads cannot be absolutely ruled out even in this scenario. There are substantial phenomenological uncertainties that can affect the calculation. For example, given certain assumptions, water co-dispersed with the debris can enhance the DCH loads substantially. Uncertainties in the analysis of the effects of co-dispersed water are especially large, however.

Detonation Threats

Using the 26-cell deck, potential detonation threats were assessed by comparing the gas compositions calculated by CONTAIN with available information on the sensitivity of steam-air-hydrogen mixtures to detonation. No calculations of actual detonation loads were performed, nor was the effect of detonations upon containment integrity assessed. It should be emphasized that it is not presently known whether occurrence of a detonation in the ice condenser could actually cause the containment to fail.

Certain limitations inherent in the CONTAIN calculations need to be kept in mind in assessing the results. One limitation is that the calculations give no direct indication as to whether detonable gas pockets might develop on a scale smaller than the containment nodalization used. Another is that the modeling is insufficiently detailed to assess detonation threats when hydrogen influx is very rapid, occurring on time scales of a few seconds or less. Due in part to the latter limitation, detonation threats were assessed only up to and at the time of vessel breach; no attempt was made to assess detonation threats associated with the conditions that develop during a DCH event.

Detonation threats are governed by the gas distributions within the containment, which are in turn strongly affected by the natural convection recirculation flows. In the ice condenser, the usual pattern was to concentrate upward flow in the central portions of the ice condenser. One consequence is that hydrogen concentrations reach detonable levels in the central regions earlier than they do in the end regions. If the lower plenum doors are forced open to the point where they do not reclose,

recirculation flows between the ice condenser and the lower containment can subsequently have a large effect upon conditions in the lower containment also.

Perhaps the most striking and consistent feature of the calculations performed is the tendency for the ice condenser to develop highly detonable atmospheric compositions in the unmodified plant (no igniters operating) for all the cases analyzed. This was true even though the cases considered involved a substantial range in the postulated behavior of the lower plenum doors and in the sources input to the containment. Detonable compositions also tended to develop in the upper plenum, although there was more variability there than in the ice condenser itself. If, after being initially opened, the lower plenum doors remained substantially open, recirculation flows could lead to detonable compositions developing in much of the lower containment volume; with door reclosure, the lower containment tended to be steam inert.

The situation is more complex when dedicated power is supplied for the existing igniter systems. When the igniters in the lower containment are effective, burns initiating there and propagating into the ice condenser (which lacks igniters) were generally effective in preventing dangerous hydrogen concentrations from developing in the ice condenser. When steam inerting defeated the igniters in the lower containment, combustion in the ice condenser would not initiate until flammable concentrations were achieved in the upper plenum, which does contain igniters. By this time, detonable concentrations had sometimes been reached in the ice condenser. Dedicated power supplies for the air return fans (both trains) resulted in significant benefits, both by reducing the likelihood that lower-containment igniters would be defeated by steam inerting, and also by reducing the differences in hydrogen concentrations between the ice condenser and the upper plenum in those scenarios for which the fans could not prevent inerting of the lower containment. Nonetheless, ice condenser detonations could not be completely ruled out, given the large uncertainties in the sources of steam and hydrogen entering the lower containment.

Installing additional igniters in the lower plenum was analyzed and was found to be helpful for the depressurized scenario. However, the strategy was largely defeated by partial steam inerting of the lower plenum in the fully-pressurized scenario.

Detonation threats in the scenario with intentional RCS depressurization proved substantially easier to mitigate by providing power to the existing ESF systems (igniters and fans) than were detonation threats in the fully-pressurized scenario. The reasons for this difference are due to the differences in the sources input to the containment. Demonstrating that detonation threats can be controlled by depressurization combined with powering the existing ESFs would require assessing the uncertainties in the sources to containment for this scenario, a task outside the scope of the present work.

It is noteworthy that the depressurized scenario was considerably easier to mitigate despite the fact that the integrated hydrogen source input to the containment prior to vessel breach is considerably greater than in the fully-pressurized scenario (722 kg vs 307 kg). Within wide limits, the source rates, and the relative timing of the steam and hydrogen sources, are more important than the total hydrogen released in determining whether powering the existing ESF systems can control the detonation threats.

The effect of containment venting was considered both with and without fans operating, with the existing igniters being powered in both cases. Although some differences in the relevant gas compositions did result, the overall implications for detonation threats were not great.

The SCDAP/RELAP calculations of the depressurized scenario indicated that the surge line might undergo thermal failure. CONTAIN calculations were performed for this scenario assuming that existing igniters would be powered. Cases with and without operating air return fans were analyzed. In neither case did events following the surge line break result in very dangerous gas compositions developing in the ice condenser. This result is, however, dependent upon the particular scenario description used as input, especially with respect to the steam and hydrogen sources entering the containment after the break occurs.

NUREG-1150 Methodology Sensitivity Studies

The response of the Sequoyah containment to severe accidents for various containment improvements was explored utilizing NUREG-1150 methodology and models. The risk assessments on which NUREG-1150 is based can generally be characterized as consisting of four analysis steps, a risk integration step, and an uncertainty analysis step. The four analysis steps include: the accident frequency analysis, the accident progression analysis, the source term analysis, and the consequence analysis. Changes to the analysis due to the proposed containment improvements for the present work were implemented only for the step involving the progression of the accident after uncovering of the top of the active fuel has occurred. Resource constraints made it impossible to perform consequence analysis and risk integration for the present study, so a method for determining risk potential was developed, as is described later in this section.

The NUREG-1150 analysis utilized uncertainty distributions for variables in the accident frequency, accident progression and source term analyses. Uncertainty distributions were provided in large part by expert panels; some uncertainty distributions were obtained from generic data bases or developed internally by the project staff. A stratified Monte Carlo sampling technique was used to incorporate the uncertainty distributions into the analysis. The risk estimates have associated distributions; however, only mean values are reported for this study.

The unmodified NUREG-1150 analysis for internal initiators is referred to as the "base case" for this study. There were five sensitivity studies performed involving containment improvements that are expected to reduce risk potential by reducing the frequency of occurrence of early containment failure (failure before or at vessel breach):

- DCH Mitigation by Depressurization of the RCS, sensitivity study Case 1. The primary system is assumed to be depressurized by intentional opening of the PORVs by the operators.

- DCH Mitigation by Depressurization of the RCS, Back-up Power Supply for Fans and Igniters, Case 2. The primary system is assumed to be depressurized by intentional opening of the PORVs by the operators. It is assumed that the air return fans and the igniters are supplied power by a back-up system.

- DCH Mitigation by Depressurization of the RCS, Back-up Power Supply for Igniters, Case 3. The primary system is assumed to be depressurized by intentional opening of the PORVs by the operators. It is assumed that the igniters, but not the fans, are supplied power by a back-up system.

- Containment Strength Increased, Case 4. The containment failure pressure and impulsive failure criteria were increased to correspond to estimated criteria for the Watts Bar plant (1.14 MPa median failure pressure).

- Elimination of Direct Contact Failure Mode, Case 5. A mode of containment failure which involves accumulation of molten core debris at the steel containment wall shortly after vessel breach was eliminated from the accident progression event tree for this case.

The method developed for integrating the results of the base case and sensitivity studies utilizes a source term partitioning process, which was developed for the NUREG-1150 project, and involves the grouping of similar source terms. The integration method utilizes early fatality and latent cancer fatality "potentials" that are based on release magnitudes and timing. Radioactive decay is taken into account, but the release energy is not considered and there are no emergency response mitigative actions taken; i.e., there is no evacuation except relocation 24 hours after the release has begun, there is no sheltering, and no crop or land interdiction. The potentials were obtained by performing consequence calculations for the Sequoyah site.

Distributions for the early fatality and latent cancer fatality potentials are obtained for the base case and sensitivity studies. Mean values are computed for the risk potential estimates, as well as contributions of particular events to the mean risk potential estimates. Comparison of NUREG-1150 mean risk estimates and mean risk potential estimates for the base case for this study and comparison of contributing events demonstrate that the use of potential risk estimates is adequate for present purposes.

The mean latent cancer fatality risk potentials for the base case and sensitivity studies as defined above are given in Table 1. The percentage reduction in mean risk from the base case is provided for the sensitivity studies. The greatest reductions in latent cancer risk potentials occur for Cases 2, 3 and 4. The reduction in risk potential is relatively small for Cases 1 and 5. Table 1 also lists the mean risk potential associated with early containment failure (CF) as well as the percentage reduction in the base case value for the sensitivity cases. For example, for Case 2, the risk potential attributable to early containment failure is 2.2E-02 latent cancers per reactor-year, which is 35% of the base case potential associated with early containment failure. The early fatality risk potential values are about three orders of magnitude less than the latent cancer fatality risk potentials for the base case and sensitivity studies; the trends indicated for the latent cancer potentials apply for the early fatality potentials also.

Table 1

Latent Cancer Risk Potentials

	Base	Case 1	Case 2	Case 3	Case 4	Case 5
Total Risk Potential	1.1E-01	1.1E-01	7.1E-02	7.8E-02	6.5E-02	1.1E-01
Reduction		3%	37%	31%	41%	3%
Early CF Risk Potential	6.2E-02	5.8E-02	2.2E-02	2.9E-02	1.2E-02	5.9E-02
	6%	65%	53%	81%	5%	

Accidents which bypass the containment are significant contributors to the potential risk profile for the Sequoyah plant. The bypass sequences are interfacing systems LOCAs and steam generator tube ruptures. The contribution that these sequences make to the base case mean risk potential is about 60% and 50% for early fatalities and latent cancer fatalities, respectively. For the sensitivity studies, these percentages increase as the total mean risk potential decreases, because the improvements considered here have little or no effect on the various bypass accidents.

Most of the mean risk not associated with bypass events results from early failures of containment. Early failures mainly involve accidents with hydrogen combustion or detonation before or at vessel breach, or accidents that proceed to vessel breach at high pressure and result in significant pressurization of the containment due to DCH. The NUREG-1150 study indicates that many sequences that are initiated at high pressure will be depressurized by unintentional temperature-induced mechanisms, thereby reducing the DCH threat. The results for the sensitivity studies indicate that deliberate depressurization alone (Case 1) does not greatly affect the potential risk profiles. This is due in part to the already frequent occurrence of unintentional depressurization for the base case, and also due to the fact that there are a significant number of early containment failures even when the system is at low pressure at vessel breach. These failures are caused by early containment failure from hydrogen burns (particularly for station blackouts) or hydrogen burns at vessel breach coupled with ex-vessel steam explosions. When the Sequoyah containment failure criteria for NUREG-1150 are used, the largest reduction in risk potential occurs for situations in which intentional system depressurization and backup power for the igniters and the air return fans are provided (Case 2).

Of all the sensitivity studies, Case 4 (Watts Bar containment failure criteria) exhibits the largest reductions in risk potentials. This is attributable to a substantial decrease in the occurrence of early containment failures. If the same accidents and accident frequencies assumed for Sequoyah were applied to a containment with the structural failure criteria assumed for Watts Bar, the importance of early containment failures would diminish and bypass accidents would be of paramount importance. This indicates that plant-specific considerations are necessary for interpreting the results of this type of analysis.

1. INTRODUCTION

Background. The Containment Performance Improvements (CPI) program is a project sponsored by the Office of Research - Division of Safety Issue Resolution of the U.S. Nuclear Regulatory Commission to review existing information on threats to containment integrity and to perform additional analyses as needed in order to determine what, if any, improvements might be made to these containments which could reduce the probability and/or consequences of containment failure. The present report describes work performed at Sandia National Laboratories (SNL) in support of the CPI evaluation of ice condenser containments. The Sequoyah plant is the representative plant which has been selected for detailed study, in order to make use of the large amount of information available on this plant through the NUREG-1150 program and other studies. Throughout this report, references to "CPI" should be understood to refer only to the SNL ice condenser work except when otherwise specified; there is, of course, a large amount of other work which has been performed for other plant types and/or at other laboratories in connection with CPI.

One major analytical technique employed in this work was application of the CONTAIN-DCH code to assess threats in the unmodified plant and to determine the effectiveness of possible improvements. CONTAIN-DCH is a developmental version of the CONTAIN 1.1 code [Mu89] which includes an interim version of partially parametric modeling of direct containment heating (DCH) phenomena [Wi87, Wi88a]; see Section 2.4.1 for some additional details on this code. In addition, sensitivity studies using the NUREG-1150 event tree and related modeling [NRC89] were employed to determine how various possible improvements would affect the overall risk profile for the plant. The SNL ice condenser studies performed for CPI also include comparison of ice condenser experiments performed at Battelle Pacific NW Laboratories with CONTAIN simulations of these experiments, in order to test the validity of certain CONTAIN predictions concerning complex recirculation patterns calculated to arise in the ice condenser region during some accident scenarios. The present report describes the CONTAIN calculations and the NUREG-1150 sensitivity studies; the results of the simulations of the ice condenser experiments are being documented separately [Ru90].

In the initial phase of this work, various combinations of potentially significant challenges to the Sequoyah containment and possible potential improvements which might mitigate these challenges were identified [Wi88b]. However, the time and resources available to this program have not permitted a treatment of all possible combinations of threats and potential mitigation strategies, nor would such a blanket approach be cost-effective. For reasons discussed in Section 2.1, it was decided to concentrate attention upon station blackout accident scenarios involving hydrogen combustion (including detonations), either by itself or in conjunction with high pressure melt ejection (HPME) and direct containment heating (DCH).

Scope and Purpose of the Present Report. The present report is limited to a description of the CONTAIN calculations and the NUREG-1150 sensitivity studies performed for the CPI program and discussion of the results. Results of CONTAIN analyses performed for the CPI program during FY 1988 were summarized previously in an informal letter report [Wi88c] and, for the sake of completeness, the results discussed there are also included in the present work. This report will not attempt to present an overview of ice condenser containment issues, nor will it discuss in any detail the risk profile for the reference plant. Ref. NRC89 and its supporting documentation may be consulted for the latter, and the former may be found in the Issue Characterization Report under preparation at Brookhaven National Laboratory [BNL90].

As of this writing, it appears that one important potential use of the results obtained in the CPI program is to provide guidance for plant-specific assessments of potential improvements which may be performed as part of the Individual Plant Evaluation (IPE) program. In this context, the importance of the results may not so much lie in the specific numerical values obtained as in the insights acquired concerning the underlying phenomenologies governing the response of the containment to the accidents considered, and how the various containment improvements analyzed alter that response. It is hoped that these insights can provide considerable guidance in performing the more detailed analyses needed in order to support a firm decision as to whether a specific improvement should or should not be implemented in a specific plant.

This report therefore places considerable emphasis upon developing the phenomenological understanding required in order to design an efficient analysis intended to support a decision as to whether a specific improvement should or should not be installed in a specific plant. An effort is made to identify instances in which either details of the assumptions made concerning code input (e.g., description of the plant and/or the accident scenario) or uncertainties in the phenomenological modeling in the CONTAIN code can significantly affect the results. Since both the input uncertainties and the modeling uncertainties are potentially significant, it is essential to appreciate these uncertainties in the present state of the analysis art, and the implications of these uncertainties for any conclusions based upon the analysis.

The next section describes the problems treated in this work: the accident sequences considered, the mitigation schemes considered, the containment nodalizations used, and other CONTAIN input and modeling assumptions used. The use of "conservatism" in the analyses is discussed, and some limitations to the scope of the analyses are also described.

The following four sections describe the main results of this study. The first of these sections considers mitigation strategies which do not involve depressurization of the primary system, while Section 4 considers strategies that do include depressurization. In both sections, the emphasis is on the quasi-static loads that are calculated to result from DCH and/or hydrogen deflagrations. Consideration of potential detonation threats is deferred to Section 5, where hydrogen distribution issues are discussed, with emphasis upon determining whether detonable atmospheric compositions can arise, and how the mitigation strategies considered can affect the answers to this question; however, the dynamic loads and containment response that would result if a detonation actually did occur are not considered. The sensitivity studies performed using the NUREG-1150 methodology and modeling are described in Section 6. Appendix A gives some additional details concerning the CONTAIN input decks used to represent the Sequoyah containment.

2. PROBLEM DESCRIPTION

2.1 Accident Scenario

As noted in the Introduction, it would be neither feasible nor desirable to analyze all possible combinations of accident scenarios and potential containment improvements. The selection of specific scenarios to analyze has been based upon the following considerations:

1. The potential contribution of the scenario to plant risk.

2. The relevance of containment phenomenology (as opposed to other issues) to assessing the scenario, and to possible mitigation strategies for the scenario.

3. The applicability and relevance for the scenario of the available analytical tools.

4. The ability to obtain useful results within the limits of the available time and resources.

2.1.1 Implications of NUREG-1150 Results

Substantial insight as to the risk significance (Criterion 1 above) of the various potential accident scenarios in the Sequoyah plant can be obtained from the NUREG-1150 report and its supporting documentation. For present purposes, it is of interest to categorize the contributions of the various accident scenarios in two different ways. The first involves classifying them according to the nature of the initiating sequences, which were grouped into categories called plant damage states (PDS) in NUREG-1150. The second involves classifying the accident scenarios according to the nature of the containment response, including especially the timing of failure and reason for failure; these containment response parameters were grouped into categories called accident progression bins (APB).

One way of determining which accident scenarios merit study is to examine the fractional contributions of the various PDS and APB to mean risk as estimated in the NUREG-1150 analysis for the Sequoyah plant. These fractional contributions are summarized in Table 2.1. Results are given for both the early fatality and the latent cancer fatality risk measures. The numbers given represent the fractional contributions to the mean risk, after averaging over the uncertainty distributions assigned to the parameters representing the many uncertainties considered in the study. The study also showed that there are large uncertainties in the relative contribution to risk of the various PDS and APB; that is, the actual fractional contribution of a given PDS or APB to risk could vary greatly as the various uncertain parameters were varied over their uncertainty ranges.

From the PDS results, it is evident that accidents initiated by containment bypass events (steam generator tube ruptures (SGTRs) and interfacing system LOCAs or "V-sequence") dominate the early fatality risk measure, with station blackouts (SBO) contributing most of the remainder. For the latent cancer fatality risk measure, bypass and SBO are about equal and together contribute about 80% of the mean risk, with LOCAs contributing much of the remainder.

The categories in Table 2.1 are defined in such a way that any bypass PDS event results in a bypass APB event. Hence, it follows necessarily from the PDS results that

Table 2.1

NUREG-1150 Fractional Contributions to Mean Risk for Sequoyah

Accident Scenario	Early Fatalities	Latent Cancer Fatalities
Plant Damage States		
Bypass (V-sequence and SGTR)	0.73	0.40
Station Blackout	0.23	0.41
LOCAs	0.02	0.14
Other	0.02	0.05
Accident Progression Bins		
Bypass (includes induced SGTR)	0.75	0.45
CF at or before VB	0.24	0.45
Others	0.01	0.10

bypass also contributes strongly in the classification by APB. (In addition, there are some accidents which do not originate as bypass sequences but in which the core melt environment results in induced SGTRs during the accident progression, and these cases also contribute to the bypass APB category.) Most of the remaining contribution to mean risk is associated with APB which involve containment failure (CF) at or before vessel breach (VB). From the PDS results, it is evident that these events primarily involve station blackout accidents.

In containment bypass accidents, containment issues are not involved in determining the probability of the sequence occurring. Furthermore, the dominant contributions to the source term are usually radionuclides which are released directly from the reactor coolant system (RCS) to either the environment or secondary buildings outside the containment; containment performance and improvements to the containment are also irrelevant to this release. Hence the bypass scenarios were excluded from detailed consideration in this work (Criterion 2 above).

In contrast with the bypass accidents, containment phenomena are heavily involved in the SBO scenarios which include CF at or before VB, and containment improvements could substantially affect these scenarios. Since this class of event strongly dominates the mean risk for all accident scenarios not involving bypass, attention was focused upon SBO scenarios with early CF in the present work. (Here, "early CF" is defined to mean containment failure at or before VB.)

Although it is not directly apparent from the results given in Table 2.1, the large majority of the SBO/early-CF cases involve hydrogen combustion (including detonation), HPME, DCH, or some combination thereof. Steam explosions and the so-called "rocket effect" scenario (i.e., blowdown reaction forces launch the vessel upward as a rocket following VB) do make a contribution, but it is quite small. In addition to being minor in the overall risk profile, the phenomenological uncertainties associated with these effects also argue against their inclusion here (Criteria 3 and 4).

Based in part upon these NUREG-1150 findings, it was decided to concentrate the CONTAIN calculations performed for the CPI program upon threats related to hydrogen combustion and DCH in station blackout accidents. The study includes threats up to and including the time of vessel breach and immediately thereafter, but response at times substantially later than VB are not considered. The reason is that if the containment survives through the events associated with VB, failure during the next few hours is not very likely, and failures later than this fall into one of the late failure APBs of NUREG-1150. These late failures are included among "others" in Table 2.1, from which it is apparent that they do not contribute heavily to the mean risk estimates.

2.1.2 RCS Pressurization

Previous studies [Wi88a, Tu89] have shown that, other things being equal, the DCH threat is greatest in accident sequences in which the RCS remains fully pressurized up until the time of VB. In the NUREG-1150 analysis, four cases were defined to represent the degree of RCS pressurization at VB, as follows:

Case 1 RCS boundary is intact (except for cycling PORV) until VB; RCS pressure remains close to PORV set pressure (16-17 MPa) until VB. This case includes the classic TMLB' sequence of WASH-1400 [NRC75].

Case 2 RCS pressures of 7-14 MPa (1000-2000 psia), which can arise in scenarios involving an S_3 size break (e.g., pump seal LOCAs). Based upon Source Term Code Package (STCP) calculations [Gi86, Le88], RCS pressure might fall to the order of 8 MPa during core degradation in SBO sequences with S_3 pump seal LOCAs and with the steam generators dry; steam generated at the time of core slump is calculated to increase this pressure to the order of 14 MPa at the time of VB in the STCP analyses. Calculations with the more mechanistic MELPROG code have yielded considerably lower pressures at VB in these scenarios [He89].

Case 3 RCS pressure is in the range 1.4-7 MPa (200-1000 psia) at the time of VB. Pump seal LOCAs and stuck-open PORVs (S_2 break) both contributed to this case, although most of the latter events contributed to the low-pressure case (Case 4) in the final NUREG-1150 analysis.

Case 4 RCS almost or totally depressurized, pressures under 1.4 MPa (200 psia) at VB. Breaks of all sizes could contribute to this case in NUREG-1150, including surge line failures due to overheating, which would lead to rapid RCS depressurization. Although DCH was assumed to be of little concern in these cases, hydrogen combusion events could still result in containment failure.

All four cases were not considered separately in all phases of the NUREG-1150 analysis. In particular, the first two cases were combined in the assessment of containment loads, which is the topic of greatest interest here.

In the final version of NUREG-1150, the expert panel evaluating in-vessel issues assigned quite low probabilities to the first of the above cases, with the other three cases having higher probabilities to a greater or lesser degree, depending upon other parameters of the scenario. Despite its lower probability in the NUREG-1150 analysis, the first case was chosen as one of the cases selected for detailed study in the present work, for the following reasons:

- Earlier assessments of the p[illegible] of Case 1, performed for the first draft of NUREG-1150 [NRC87], g[illegible]nsiderably higher values, and the CPI analyses were begun before the final values became available; in addition, primary system sources were available for the fully-pressurized scenario (see Section 2.4).

- Case 1 is the worst case in terms of DCH threat, and it is desired to be somewhat conservative in the present work, as is discussed in Section 2.2.

- Case 1 and Case 2 were combined and considered together in the NUREG-1150 analysis of containment loads because Case 2 is not expected to be substantially less severe than Case 1, and use of Case 1 to represent this combination of Cases 1 and 2 is not excessively conservative. (The probability assigned to the combination of Cases 1 and 2 was quite significant in NUREG-1150; the combined case clearly does require detailed consideration.)

- The probabilities assigned by the NUREG-1150 experts were admittedly highly subjective, being based largely upon interpretation of a very limited number of code calculations with no direct experimental validation for some of the key assumptions involved. It therefore seemed prudent to include the more severe case among those studied in detail, lest changes in the estimated probability for the fully-pressurized case invalidate the findings of this study.

Station Blackout with Intentional Depressurization. As will be seen in Section 3 of this report, the results obtained for various mitigation schemes applied to the fully-pressurized station blackout accident do not appear especially promising, in terms of the feasibility of dramatically reducing the probability of early containment failure. Hence, later calculations in this program emphasized mitigation strategies that involved intentionally opening the PORVs to depressurize the RCS prior to VB. In the particular case selected for detailed study, the pressure of the RCS at VB was about 1.5 MPa (see Section 2.4). This is close to the borderline separating Case 3 and Case 4 in the NUREG-1150 classification of the possible RCS states with respect to pressure at VB. Results obtained for this case may therefore be taken as reasonably representative of the low end of the RCS pressure range in Case 3 of the NUREG-1150 study, even though the events assigned to Cases 3 and 4 generally did not involve intentional depressurization. (In the existing plant, intentional depressurization by opening the PORVs is not possible in SBO accidents because AC power is required; even in other scenarios, it generally would be precluded by the existing operator procedures in the relevant accident sequences.)

2.2 Mitigation Strategies Considered

2.2.1 Selection of Specific Improvements Considered

Potential containment improvements chosen for analysis in this work were selected following a considerable amount of consultation with NRC staff and with other participants in the Containment Performance Improvement Program. Selection criteria included the following:

1. Potential for effective mitigation

2. Technical and economic feasibility

3. The applicability and relevance for the proposed improvement of the available analytical tools.

4. The ability to obtain useful results within the limits of the available time and resources.

As the work progressed, a de facto fifth criterion emerged: mitigation schemes were emphasized that reduced containment loads and hence failure probabilities, as opposed to schemes that would reduce the source term if the containment did fail. One key reason was simply the additional effort required for including the latter. In addition, considering source term mitigation would introduce an additional large class of phenomenological uncertainties. The historical experience suggests that it could prove difficult to establish source term reduction with sufficient rigor to take credit for source term mitigation strategies in the regulatory arena, even though PRA results sometimes imply that source term mitigation strategies can significantly reduce risk.

The basic approach used in this work was to assess containment loads for the unmodified plant, and then repeat the analyses for the various containment improvements to be considered and compare results with the unmodified plant results. The containment improvements considered were as follows:

1. Backup power sources for existing igniters
2. Augmented igniter systems
3. Filtered vents in either the upper or lower compartment
4. Containment inerting
5. Operating the containment at subatmospheric pressures
6. Reduction of leakage paths past the ice condenser
7. Backup power sources for recirculation fans (both trains)
8. RCS depressurization

"Augmented igniter systems" (item 2 above) includes installation of igniters in locations where they are currently absent. The most important of these locations are the ice condenser and the lower plenum of the ice condenser. Backup power for all igniters is also assumed in this case.

In the above list, improvements 1, 2, 3, 4, and 8 were assessed individually (i.e., not in combination with any other improvement). All the improvements were assessed in combination with augmented igniters, with the exception of inerting, for which igniters are irrelevant. Additional combinations of improvements were considered when it appeared that they might offer advantages, as is discussed in Sections 3-5 of this report.

One potential improvement that was initially considered for inclusion but ultimately excluded is deep flooding of the cavity as a method of mitigating DCH threats. This strategy was dropped from consideration primarily because of the large uncertainties associated with fuel-coolant interactions (FCIs). Although there is a general consensus that deep flooding would substantially reduce HPME/DCH risks, there is not a complete consensus that the associated FCI threats could not result in making this cure worse than the disease. The phenomenological questions involved are not likely to be resolved within the time scale of the current study and, hence, this approach was not analyzed in detail.

As noted previously, containment bypass accidents are dominated by issues which do not, strictly speaking, involve containment phenomenologies. However, mitigation strategies have been proposed for these sequences which actually could be analyzed to at least some degree using the available containment analysis tools. These strategies generally involve scrubbing of the radionuclide release, either by introducing water in the release pathway or by operating sprays in the auxiliary building, for those scenarios in which the release is via the auxiliary building. Ultimately, these strategies were dropped from detailed consideration, in part because of the substantial effort required to set the problem up for analysis and in part because these strategies only involve a potential for source term mitigation; i.e., they do not reduce the probability of containment bypass occurring.

2.2.2 Role of "Conservatism" in the Study Design

If a given containment improvement is to be judged effective, it must yield a substantial mitigation of the threat it is intended to address. Some care is required in the evaluation of mitigation schemes when there are important uncertainties in the analysis (either uncertainties in the input parameters or in the modeling), as is known to be the case in the present study. Clearly, it will be difficult to justify an improvement which is effective given one specific scenario description (or modeling assumption), but which becomes ineffective given another, equally plausible, specific scenario description (or modeling assumption). In order to be justifiable, the improvement should be effective throughout most, if not all, of the parameter space spanned by the uncertainty ranges of the dominant uncertain parameters. This means that the potential improvement must be effective even when reasonably conservative assumptions are employed in the analysis.

Although the class of accident threats "DCH and hydrogen burns" might seem limited, there are actually a wide range of accident scenarios which fall into this category. In addition, there are important phenomenological uncertainties involved in the analysis of any given scenario. There are a number of mitigation systems which need to be considered, including combinations of systems; this leads to a substantial number of strategies which should be assessed. The number of possible combinations of accident scenarios, phenomenological uncertainties, and mitigation strategies which would have to be treated in an exhaustive examination is prohibitively large. Hence, considerable selectivity must be exercised in the choices of cases to be analyzed. The following guidelines have been employed:

1. Input parameters and modeling assumptions should be moderately but not excessively conservative; e.g., between the 50th and 90th percentiles of their uncertainty distributions, where such distributions have been established.

2. In general, a potential mitigation scheme has been dropped from further consideration if it appears to be ineffective for any reasonably plausible scenario description, and additional sensitivity studies are not performed for such schemes. Additional sensitivity studies are performed for the more promising options identified. However, no attempt has been made to analyze any option to the degree of detail that would be required to justify a definite decision to implement that option. Such a decision would require a detailed study of the given option in a highly plant-specific context.

In applying the first guideline, it must be remembered that some modeling assumptions are "conservative" for one set of conditions but "nonconservative" for others. When the uncertainty involved is potentially important, sensitivity studies were

sometimes performed to evaluate its impact. Performing comprehensive uncertainty studies for any of the containment improvements considered was, however, outside the scope of the present work.

CONTAIN is intended to be a detailed mechanistic code, and the code modeling is not generally designed to give either an inherently conservative or an inherently nonconservative result. Of course, there are significant uncertainties in some of the models employed and, in any given case, the resulting error may be in either a conservative or a nonconservative direction. Overall, however, there is no known reason to believe that the results of the calculations will have consistent built-in conservative (or nonconservative) bias. The degree of conservatism in a given calculation is primarily governed by the degree of conservatism of the input specified, including the specification of the modeling options to be used. Specific instances where it is believed that the input and/or modeling options used may be conservative or non-conservative are discussed further in Section 2.5 of this report.

One exception to the tendency toward conservatism in this work involves hypothetical phenomena for which mechanistic models are not available and for which the magnitude and even the existence of the effect is speculative. Often such effects can be represented using the CONTAIN-DCH code, but the representation is parametric, with the results being governed largely by user-specified input. In cases where there is little basis for the selection of the governing input parameters, and for which even the existence of a significant effect is uncertain, it does not seem useful to include the effect in the main body of calculations performed for this work, even when omitting the effect is potentially nonconservative. In a few cases, limited sensitivity studies were carried out for the effect in question (an example is the effect of water co-dispersed with the debris; see Section 2.5 and Section 4.5.1). In many cases, the existence of the possible effect is simply acknowledged as an uncertainty in Section 2.5. Similar principles also apply to the omission of highly speculative phenomena which could have mitigative effects.

2.3 Containment Nodalizations

CONTAIN-DCH calculations described in this report were performed using 4-cell, 6-cell, and 26-cell representations of the Sequoyah containment. (In some versions of the most detailed deck, 27 containment cells were used.) In all three decks, an additional cell was used to represent the reactor coolant system; this cell was only used to generate sources of blowdown steam and hydrogen entering the containment at the time of vessel breach (see Section 2.4). A second "extra" cell was used to represent the environment in scenarios involving containment failure or containment venting. Throughout this report, the decks are referenced by the number of cells used to represent the containment itself, with the actual number of cells in the complete deck being two greater than this number; thus, the "26-cell deck" actually has a total of 28 cells, counting the RCS and environment cells.

The 4-cell deck was used only in early phases of this work. Comparison between the 6-cell and the 26-cell results indicated that the former was usually adequate to predict gross containment pressurization. The more detailed deck was required to analyze questions involving hydrogen distribution (e.g., assessment of whether detonable atmospheric compositions could arise), uneven melting in the ice condenser, natural circulation flow patterns, etc. The more detailed deck proved rather expensive to run, typically requiring about 1 hour (or somewhat more) of CRAY CPU time for each two hours of actual problem time.

2.3.1 4-Cell Nodalization

A 4-cell deck was constructed by collapsing the 9-cell model used in the Sequoyah MARCH-HECTR study [Ca84] to three cells and adding a cavity cell separate from the remainder of the lower containment. The 4-cell representation is sketched in Figure 2.1. The four cells correspond to the cavity, the remainder of the lower containment, the ice compartment, and the upper containment. The volume of the lower and upper plena of the ice condenser are included in the upper and lower containment compartments, not the ice condenser.

The ice condenser doors were modeled as flow paths with a pressure-dependent area which can vary, reversibly, from a value equal to one quarter of the fully open value up to the fully open value. The choice of the minimum door area to be a quarter of the fully open value (rather than something much smaller) provided a crude representation of the fact that the doors, once opened by a strong flow, are not expected to fully reclose. Modeling of the door behavior is discussed further in connection with the 6-cell and 26-cell decks.

This 4-cell deck was used to study the unmodified plant and possible benefits from potential improvements including filtered venting of both the upper and lower compartments of the containment, independent power to igniters (including addition of igniters to the ice compartment), subatmospheric containment, and containment inerting.

2.3.2 6-Cell Nodalization

A 6-cell nodalization was developed from the 4-cell nodalization by adding two additional cells to represent the lower and upper plena of the ice condenser. Some additional refinements to the model were made based upon information obtained from the 40-cell HECTR representation of Sequoyah used in Ref. Di85, plant drawings, and information provided by TVA [TVA88]. The 6-cell nodalization is sketched in Figure 2.2.

Ice Condenser Doors. The three sets of ice condenser doors open under a forward pressure differential but may not fully reclose when the pressure differential is removed. In CONTAIN, flow paths with pressure-dependent areas may be defined, but these paths must be either fully reversible or fully irreversible as the pressure differential decreases. More complex behaviors may be simulated by using several parallel flow paths (some reversible and some irreversible), by opening and closing various flow paths at specified times, etc. However, specifying multiple flow paths increases the complexity of the analysis of the results and also increases the computer running time.

After some experimentation, a compromise representation was developed which involved specification of one reversible flow path and one irreversible path for each set of doors. Parameter values for the doors are summarized in Table 2.2; they are based upon information in Refs. Ca84, Di85, and TVA88. In some of the 6-cell calculations performed later in the program, the representation of the lower plenum doors was changed to conform to that used in the 26-cell deck. It should be noted that the 6-cell and 4-cell decks are much less sensitive to details of the door representation than is the 26-cell deck, since the simpler decks are not sufficiently detailed to represent recirculation flows through partially open doors.

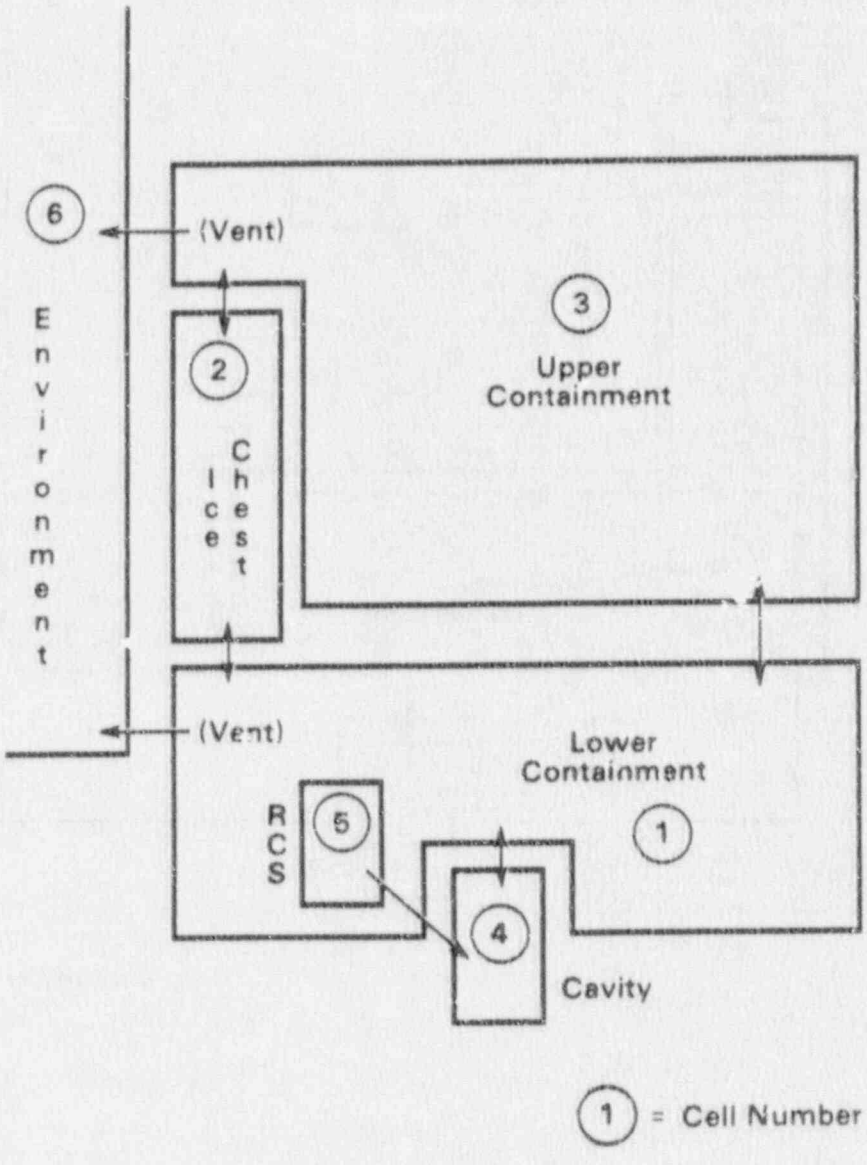

Cell	Volumes (m^3)	Flow Path	Areas (m^2)	ΔP Range (Pa)
1	10415	(1,4)	5.58	------
2	2444	(1,3)	0.204	------
3	22891	(1,2)	19.5-79	0.0-142.0
4	430	(2,3)	22.8-91.3	263-37910

Figure 2.1 4-Cell CONTAIN model for the Sequoyah containment.

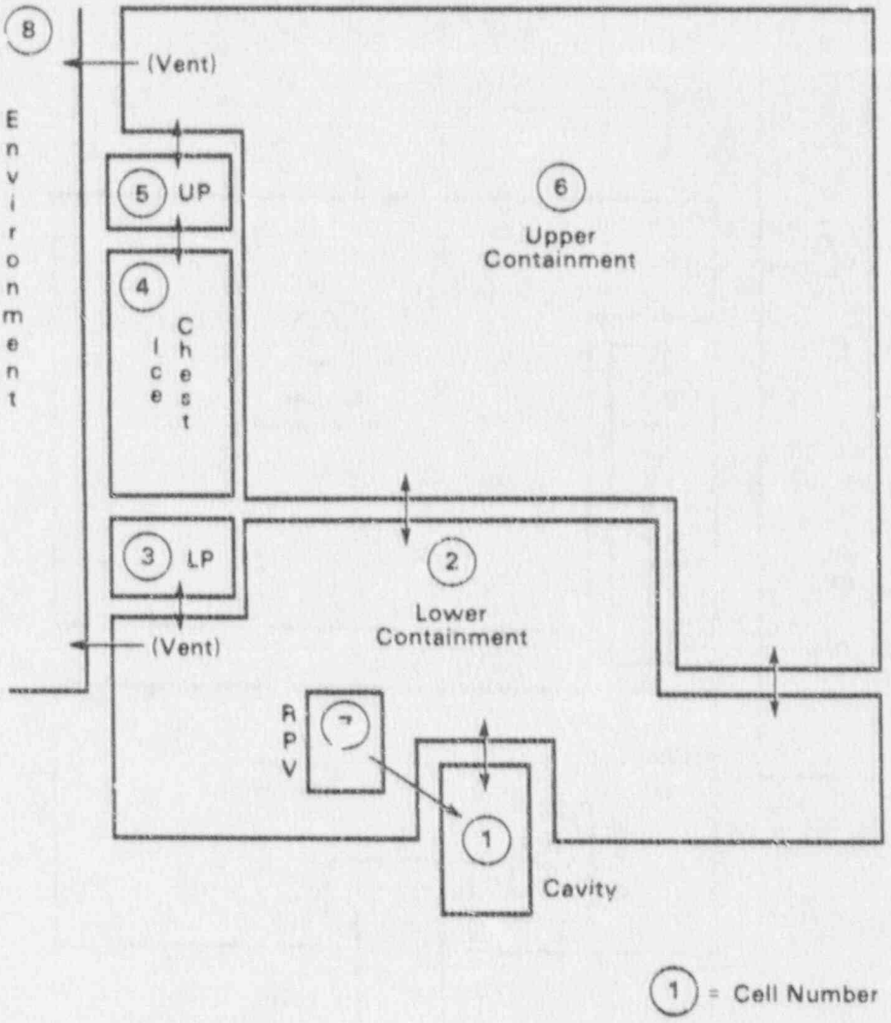

Cell	Vol. (m^3)	Elev. (m)	Cell	Vol. (m^3)	Elev. (m)
1	430	0.0	4	2444	27.8
2	9731	12.9	5	1330	37.6
3	685	19.0	6	21561	38.5

Flow Junctions

Junction	(1,2)	(2,3)	(2,6)	(2,6)	(3,4)	(4,5)	(5,6)
Flow area (m^2)	5.58	Door[a]	0.175	0.29	91.5	Door[a]	Door[a]
Elevation	8.53	19.0	6.47	20.6	20.4	35.0	35.0[b]

[a] Ice condenser door behavior is summarized in Tables 2.2 and 2.4.
[b] Value used was in error; it should have been 40.2 m. Correct value was used in the 26-cell deck.

Figure 2.2 6-Cell CONTAIN model for the Sequoyah containment.

Table 2.2

CONTAIN Representation of the Ice Condenser Doors
(6-Cell Deck, Initial Version)

Door		Flow Area (m^2) Min.	Max.	ΔP Range Over Which Doors Open (Pa) Min.	Max.
Lower Plenum	Reversible	0.0	37.89	27.3	142.07
	Irrev.	0.004	40.11	23.9	142.07
Intermed. Deck	Reversible	0.0	68.38	263.	37910.
	Irrev.	1.86	24.65	263.	37910.
Upper Plenum	Reversible	0.0	92.08	263.	8619.
	Irrev.	1.83	93.9	263.	8619.

Ice Condenser Bypass Leakage Paths. According to Refs. TVA74 and TVA88, there is about 0.465 m^2 (5 ft^2) of flow path area between the lower and upper containment that bypasses the ice condenser. Of this, 0.175 m^2 represents the refueling canal drains, while the remainder is unspecified leakage. These bypass paths can play a significant role in accidents of long duration in which steam and gas sources to the lower containment are low; under such conditions, the lower containment may not pressurize sufficiently to overcome the weight of the cold, heavy gas in the ice condenser and much of the flow may be through the bypass. Since this flow is largely governed by buoyancy effects under these conditions, the elevation of the bypass paths is important. The refueling canal drains are at an elevation of about 6.5 m; the elevation of the remaining bypass flow paths is not known. The latter bypass flow (which will be called "deck leakage" in this work) was assumed to be leakage in and around the main floor separating the upper and lower compartments, at an elevation of about 20.5 m. (All elevations are referenced to the elevation of the center of gravity of the cavity cell.)

2.3.3 26-Cell Nodalization

In the 4- and 6-cell nodalizations, most of the volume of the lower containment is in a single cell, and most of the volume of the upper containment is likewise in a single cell. This degree of detail is quite inadequate to treat questions such as detonation threats, which depend upon details of the hydrogen distribution. The degree of spatial resolution is inherently inadequate and, furthermore, the degree of detail in the flow path representation is not adequate to simulate the relatively complex natural circulation patterns that can develop and that can significantly affect the hydrogen distributions. (It was also thought possible that such simple representations might yield overly conservative results for the containment pressures in DCH calculations. However, the benchmarking exercises described in Section 3.3 suggest that this is generally not the case, at least for the 6-cell deck.) Hence, a more detailed deck was constructed, based in part upon an earlier HECTR code deck [Ca84, Di85], but with substantial modifications based upon the FSAR [TVA74], information supplied to the NRC in support of the Sequoyah hydrogen control program [TVA81], and information supplied by TVA for the NUREG-1150 effort [TVA88].

The more detailed nodalization represented the containment using 26 cells. Major features of this representation are summarized in Figure 2.3 and Table 2.3. In some earlier versions of the deck, Cell 26 in Figure 2.3 was subdivided into a cell representing the refueling canal and a cell representing the remainder of the lower portion of the upper containment, making 27 cells in all; because CONTAIN flow modeling does not include countercurrent flow through a single opening, this division introduced artificial gas stratification effects and was later eliminated. Additional information on this containment representation, including a complete listing of the deck itself, is given in Appendix A of this report.

Ice Chest Nodalization. Four cells were used to represent the ice condenser. The nodalization was azimuthal; that is, each cell represented an ice column that was the full height of the ice condenser and that included one quarter of the total ice chest volume and associated ice mass. Adjacent ice columns were modeled as being connected by two flow paths, at elevations of one quarter and three quarters of the cell height, respectively. Providing two connections at different heights between adjacent cells permitted at least a highly simplified representation of recirculation flows within the ice condenser. In addition, recirculation loops involving the lower and/or upper plena were modeled. Additional discussion on the modeling of recirculation flows driven by buoyancy heads (i.e., natural circulation) is given in Section 2.4, including discussion of some limitations inherent in CONTAIN and other lumped-parameter control volume codes of this type.

Ice Condenser Doors. Sensitivity of the calculated flow patterns to the modeling of the ice condenser doors was examined, and it appeared that the greatest sensitivity

Table 2.3

Summary of Sequoyah 26-Cell Nodalization

Cell Nos.	Location
1	Reactor Cavity
2-5	Steam. Gen. Doghouses
6	Upper Reactor Space
7	Pressurizer Doghouse
8-10	Lower Containment (Inside Crane Wall)
11-13	Lower Annulus (Between Crane Wall, Shell)
14-17	Lower Plenum
18-21	Ice Condenser
22,23	Upper Plenum
24,25	Upper Dome
26	Lower Dome & Operating Floor

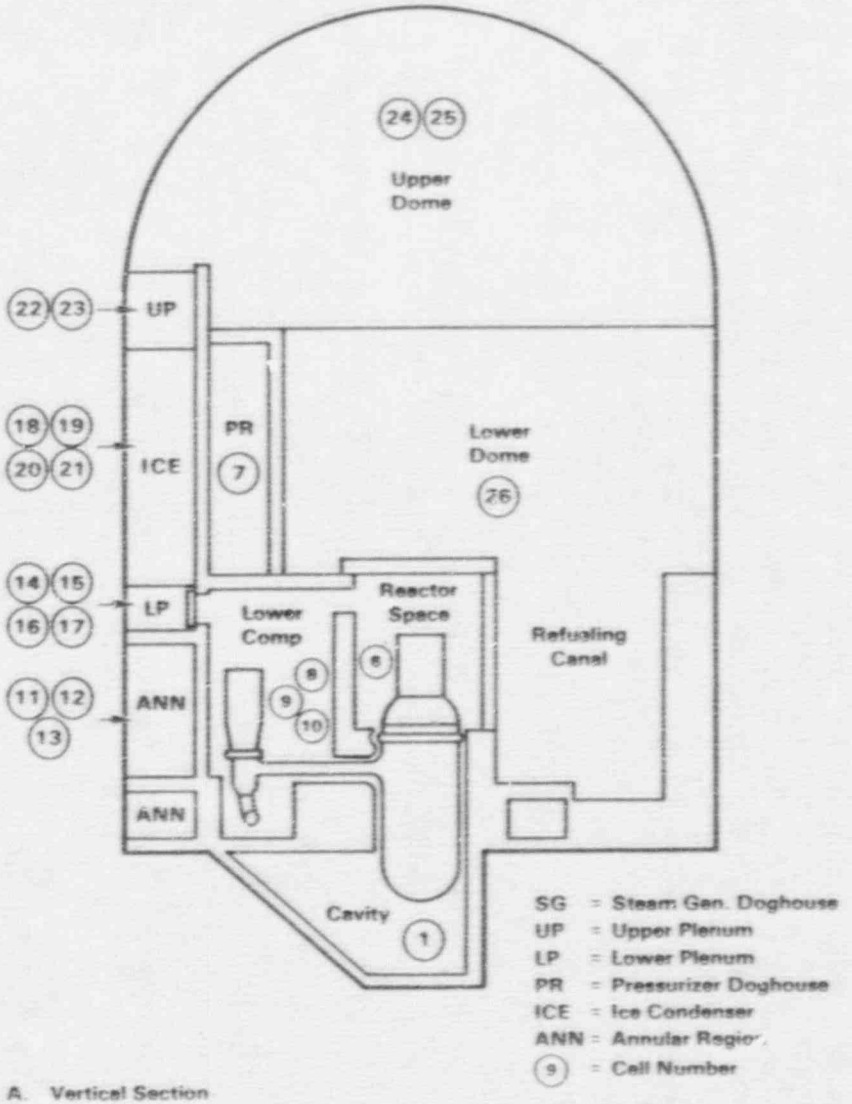

A. Vertical Section

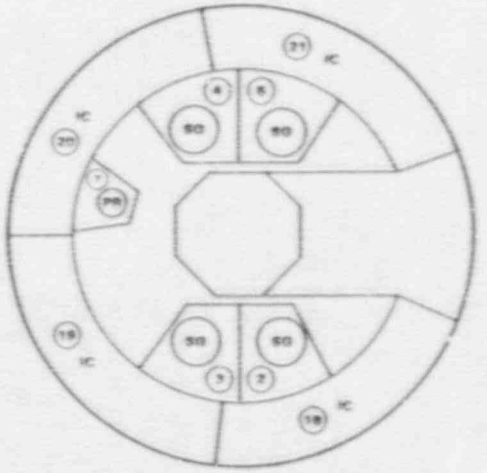

B. Top View of Ice Condenser Nodalization

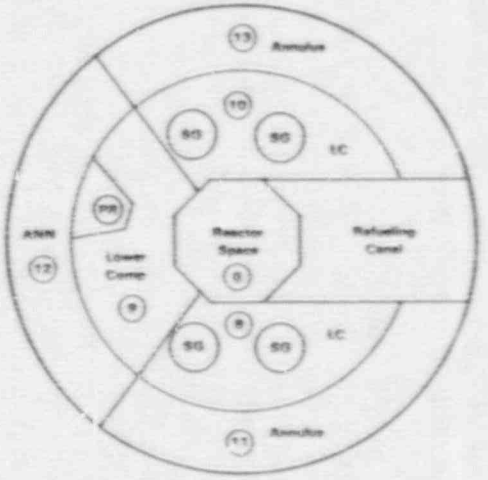

C. Nodalization of Lower Compartment

Figure 2.3 26-cell CONTAIN model for the Sequoyah containment.

was to the modeling of the lower plenum doors. After some initial sensitivity studies, the pressure vs. area curve for the plenum doors was modified to correspond to the behavior summarized in Table 2.4.

In Table 2.4, modeling of the upper and intermediate deck doors is essentially the same as in Table 2.2 except that the irreversible portion does not begin to open until the reversible portion has been fully opened; thus, if the opening is less than the maximum opening of the reversible portion, the doors can reclose fully. The lower plenum doors are modeled as being fully reversible except that, once fully opened, they are assumed to remain fully open due to deformation of crushable hinges. Note that a small reverse pressure (14 Pa) is required to fully close the lower plenum doors; at the neutral point (zero pressure differential) the open area is 2 m^2. These details of the door behavior are quite uncertain, and some results of the CONTAIN calculations do show significant sensitivity to these details (e.g., ice condenser bypass flows and recirculation between the ice condenser and the lower plenum). The response of the ice condenser doors assumed here is based upon information in Refs. TVA74 and TVA88; see also Appendix A.

The main volume of the lower containment between the cavity shield wall and the crane wall was modeled using three cells (Cells 8-10 in Figure 2.3), four cells were used to represent the lower plenum, and a total of six variable-area flow paths connecting the lower containment to the lower plenum were needed to represent the lower plenum doors. For each of these paths, the fractional area versus pressure curves were identical; however, due to recirculation flows and uneven ice melting, the pressure differential seen by the various flow paths representing the doors were not necessarily the same and, hence, the doors could open to different degrees. The doors are designed to open under low pressure differentials, and the pressure differentials involved in the buoyancy flows and the ice condenser cold head are far from negligible

Table 2.4

CONTAIN Representation of the Ice Condenser Doors
(26-Cell Deck and 6-Cell Deck, Final Version)

Door		Flow Area (m^2) Min.	Flow Area (m^2) Max.	ΔP Range Over Which Doors Open (Pa) Min.	ΔP Range Over Which Doors Open (Pa) Max.
Intermed. Deck	Reversible	1.86	70.24	263.	28498.
	Irrev.	0.0	22.79	28498.	37910.
Upper Plenum	Reversible	1.86	93.9	263.	4441.
	Irrev.	0.0	92.08	4441.	8619.

Lower Plenum Doors:

ΔP (Pa)	≤ -14.0	0.0	4.788	9.576	19.15	28.73	38.30	≥ 46.92*
Area (m^2)	0.00403	2.0	2.60	3.75	6.23	20.24	44.6	78.0*

* Lower plenum doors remain open once pressures exceed the value required to produce the maximum opening.

in influencing door behavior. (The term "cold head" refers to the differential pressure head developed by the cold, relatively heavy gas that normally fills the ice condenser; the cold head is sufficient to keep the lower plenum doors fully closed under normal operating conditions.)

Among other things, this meant that the doors would not fully reclose when there was a zero pressure differential across them, although they would close when a small reverse pressure was present. A small reverse flow through the doors could occur without closing them, but when this flow exceeded a few kg/s, the doors would in effect slam shut. Although the convergence checks built into the CONTAIN implicit flow solver tended to complain about the near-discontinuous behavior that resulted, and computer execution times sometimes suffered, the behavior calculated actually appeared to be quite reasonable, physically.

Bypass flow. The bypass flow paths representing the refueling canal drains connect Cells 8 and 10 to Cell 26 (see Table 2.3), while the additional leakage (deck leakage) was equally distributed between Cells 8, 9, and 10, and was also connected to Cell 26. The total bypass flow areas, and the elevations of the bypass flow paths, were as in the 6-cell deck.

2.4 CONTAIN Modeling and Input

2.4.1 CONTAIN Version and Modeling

Code Version. Modeling for direct containment heating (DCH) is not yet included in any formally released and documented version of CONTAIN. All calculations to be discussed here were performed using a code variation which will be referred to throughout this report as "CONTAIN-DCH", although the code will sometimes be referred to simply as "CONTAIN" when the description is equally applicable to CONTAIN 1.1. CONTAIN-DCH is built upon the released version of CONTAIN 1.1 documented in Ref. Mu89, and includes all standard modeling and features of that code. CONTAIN-DCH also includes interim models for DCH that are described in Refs. Wi87 and Wi88a. In addition, this code includes three major updates to CONTAIN 1.1, as well as some much less extensive modifications introduced specifically for the present work. These enhancements together with several others comprise CONTAIN 1.11, which did not become available in time for the present study. (CONTAIN 1.11 combined with the DCH models will be released as CONTAIN 1.12.)

The descriptions of the standard CONTAIN 1.1 models in Ref. Mu89, and of the interim DCH models in Refs. Wi87 and Wi88a, are generally sufficient for present purposes. Hence the present discussion will be limited to features not in the code versions described in these references, plus some special considerations not immediately obvious from a simple description of the relevant modeling itself.

Modeling of Hydrogen Combustion. In the CONTAIN default model for hydrogen combustion (which is essentially the same as the default burn model in the HECTR code [Di86]), hydrogen combustion is assumed to occur whenever hydrogen and oxygen mole fractions exceed 7% and 5%, respectively, provided that the steam mole fraction is less than 55%. In addition, a combustion event initiated in one cell is allowed to propagate into any cell connected to it provided atmospheric concentrations in the connected cell meet certain criteria for propagation; in the default model, the oxygen and steam concentration limits for propagation are the

same as the ignition limits, while the hydrogen concentration limits for propagation are 4.1%, 6%, and 9% for upwards, sideways, and downward propagation, respectively.

In the default burn model, the flame speed (which controls the rate of combustion) is calculated from correlations that are rather complex functions of the hydrogen and steam concentrations. Both the combustion rate and the degree of completeness of combustion increase with increasing initial hydrogen concentration, with almost complete combustion being assumed for initial concentrations greater than 8%. On the other hand, combustion rates decrease substantially with increasing steam concentrations, and high steam concentrations result in long burn times, which often permits gas-structure heat transfer to substantially mitigate the peak pressures calculated.

The correlations used in this model are based upon experiments in which the initial atmosphere temperature was less than 400 K. In DCH scenarios, the atmosphere is often heated to substantially higher temperatures, even prior to the initiation of any hydrogen combustion. As discussed in Refs. Wi87 and Wi88a, there is theoretical and experimental reason to believe that the default correlations may be inapplicable under these conditions. In particular, the flammability limits are expected to be wider, and flame speeds higher, than the default correlations imply. In DCH calculations for PWR large dry containments, temperatures commonly become so high (800-2000 K) that the "unconditional hydrogen burn" (UCHB) assumption becomes plausible; i.e., it is possible that hydrogen and oxygen will react whenever both gases are present in the same cell, regardless of concentration criteria. Many of the DCH calculations that have been carried out for large dry containments have employed the UCHB assumption. In station blackout calculations for large dry containments, steam fractions were generally sufficiently high so that the default model either permitted no hydrogen burns at all, or else imposed such long burn times that the hydrogen burn did not augment the peak DCH loads greatly. Invoking the UCHB model substantially increased the calculated loads for large dry containments.

In ice condenser containments, the situation is less clear-cut. Since the upper containment generally has relatively low steam concentrations, even in station blackout accidents, hydrogen burns are very important contributors to DCH loads even when the default model is assumed. Indeed, the default model sometimes yields higher loads than does the UCHB model [Wi87], since the default model allows more hydrogen to accumulate in an oxygen-bearing cell prior to ignition. Furthermore, the ice condenser keeps pre-ignition temperatures lower in the upper containment, especially when the amount of corium participating in DCH is relatively small (e.g., 25% of the total corium inventory). Under these conditions, the arguments supporting the UCHB assumption are weaker than they are for DCH events in large dry containments, and it is likely that both the default model and the UCHB model are only crude approximations at best. Refinements to more mechanistically take into account hydrogen behavior under conditions existing during DCH events in ice condenser plants are a clear need.

In the present calculations, the default ignition limits have been used except in some sensitivity studies discussed in Section 3.1 (when igniters are absent or not operating, ignition prior to VB was generally suppressed completely; see Section 2.4.3.) In the initial phases of the study, the default flame speeds were also used. However, it was found that burns initiated in the upper containment sometimes did so under conditions for which the default model predicted long burn durations (tens of seconds). These long burn durations may be nonconservative for events involving DCH, and later calculations in this study generally used a flame speed of 5 m/s in the

upper and lower containment compartments, giving burn durations of the order of 5 s. This flame speed was chosen to give burn durations sufficiently short so that substantial mitigation by heat transfer to structures during the burn usually does not occur; the choice of 5 m/s is otherwise arbitrary. The default model was generally used in the ice chest and the dome. Often conditions in these volumes (especially the ice condenser) were such that the default criteria gave flames speeds at least as great as 5 m/s, although this was not always the case.

Ice Condenser Modeling: Heat and Mass Transfer. In CONTAIN, convective heat transfer to structure surfaces in general is modeled using Nusselt number correlations, and mass transfer (condensation and evaporation of coolant) is modeled using a heat transfer - mass transfer analogy. The presence of a water film (default thickness = 0.5 mm) is allowed for. In CONTAIN 1.11, the treatment was refined in a number of ways, and these refinements are included in CONTAIN-DCH, but the description given in Ref. Mu89 still generally applies.

In CONTAIN 1.1, the treatment of convective heat and mass transfer to ice surfaces was basically equivalent to heat transfer to a structure whose surface temperature is constrained to remain at or below 273.15 K. (In addition, ice melt and heat transfer to effluent water were allowed for.) However, there is evidence that roughness-induced turbulence in the ice chest could actually enhance heat and mass transfer rates substantially, and, in CONTAIN-DCH, a user-specified enhancement factor is provided, with a default value of 5. Without this enhancement, the code was found to calculate excessive containment pressurization in an approximate simulation of a large LOCA accident. A factor of 5 has also been found to give reasonable results in the HECTR code. It should be emphasized that there is little true validation of this treatment, largely because of the unavailability of suitable experimental data for comparison purposes; see Section 2.5. All calculations reported here were performed with the default value (5) of this enhancement factor.

Natural Circulation. In the accident situations analyzed here, flows are dominated by natural circulation for substantial periods of time, and these circulation patterns will heavily affect the hydrogen concentrations calculated by the code. The CONTAIN flow equations include pressure terms representing the gravitational heads in the various flow paths and cells. Hence, the calculation does include natural circulation effects. However, there are some limitations to the treatment which must be taken into account in interpreting the results.

One limitation is that the code does not model countercurrent flows when a single flow path connects two cells. This countercurrent flow could be important when two cells are connected by a single path of relatively large area, if the atmospheric densities and the geometries are such that convective interchanges between the cells would be expected. In CONTAIN, convective flow can be calculated only when the flow paths specified include a return path, so that a complete loop is modeled. Even when this is done, there are some limitations to the treatment which must be kept in mind when interpreting the results. These effects can be divided into three categories:

1. Even the 26-cell nodalization used here is very coarse in comparison with the nodalizations used in finite difference codes, which may involve many thousands of computational cells. Hence, spatial resolution is comparatively crude and numerical diffusion effects may be large.

2. CONTAIN treats each cell as being well-mixed, with gas properties being the same in all parts of the cell. In addition to the limits imposed upon spatial

resolution that were noted above, the fact that gas density throughout a cell, or within the full length of a flow path, is assumed to be constant means that the gravitational heads calculated by the code will not be the same as would be calculated if more detailed information were available for the gas density as a function of location. Hence, some error is introduced into the driving forces for convection. Numerical experiments have shown that even the failure to treat the small density gradients introduced by the gravitational heads themselves can introduce significant spurious effects, although usually this gravitational density gradient is small compared with the density differences associated with temperature and with gas composition in realistic containment calculations.

3. CONTAIN, like other control volume codes, does not treat momentum convection in its flow solution. The impact of this simplification is believed to be minor in many calculations for which the code is normally used. However, it may be significant when driving pressure differentials are small, as in natural circulation calculations, and is especially likely to be of concern if one attempts to treat circulation patterns within large, open volumes by artificially subdividing these volumes into a number of computational cells separated by "virtual" boundaries.

Little information permitting a direct evaluation of these effects is available. It should be noted that, to the best of the authors' knowledge, all currently-available codes of the same class as CONTAIN (i.e., lumped-parameter, control volume codes) are subject to all the same limitations noted above. Codes based upon finite difference solutions of the Navier-Stokes equations reduce or eliminate these limitations in principle, but their use for the analysis of complex containment systems has been severely restricted in practice because of the codes' complexity and running expense. At this time, it is not clear that such codes can give better results than the control volume codes [Ti90].

Some validation work has been done on the ability of CONTAIN and other reactor safety codes to treat gas mixing problems in complex geometries, including some experiments performed at relatively large scales. Without going into details, the results suggest that CONTAIN gives reasonably satisfactory results in situations where gas flows are vigorous and in situations where buoyant plumes are released at low elevations within the containment. However, recent large-scale experiments have shown that, when buoyant plumes are released high in the containment, without strong mixing forces other than natural circulation being present, the gases may tend to stratify more than is predicted; that is, the degree of mixing may be overpredicted by the codes. Hence, the possibility of detonations in regions of containment having high hydrogen concentrations could be greater than implied by the code calculations. A recent review summarizing the state of the art for the analysis of hydrogen mixing may be found in Ref. Ti90.

In general, buoyant gas sources (steam and steam-hydrogen mixtures) will not initially enter the Sequoyah containment at high elevations in the accident sequences analyzed here, and the worst-case situation noted above probably will not arise directly as a result of the sources from the primary system. However, under some circumstances, in the absence of igniters, hydrogen-rich plumes could enter the upper containment from the ice condenser upper plenum, and tend to stratify in the upper dome. No attempt will be made to assess this problem, as it is believed that the results could be quite unreliable. Note that this situation does not arise if igniters are provided to burn off the hydrogen in the ice condenser, the upper plenum, and/or the

upper dome. If igniters are not available, it will be seen in Section 5 that detonable gas concentrations are generally calculated to arise in the ice condenser region. The possibility of additional detonable regions developing in the upper containment would only add to the existing concern over detonations in the ice condenser.

For the most part, the qualitative conclusions concerning the development of detonable gas mixtures that will be offered in this work are not believed to be invalidated by the uncertainties discussed here, primarily because no conclusions will be drawn for the situations in which these uncertainties are expected to be the most severe. Nonetheless, it must be remembered that the uncertainties will be substantial, not only because of the modeling limitations discussed here but also because of the large uncertainties in some of the input required, e.g., concerning the sources of steam and hydrogen entering the containment from the primary system. In particular, care should be taken not to overinterpret a particular quantitative result concerning whether hydrogen concentrations in a specific scenario are above or below a presumed detonation limit. In many such cases, changes to the scenario description that are well within the uncertainty range could reverse conclusions that might be drawn from such a simplistic comparison with detonation limits.

Momentum-Driven Mixing. As noted above, the CONTAIN code, like other lumped-parameter control-volume codes, does not treat momentum as a conserved field; in effect, it is assumed that momentum of a flow entering a cell is dissipated within the cell. If, in reality, a high-momentum jet enters one cell, transport across this cell to the next cell may be governed in part, at least, by the momentum of the flow. In this event, the CONTAIN code may underestimate the extent of intercell mixing. The effect is, in a sense, the opposite of the effect discussed in connection with natural convection above: in the latter, the result can be a tendency to overestimate mixing in relatively long-duration accident sequences with flows governed by natural convection, while the result in the present case can be a tendency to underestimate intercell mixing in short-duration energetic scenarios for which momentum-driven transport and mixing processes are important.

Despite the limitations in the CONTAIN flow modeling that have been discussed here, it should be remembered that they involve situations that are the exception, not the rule, in containment analyses. For many of the situations routinely encountered, flows and resulting gas mixing will be governed by pressure differences associated with sources and sinks of mass and energy to the containment atmosphere, as opposed to flows governed by buoyancy effects. The inability of the code to model momentum-driven mixing effects is probably important only in scenarios involving high flow rates and short time scales, during which other mixing processes may not be fully effective. The code is expected to do a satisfactory job in analyzing many of the more common containment scenarios, and this expectation is supported by a number of experimental validation efforts [Mu83, Al87, La89], including some cases involving natural circulation [La89]. Even in some recent simulations of ice condenser experiments, involving complex gas stratification and recirculation flows driven by buoyancy effects, the code was found to provide a good qualitative description, although the degree of thermal stratification was underpredicted significantly [Ru90]. In the present work, any cases that have been identified in which the uncertainties discussed here could be important will be explicitly flagged when the relevant results are discussed.

2.4.2 Code Input

Primary System Sources. The CONTAIN code does not include models for analyzing the in-vessel phase of the accident progression. Hence, sources of steam,

hydrogen, aerosols, radionuclides, etc., entering the containment from the primary system must be input to the code. In typical CONTAIN analyses, these sources are obtained from calculations using primary system analysis codes and are input to CONTAIN in the form of source tables, and this approach was used in the present work.

For the fully-pressurized station blackout analysis, sources of steam and hydrogen to the containment prior to VB were taken from MARCH calculations performed at Battelle Columbus Laboratories. Sources for the scenario of interest were not available for Sequoyah, and the scope of the present program did not include performing primary system analyses specifically for this purpose. Hence, sources were estimated by scaling up sources that had been calculated for Surry using the ratio of the primary system coolant inventories as a scale factor. The additional uncertainty introduced by this procedure is discussed briefly in Section 2.5. The MARCH calculation employed was the same one that was used to provide primary system sources in the Surry DCH analyses described in Ref. Wi88a. The accident analyzed was a station blackout with loss of all feedwater and with the primary system remaining intact prior to VB; thus the accident corresponds to the classic TMLB' sequence in WASH-1400 terminology. Vessel failure occurred at 10090 seconds after reactor shutdown in this calculation. The sources of primary system water, steam, and hydrogen to containment prior to VB are plotted in Figure 2.4.

The potential for mitigating DCH in PWRs by intentionally opening the PORVs and head valves to depressurize the RCS has been studied at the Idaho National Engineering Laboratory (INEL) using the SCDAP/RELAP code, which provides a more mechanistic description of the in-vessel accident progression than does MARCH [Ch88, Go89]. Again, the plant studied was Surry, not Sequoyah; there have been no comparable analyses using any code for Sequoyah. Hence the the sources of steam and primary system water to containment were scaled up to Sequoyah by multiplying by the coolant inventory ratio, while the hydrogen sources were scaled by multiplying by the ratio of zirconium inventories in the respective cores.

The INEL work assessed two basic scenarios for intentional depressurization. In the first, designated "early depressurization," the PORVs were assumed to be latched open at the time of steam generator dryout. In the second, designated "late depressurization," the PORVs were not latched open until high core exit temperatures (i.e., above 1200 F or 886 K) signaled the approximate onset of core degradation. In terms of potential containment response, the most important difference between them was in the timing of hydrogen generation. In the early scenario, initial accumulator discharge rates were not sufficiently rapid to cool the core and halt oxidation, and the strongest hydrogen sources to containment were early in the accumulator discharge phase of the accident; there was a second, smaller release of hydrogen that took place during core reheat after accumulator discharge was complete. In the late depressurization scenario, the initial accumulator discharge did cool the core sufficiently to terminate oxidation, and the principal period of hydrogen generation began after accumulator discharge was complete. However, the SCDAP/RELAP calculation was terminated during the period of strong hydrogen generation, and a complete hydrogen source for this scenario is unavailable.

The investigators in Ref. Go89 concluded that late depressurization was preferable to early depressurization, for the good reason that early depressurization was calculated to hasten the onset of core degradation (relative to taking no action), while late depressurization did not. However, since the late depressurization calculation was less complete (especially with respect to hydrogen sources, which are

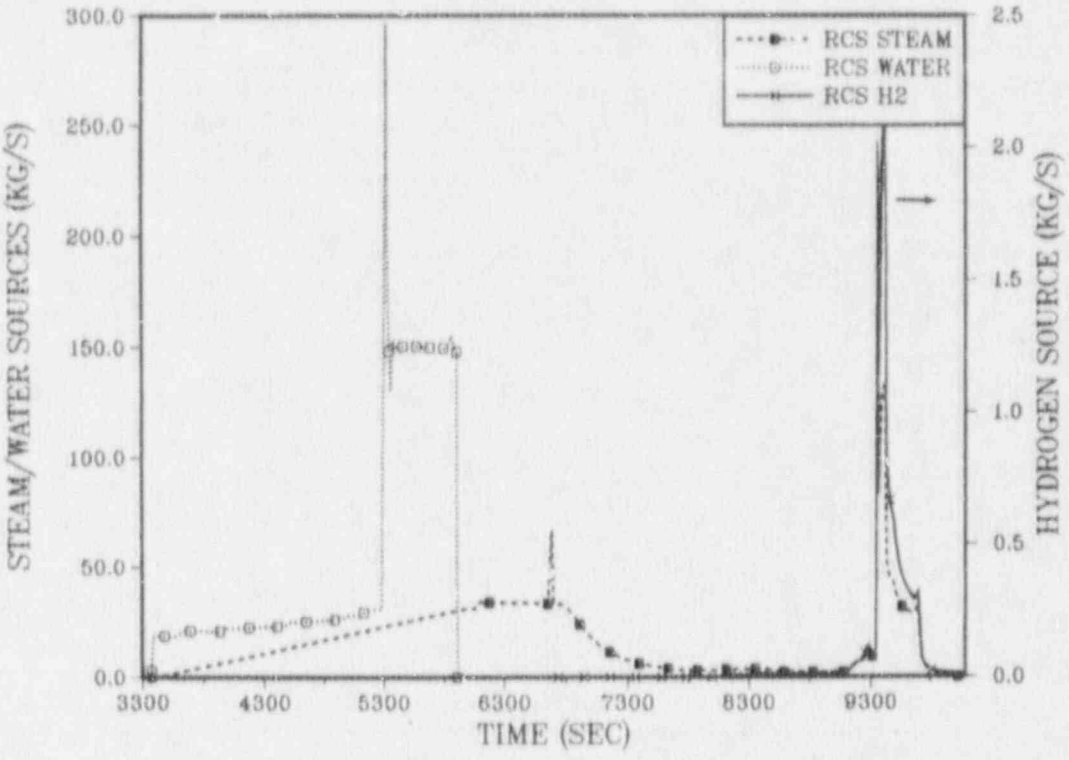

Figure 2.4 Sources of primary system water, steam, and hydrogen to the containment in the fully-pressurized station blackout scenario.

central to this work), only the early depressurization scenario has been analyzed here. The sources of primary system water, steam, and hydrogen, as input to CONTAIN in the early depressurization scenario, are plotted as a function of time in Figure 2.5. Note that the duration of this scenario, to 33000 s after shutdown, is much greater than the duration of the fully-pressurized scenario up to the time of vessel breach. The SCDAP/RELAP analysis of the depressurized sequence was not carried out clear to vessel breach, but sources to the containment later after 33000 s would have been small. In the CONTAIN calculations, VB was assumed to occur at 33000 s.

In the intentionally depressurized scenarios, threats to containment fall into two categories: those posed by hydrogen prior to and at the time of VB, and any residual DCH threat arising at the time of VB. The latter, but not the former, will be sensitive to the residual RCS pressurization remaining at the time of VB. Based in part upon early information from the INEL calculations, a value of 1.5 MPa was taken to be a reasonable, though somewhat conservative, estimate of the primary system pressure at the time of VB. This value is also consistent with the NUREG-1150 assessment that there was an 80% probability that stuck-open PORVs would result in depressurization to 1.4 MPa or less at VB, with a 20% probability that the pressure would be in the 1.4 - 7 MPa range. Later refinements in the INEL analyses [Go89] indicated that the RCS pressure at VB implied by the SCDAP/RELAP calculations actually would be under 1 MPa, which should essentially eliminate the residual DCH threat except, possibly, for the co-dispersed water scenario (see Section 4.5.1). If subsequent work confirms the essentially complete RCS depressurization implied by the SCDAP/RELAP results,

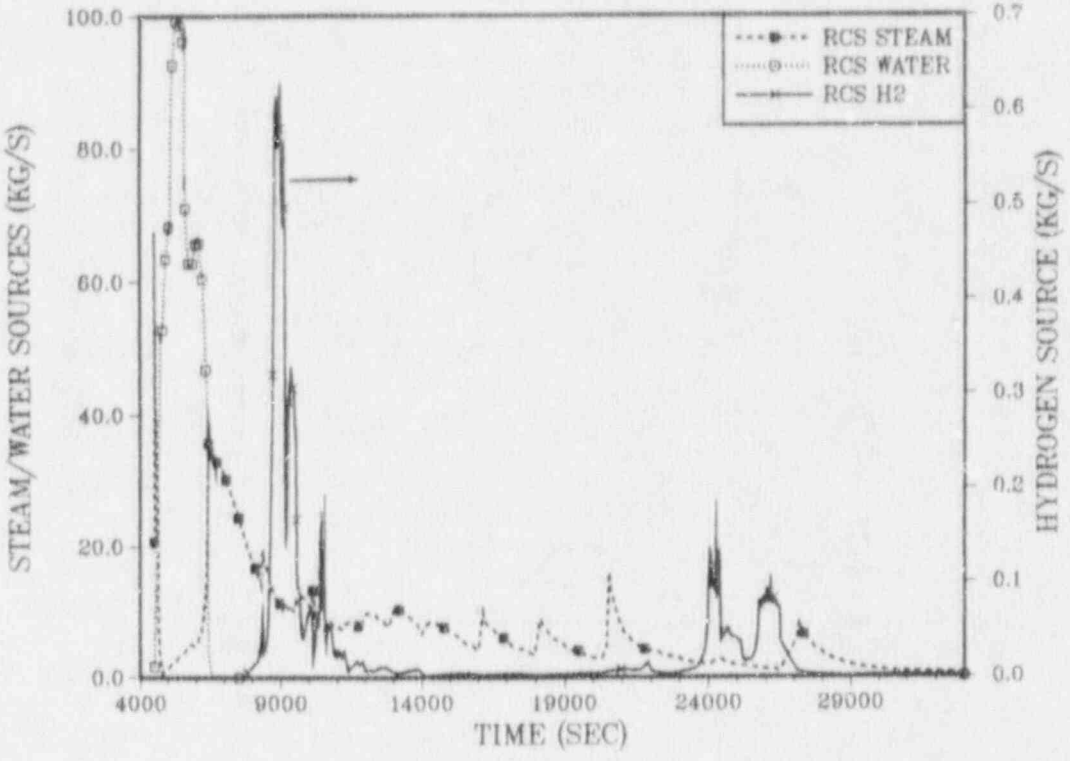

Figure 2.5 Sources of primary system water, steam, and hydrogen to the containment in the depressurized station blackout scenario

parts of the discussion of residual DCH threats in Section 4 of this report may be less relevant; however, the assessment of hydrogen distribution and detonation threats (Section 5) will remain applicable.

Debris and Blowdown Sources. Previous work [Wi87, Wi88a] has shown that DCH loads can be sensitive to the rate of steam blowdown from the primary system. Blowdown sources were calculated by CONTAIN-DCH with the primary system modeled as an additional cell filled with saturated steam (and hydrogen). CONTAIN uses an ideal gas equation of state (EOS) for water vapor which can, in principle, introduce substantial error when applied to primary system conditions. However, comparison with blowdown rates estimated using critical flow charts [Mo78] showed that quite satisfactory results (agreement to within 10%) were obtained when the orifice coefficient in the CONTAIN flow model was adjusted so that the initial flow rate matched the values given by the critical flow charts, and furthermore, the volume of the "RCS cell" was increased so that it would hold the correct mass of steam, as calculated by CONTAIN's ideal gas EOS.

In the SCDAP/RELAP analyses of the early depressurization scenario, it was calculated that the surge line would become hot enough so that failure would be expected early in the accumulator discharge phase. Surge line failure would quickly depressurize the RCS fully, thereby eliminating any residual DCH threat, but hydrogen distributions during and shortly after the blowdown following failure are still

of interest. SCDAP/RELAP sources for the surge line failure scenario were unavailable, and the resulting blowdown was therefore calculated by CONTAIN as was the blowdown following vessel breach. RCS conditions were assumed to be those calculated by SCDAP/RELAP at the time the surge line was predicted by the latter to fail, although only a highly simplified representation of these conditions was attempted in the CONTAIN simulation of the blowdown.

Vessel breach was assumed to occur as the result of the failure of a single instrument tube, followed by ablation of the hole as the melt is ejected. Vessel ablation, melt ejection from the vessel, and the gas "blow-through" phenomenon were modeled by the GASBLOW2 code, written by M. Pilch at SNL [Pi85]. In the CONTAIN-DCH calculation of the blowdown, the orifice area available for gas flow, as calculated by GASBLOW2, was input to CONTAIN-DCH as a time-dependent flow area between the cavity cell and the cell representing the primary system. Once the blowdown commences, debris in the cavity was assumed to be entrained in the gas flow at a rate that was also calculated using GASBLOW2. The entrainment rate thus calculated was used as the debris source rate which was input to the CONTAIN cavity cell, using CONTAIN's source table input option.

The models for vessel ablation, melt ejection from the vessel, and gas discharge in GASBLOW2 are considered to be reasonably well validated by experiment [Ta86], but the debris entrainment modeling is not considered adequate for a fully mechanistic calculation. Hence, the entrainment model was used in a semi-empirical fashion. Scaled cavity ejection experiments have been performed at Brookhaven National Laboratory for models of a number of reactor cavities, including the Watts Bar cavity, which is very similar to the Sequoyah cavity [Tu87]. GASBLOW2 was first used to simulate the same accident scenario which was simulated in the Brookhaven experiments, and the cavity cross section parameter in GASBLOW2 (which governs the gas flow velocity and hence the entrainment rate in the code) was adjusted to give a debris ejection fraction equivalent to that inferred from the experiments as reported in Ref. Tu87. GASBLOW2 was then applied to the scenario of interest in the present work without any further adjustment to the input except those directly dictated by the scenario of interest (e.g., the vessel pressure and the mass of melt in the vessel).

Because there are important uncertainties in the entrainment modeling, the total mass of debris participating in DCH was viewed as a sensitivity parameter to be specified upon input, and to be varied in the course of the study. Hence, the sources calculated by GASBLOW2 were renormalized to give the desired total mass. This means that GASBLOW2 was only used to obtain the time-dependence of the debris sources, not the total debris mass involved. However, it should be noted that, for the fully-pressurized experiments, both GASBLOW2 and the experimental results imply that ejection of melt from the cavity should be essentially 100% and the effect of renormalizing the sources was very minor. The same is not true for the depressurized scenario, however, and the procedure used here may be rather conservative; see Section 4 for some additional discussion.

In early phases of this work, calculations were run assuming either 75% or 25% of the total corium inventory was molten and available for ejection at the time of VB. Corium composition was based upon Battelle calculations reported in BMI-2104 for the TMLB' sequence. The debris sources input to CONTAIN-DCH and the steam blowdown rates are shown in Figure 2.6 for both the 75% and the 25% core ejection fractions, with both cases being calculated for the fully-pressurized scenario. It is seen that the debris ejection time is shorter, and the steam blowdown rates higher, in the

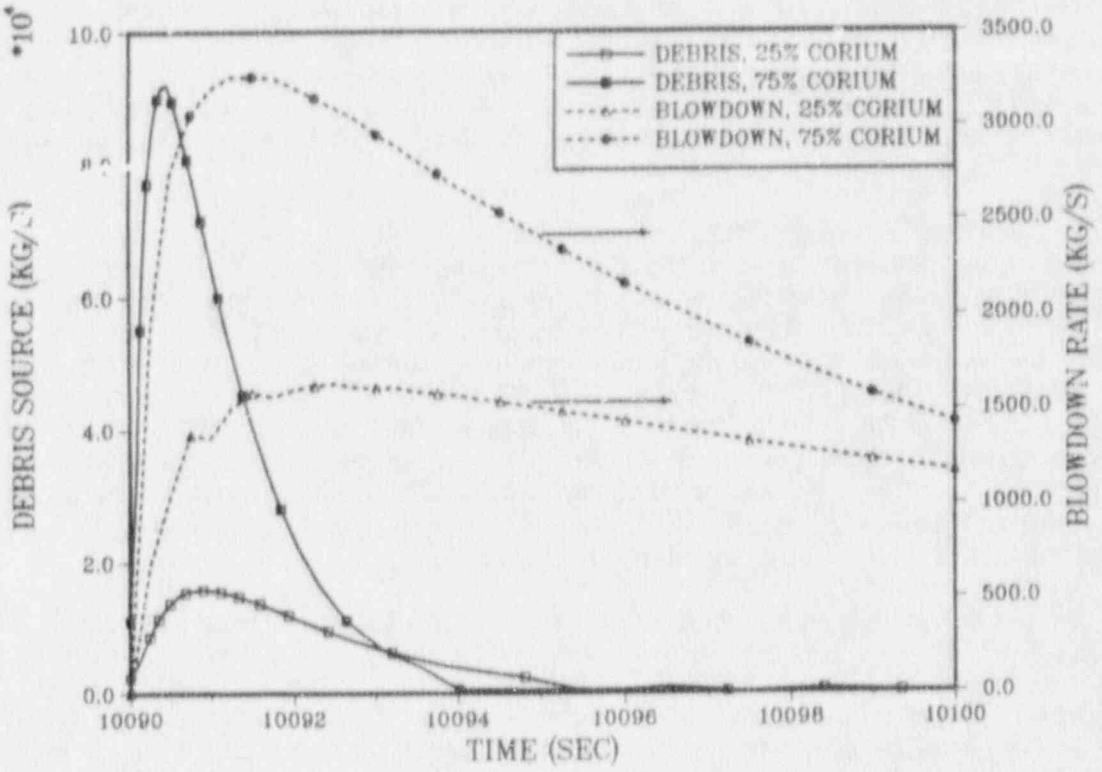

Figure 2.6 Debris and steam sources to containment following vessel breach (VB), fully-pressurized scenario.

75% ejection case than in the 25% ejection case. Both these effects are consequences of the larger hole size ablated by the larger mass of melt in the 75% case.

Definition of the Base Case. Important parameter values defining the base case are summarized in Table 2.5. Except where otherwise specified, parameters were left equal to their base case values in this study.

The trapping rate parameter, λ_{tr}, requires some explanation. It describes the fractional rate at which debris is de-entrained from the gas stream by debris-structure interactions; at present, there are no mechanistic models for the de-entrainment process and it is represented parametrically in CONTAIN-DCH. In the present work, $\lambda_{tr} = v_t/L$ was assumed, where v_t is the terminal fall velocity of a debris drop and L is a characteristic length for the cell. The latter was taken to be either $V^{1/3}$ or the cell height, where V is the cell volume.

Using the 4-cell nodalization, calculations were performed for both the 25% and the 75% corium participation fractions. In NUREG-1150, the expert panel dealing with containment loads issues considered two values of the participation fraction, 33% and 75%. Thus, their high value is the same as that considered here, while their low value was somewhat higher than the low value in the present work.

After this work had been initiated, results became available for the elicitations of the expert panel treating the in-vessel accident progression. Their distribution for the

Table 2.5

Base Case Parameters and Modeling Assumptions

Parameter or Model Assumption	Value
Initial Ice Mass (kg)	1.11×10^6
Initial Ice Area (m^2)	2.48×10^4
Ice Condenser Flow Area (m^2)	167
Ice Condenser Bypass Area (m^2), 4-Cell Model	0.204
Ice Condenser Bypass Area (m^2), 6-Cell Model	0.465
Corium Inventory (kg)	
UO_2	100992
ZrO_2	15260
Zr	11800
Steel (modeled as Fe)	61989
Corium Participation Fraction	25%, 75%; 50%
Corium Temperature (K)	2550
In-Vessel Zr Oxidation	49%, 71%[a]
Natural Convection	Included
Hydrogen Burn Model	Default
Debris Particle Diameter (m)	0.0005
Chemical Reaction Equilibria	Fe-H_2O treated[b]
Drop-side reaction rate limits	None
Trapping Rate (s^{-1})	$\lambda_{tr} = v_t/L^c$, = 0.2 in cavity

[a] 49% and 71% for the fully-pressurized and depressurized scenarios, respectively.
[b] Other reactions assumed capable of going to completion
[c] $L = V^{1/3}$, except $(V/10)^{1/3}$ for the ice compartment

fraction of the core ejected has a median value of about 30% and a maximum value of about 60% [Ha90]. If their judgments are to be accepted, the 75% case considered here is outside the plausible range and is excessively conservative. Hence, the discussion of the calculations performed in the earlier phase of this study emphasizes the 25% case in a number of instances. It must be remembered that the 25% case is only a representative value, and by no means a conservative one: it is, in fact, somewhat less than the median value given by the in-vessel review group.

As a result of the NUREG-1150 elicitations, a third case was defined involving a 50% corium participation fraction, which corresponds approximately to the 85th percentile of the NUREG-1150 distribution. Thus this case meets the desired criterion of being conservative and yet within the indicated uncertainty range. It was used in later stages of the present work.

Since source term issues were not addressed in the main part of this study, containment failure was not modeled. However, it will obviously be of interest to compare the pressures calculated in this work with failure pressures that have been estimated for the Sequoyah plant. For reference purposes, the median failure pressure estimated for Sequoyah by the NUREG-1150 panel considering containment

performance issues was 0.54 MPa (absolute). The uncertainty range (5% to 95% failure probability) was 0.36 to 0.75 MPa. The most likely containment failure mode was judged to be a function of the pressure at the time of failure. Rupture failure (as opposed to more gradual leakage) was judged to be the dominant failure mode except for the lowest portions of the range in failure pressures, for which leakage failures dominate. Catastrophic rupture was considered to be the most likely failure mode if failure occurred at pressures in the upper part of the uncertainty range. Here, "catastrophic rupture" was taken to mean complete failure of a substantial portion of the containment boundary, with ice condenser bypass assumed to result in all cases.

2.4.3 Representation of Containment Improvements

Unmodified Plant. In the unmodified plant, no engineered safety features operate during station blackout accidents (except for the ice condenser itself), and the basic CONTAIN decks used to represent the plant require no modifications for this case except for some questions concerning the treatment of hydrogen burns. In the default burn model, ignition occurs in a cell as soon as the flammability criteria are met within the cell. In effect, the default model assumes ignition sources are always available. In station blackout accidents, this assumption may not be valid. Hence, some analyses of the unmodified plant were performed with no burns permitted up until the time of vessel breach, at which time it was assumed that dispersal of hot corium would provide ample ignition sources.

Even in station blackout accidents, the absence of random ignition sources cannot be guaranteed. For example, opening and closing of ice condenser doors (especially the intermediate deck doors) are likely to be accompanied by considerable metal-metal contact. Under these conditions, sufficient sparking to provide ignition seems possible. The existence of random ignition sources may be especially plausible when highly flammable mixtures within the potentially detonable range are involved, since even extremely small spark energies are adequate to ignite such mixtures [Ti90]. Given ignition of a detonable mixture, there is no guarantee that deflagration to detonation transition (DTT) will actually occur, but DDT is difficult to rule out in such cases. Hence, in assessing potential detonation hazards in this work, it is assumed that ignition might occur at any time, and that even the temporary presence of detonable compositions represents a potential detonation hazard. In particular, it is not assumed that detonation hazards exist only if detonable compositions are present at the time of VB, when ignition sources are known to become available.

In assessing the deflagration and DCH-related loads in the unmodified plant, the possibility of ignition prior to VB should also be considered, in principle. However, comparison with the cases with igniters operational consistently indicate that the latter are less severe, although the magnitude of the effect depends substantially on the scenario. When explicitly considering the unmodified plant, therefore, ignition sources will be assumed to be absent, except as discussed above in the case of detonations.

Igniters. The operation of igniters in any cell was modeled simply by allowing the CONTAIN default ignition criteria to apply, without modification. Three cases involving igniters were considered:

1. Existing igniters powered, but no additional igniters were assumed to be installed. In the six-cell deck, this means that the default ignition criteria apply in Cells 2, 5, and 6 but not in Cells 1, 3, and 4. In the 26-cell deck, igniters are located in Cells 6-13 and 22-26 (see Table 2.3). In cells which do not contain igniters, the CONTAIN input options are used to set the ignition

criteria to impossible values, but the burn model is still active and the criteria for propagation of burns into these cells remain at their default values. Thus, if a burn initiates in a cell with igniters, propagation of the burn into cells without igniters is allowed for in the modeling.

2. Igniters present and operational in all cells. Default ignition criteria are used throughout.

3. Existing igniters are powered, and additional igniters are installed in the ice condenser lower plenum. This case is modeled as is Case 1, except that the default ignition criteria are also applied in Cells 14-17 (Table 2.3).

It is generally accepted that hydrogen control will be required for effective improvements to ice condenser plants, a conclusion which is also consistent with the present work. In any case, ignition cannot be precluded, even if it were desirable to do so. Most other improvements are therefore assessed in conjunction with the assumption that ignition sources are available. In this sense, then, the plant with igniters serves as the "base case" when assessing other improvements.

Venting of the Containment. Venting the containment prior to VB during station blackout accidents is calculated to mitigate DCH loads to some extent in PWR large dry containments, and it therefore seemed reasonable to consider its possible effects in ice condenser plants. Two possible mitigating effects are involved. The first effect is reduction of the base pressure existing at the time of VB, which tends to reduce the maximum pressure resulting from the DCH event. The second is that steam released from the primary system prior to VB partially purges the containment of atmospheric oxygen, thereby reducing the oxygen supply at VB.

No criteria have been defined for the vents that might be used for this purpose, and therefore the vent characteristics assumed were simply selected based upon what seemed reasonable but were otherwise arbitrary. It was assumed that filtering would be required to reduce radionuclide releases, and that design of filtered vents capable of removing very large radionuclide loads under severe accident conditions would be difficult, especially if the vent were to be required to function with unimpaired filtration during the DCH event itself. Likewise, very large vents capable of effective pressure relief during DCH time scales (seconds) were deemed impractical. Hence, it was assumed that the vent would be closed once high radiation levels within containment signaled the onset of serious core damage, which was assumed to occur at 8144 s after shutdown in the fully-pressurized scenario, based upon the MARCH in-vessel analysis. The flow area of the vent was assumed to be equivalent to a CONTAIN flow path with a 0.1 m^2 orifice area when the vent was open. It was also assumed that the vent would allow only one-way flow from the containment to the environment; that is, when the containment pressure dropped below one atmosphere (as sometimes happened due to steam condensation), flow back into the containment was assumed not to occur. Venting from the lower containment and venting from the upper containment were both studied for the fully-pressurized scenario; venting was not studied for the intentionally depressurization scenario.

In a few cases, some of the above assumptions concerning the vent parameters were modified in sensitivity studies. Since source term issues were not studied in this work, no actual filter modeling was included.

Containment Inerting. Containment inerting was simulated by using switches in the CONTAIN input options to turn off all oxygen chemistry (metal-oxygen reactions

during DCH and all hydrogen combustion). This approach was more convenient than replacing all oxygen with nitrogen in the containment atmosphere. (The differences in properties between nitrogen and oxygen, other than the chemical properties, are quite small and would have a trivial impact upon the calculation.) Metal-steam reactions during DCH were still modeled in these calculations.

Subatmospheric Containment. One option considered was to operate the containment at subatmospheric pressures, low enough to reduce oxygen supplies somewhat but not low enough to prevent entry by personnel when needed to meet operational requirements. The effects of this option were simulated by setting the initial containment pressure to 0.0693 MPa, as in the Surry plant, which has a subatmospheric large dry containment.

Reduced Leakage Paths Bypassing the Ice Condenser. Flow paths between the lower and upper containments which bypass the ice condenser were assumed to be either eliminated entirely or else reduced by a factor of ten in order to determine what effects steps to reduce this bypass flow might have upon containment response.

Backup Power for Air Return Fans. CONTAIN does not include a fan model; however, it does include provisions by which user-specified flow rates can be defined to exist between any pair of cells. This provision was used to simulate the effects of operating the air return fans. Based upon information from Refs. Ca84 and TVA81, fans were simulated by imposing a flow rate of 54.7 m^3/s between the upper and lower containment compartments (Cells 1 and 6 in the 6-cell deck) whenever the fans were assumed to be on. This rate corresponds to full operation of both trains of existing fans, with no backpressure; no calculations were performed for cases with only one train of fans operating. The effect of back pressure upon fan operation was not modeled, but this effect would be minor except during short periods of rapid flow into the lower compartment. Fan operation was assumed to commence 600 s after pressures in the upper compartment first exceeded 0.122 Mpa. In the 26-cell deck, the effect of the hydrogen skimmers was also approximately simulated; see Appendix A for details of the representation.

Fans were assumed to continue to operate after VB. It might have been more reasonable to assume that fans would fail at VB as a result of the DCH environment, but the time scale of the events of interest around the time of VB (of the order of 10 seconds) is too short for the fans to make a significant difference in any case. The present work did not include longer-term study of containment conditions after VB.

RCS Depressurization. The influence of RCS depressurization upon the containment response is governed by the sources input to the containment before and at the time of vessel breach. Modeling of these sources was discussed in Section 2.4.2

2.5 Some Limitations and Uncertainties in the Present Study

2.5.1 Discussion of Selected Limitations and Uncertainties

The main purpose of this work has been to examine a considerable number of possible containment improvements (including selected combinations of improvements) in order to identify promising approaches and weed out approaches which appear to offer little benefit. For this purpose, it was judged unnecessary to perform comprehensive sensitivity and/or uncertainty studies in order to evaluate all of the many uncertainties in the analysis. With some qualifications, it is believed that

the uncertainties will not radically alter the relative benefits of a given mitigation scheme, either in comparison with the response of the unmodified plant or in comparison with other mitigation schemes. That is, it is not deemed likely that there will be a qualitative change in the nature of the effect of a given mitigation scheme upon a particular category of threat as the uncertain parameters describing a scenario are varied over their uncertainty range, even though substantial quantitative variations are likely.

The requirements could be more demanding if one were attempting to decide whether to actually implement a given containment improvement. For example, it would be desirable to obtain an estimate of the degree to which a given improvement would reduce the probability of containment failure in the class of accidents for which the improvement is supposed to provide protection. One approach would be to perform a full uncertainty study for the containment failure probability in both the unimproved plant and the improved plant. Both the uncertainty in the failure pressure and the uncertainty in the loads would require consideration, and treating the latter would require consideration of the full range of relevant accident scenarios in addition to treating the various uncertainties in the CONTAIN input and in the modeling. Clearly, performing a complete study of this type would be a substantial task, and it was not attempted here.

To some extent, an effort was made to allow for the uncertainties by building in a moderate degree of conservatism into the calculations (see Section 2.2.2). However, this approach cannot provide a complete substitute for a true uncertainty study, for several reasons. Not all input and modeling choices are conservative (some may even be nonconservative), in some cases it is not known whether the choices are particularly conservative or nonconservative, and a given parameter choice can be conservative in one context and nonconservative in another (see, e.g., the discussion of in-vessel zirconium oxidation given later in this subsection). Without a systematic uncertainty assessment, the degree to which the overall results are conservative or nonconservative is difficult to estimate.

In the remainder of this section, a brief discussion is given of some uncertainties not considered in detail in the present study. Judgments are offered as to whether the present treatment is conservative or nonconservative when there is some basis for such judgments. The discussion of selected aspects of CONTAIN modeling in Section 2.4.1 is also relevant in this context.

Review of the Plant Decks. The input decks used to represent the Sequoyah containment were developed from information taken from a number of sources (see Section 2.3) and considerable effort was made to generate a reasonable representation of this containment. However, it can sometimes be surprisingly difficult to obtain information needed for severe accident analyses from publicly available documents; for example, plant FSARs are often out of date in significant respects and, more fundamentally, are oriented toward supplying information supporting analyses of normal operations and design basis accidents (DBAs), not supplying information required for analyzing core melt accidents.

Ideally, an analysis of this type would include a close working relationship with plant personnel permitting exchange of technical information on a day-to-day basis. However, TVA policies did not permit this type of information exchange. An effort to arrange a review of the 26-cell deck by knowledgable plant personnel was also unsuccessful. There is no known instance in which it is believed that inadequate plant

information has introduced major uncertainties into the findings of this study, but the possibility of significant error from this source does exist.

Variations in the Accident Scenario. Both the fully-pressurized and the depressurized station blackout accidents analyzed here fall in the category of "early" or "fast" station blackouts, meaning that the auxiliary feedwater (AFW) fails at the time of accident initiation. In addition, there is a class of "late" or "slow" station blackouts, in which the steam turbine-driven AFW systems initially function, but core melt results either when DC battery exhaustion results in loss of AFW, or when thermally-induced pump seal LOCAs result in loss of primary system inventory. So long as AFW is available, the operators may achieve partial RCS depressurization by depressurizing the secondary side, although the primary system will repressurize if AFW is eventually lost. None of these scenarios have been analyzed in this work. No opinion is offered as to whether the present calculations should be considered more conservative or less conservative if applied to these alternative scenarios. There is no known reason to believe the alternative scenarios would be very different from those considered here, provided parameters known to be important (e.g., RCS pressure at vessel breach) are similar. There is, however, little information upon which firm judgments can be based.

As was discussed in Section 2.1.2, the NUREG-1150 PWR studies indicated that, even without intentional depressurization, a range of thermally-induced RCS failures may occur which can result in partial or complete RCS depressurization; they can also substantially affect (delay) the time of VB. These variations have not been analyzed, although comparison of the fully-pressurized sequence with the intentionally depressurized case provides considerable insight as to the effects to be expected. Assuming full RCS pressurization at VB is conservative with respect to DCH loads, although some of the partially depressurized sequences can involve greater steam loads prior to VB and, hence, greater ice depletion at VB.

Uncertainties in the Primary System Sources. There are substantial uncertainties in the analyses of the in-vessel accident progression and the resulting steam and hydrogen sources to the containment. There are no known reasons for believing that DCH results will be very sensitive to uncertainties in timing of the pre-VB steam sources or uncertainties in the time of vessel breach, although these questions have not been investigated to any great extent. Uncertainty in the total steam source prior to VB is of some significance because of its effect upon the amount of ice remaining unmelted at the time of VB. It is likely that there will be some sensitivity to the amount of hydrogen released prior to VB if it is assumed that this hydrogen does not burn for lack of an ignition source. If ignition sources are available prior to VB, sensitivity to the quantity of hydrogen released during this period is probably less, although the increased thermal loads on the ice condenser due to combustion of large amounts of hydrogen could still have some effect. For the same reason, there will be some sensitivity to the quantity and enthalpy of steam released prior to VB.

Detonation threats will be quite sensitive to the rates of both hydrogen and steam release, as well as sensitive to the relative timing of the hydrogen and steam sources. Little is known about the uncertainty range in these rates, except that the uncertainties are undoubtedly large. Some insight as to the dependence of the detonation threats upon these uncertainties can be obtained by comparison of results of the calculations for the fully-pressurized and the depressurized scenarios, which have rather different source rate histories (see Figures 2.4 and 2.5, and the discussion in Section 5). It is not known whether either of these two cases should be considered conservative or nonconservative, in terms of detonation threats.

For both the fully pressurized and the depressurized sequence, sources were estimated for Sequoyah by scaling up the results of calculations that were actually performed for the Surry plant (Section 2.4.2). There is little information permitting a direct assessment of the magnitude of the uncertainty that is introduced by this procedure. Comparison of results of STCP calculations (Gi84, De86, Le88) suggest that, for the MARCH calculations used for the fully-pressurized scenario, these uncertainties are not very large, although judgments are difficult to make because of the lack of detailed information for otherwise-equivalent calculations performed for the two plants. No SCDAP/RELAP calculations for Sequoyah are available for comparison purposes for the depressurized sequence. For what it is worth, it does seem likely that uncertainties resulting from the use of the scaled-up Surry sources are less than the phenomenological uncertainties involved in the in-vessel accident progression analysis. Nonetheless, it would obviously be desirable to perform analyses using sources calculated specifically for Sequoyah before making firm decisions to implement any of the containment improvements considered here.

Blowdown Sources at VB. The availability of large supplies of steam to interact with the debris favors high DCH loads [Wi87, Wi88a], which in turn implies that rapid blowdown favors high DCH loads. The rate of vessel blowdown is determined primarily by the size of the hole that develops at vessel breach. If the initial failure mode is failure of a single instrument tube penetration, as is assumed in this work, the size of the hole at the time of gas blowthrough is determined almost entirely by the amount of ablation that occurs, since the initial hole size is small. The GASBLOW2 ablation model may be somewhat conservative here, in that some other ablation calculations yield somewhat smaller hole sizes. However, uncertainties in the ablation model may be of less importance than the uncertainty in the basic failure mode, which is considered to be large. If, for example, the initial failure mode is a creep rupture failure of the bottom head, the failure size could be considerably larger than is assumed here, and the assumption of vessel breach due to failure of an instrument tube penetration could prove rather nonconservative.

The influence of vessel failure size was not studied in the present work. Results obtained for the PWR large dry containments suggest that it is quite important for the fully-pressurized station blackout sequence and that sensitivity to failure size may be less for lower RCS pressures [Wi87, Wi88a]. Extrapolation of large dry containment results to ice condenser plants can be risky, however, and it is clear that this question would require examination in any detailed uncertainty study for ice condenser plants.

Water Co-Dispersed with Core Debris. Previous calculations [Wi87, Wi88a, Tu89] have shown that DCH loads can be substantially altered if water is co-dispersed with the debris in such a manner that there is rapid, effective heat transfer between the debris and the water. If only a moderate amount of water interacts with the debris (e.g., a water mass half or less of the debris mass), the dominant effect of the water is calculated to be an increase in the steam supply which enhances the DCH loads. If the mass of water interacting with the debris is large (e.g., equal to or greater than the debris mass) the dominant effect is to quench the debris and thus decrease the loads. Note that the critical parameter is the amount of water that undergoes a rapid thermal interaction with the debris. This quantity cannot a priori be equated to the total water supply potentially available; for example, if there is water in the cavity, an initial FCI might blow a substantial fraction of it out of the cavity without its having a chance to effectively interact with the debris.

According to the NUREG-1150 analysis of Sequoyah, substantial water is not likely to be present in the cavity unless the RWST has dumped; hence a dry cavity is

generally expected in station blackout accidents. It is possible, however, that debris will form in a noncoolable layer in the reactor vessel bottom head, with a pool of primary system water being present on top of the debris; debris crusting and/or film boiling conditions could prevent rapid debris-water heat transfer prior to VB. After VB, debris and water could be co-dispersed in the cavity together. In this scenario, the amounts of water available would be limited and the effect of the water would likely be such as to augment DCH loads. Because the cavity is expected to be dry at VB in most station blackout accidents, and because the possibility of RCS water being co-dispersed with the debris is rather speculative, the large majority of calculations performed for this work were run without co-dispersed water. Although this treatment is believed to be justified, the possibility that the results are nonconservative if co-dispersed water actually is present must be acknowledged.

Two sensitivity studies were performed for the intentionally depressurized case in which co-dispersed water was assumed to be present. There are major uncertainties in the modeling of the effects of co-dispersed water in CONTAIN-DCH. Very briefly, the water is introduced into the atmosphere, at a user-specified rate, as a source of low-quality (i.e., low-enthalpy) steam. The rate-limiting heat transfer process in the calculation is debris-atmosphere heat transfer; subsequent atmosphere-water heat transfer is assumed to be instantaneous. No direct heat transfer between debris and liquid water is modeled. Thus, the latent heat of vaporization and the steam produced by vaporization are accounted for, but many of the processes that might affect the rate of heat transfer are omitted, and there is no treatment of such FCI phenomena as triggering, fine fragmentation, and FCI propagation. Overall, the treatment is believed to be conservative in terms of the effects of the water upon the quasi-static pressurization resulting, but there is no consideration of the dynamic loads potentially associated with the FCI at all.

Other Sources of Steam. Based upon PWR large dry containment calculations, the DCH loads could be augmented by vaporization of water films condensed upon structures [Wi88a], and by steam generated by rapid quench of de-entrained debris in water pools within the containment [Wi87, Wi88a, Tu89]. In both cases, the augmentation is due to the increased steam supply available for interaction with the debris. In CONTAIN, the default maximum thickness for water films is assumed to be 0.5 mm, with any additional water condensed assumed to be drained to the containment pools. The default film thickness may be on the high side, which would be conservative in the present context.

Large quantities of ice melt and condensed primary system water will have accumulated in the lower containment by the time of vessel breach, and the heat capacity of this water is sufficiently large that little steam would be generated if all this heat capacity is available for quenching debris de-entrained in the lower containment; that is, the enthalpy content of the debris would probably be insufficient to bring the entire pool to boiling. However, it is possible that de-entrained debris falling into the water would interact directly with only a small fraction of the total water present, and that significant steam could be generated by vaporizing this water. This steam would tend to increase the DCH loads. Mechanistic models for these effects are not available, although they can be simulated parametrically in CONTAIN-DCH through user-controlled input. Since much arbitrariness is involved in any such simulation, these effects were not included in the present calculations, which would be nonconservative if they should actually turn out to be significant.

To summarize these effects, the representation of the condensate films is probably somewhat conservative, while the neglect of steam produced by rapid

quenching of de-entrained debris is potentially nonconservative. In PWR large dry containments, the uncertainties introduced by these effects were fairly significant [Wi88a]. Again, it is risky to assume that the latter results would apply directly to ice condenser containments, but it is likely that qualitatively similar effects would exist.

Debris Sources. The mass of debris participating in a DCH event is one of the most uncertain of all DCH-related parameters; the masses assumed here, and their relation to the NUREG-1150 uncertainty distributions, were discussed in Section 2.4.2. The debris temperature was taken to be 2550 K, which may be slightly conservative (high), but the uncertainty in this parameter in either direction is substantial; the limited sensitivity studies available [Wi87] suggest that results are not very sensitive to the debris temperature for the cases that were considered. The corium composition, especially the unoxidized metallic content, is also quite uncertain. Some mechanistic code calculations of the in-vessel accident progression [Ke87] suggest that the amount of steel assumed to be present in the melt (Table 2.5) in this work is high. On the other hand, when only a fraction of the total corium mass is assumed to be molten and available for participation in DCH, it is likely that this molten mass will be preferentially enriched in metals, which are lower-melting than the oxides; the calculations discussed in Ref. Ke87 exhibit this effect.

The extent of in-vessel Zr oxidation assumed here is somewhat above the medians of the relevant NUREG-1150 uncertainty ranges, especially for the depressurized case. Whether this is conservative or nonconservative depends entirely upon the context. It is probably conservative to assume a large degree of in-vessel zirconium oxidation when assessing detonation threats and hydrogen deflagration threats in the absence of igniters. On the other hand, it is probably nonconservative when evaluating DCH threats, especially when large steam supplies and/or co-dispersed water are present. For the one sensitivity case considered (Section 4), the sensitivity to the amount of unoxidized Zr in the melt was not large, however.

At present, there are no known reasons for believing the choices of corium temperature and corium composition used here to be either conservative or nonconservative to any large extent. The associated uncertainty in the results is probably significant, but less than that introduced by the uncertainty in the molten corium mass.

Other DCH Phenomena. There are a substantial number of DCH-related phenomenological uncertainties and input parameters whose magnitude is uncertain, and sensitivity to a number of these is discussed in Refs. Wi87 and Wi88a, although largely in the context of PWR large dry containments. Some of the more important of these include the following:

- Rate of debris de-entrainment from the atmosphere. No mechanistic models are available for this process, and the rate of de-entrainment is controlled by the user-specified "trapping" parameter. The values used in this work are based upon gravitational fall-out of the suspended particles (see Table 2.5) and are probably on the low side, which will be conservative. The degree of conservatism is only moderate unless actual trapping rates are much greater than is assumed here.

- Debris particle size. A number of HPME experiments [Ta88] have yielded debris particle mass median diameters of the order of 5×10^{-4} m, and this value was used in the present work. The actual particle size in a full-scale DCH event is still quite uncertain. The "particle size" is best thought of as a

parameterization of the debris surface/volume ratio for debris-gas mass transfer (controlling chemical reaction rates) and heat transfer. Since the rates calculated for this particle size are quite rapid, much smaller particles would not have a major effect but much larger particles could reduce heat transfer and chemical reaction significantly; hence, the particle size assumed here is unlikely to be very nonconservative but could be conservative. The latter may be more likely to be the case for the depressurized scenario than for the fully-pressurized case.

- Direct debris-structure radiation. In CONTAIN-DCH, airborne debris can radiate energy both to the atmosphere and to the structures. However, the fractional split for these two processes is governed by a user-specified input parameter; no mechanistic modeling is available. If the atmosphere were transparent, direct debris-structure radiation could be an important mitigative effect. However, HPME experiments have shown that melt ejection is accompanied by dense aerosol clouds [Ta88], which are likely to result in mean optical extinction lengths much less that one meter, while containment optical path lengths are at least a few meters or more. Hence, it is believed that most of the airborne debris will be unable to "see" the surrounding structure. In the present work, the debris-structure radiation was set equal to zero, and all radiant energy transfer from the debris was to the atmosphere. The resulting error is conservative, and its magnitude is believed to be small.

- No Slip in the Debris Transport Modeling. In the CONTAIN-DCH model, airborne debris is assumed to flow with the gas as the latter flows from one cell to another, except for debris that is removed from the atmosphere by trapping. No debris-gas slip is modeled in the transport calculation. One consequence of this assumption may be to overestimate the degree to which the cavity pressurizes in a DCH event; examples are cited in Section 3.

Effect of the Ice Condenser Upon DCH Loads. The ice condenser exerts a substantial mitigating effect upon DCH loads [Wi87], and the magnitude of this effect will depend upon the amount of ice remaining unmelted at VB, and may also depend upon the degree of nonuniformity in ice melting prior to VB. The state of the ice condenser at VB will obviously depend upon the total enthalpy of the steam source prior to VB. It will also depend upon a number of more complex phenomena, e.g., hydrogen burns prior to VB, recirculation flows, the extent to which ice condenser doors reclose once they have been opened, and the extent of ice condenser bypass. These effects were generally modeled to at least some degree in the calculations, but no systematic study of the sensitivity of DCH loads to the ice condenser state at VB was made.

Another potentially important source of uncertainty is uncertainty in the ice condenser modeling itself. There are no experimental test data at all for ice condenser performance under DCH conditions. The most nearly relevant data on ice condenser performance under high-flow, high-enthalpy-load conditions appear to be the Waltz Mill test data [WC74], cited in the FSAR in the discussion of ice condenser performance under large LOCA conditions. These data are proprietary, and efforts to obtain the data for CONTAIN validation purposes were unsuccessful.

Still another potential source of uncertainty in DCH calculations concerns the behavior of the ice meltwater. In CONTAIN, the user specifies the temperature of the effluent water. The energy transfer required to heat the meltwater to this effluent temperature is taken into account, but there is no other mechanistic modeling of the

meltwater behavior. Under normal conditions, this may not matter greatly. However, under DCH conditions, tens of thousands of kilograms of ice are calculated to melt within a few seconds, during a time that there is a strong upward flow through the ice condenser. It seems plausible, at least, that some of this water could become entrained in the gas flow, perhaps vaporizing. This could have a quite significant impact upon the response of the containment to a DCH event. Intuitively, mitigation would be expected, but no detailed analysis is available to support this supposition.

2.5.2 Significance of the Limitations and Uncertainties

It should be clear from this discussion that the uncertainties in the absolute magnitude of the containment loads calculated in this work are substantial. This fact must be taken into account in drawing conclusions from the results, especially concerning containment failure probabilities. Although calculated pressures will occasionally be compared with the estimated Sequoyah failure pressure, this is done only to provide perspective for the particular calculation being discussed. In all such cases, the calculation itself only represents the implications of the particular set of input and modeling assumptions used in that calculation. Comparison of the results with estimates of the failure pressure in no sense represents a prediction that the containment will or will not fail in a given accident sequence.

Fortunately, the impact of the uncertainties is not overwhelming in the context of assessing the benefits of the various containment improvements considered, which is the principal purpose of this work. All such assessments are based upon comparing calculations that include the improvement to otherwise-similar calculations without the improvement. In the large majority of cases, the impact of the various uncertainties upon these differences is believed to be a second order effect. For example, it is generally expected that the effects of uncertainties in ice condenser performance, DCH phenomena such as trapping, etc, will not differ qualitatively for the unmodified plant from the effects of these uncertainties with various mitigation strategies implemented. Hence, differences calculated between the behavior of the unmodified containment and that of the modified containment should not be excessively sensitive to the modeling uncertainties discussed here, especially when the differences between the unmodified and the modified containment responses are large enough to be of much practical interest.

When the differences between the unmodified and the modified containment responses are smaller, care must be used in interpreting these differences. This care is required both because of the uncertainties discussed here and because the calculations can be sensitive to minor changes that might affect, for example, whether a hydrogen combustion threshold is or is not exceeded. When the differences are small, however, the principal result of practical interest is the fact that the differences are indeed small; once again, the uncertainties are not likely to invalidate conclusions to that effect.

There are, of course, possible exceptions to these conclusions concerning the impact of the modeling uncertainties upon the assessment of mitigation strategies, and these exceptions will be acknowledged in any cases where they have been recognized. Perhaps the most important exception involves cases in which the modeling describing the mitigation strategy itself would be especially uncertain. Such strategies have been excluded from the present study. An example is deliberate flooding of the cavity as a DCH mitigation strategy.

In brief, the uncertainties do warrant caution in interpreting the results obtained in this work, but they do not warrant despair as to the potential usefulness of these results.

3. MITIGATION OF DCH/DEFLAGRATION LOADS W/O RCS DEPRESSURIZATION

In this section, results for the analysis of the station blackout sequence with the RCS at full system pressure until vessel breach are described. The emphasis is on the containment loads associated with DCH and hydrogen combustion immediately following vessel breach. All three decks (4-, 6-, and 26-cell) described in Section 2.3 are used, and results obtained using different decks should not be directly compared without making due allowance for the differences in nodalization. Some explicit comparisons between results obtained using the different decks for otherwise-similar scenarios are presented in Section 3.3.1. However, the dependence upon the nodalization used does not directly affect the assessments offered in this section for the various containment improvements considered, since all such assessments are based upon comparisons between the modified plant and the unmodified plant performed using the same deck.

Except where otherwise noted, the default flame speed correlations of the CONTAIN hydrogen burn model were used in these calculations. The assumptions made concerning the availability of ignition sources prior to VB are noted for each calculation as it is discussed.

3.1 4-Cell Calculations

Results for the 4-cell calculations are summarized in Table 3.1. The first column gives a case number used for identification purposes in the discussion that follows. The second column gives the corium mass assumed to participate in DCH; this mass is expressed as a percentage of the total potentially available, i.e., a percentage of the corium inventory given in Table 2.5. The third column indicates whether ignition sources were assumed to be available prior to vessel breach. Providing the plant with an augmented igniter system (igniters in all cells, with dedicated power supplies provided) would assure behavior corresponding to a "yes" in this column, while a "no" corresponds to the unmodified plant if ignition sources are assumed to be absent until vessel breach. In the unmodified plant, ignition sources prior to vessel breach could arise to some degree as a result of random spark generation. In this event, the behavior would not necessarily correspond exactly to either the "no" or the "yes" cases, since the latter involve the assumption that ignition sources are always available, which need not be true for random, unintentional ignition.

Calculations for PWR large dry containments have indicated that controlled venting can lead to significant mitigation of DCH loads [SNL89], and a number of cases were therefore run in which it was assumed that a vent was installed in the Sequoyah containment. The fourth column of Table 3.1 indicates whether the vent was installed in the upper containment or the lower containment; a dashed line in this column indicates unvented cases. The fifth column gives any additional modifications to the base case, and the last column in Table 3.1 gives the maximum pressure that was calculated for the upper containment (Cell 3 in Figure 2.1).

3.1.1 Results for the Base Case

Before considering potential improvements, it is important to understand the response of the unmodified plant to DCH events. In particular, hydrogen combustion plays a very important role in determining the loads developed in an ice condenser

Table 3.1

Results of 4-Cell Calculations, Fully Pressurized RCS

Case No.	Corium Fraction	Ignition Prior to VB	Vent Location	Other	Max. P (MPa)
1	25%	Yes	---	---	0.55
2	75%	Yes	---	---	0.85
3	25%	Yes	Upper[a]	---	0.44
4	25%	Yes	Lower[a]	---	0.46
5	75%	Yes	Upper	---	0.73
6	75%	Yes	Lower	---	0.75
7	25%	No	---	---	0.56
8	25%	No	Upper	---	0.48
9	25%	No	Lower	---	0.48
10	25%	No	Lower	Large Vent[b]	0.42
11	75%	No	---	---	0.92
12	75%	No	Upper	---	0.86
13	75%	No	Lower	---	0.84
14	25%	No	---	UCHB[c]	0.56
15	25%	No	Upper	UCHB	0.47
16	25%	No	---	UCHB, Continuous[d]	0.48
17	25%	No	Upper	UCHB, Continuous[d]	0.46
18	25%	---	---	Inerted	0.28
19	50%	No	---	---	0.80
20	50%	---	---	Inerted	0.45
21	75%	---	---	Inerted	0.62
22	25%	---	Upper	Inerted	0.24
23	75%	---	Upper	Inerted	0.57
24	25%	Yes	---	Subatmospheric[e]	0.44

Notes:

[a] "Upper" and "lower" refer to vents located in the upper and lower containment, respectively.

[b] Large vent area (1 m^2) was assumed, and the vent was not closed until vessel breach.

[c] "UCHB" means that the unconditional hydrogen burn assumption was invoked.

[d] "Continuous" means that the dead time following a hydrogen burn in the standard CONTAIN model was substantially shortened (Section 3.1.4).

[e] Containment was assumed to be at 0.0693 MPa during normal operation.

plant during DCH. The calculated pressures can depend strongly upon when and whether combustion thresholds are exceeded in the various cells, and accidents of timing of burns in different cells can also affect the results. In comparing any two calculations, minor changes can have disproportionate effects and lead to misleading conclusions concerning the effectiveness of a given plant modification. To use a simple example, it could happen that the hydrogen concentration could marginally exceed the burn threshold in one calculation, while it fails to reach the threshold by a small margin in a second calculation. The resulting pressures might then differ substantially; however, if minor changes were made to some of the other uncertain

parameters involved, both calculations might then exceed the threshold (or fail to exceed it), and the differences between them could then be much smaller.

As was discussed in Section 2.4.3, ignition sources may or may not be present in the unmodified plant. In base case discussed below, ignition sources are assumed to be present throughout the calculation. However, the points to be made here concerning accidents of timing of the hydrogen burns do not depend upon this assumption; they basically apply to any calculation involving hydrogen burns. Discussion of the possible benefits of installing igniters with independent power supplies, and thereby assuring the availability of ignition sources, is deferred until Section 3.1.3, where calculations with and without ignition sources prior to VB are compared.

25% Corium Participation Case. In Figure 3.1, pressure is plotted as a function of time for the four containment cells in the base case with 25% corium participation (Case 1 in Table 3.1). The cavity cell is a rather constrained volume, with a relatively small (5.6 m²) flow path connecting it to the rest of the lower containment. As a result, the cavity cell (dotted curve and right-hand axis in Figure 3.1) quickly pressurizes to very high levels soon after VB, which occurs at 10090 seconds. The pressure then falls almost as quickly, following the rapid decline in the debris source (Figure 2.6). At its maximum, the cavity pressure is over 1 MPa higher than the pressure in the adjacent portions of the containment. Little analysis has been performed as to the possible implications of this degree of cavity pressurization; e.g.,

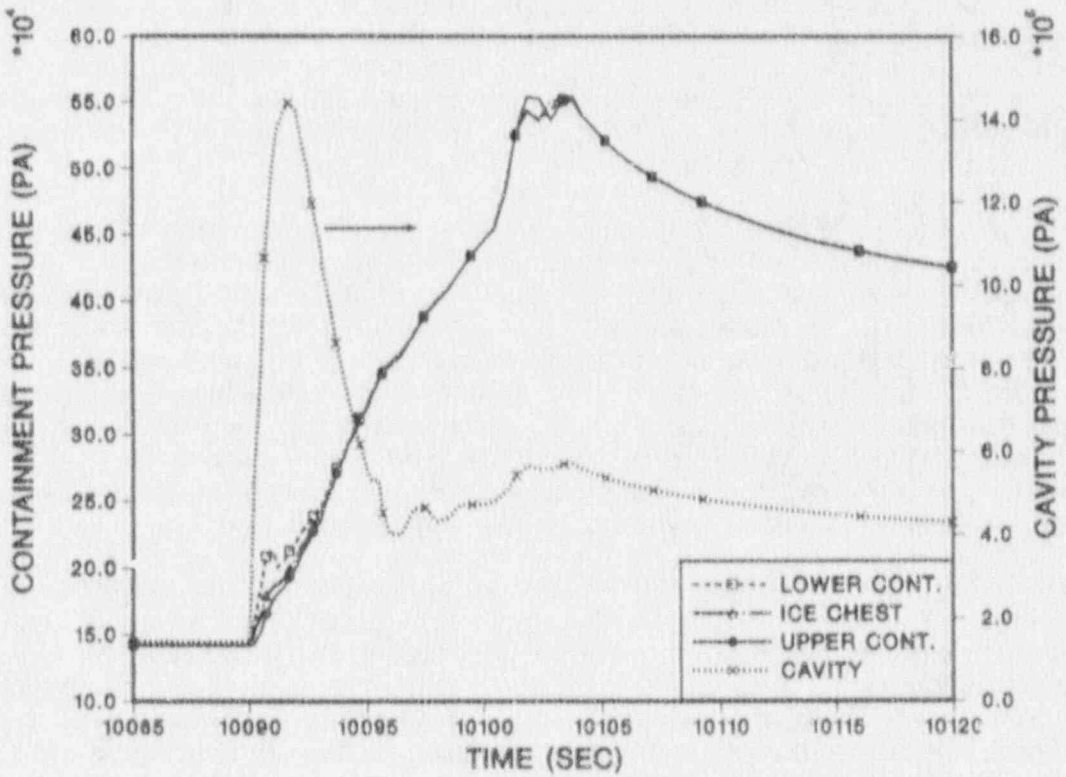

Figure 3.1 Containment pressure-time histories following VB in the 4-cell base case with 25% corium participation.

whether it could cause vessel lifting and/or failure of cavity structures. At the very least, seal table failure appears to be highly likely. The possibility of larger scale failures needs to be investigated. Large-scale structural failures and/or vessel lifting could damage the containment boundary; in addition, they might open direct paths to the upper containment bypassing the ice condenser, which could substantially augment DCH-related loads.

In connection with the cavity pressurization question, it should be noted that the CONTAIN-DCH model provides no provision for debris-gas slip. Thus, the debris is assumed to move with the gas as the latter flows from one cell to another, except for that debris which is removed from the atmosphere by trapping. As a result, the calculated rate of gas flow out of the cavity is slower, and pressurization is greater, than would be the case if slip were to be taken into account. Hence, the current model is expected to overestimate the extent of cavity pressurization somewhat. However, sensitivity studies performed for a similar scenario in the Grand Gulf plant (pressurization of the pedestal region during DCH) indicated that this effect may not be very large [Mu88]. Hence, the conclusion that the cavity can pressurize severely during a DCH event is likely to be valid.

Pressure differences among the other cells of the containment are relatively small due to the large flow paths connecting them when the ice condenser doors are open. The maximum containment pressure outside of the cavity, about 0.55 MPa, is much lower than in the cavity region, but it is still high enough to constitute a substantial threat to containment integrity at Sequoyah.

It is instructive to consider the various processes responsible for the detailed shape of the pressure history curve for the upper containment in Figure 3.1: the initial steady rise, the sharper rise after 10100 s, and the double peak. Some relevant information is given in Figures 3.2-3.5. Figure 3.2 portrays the temperature histories of the four containment cells, Figure 3.3 shows the cumulative quantities of hydrogen burned in each cell, atmospheric compositions are given in Figure 3.4, and flow rates into and out of the ice condenser are plotted in Figure 3.5.

In Figure 3.2, it is apparent that temperatures in the lower containment quickly rise to very high values (> 1500 K) in response to debris injection into the containment, and then fall rather rapidly. Temperatures in the ice condenser rise to moderately high levels (~ 700 K), and then also fall rapidly after the first few seconds. During the debris injection period, temperatures in the upper containment are relatively low (< 500 K), but they then begin a steady rise due to a hydrogen burn in the upper containment which initiates about 3 seconds after VB and continues for about 10 seconds (Figure 3.3). During most of this time, the ice condenser atmosphere is over 50% hydrogen (Figure 3.4), but oxygen concentrations are too low to permit combustion to initiate in the CONTAIN default burn model.

Before the upper containment burn is complete, flow reversal occurs in the junction between the ice condenser and the upper containment (dashed curve, Figure 3.5). This permits enough oxygen to enter the ice condenser so that a rapid burn occurs there, accelerating the pressure rise. Since there is a large excess of hydrogen in the ice condenser, the temperature rise in the ice condenser forces hydrogen-rich gas into the upper containment, augmenting the burn which is still in progress there, which increases the effect of the ice condenser burn upon the total containment pressure. The first peak in the pressure trace occurs at about the time that these burns terminate. Shortly thereafter, a renewed influx of oxygen permits a second burn to

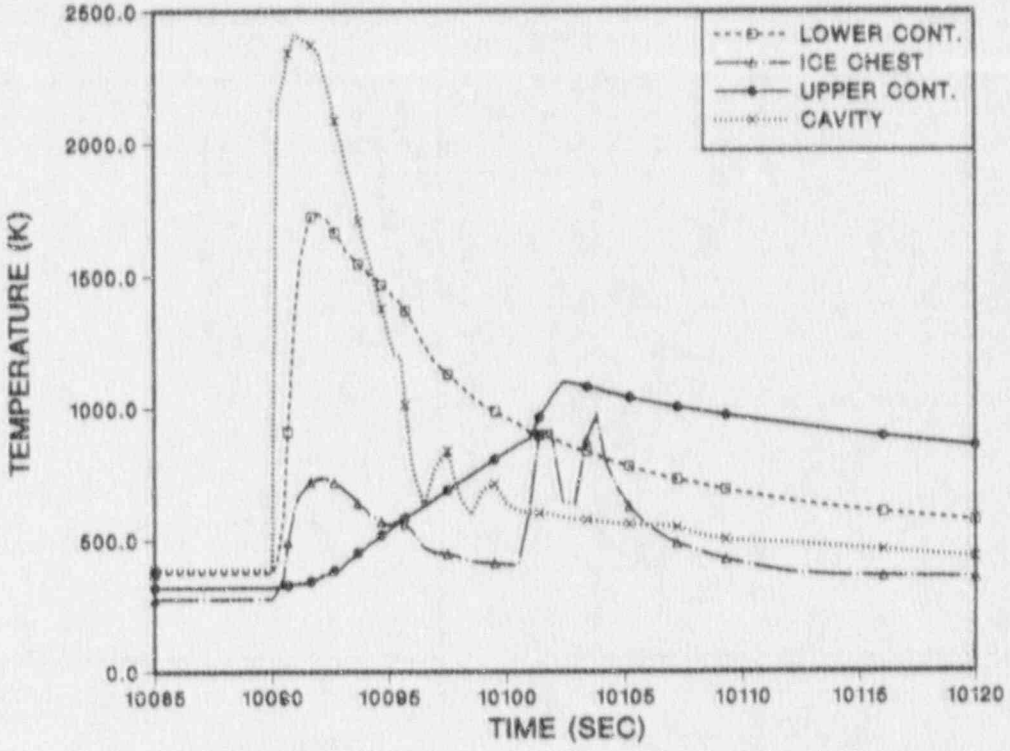

Figure 3.2 Containment temperature-time histories following VB in the 4-cell base case.

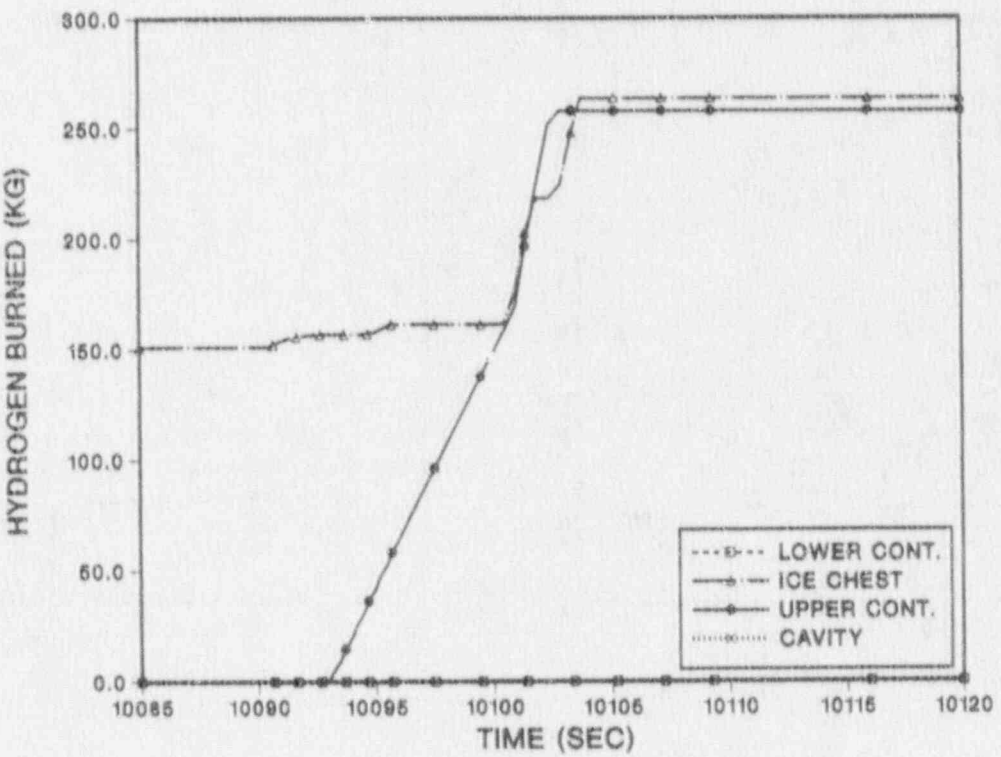

Figure 3.3 Cumulative quantities of hydrogen consumed as a function of time in the 4-cell base case.

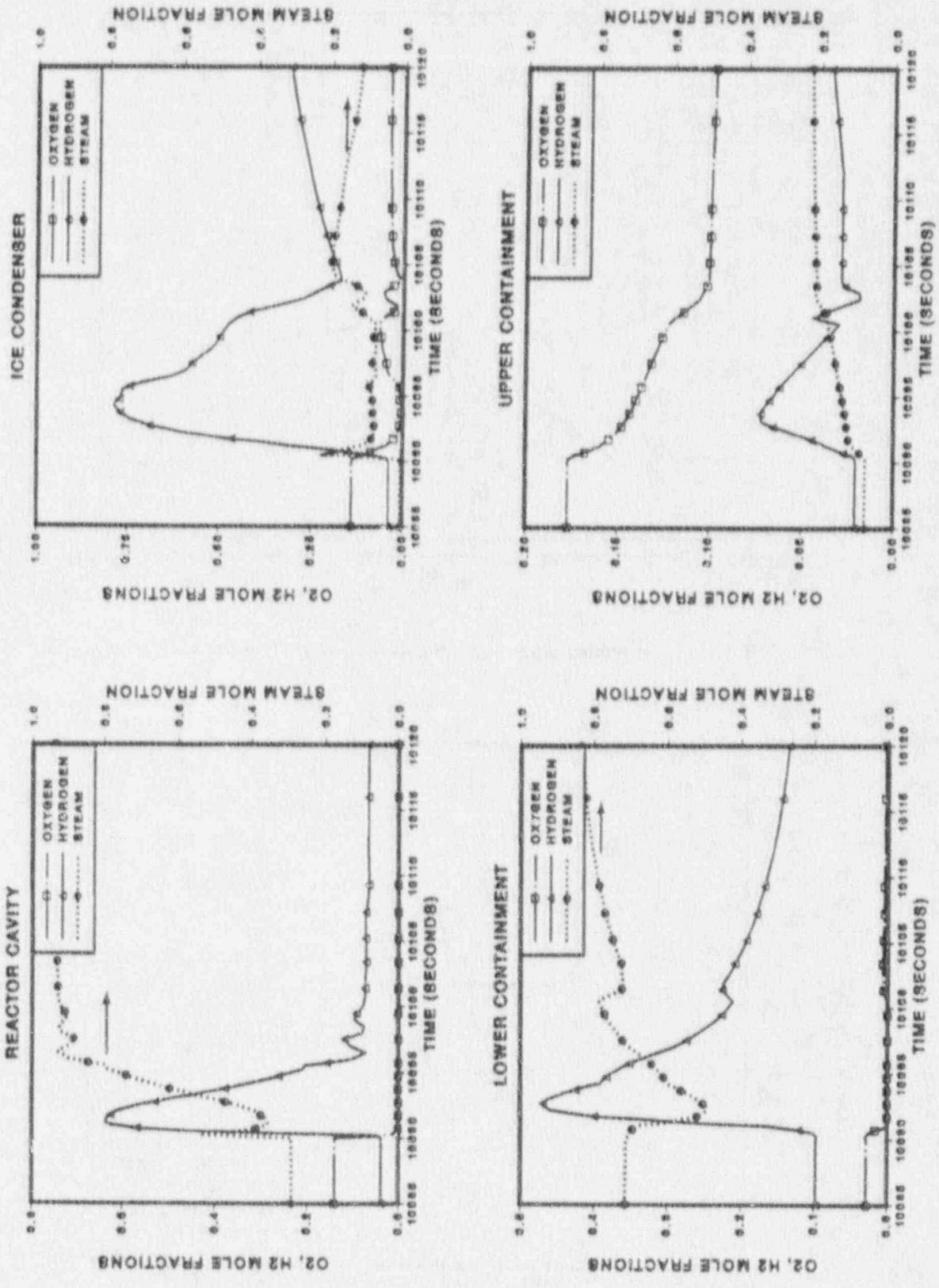

Figure 3.4 Atmospheric compositions following VB in the 4-cell base case.

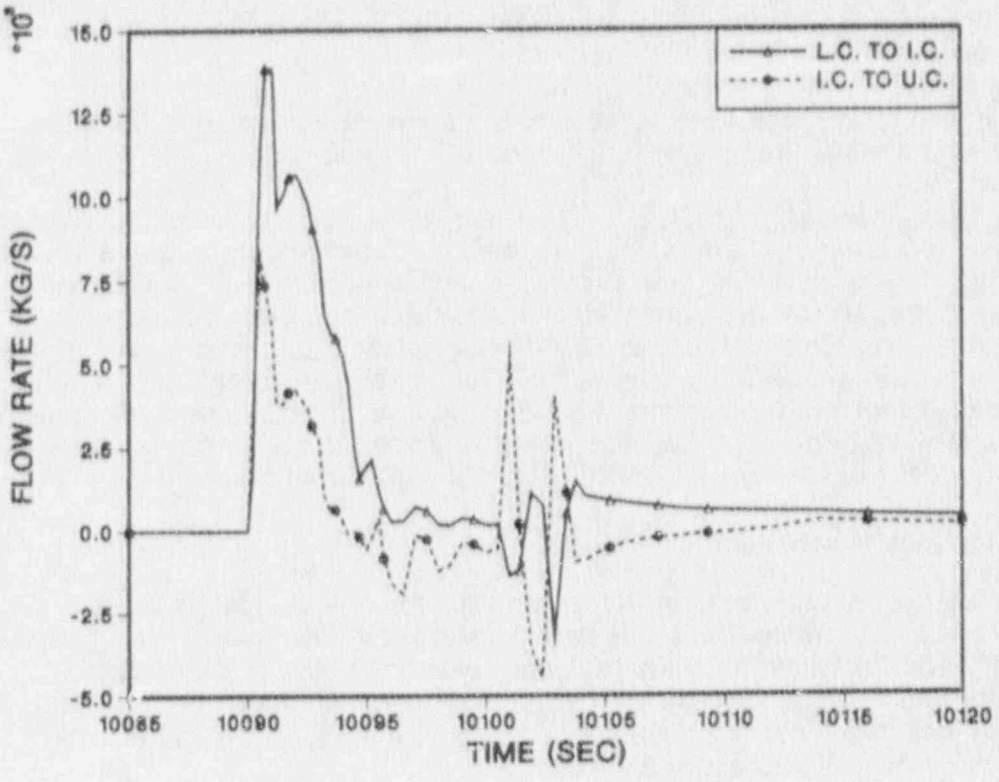

Figure 3.5 Flow rates into and out of the ice condenser in the 4-cell base case.

occur in the ice condenser, producing the second peak in the pressure trace. At this time, no burn is occurring in the upper containment and hydrogen concentrations there are insufficient to initiate a second burn. Hence, hydrogen driven into the upper containment by the second ice condenser burn is not calculated to undergo combustion.

This interplay between burns in the two different cells illustrates one way that the exact pressures obtained can be somewhat sensitive to what may be regarded as accidents of timing. If the first ice condenser burn had happened to occur after the upper containment burn had terminated, peak pressures would have been somewhat lower. On the other hand, they could have been somewhat higher if the second ice condenser burn had occurred before the upper containment burn had terminated. Since there is much uncertainty in the exact timing and durations of these burns, differences between different calculations which depend upon this kind of detail cannot be viewed as being very significant. Experience suggests that pressure variations of up to 0.1 MPa can result from effects such as these.

At least to some extent, this behavior is an artifact of the model. In these calculations, it is assumed that each cell is well mixed and that it will not burn until the average gas concentrations in the entire cell meet the burn criteria. In reality, it is likely that, in the scenarios considered here, a hydrogen-rich gas entering an oxygen-rich atmosphere (or vice versa) will burn as it enters, in a more nearly continuous

fashion. A considerably more detailed model would be required to track this behavior with any accuracy.

Some sensitivity studies further illustrating the dependence upon hydrogen modeling assumptions are presented in Sections 3.1.4 and 3.2.1.

75% Corium Participation Case. Pressures and temperatures for the base case with 75% corium participation (Case 2 of Table 3.1) are shown in Figures 3.6 and 3.7, respectively. Not surprisingly, both pressures and temperatures (including ice condenser temperatures) are much higher than in the 25% case. Pressures are much higher than any reasonable estimate of the Sequoyah failure pressure, and it is evident that only very substantial mitigation would be of any help in this plant. Nonetheless, moderate degrees of mitigation might be of interest for ice condenser plants with stronger containments, e.g., Watts Bar. Possible effects of the extreme pressures calculated for the cavity region (> 4 MPa) also require evaluation.

3.1.2 Mitigation by Containment Venting

Venting the containment offers the potential for reducing DCH loads due to at least two effects: it reduces the DCH base pressure (i.e., the containment pressure at VB), and it permits steam to partially purge oxygen from the containment. CONTAIN-DCH calculations for the Surry plant have indicated that both these effects can be significant in PWR large dry containments [SNL89]. Vent characteristic assumed were discussed in Section 2.4.3.

Figure 3.8 compares pressure histories for the 25% base case with the results of some venting calculations. The chain dot curve and the dashed curve give, respectively, results for a vent in the upper containment and a vent in the lower containment (Cases 3 and 4 in Table 3.1). There is a significant reduction in pressure, but the effect is not dramatic. The dependence upon the location of the vent (i.e., upper vs lower containment) is minor.

In Figure 3.9, the effect of venting upon the 75% base case is illustrated (Cases 5 and 6). The reduction in maximum pressure is comparable to that obtained for the 25% case. The pressures calculated remain well above the estimated Sequoyah failure pressures.

When one considers the large uncertainties in many of the parameters that govern DCH loads (e.g., corium participation fraction), it is evident that the effect of venting is less than the variations in DCH loads that result from these other parameters. Hence, these calculations do not indicate that venting could greatly increase containment survivability.

3.1.3 Effect of Augmented Igniters

In the calculations presented previously, it was assumed that hydrogen combustion would occur whenever the default burn criteria were met. Thus, these calculations are applicable for the case in which an augmented igniter system is available, with independent power supplies and with igniters installed in the ice condenser. The calculations are also applicable to the unmodified plant if it is assumed that sparking associated with ice condenser door movements (or other effects) provides ignition sources. As can be seen from Figure 3.3, these assumptions do result in considerable hydrogen combustion in the ice condenser prior to VB; combustion prior to VB does not occur in any of the other three containment cells.

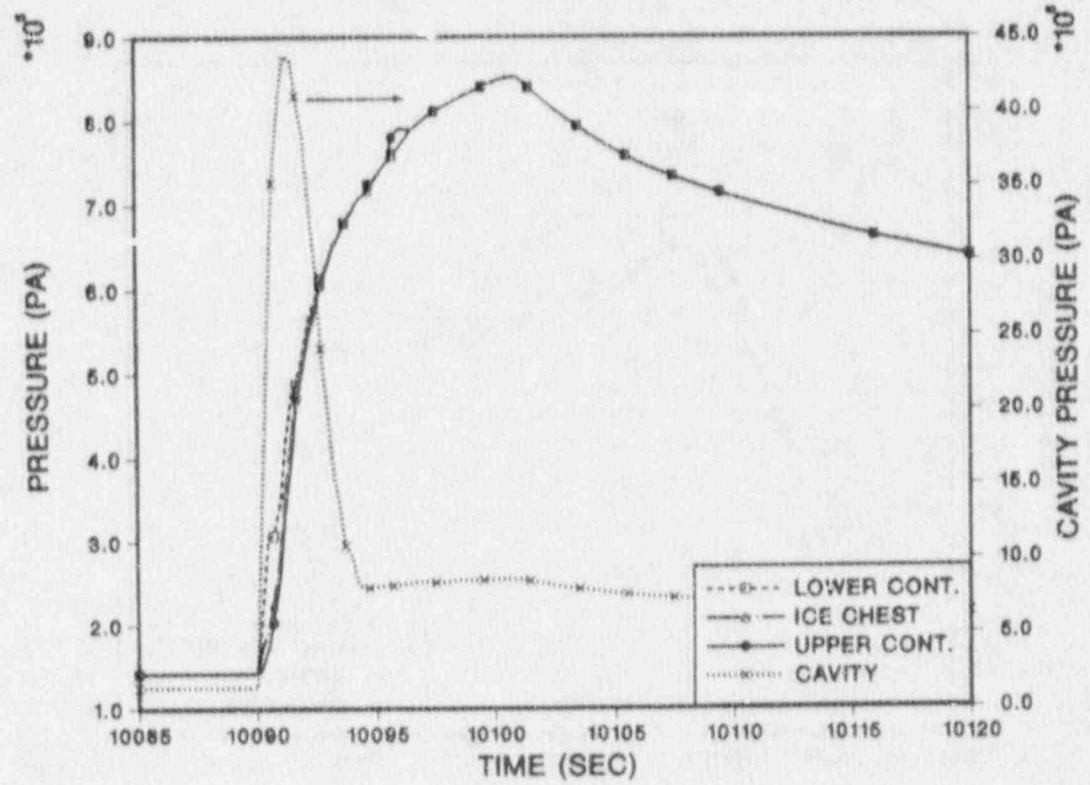

Figure 3.6 Containment pressures in the case with 75% corium participation.

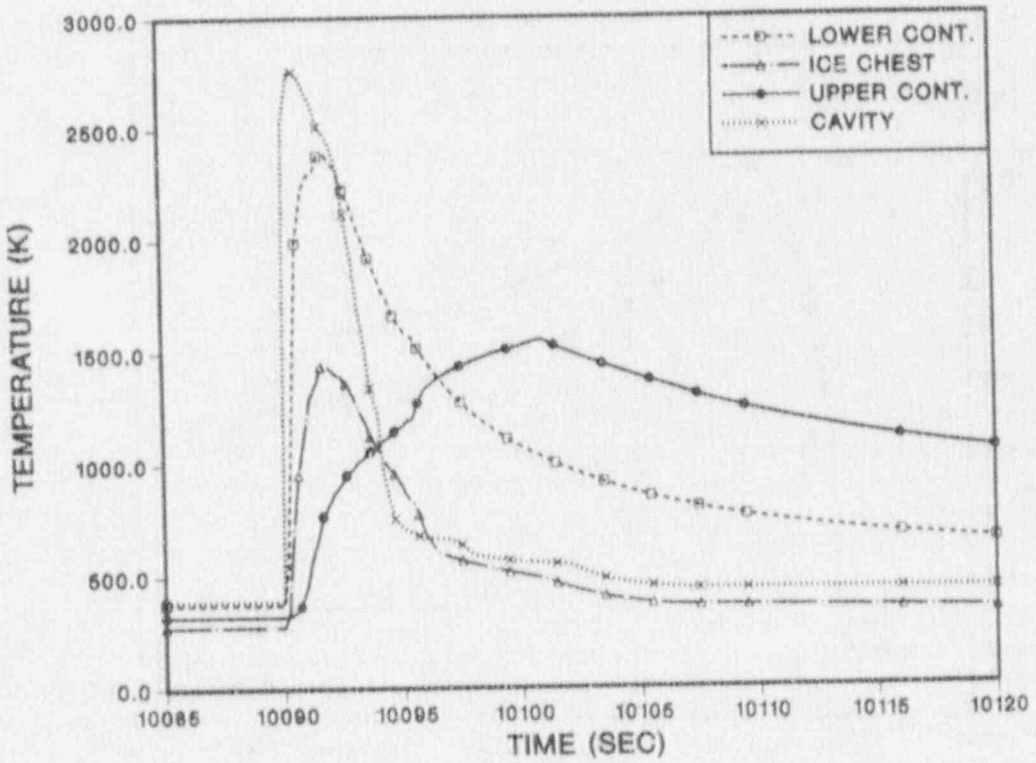

Figure 3.7 Containment temperatures in the case with 75% corium participation.

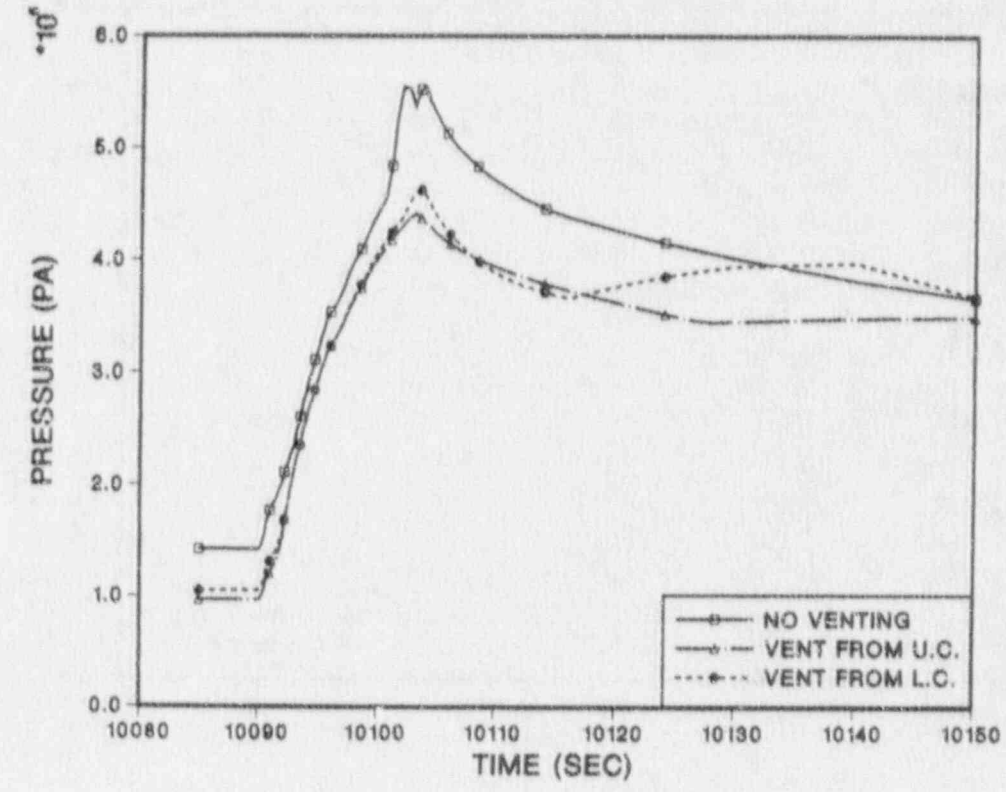

Figure 3.8 Effect of containment venting, 25% corium participation.

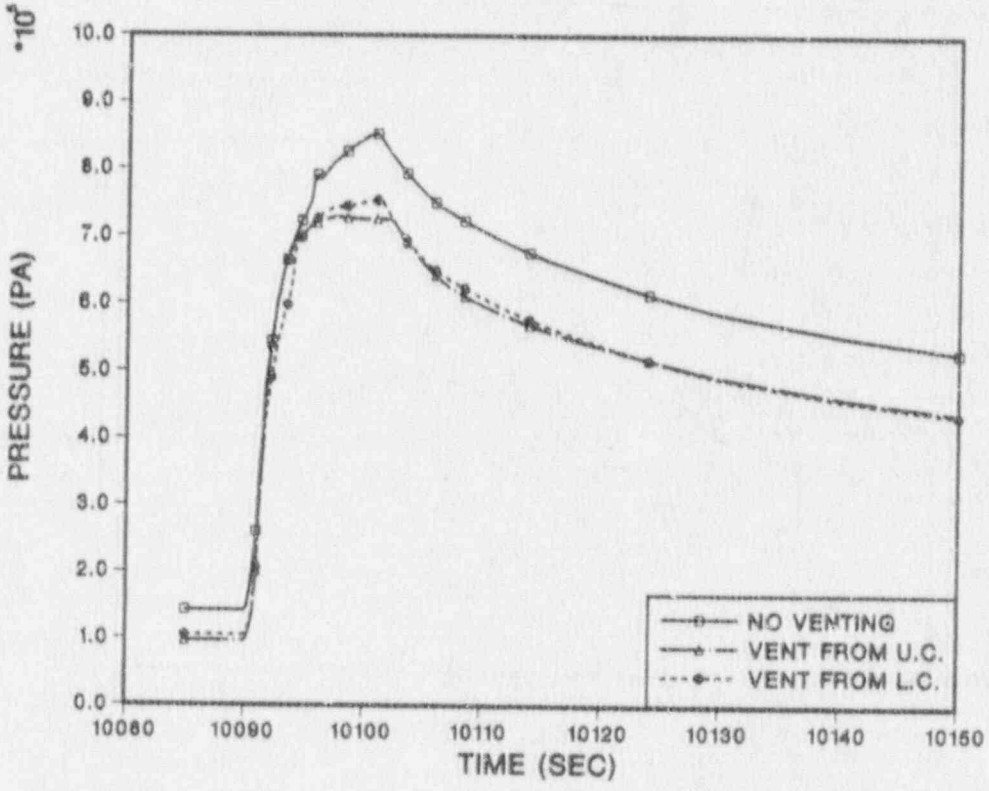

Figure 3.9 Effect of containment venting, 75% corium participation.

Since ignition cannot be assured in the unmodified plant, calculations were performed assuming no ignition prior to VB. Both the vented and the unvented cases were considered. Results are given for the 25% and the 75% corium fractions in Figures 3.10 and 3.11, respectively (Cases 7-13, Table 3.1). It is evident that venting has about the same effect as was observed when pre-VB ignition was assumed.

Case 10 (dotted curve, Figure 3.10) gives the results obtained if one assumes a larger vent (1 m^2) which is not closed off until the time of VB. Some additional reduction in the maximum pressure results.

Augmented igniters would have the effect of assuring ignition sources are available as assumed in Figures 3.8 and 3.9. The results with and without pre-VB ignition are compared more directly for the unvented cases in Figure 3.12. (Compare Cases 1 and 2 with Cases 7 and 11, respectively, in Table 3.1.) For the 75% corium fraction, the pressure increase in the no-ignition case is less than 0.1 MPa, and there is almost no difference between the maximum pressures in the two 25% cases.

Comparison of the curves for the vented scenarios in Figures 3.8 and 3.9 with those in Figures 3.10 and 3.11, respectively, shows that guaranteeing ignition prior to VB yields only relatively minor benefits in the vented cases also. Thus, there is no indication that augmented igniters could greatly alter the DCH threat spectrum for ice condenser plants in those accidents in which the RCS remains highly pressurized until vessel breach.

3.1.4 Sensitivity to Hydrogen Combustion Uncertainties

As discussed in Section 2.4.1, neither the default burn model nor the unconditional hydrogen burn (UCHB) model can be expected to give a fully adequate representation of hydrogen combustion associated with DCH events in ice condenser plants. Nonetheless, comparison of the results obtained using the different models does provide insights as to the magnitudes of the uncertainties resulting from the current limitations in the modeling of hydrogen behavior.

Calculations were run for the 25% cases with and without venting using the UCHB model. No ignition prior to VB was assumed. Burn duration times of 0.5 s and 2 s were assumed for the ice condenser and the upper containment, respectively.

Results are given by the curves without symbols in Figure 3.13 (Cases 14 and 15, Table 3.1). The ragged appearance of the curves is an artifact of the model in which a burn in any cell is followed by a "dead time" of equal duration, during which no burn can occur in that cell. The code was then modified to shorten the dead time to be no greater than the system timestep, thereby obtaining a more continuous combustion of the hydrogen. The results are given by the curves with symbols (squares or circles) in Figure 3.13 (Cases 16 and 17, Table 3.1). The curves are considerably smoother and the maximum pressures somewhat lower in the unvented case.

Comparison of the curves for the UCHB (with the shortened dead time) with the analogous curves for the default burn model (Figure 3.10; Cases 7 and 8) shows that the UCHB model gives somewhat lower maximum pressures for the unvented scenario (Cases 7 and 8) while the results are more nearly equal for the vented cases. Thus the UCHB assumption reduces somewhat the effects of venting, in this particular instance.

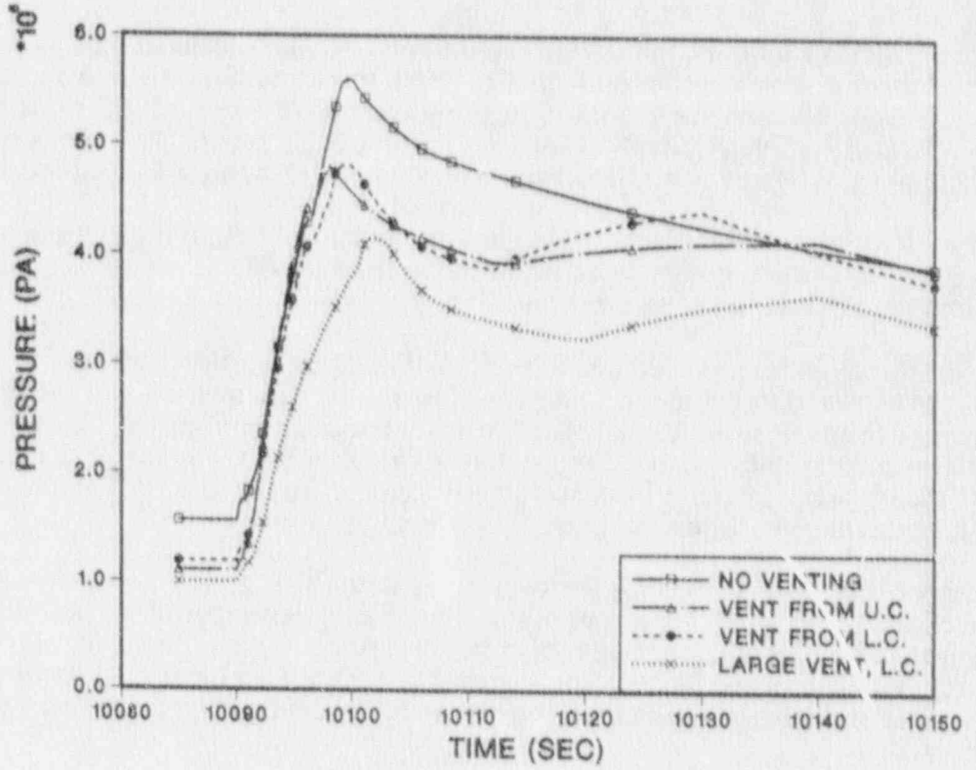

Figure 3.10 Containment pressures with and without containment venting, no ignition prior to VB, 25% corium participation.

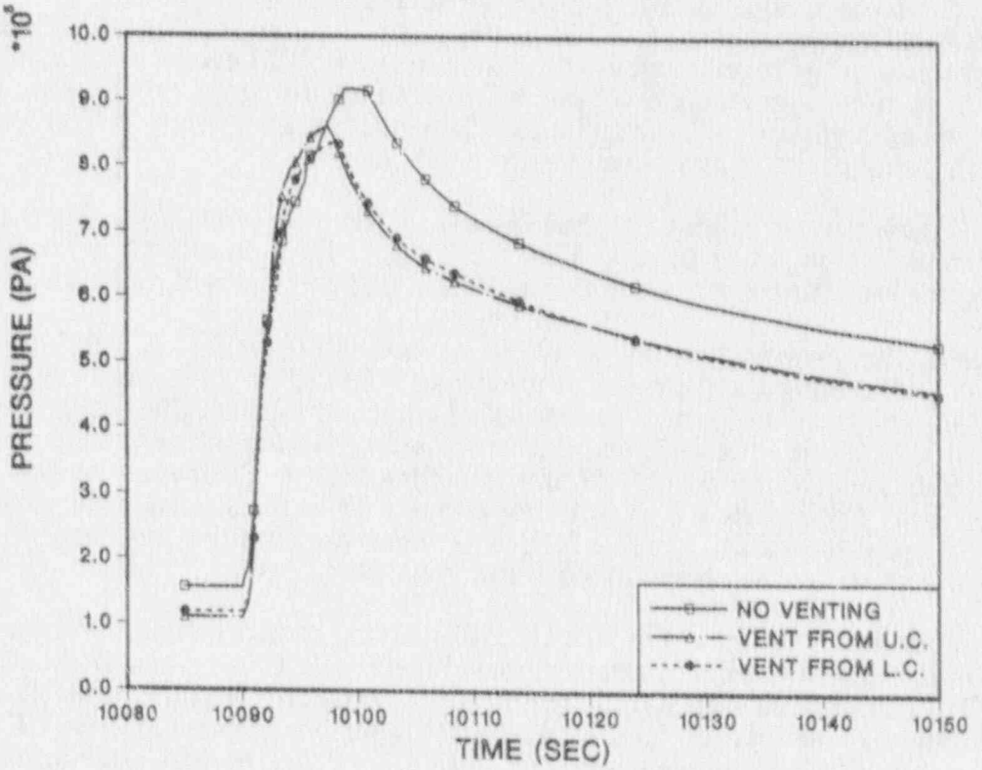

Figure 3.11 Containment pressures with and without containment venting, no ignition prior to VB, 75% corium participation.

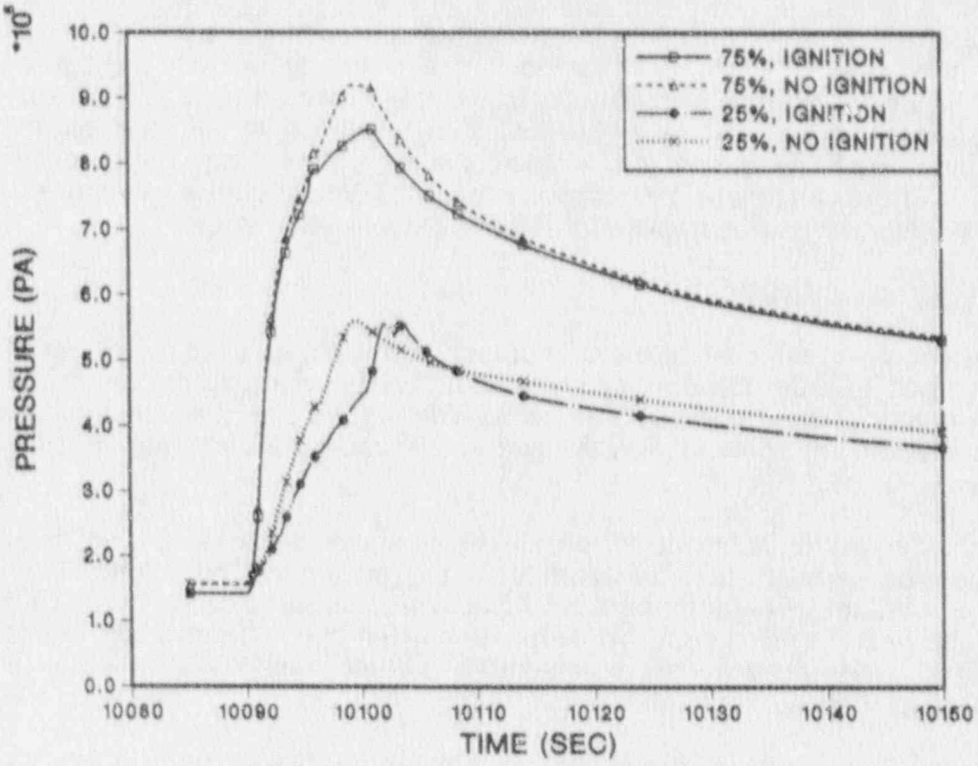

Figure 3.12 Effect of ignition sources prior to VB, 25% and 75% corium participation.

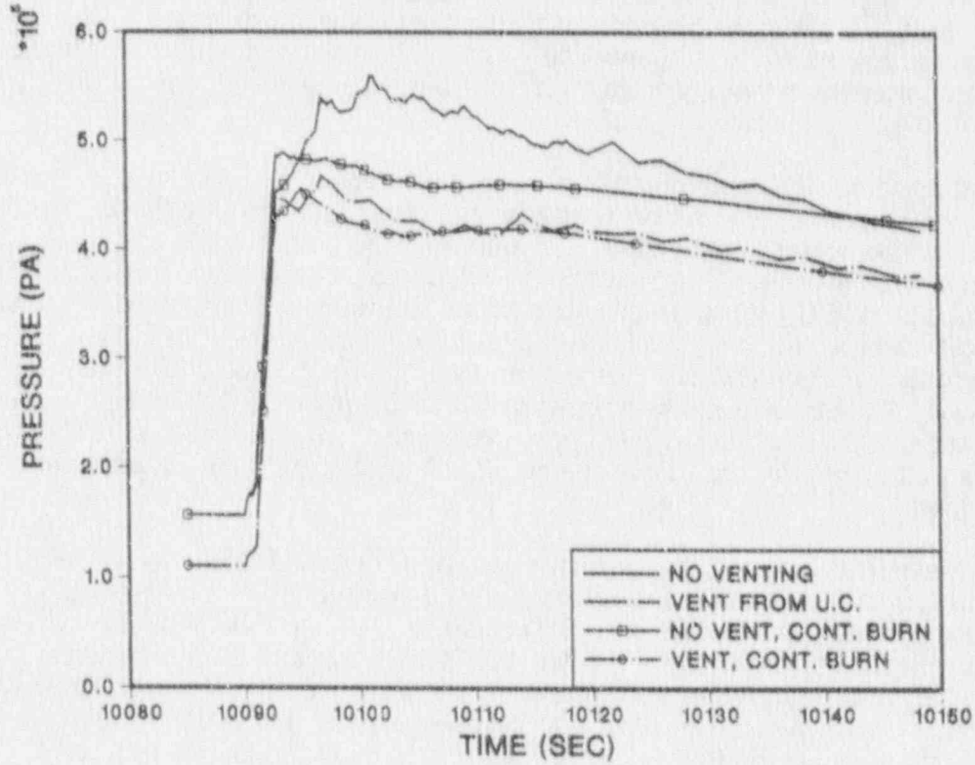

Figure 3.13 Containment pressures calculated with the unconditional burn assumption, 25% corium participation.

The effects of these variations in the hydrogen burn model are of the same order of magnitude as are the differences associated with venting and with augmented igniters. Thus, the relative uncertainties in the magnitudes of the effects of the improvements may be substantial. However, the results do not indicate that these uncertainties are large enough to alter the conclusions drawn as to the order of magnitude of the benefits of the improvements considered. Hence, the modeling is probably adequate for the purposes of the present screening study.

3.1.5 Containment Inerting

It is not clear that inerting the containment atmosphere in ice condenser plants is feasible, since it would introduce operational difficulties that might ultimately do more harm than good. Nonetheless, it is worth considering inerting in a screening study, partly to identify any potential benefits and also because it is phenomenologically instructive.

In the Sequoyah DCH calculations discussed above, almost all of the metal oxidation is due to reactions with steam in the oxygen-starved lower containment. Hence, elimination of oxygen would not have a large direct effect upon the DCH energy release itself. However, hydrogen combustion plays an important role in all the calculations, and eliminating oxygen obviously eliminates this contribution to the total pressurization of the containment.

The effects of inerting were investigated by exercising code options which permit the user to switch off all chemical reactions involving oxygen. Results are shown in Figure 3.14; see also Cases 18-23 in Table 3.1. The solid, chain dot, and dotted curves in Figure 3.14 give results for the 25%, 50%, and 75% corium participation cases, respectively; the noninerted cases and the inerted cases are distinguished by open symbols and closed symbols, respectively. In this comparison, the noninerted cases were run under the assumption that ignition sources would not be available prior to VB.

It is apparent that inerting results in very substantial decreases in the pressure rise following VB in all cases. Proportionately, the effect is largest for the 25% case; evidently, most of the pressure rise in the unmodified plant for the 25% case is associated with hydrogen combustion and eliminating this combustion essentially eliminates the DCH threat. In absolute terms, the reduction is somewhat greater for the larger corium fractions, but the fractional reduction is less than for the 25% case. In the context of the NUREG-1150 estimates of the Sequoyah failure pressure (Section 2.4.2), the 50% case with inerting (Case 20) presents a marginal threat of containment failure, while the peak pressure for the 75% case, even with inerting, remains well above the median of the Sequoyah failure pressure uncertainty distribution.

These results indicate that containment inerting would substantially mitigate DCH threats in Sequoyah, but would not offer a complete panacea, at least if scenarios as severe as the 75% case are credible. If the NUREG-1150 uncertainty distributions for corium fraction ejected at VB are accepted, the 75% case actually is outside the credible range and is excessively conservative in this sense. However, this case is not necessarily conservative with respect to other defining assumptions; for example, the assumption that vessel breach results from the failure of a single instrument tube penetration could prove to be nonconservative (Section 2.5). Without additional study, results as severe as those calculated for the 75% case cannot be

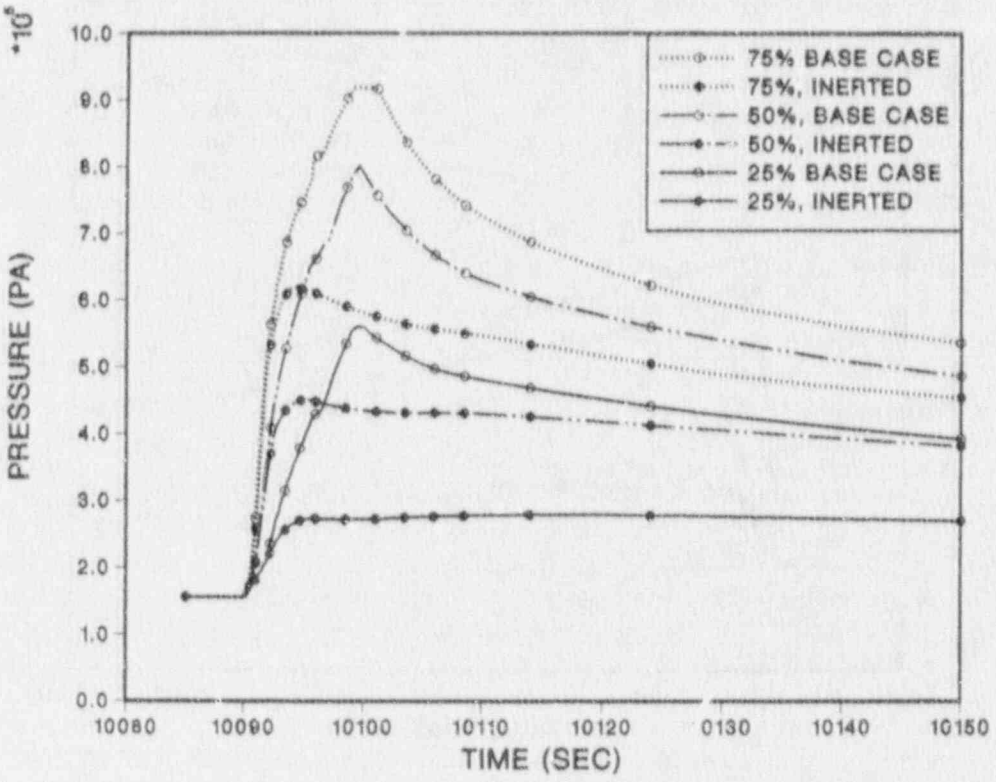

Figure 3.14 Effect of inerting the containment atmosphere.

absolutely ruled out, even if the 75% participation assumption is itself rejected as excessively conservative.

Combining inerting with containment venting (Figure 3.15; Cases 22 and 23 in Table 3.1) yields only a small additional reduction in the maximum pressures following VB. For the 75% corium fraction calculation, the maximum pressure (0.57 MPa) is still above the median in the NUREG-1150 uncertainty distribution for the Sequoyah failure pressure.

It is evident that only a very large mitigation factor could completely eliminate the DCH threat for the 75% corium participation fraction case. However, this conclusion is plant-specific for Sequoyah. For an ice condenser plant with a stronger containment (e.g., Watts Bar), a more detailed examination might succeed in establishing that inerting could largely eliminate the DCH threat.

3.1.6 Subatmospheric Containment

A potential containment improvement option that is less drastic than inerting would be to maintain subatmospheric pressures in the containment, e.g., as is done at Surry and other PWR subatmospheric large dry containments. Calculations were performed assuming a containment pressure of 0.0693 MPa at the time of reactor shutdown (Case 24). Results are compared with the base case in Figure 3.16 for the 25% corium assumption. In both calculations, ignition sources were assumed to be available at all times.

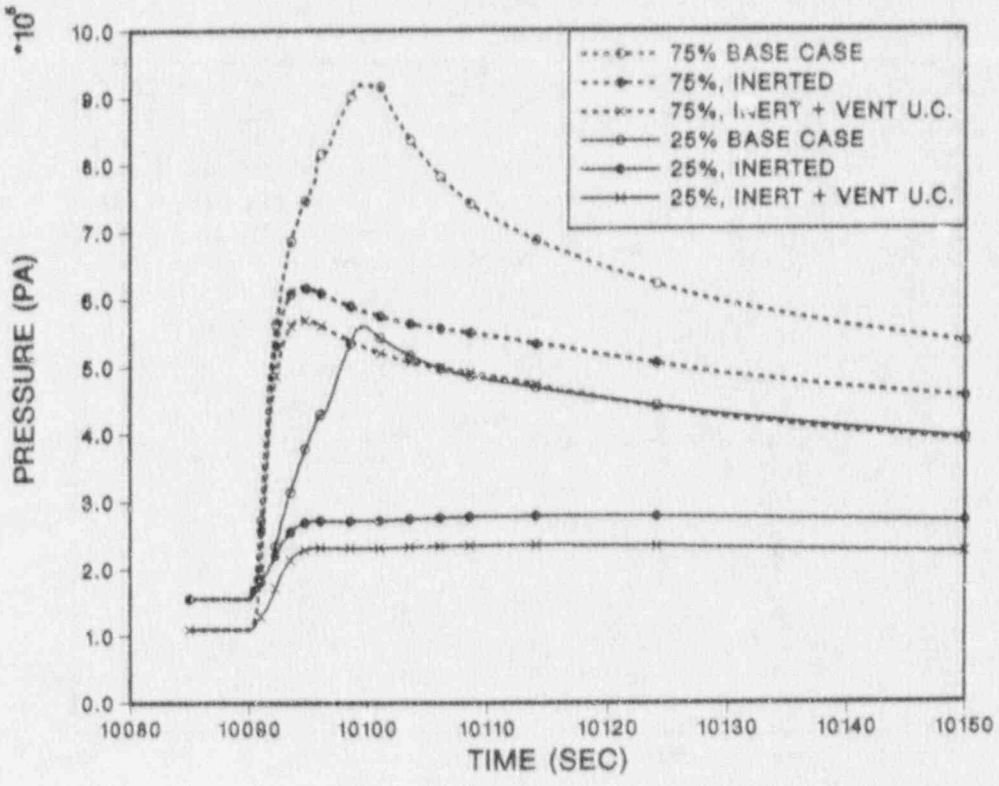

Figure 3.15 Effect of containment inerting, and of inerting combined with venting.

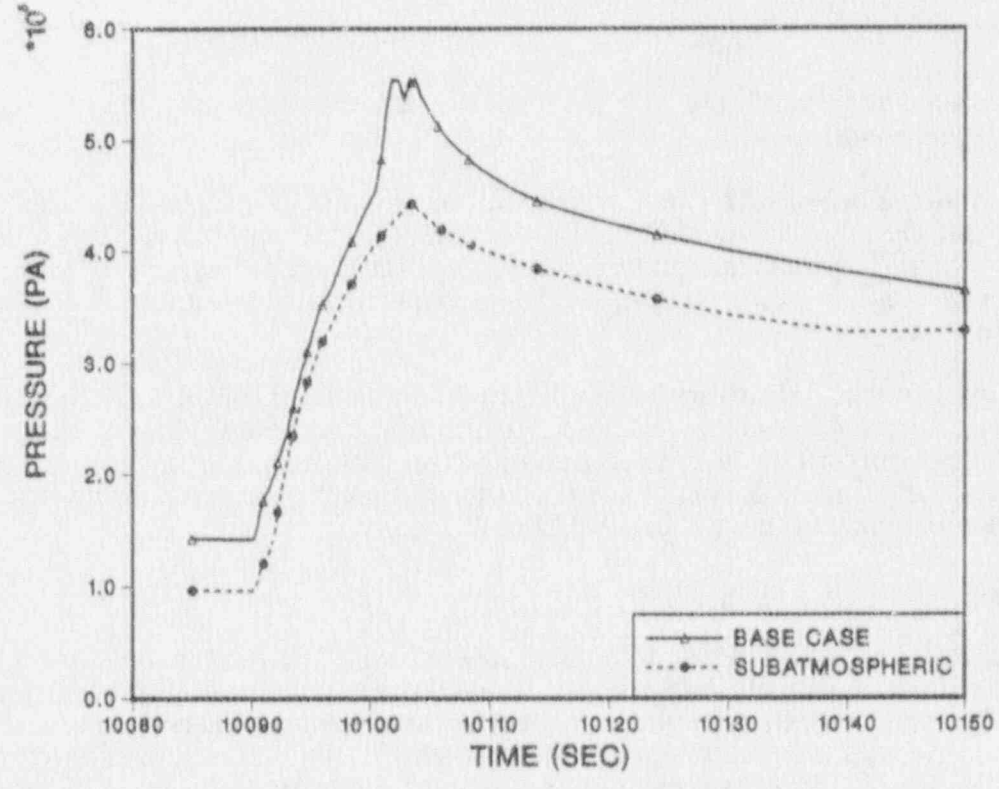

Figure 3.16 Effect of a subatmospheric containment.

The extent of mitigation is comparable to that calculated previously for venting. This is not surprising, since conditions at VB (containment pressure, oxygen inventory, oxygen distribution) in the subatmospheric case are fairly similar to those calculated for the venting cases. The extent of mitigation, though not negligible, is not sufficient to offer a major reduction in the overall DCH threat spectrum.

3.2 6-Cell Calculations

The 6-cell model was derived from the four cell model by adding cells to represent the lower and upper plena of the ice condenser. In addition, a number of other refinements based upon data in Refs. Di85 and TVA88 were added. As discussed in Section 2.3, these included more detailed representations of the ice condenser doors and of flow paths between the upper and lower containment that bypass the ice condenser. The net effect of the latter was to increase the bypass flow, allowing somewhat more steam to reach the upper containment prior to VB, without passing through the ice condenser.

Calculations using the 6-cell model were performed primarily for the cases with a 25% corium participation fraction, with a few 50% cases also being treated. No calculations for the 75% corium fraction were performed. Results are summarized in Table 3.2. The meanings of the column heads are the same as in Table 3.1 except for the third column headed "igniters". Here "all" denotes an augmented igniter system with igniters in all cells and with a dedicated power supply operational, while "existing" denotes independent power supplies for existing igniters but with no additional igniters installed. "None" means that no igniters are powered, and corresponds to the unmodified plant. In the discussion that follows, the presence or absence of powered igniters in a cell is assumed to be equivalent to the presence or absence of ignition sources in that cell prior to VB; the possibility of chance ignition in the absence of igniters is not considered. It is assumed that ignition sources always become available at VB.

3.2.1 Results for the Base Case

Pressures and temperatures for the 25% 6-cell base case (Case 1, Table 3.2) are shown in Figures 3.17 and 3.18, respectively. Figure 3.19 gives the cumulative hydrogen combustion in the various cells, while the atmospheric compositions are displayed in Figure 3.20. The default hydrogen burn model was used, with ignition sources assumed to be available in all cells at all times.

As in the 4-cell model, the cavity cell initially pressurizes severely with respect to the rest of the containment, while the pressures in the other cells are about equal to one another except for short periods during the maximum DCH heating rates. As in the 4-cell calculations for the 25% corium cases, much of the pressurization outside the cavity cell is due to hydrogen combustion rather than the immediate effects of DCH. Hydrogen combustion occurs in the upper containment and in the upper plenum during the time of interest, but only a small amount occurs in the ice condenser (Figure 3.19). Substantial hydrogen combustion has occurred in the ice condenser prior to VB, however.

The maximum pressure in the 6-cell case is over 0.1 MPa lower than in the 4-cell base case. (As will be seen below, this result is sensitive to modeling details and should not be taken too seriously.) One reason is that the increased bypass flow leads to somewhat higher steam concentrations in the upper containment (about 20%, see

Table 3.2

Results of 6-Cell Calculations, Fully Pressurized RCS

Case No.	Corium Fraction	Powered Igniters	Other	Max. P (MPa)
1	25%	All	---	0.44
2	25%	All	Burn propagation inhibited[a]	0.53
3	25%	All	No deck leak	0.49
4	25%	All	No deck leak, Note a	0.49
5	25%	All	No ice bypass	0.45
6	25%	All	Fans operate	0.43
7	25%	All	Fans operate, Note a	0.47
8	50%	Existing	---	0.65
9	50%	All	---	0.61
10	50%	None	---	0.65
11	50%	Existing	Vent upper containment	0.60

Notes:
[a] Burn propagation from the upper plenum to the upper containment was artificially inhibited.

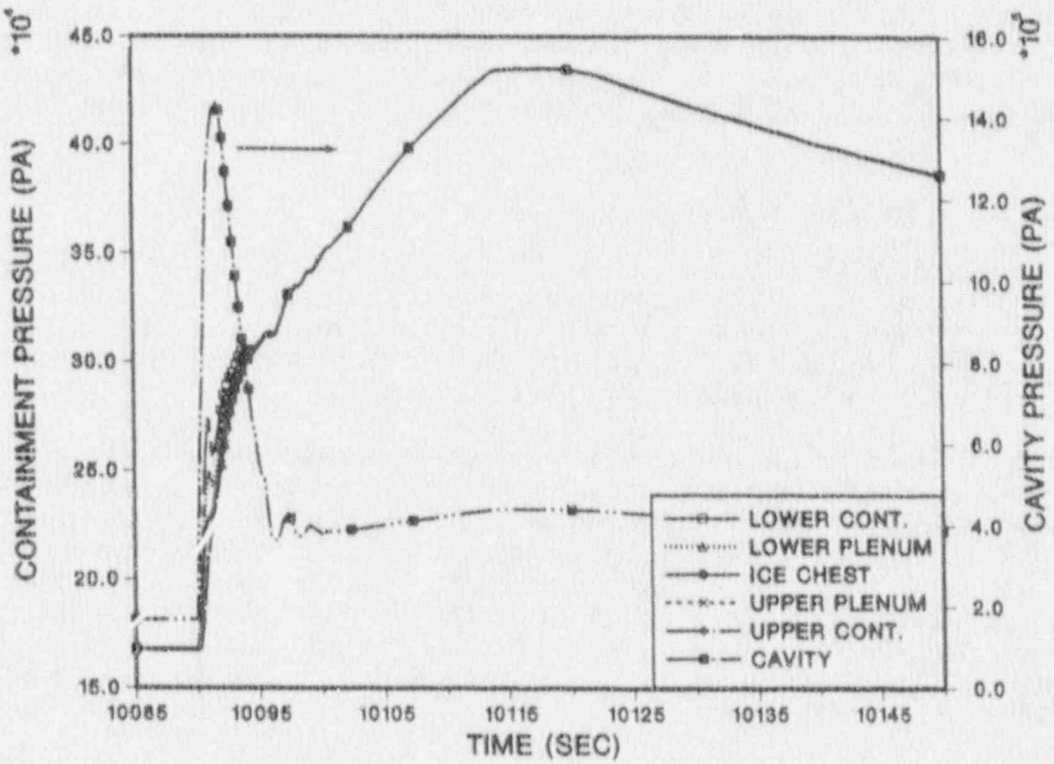

Figure 3.17 Containment pressures after VB calculated using the 6-cell deck, 25% corium participation.

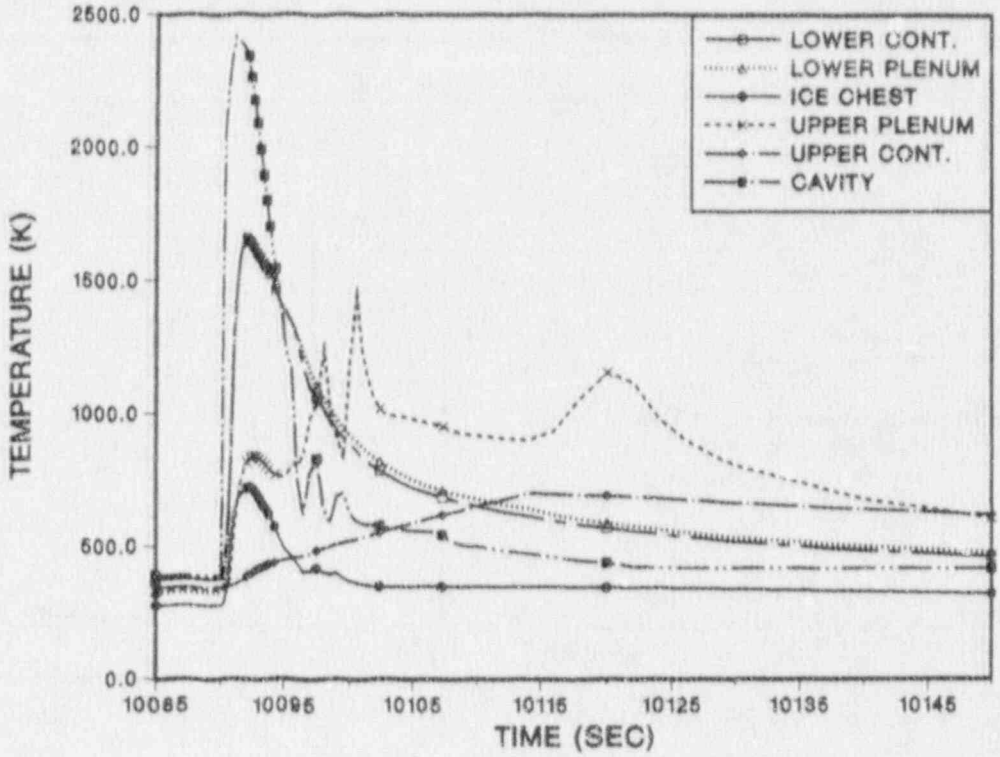

Figure 3.18 Containment temperatures after VB calculated using the 6-cell deck, 25% corium participation.

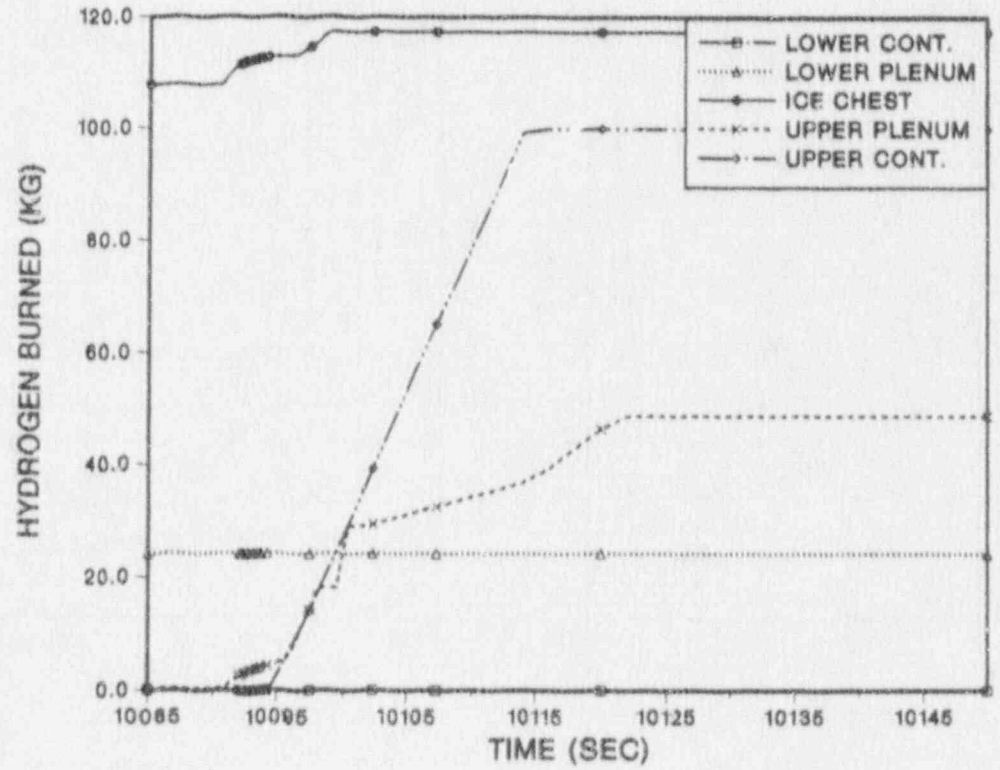

Figure 3.19 Cumulative hydrogen consumption, 6-cell deck.

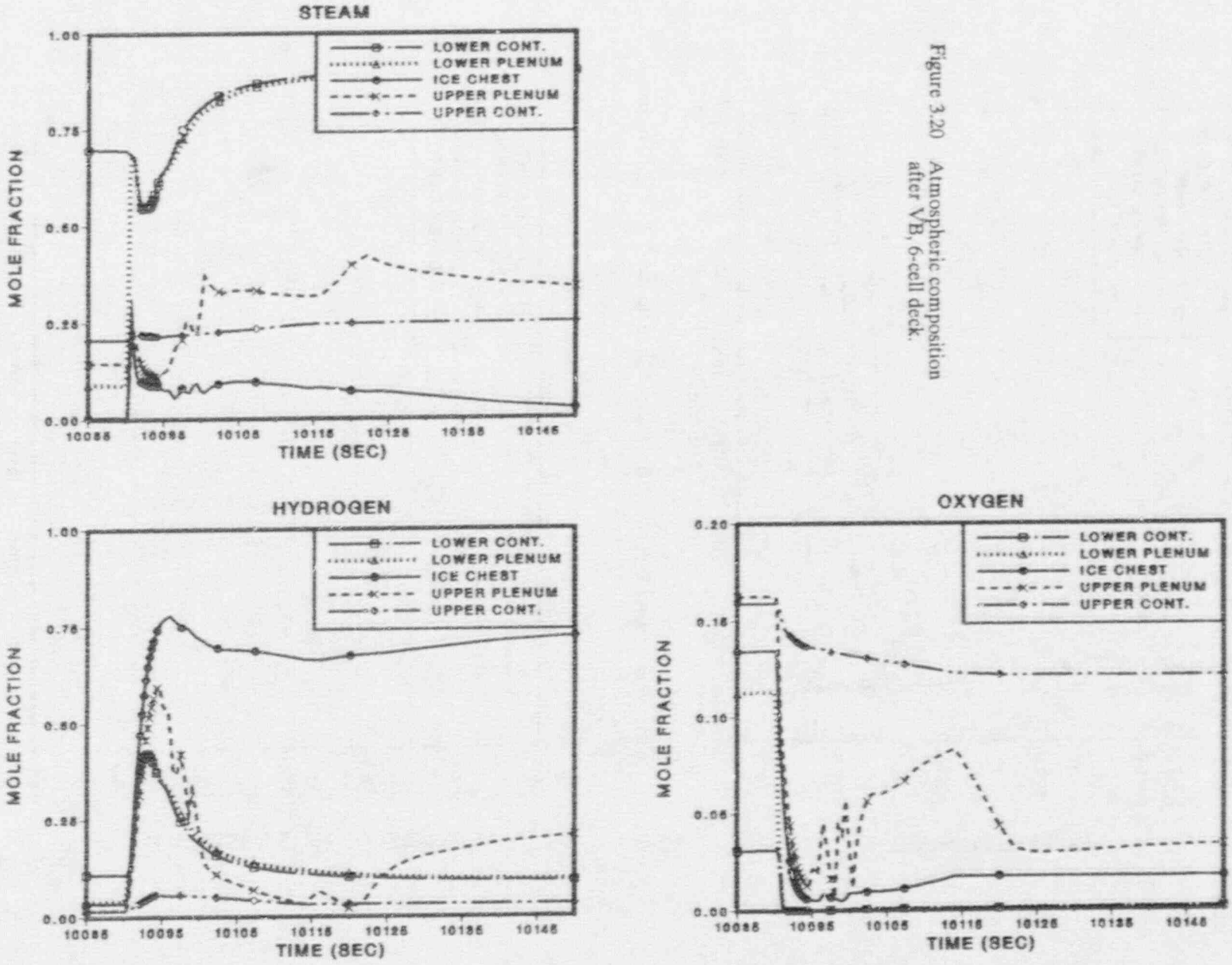

Figure 3.20 Atmospheric composition after VB, 6-cell deck.

Figure 3.20), which results in a slower hydrogen burn and, hence, greater mitigation from energy losses during the burn.

Sensitivity to Burn Propagation Criteria. A more subtle reason for the lower pressure in the 6-cell case has to do with details of the default burn model with respect to burn propagation. In CONTAIN, burns may propagate from one cell to an adjacent connected cell provided the flammability limits for propagation are satisfied. These limits depend upon whether the elevation of the receiver cell is greater than, equal to, or less than the elevation of the donor cell. In the 6-cell model, the center of gravity of the upper containment is about 1 m greater than that of the upper plenum, so that the criterion for upward propagation (4% H_2) is used by the code.

In the 6-cell base case, a burn initiates in the upper plenum (Figure 3.19) and propagates into the upper containment at a time when the hydrogen concentration there is less than the lower flammability limit for independent ignition (7%). Since the correlations for burn duration and burn completeness are functions of the initial hydrogen concentration, the resulting burn is relatively slow and incomplete. During the burn, additional hydrogen flows into the cell; although this additional hydrogen is allowed to burn, it is not taken into account in setting the burn duration and completeness parameters.

The location at which a burn in the upper plenum could propagate into the upper containment is the upper plenum doors, which are actually higher than the center of gravity of the upper containment volume. When the hydrogen concentrations are low, it is possible that the burn would not actually propagate into the lower portions of the upper containment volume. As a test of the sensitivity to the burn propagation parameters, a calculation was run with the elevation specified for the upper containment in the burn model reduced by two meters. This change results in the propagation criteria for downward propagation, rather than upward propagation, being used in the calculation. Since the flammability limit for downward propagation (9%) is higher than the limit for independent ignition, this choice in effect eliminates propagation in the present case.

Results are compared with the base case in Figure 3.21, where the chain dot curve gives the base case pressure history while the pressure history for the modified case (Case 2, Table 3.2) is given by the dashed curve. It is seen that the maximum pressure is increased by about 0.1 MPa. The upper containment burn is delayed until the 7% threshold for independent ignition is reached, and the resulting burn is stronger as can be seen from the quantities of hydrogen consumed (Figure 3.22; compare with Figure 3.19 for the base case). The upper containment burn results in sufficient oxygen being forced back into the upper plenum and the ice condenser so that strong burns initiate in these locations also. These burns are responsible for the sharper pressure spike at the top of the more gradual rise in the dashed curve of Figure 3.21.

These results should not be viewed as simply representing the uncertainty resulting from ambiguity in the appropriate burn propagation criteria. Instead, they basically represent uncertainty associated with details of the hydrogen behavior such as the timing, duration, and completeness of hydrogen burns, and also the relative timing of burns in different locations. Many other uncertainties affect these hydrogen behavior details in addition to the propagation uncertainties.

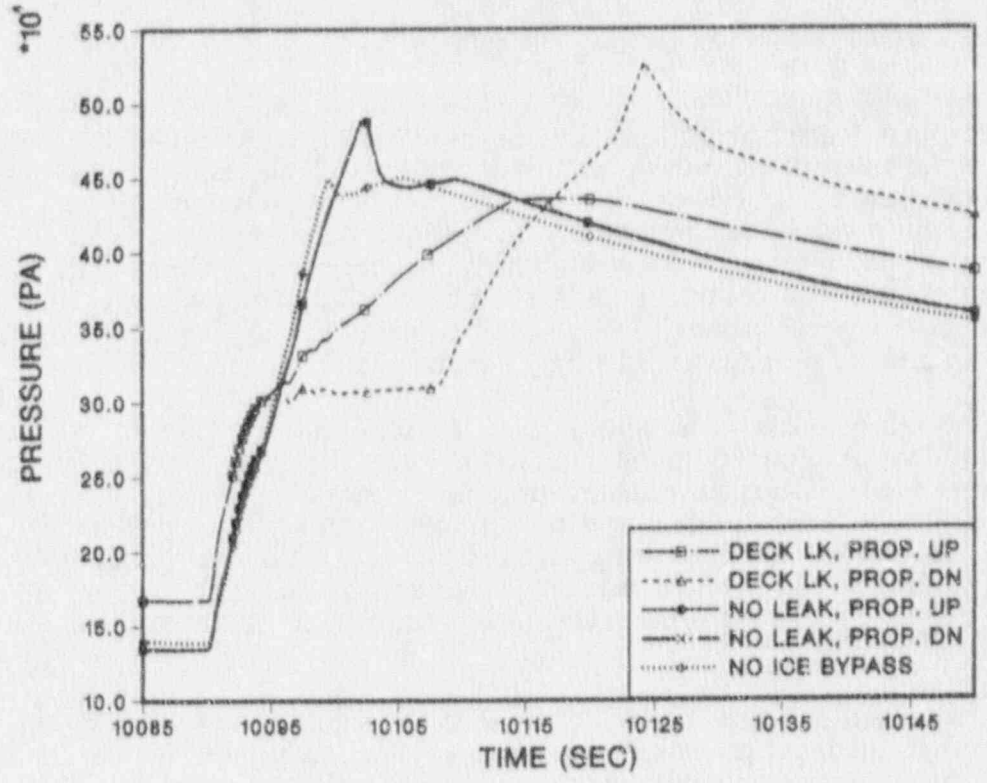

Figure 3.21 Effect of reduced ice condenser bypass flows and of altered hydrogen burn propagation parameters.

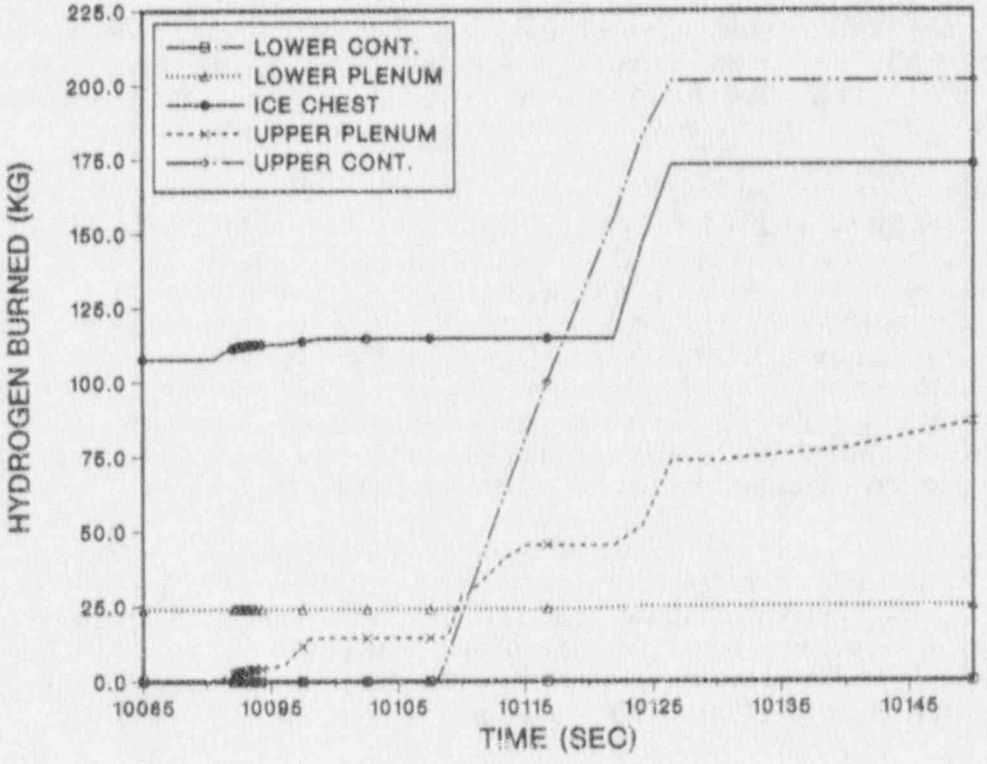

Figure 3.22 Cumulative hydrogen consumption following VB for the case with partial inhibition of hydrogen burn propagation.

3.2.2 Reduced Ice Condenser Bypass

One possible containment modification would be to reduce the assumed ice condenser bypass leakage in the deck separating the upper and lower containments. Case 3 in Table 3.2 was calculated with this leakage eliminated, and the solid curve in Figure 3.21 gives the pressure history resulting. The bypass flow through the refueling canal drains is still included in this case. The maximum pressure calculated is intermediate between the two calculations for the case with deck leakage that were discussed above. In this calculation, no burn happened to occur in the upper plenum at a time which would lead to early propagation into the upper containment, and changing the propagation criteria therefore made no difference (chain-dot curve with crosses superposed upon the solid curve in Figure 3.21). Eliminating all bypass (including the refueling canal drains) reduced the maximum pressure by about 0.04 MPa (dotted curve in Figure 3.21; Case 5 in Table 3.2). This calculation also showed no dependence upon the propagation criteria.

For this scenario, it is evident that any effects resulting from eliminating the bypass flow are within the uncertainty resulting from uncertain details of the hydrogen phenomenology. This may not always be the case, especially in accidents of longer duration such as the station blackout sequence with intentional depressurization of the RCS. Effects of the bypass flows in that scenario are discussed in Section 4.3.

3.2.3 Independent Power Supplies for the Air Return Fans

Ice condenser plants are equipped with air return fans that move air from the upper containment back to the lower containment. Among other things, these fans may reduce the accumulation of high local concentrations of hydrogen in the ice condenser. The fans would not operate during a station blackout accident in the unmodified plant, since they require AC power. One proposed improvement would be to provide an independent power supply for the fans.

In the present work, the fans were modeled as described in Section 2.4.3. Hydrogen ignition sources were assumed to be available at all times, since it would seem to make little sense to provide power for the fans and yet leave the igniters unpowered. Results are shown in Figure 3.23 and in Table 3.2 (Cases 6 and 7). The solid curve gives the base case pressure history, while the dashed curve gives the pressure history for the base case without upward burn propagation into the upper containment as was discussed previously. The chain dot and dotted curves give the results for the analogous cases with fans on. With upward propagation assumed, the fans make little difference between the two cases, while the fans give some improvement when no propagation is assumed.

One effect of fan operation is to increase the rate of ice melting. This effect is illustrated in Figure 3.24, in which the height of the ice column is plotted as a function of time for the base case and the case with fans on (Cases 1 and 6, Table 3.2). In CONTAIN, certain parameters describing the ice bed geometry (including the ice height and ice surface area) are decreased in proportion to the remaining ice mass as the ice melts; hence, the ice height is a directly proportional to the amount of ice remaining. It is evident that, at the time of vessel breach, almost twice as much ice has melted in the fans-on case as in the fans-off case. The reason for this difference is that, without fans, substantial steam condensation on the heat sinks in the lower containment occurs. With fans operating, the steam is transported to the ice condenser more rapidly, less steam is condensed upon the lower-containment heat

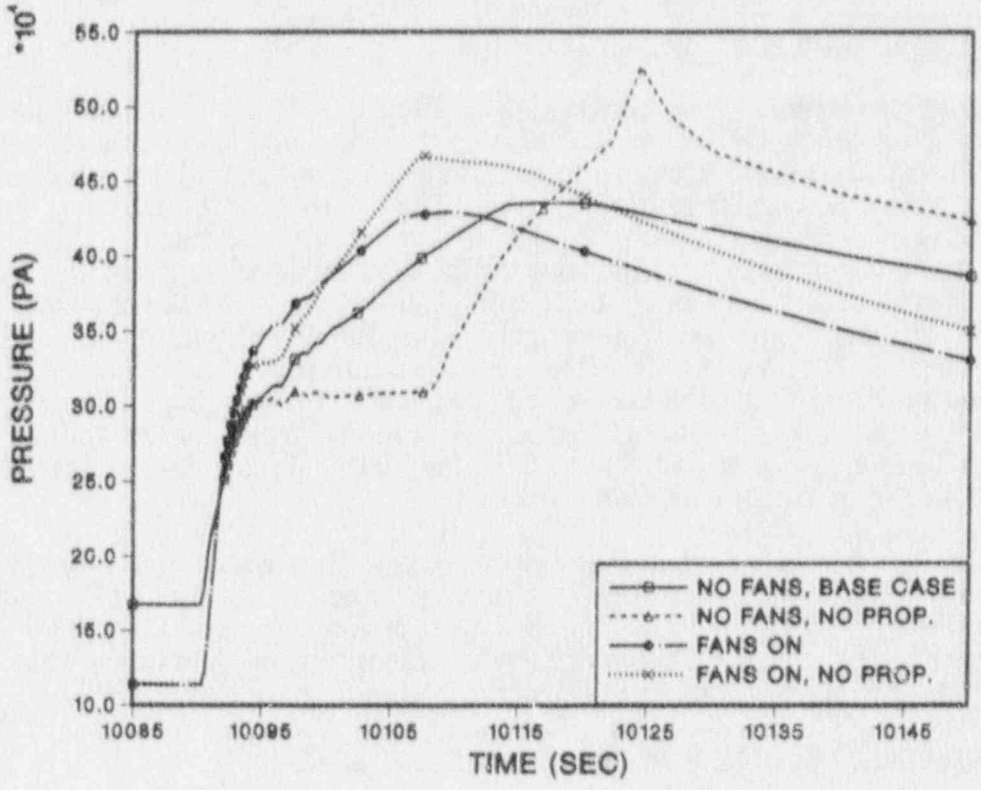

Figure 3.23 Effect of independent power supplies for the air return fans, and of altered hydrogen burn propagation parameters.

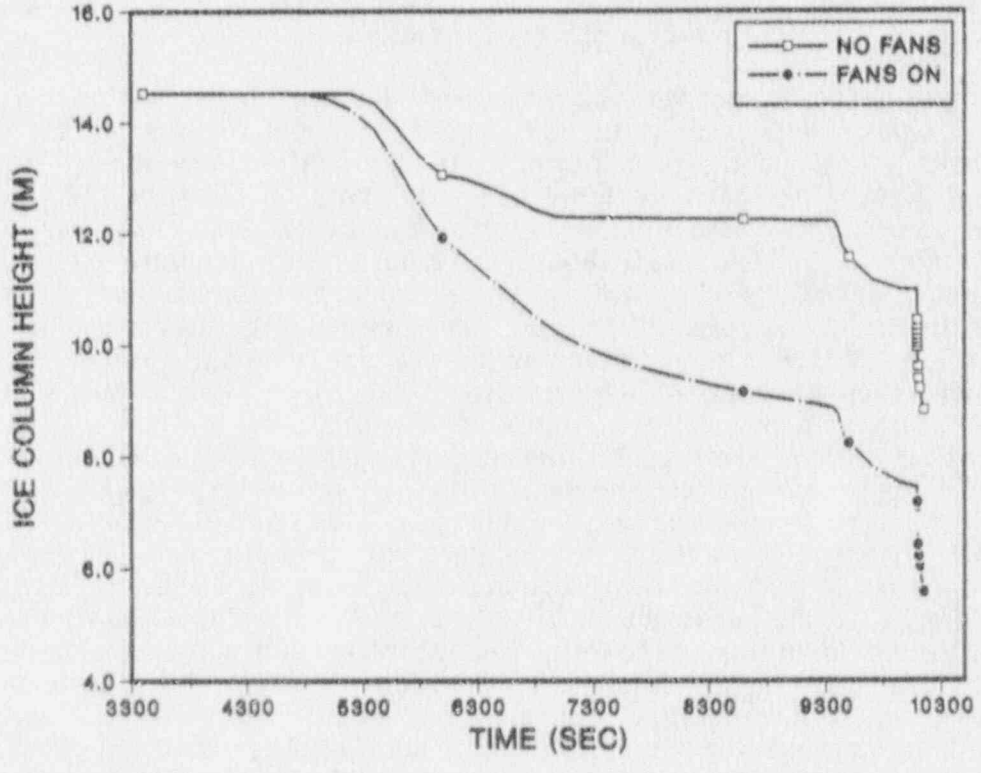

Figure 3.24 Ice remaining as a function of time, with and without fan operation.

sinks, and correspondingly more steam is condensed in the ice condenser. The effects of fans on ice melt are discussed in more detail in connection with calculations performed using the 26-cell containment representation.

It is evident that any effects of fan operation on the maximum pressures calculated are not large compared with the uncertainty introduced by uncertain details of the hydrogen phenomenology. It is possible that the enhanced ice melting prior to VB vitiates any beneficial effects that fan operation might otherwise be expected to have.

3.2.4 Calculations for 50% Corium Participation

Calculations performed assuming a 50% corium participation fraction were performed later in the CPI program than were the other calculations discussed in this section, and some changes were made to the deck, based upon the experience obtained in the earlier work. The change with the greatest potential importance is the imposition of a flame speed of 5 m/s in the upper and lower containment compartments, rather than use of the default correlations for flame speed. The motivation was concern that the default correlations could be nonconservative under some of the conditions involved (see the discussion of hydrogen burn modeling in Section 2.4.1). The default ignition criteria were still used whenever ignition sources were assumed to be available. In addition, the area vs pressure response function of the ice condenser lower plenum doors was modified to conform more closely with that given in the FSAR; see Table 2.4.

The 50% corium-fraction cases were studied further using the more detailed 26-cell containment representation (Section 3.4). Hence, the 6-cell results are discussed only very briefly here.

For the base case (Case 8 in Table 3.2), it was assumed that dedicated power supplies were available for the existing igniters, but without additional igniters installed. Pressures and atmospheric temperatures calculated as a function of time are plotted for the 50% base case in Figures 3.25 and 3.26, respectively. The results are generally intermediate between those obtained previously for the 25% and 75% corium fractions, as would be expected. The maximum pressure calculated, over 0.6 MPa, would constitute a serious threat to Sequoyah containment integrity. Note also the severe, albeit brief, pressurization of the cavity cell indicated in Figure 3.25.

Variations considered include a case with igniters in all cells, a case with no igniters powered (i.e., the unmodified plant), and a case with the existing igniters powered plus venting of the upper containment (Cases 9-11, respectively). Pressure-time histories are compared with that of the base case in Figure 3.27. These variations resulted in relatively small changes in the maximum pressures calculated.

3.3 Comparison of 26-Cell Results With 4- and 6-cell Results

The 26-cell containment representation was used for two distinct purposes in this work. The first was to compare with the results of the simpler 4- and 6- cell decks, in order to study the dependence of the results upon the nodalization used. The second is to study certain phenomena (especially hydrogen distribution and associated detonation threats) which cannot be realistically assessed using the simpler decks. The

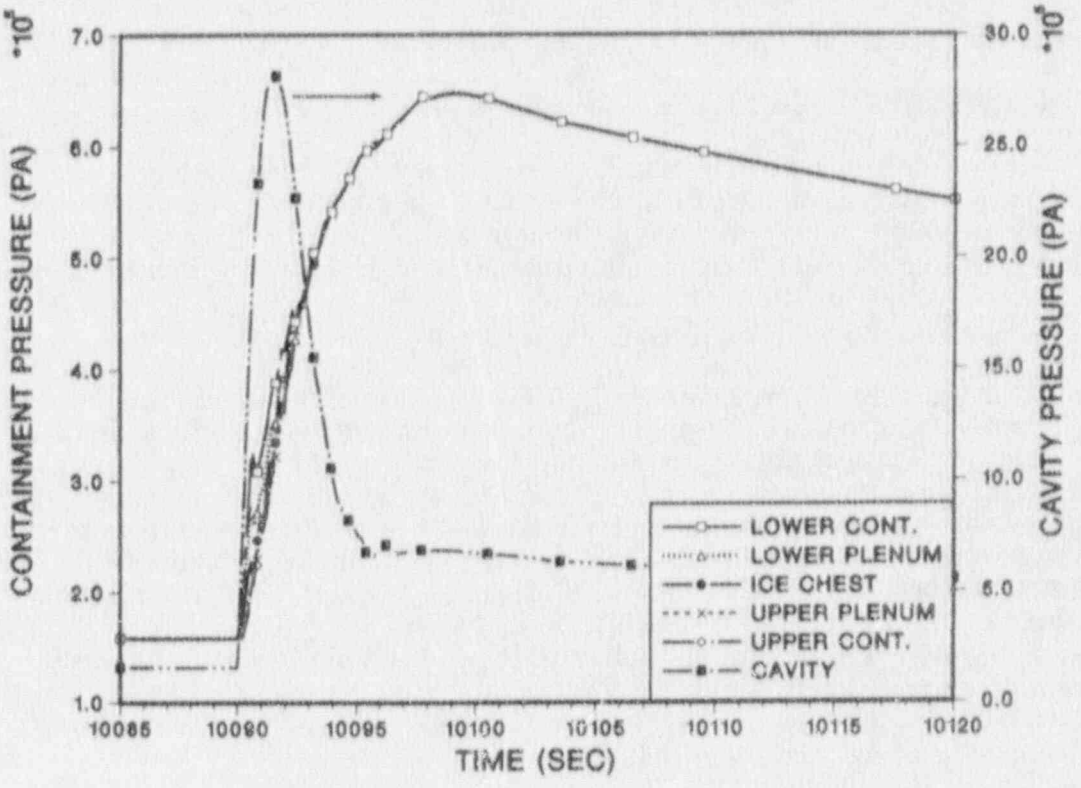

Figure 3.25 Containment pressures following VB calculated using the 6-cell deck, 50% corium participation.

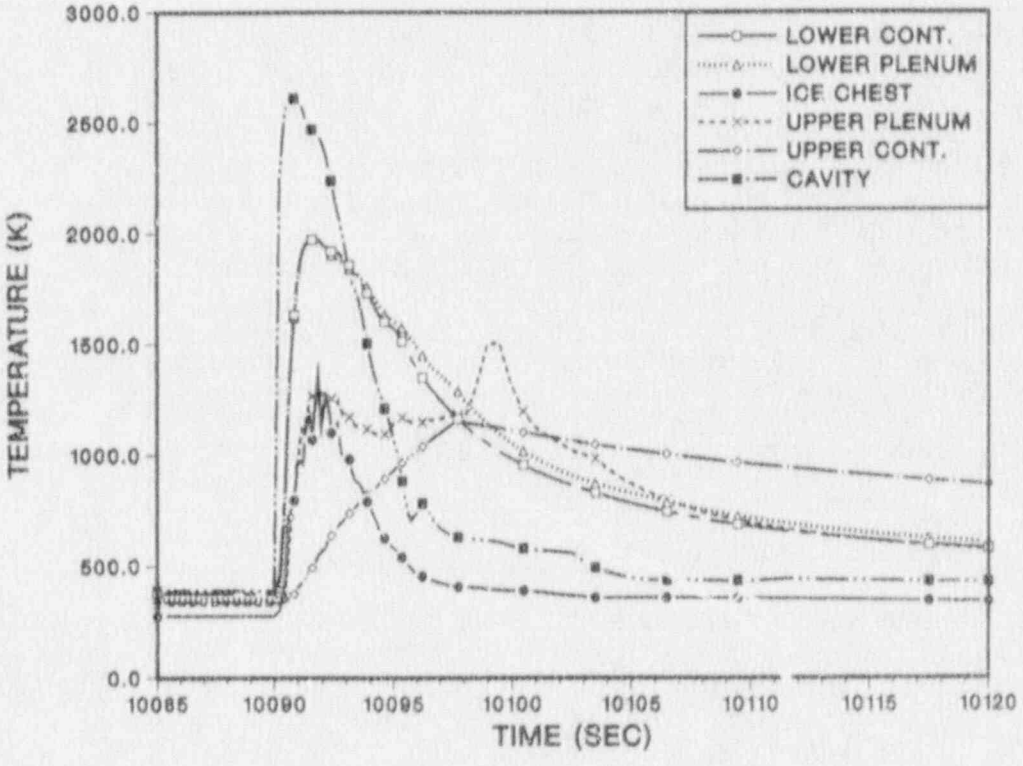

Figure 3.26 Containment temperatures following VB calculated using the 6-cell deck, 50% corium participation.

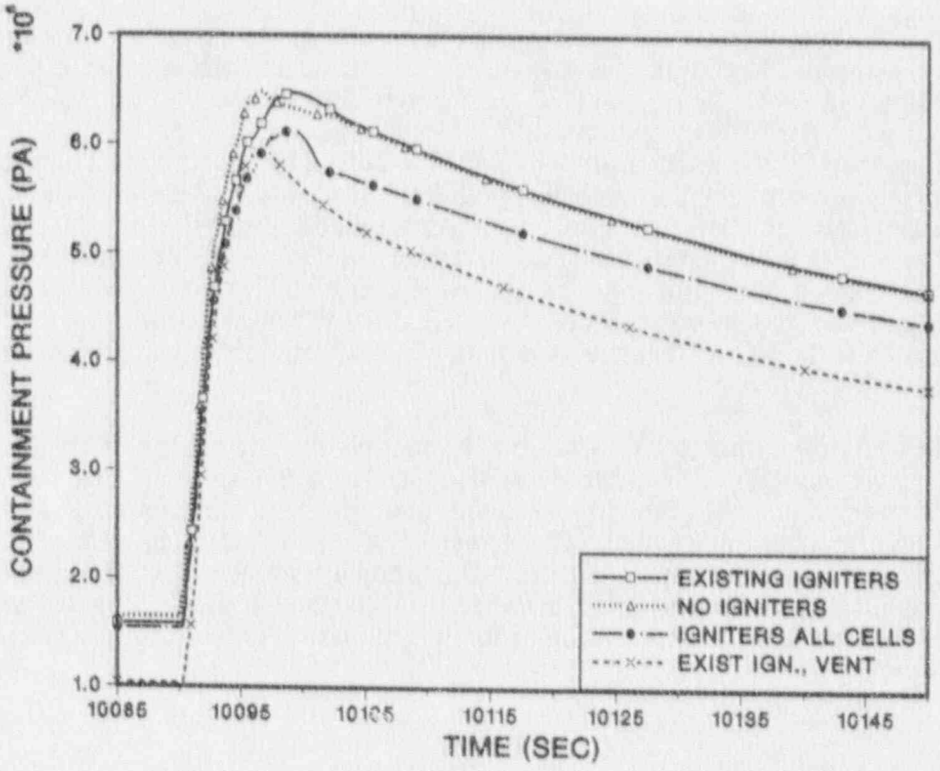

Figure 3.27 Effect of igniter operation prior to VB on containment pressures, 50% corium participation, 6-cell calculation.

first topic will be considered in this section, while the second wi" :e considered primarily in Section 5.

In order to minimize sensitivity to nodalization, judgments concerning the effectiveness of mitigation schemes in this work were always based upon calculations performed with the same containment nodalization. Hence, in the course of this study, it happened that similar scenarios were sometimes calculated using different nodalizations, and comparisons between these cases may be used to explore the degree of sensitivity to nodalization. In addition, a few calculations were run explicitly to provide additional comparison cas[illegible] section, comparisons will be made between results obtained using the d[illegible]lizations to calculate otherwise-similar (though not necessarily ident[illegible]os.

To some extent, this exercise r[illegible]ed as "benchmarking" the simpler decks, insofar as one is justified in assuming [illegible]nore detailed deck necessarily gives more accurate results. Such an assumption [illegible] often justified, but not always; some of the issues involved are discussed in connection with the comparisons that follow. Since the detailed deck is expensive to run, it is obviously desirable to determine when the simpler decks can be used without introducing substantial additional uncertainty.

3.3.1 Comparison of Maximum Pressures

Table 3.3 summarizes the pressures obtained for those cases in which two or more decks were applied to analyze scenarios which were sufficiently similar to permit useful comparisons for benchmarking the simpler decks. The first column gives a case number used in the following discussion, while the second column gives the corium fraction assumed. The third column gives the assumptions used concerning igniter availability. The fourth column indicates the assumptions made concerning hydrogen burn flame speeds in the upper and lower containment compartments (the default model flame speed was used in the ice condenser in all cases). The fifth column is used to note any other significant features of the calculation, while the last three columns give the maximum pressures calculated for the upper containment using the 4-, 6-, and 26-cell decks. Absence of an entry in the latter columns indicates that the case was not run.

One significant observation that may be made from the results in Table 3.3 is that the maximum pressures calculated using the 6-cell and the 26-cell decks are within 10% of one another in all six cases for which comparable problems were analyzed with the two decks. As already noted, differences between runs with the same deck are not to be regarded as being very significant unless they are greater than this, in part because such differences can arise as the result of details in the hydrogen combustion behavior that are known to be sensitive to chance factors and to modeling uncertainties.

Table 3.3

"Benchmark" Comparisons of 4- and 6-Cell Results with 26-Cell Results

Case No.	Corium Fraction	Igniters Powered	Flame Speed	Other Other	Max. Containment P (MPa) 4-Cell	6-Cell	26-Cell
BM-1	25%	None	Default	Note a	0.56	---	0.47
BM-2	25%	All	Default	Note a	0.55	0.44	0.43
BM-3	50%	None	5 m/s[b]	---	---	0.65	0.70
BM-4	50%	All	5 m/s[b]	---	0.71[c]	0.61	0.66
BM-5	50%	Existing	5 m/s[b]	---	0.71[c]	0.65	0.68
BM-6	50%	Existing	5 m/s[b]	Vented	---	0.60	0.58
BM-7	50%	Existing	5 m/s[b]	Depress.[d]	---	0.41	0.41

Notes:

[a] Ice condenser doors modeled as in Table 2.2; in all other cases, the 6-cell and 26-cell decks had doors modeled as in Table 2.4.

[b] 5 m/s flame speed specified for upper and lower containment; default model used in ice condenser.

[c] Represent the same calculation: the 4-cell deck has insufficient spatial resolution to distinguish the existing igniters case from the case with igniters in all cells.

[d] Station blackout sequence with intentional RCS depressurization.

The differences between the pressures calculated with the 4-cell deck and the other decks are somewhat larger, especially for Cases BM-1 and BM-2. In all cases, the 4-cell decks gives the higher pressures. One reason may be the absence of an upper plenum cell between the ice condenser cell and the upper containment cell. In the 4-cell deck, the hydroge..-rich ice condenser cell communicates directly with the oxygen-rich upper containment cell, and flows surging between these cells can tend to enhance the hydrogen combustion events in some cases (see Section 3.1.1). The presence of intervening upper plenum cells in the 6- and 26-cell decks may tend to moderate this behavior.

Such as they are, the differences between the 6-cell results and the 26-cell results are in the direction of the 26-cell deck giving somewhat higher pressures. Thus, the common supposition that coarser noding is necessarily conservative is not true in this case. The reason for this tendency is not fully known, although a contributing factor may be the uneven ice melt calculated to result from recirculation flows when the 26-cell deck is used (see Section 3.3.3). In any case, not too much should be made of these differences, in view of the sensitivities to relatively minor details that have been discussed in this work.

A more detailed comparison of the responses of the three decks is given for Cases BM-5 and BM-6 in Figure 3.28, in which pressure-time histories are plotted for all five calculations involved. Although deck-dependent differences are clearly present, they

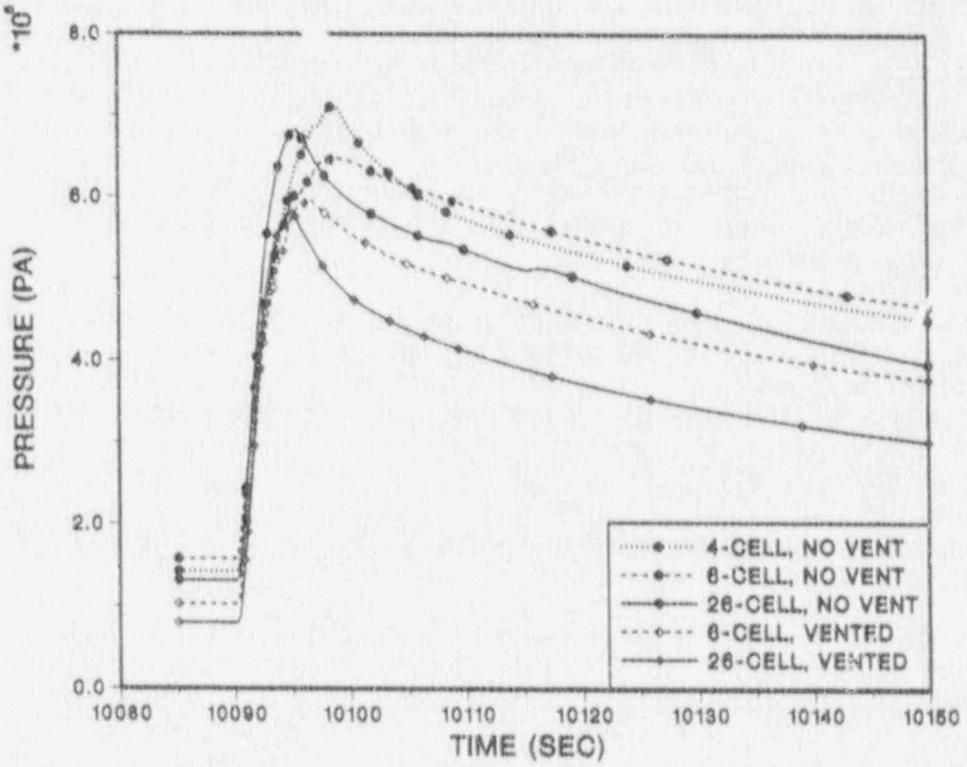

Figure 3.28 Comparison of pressure-time histories calculated with the 4-, 6-, and 26-cell decks, 50% corium participation.

are not very dramatic. Cases BM-3 and BM-4 exhibited slightly smaller differences in the shapes of the pressure-time curves, while the differences were greater for BM-1 and BM-2 but considerably smaller for BM-7.

The cases given in Table 3.3 permit comparisons illustrating the effects of dedicated power for the igniters, the effects of venting, and the effects of depressurization of the primary system. In no case would the conclusions to be drawn concerning the effectiveness of these mitigation strategies depend strongly upon which deck was used, although one might conclude that the benefits of containment venting were somewhat larger when the 26-cell deck is used rather than the 6-cell deck. In terms of the primary purpose of the present work, the lack of a strong dependence upon nodalization when assessing the various improvements may be the most important conclusion to be drawn from these comparisons.

3.3.2 Hydrogen Combustion Comparisons

In Figure 3.29, the cumulative quantities of hydrogen burned are plotted as a function of time for the period immediately following VB for all of the cases listed in Table 3.3. In terms of the containment pressurization, the most important quantity is the amount of hydrogen burned at this time, i.e., the amount by which the curves in the figure rise immediately following VB. (Burn location, i.e., lower vs upper containment, could also be very important; however, little combustion can occur in the oxygen-starved lower containment in these scenarios and therefore there is not much variation in burn location in the cases considered here.) Not surprisingly, the simpler decks give a larger quantity of hydrogen combustion following VB, with the effect being largest for the 4-cell deck. Differences between the 6-cell deck and the 26-cell deck range from essentially negligible (Cases BM-2 and BM-7) to a difference of about 130 kg in the amount of hydrogen burned following VB (Case BM-6, the vented containment case). The adiabatic isochoric combustion of this much hydrogen in a volume the size of the Sequoyah containment would yield a pressure rise of about 0.10 to 0.12 Mpa, depending upon the initial conditions. Hence, these differences in hydrogen combustion following VB are not negligible, although it should be remembered that the actual pressure rise due to a hydrogen burn can differ substantially from the adiabatic values.

It is not immediately obvious which representation is the most realistic in the present context, at least in comparing the 6-cell and the 26-cell results. (The 4-cell results are definitely believed to be less realistic, in part because of the absence of an upper plenum cell.) The 6-cell deck represents the entire upper containment (which includes about 60% of the total containment free volume) as a single cell. Immediately following VB, there is a rapid influx of hydrogen into this cell at an elevation higher than the cell center of volume. Use of a single cell to represent this volume is equivalent to assuming instantaneous mixing and can overestimate the coherence and magnitude of the resulting hydrogen burns.

In the 26-cell deck, the upper containment is somewhat artificially divided into two equivalent upper dome cells (6387 m^3 volume each) and a "lower dome" cell (5852 m^3 volume). Hydrogen and oxygen concentrations in these three cells are plotted as a function of time following VB in Figures 3.30a and 3.30b for the 26-cell calculations of Cases BM-5 (unvented containment) and BM-6 (vented containment), respectively. The solid and dashed curves represent, respectively, the hydrogen and the oxygen concentrations; concentrations for the two upper dome cells are portrayed by closed symbols while the curves with open symbols give the results for the lower dome cell.

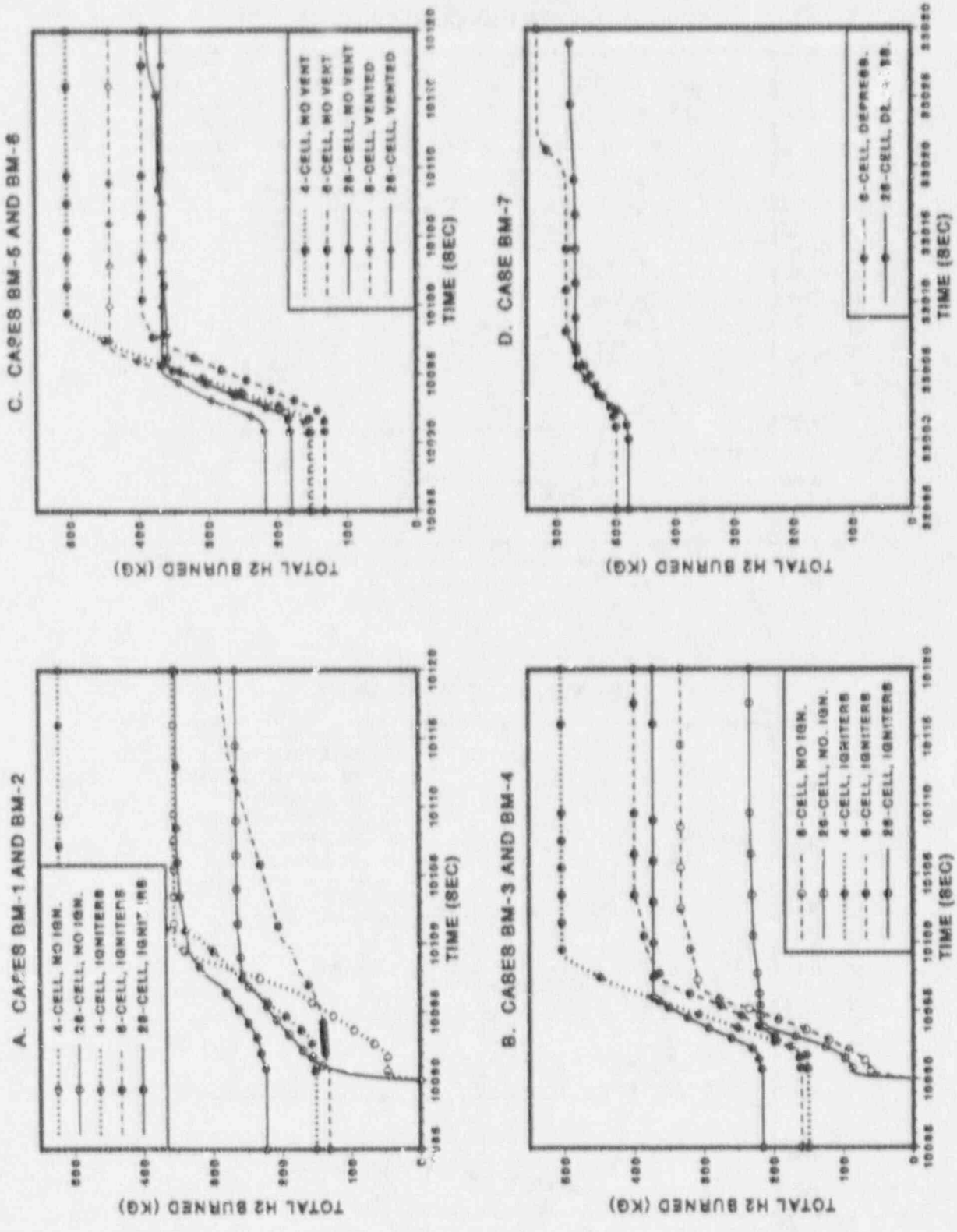

Figure 3.29 Comparison of cumulative hydrogen consumption for the 4-, 6-, and 26-cell decks, 50% corium consumption.

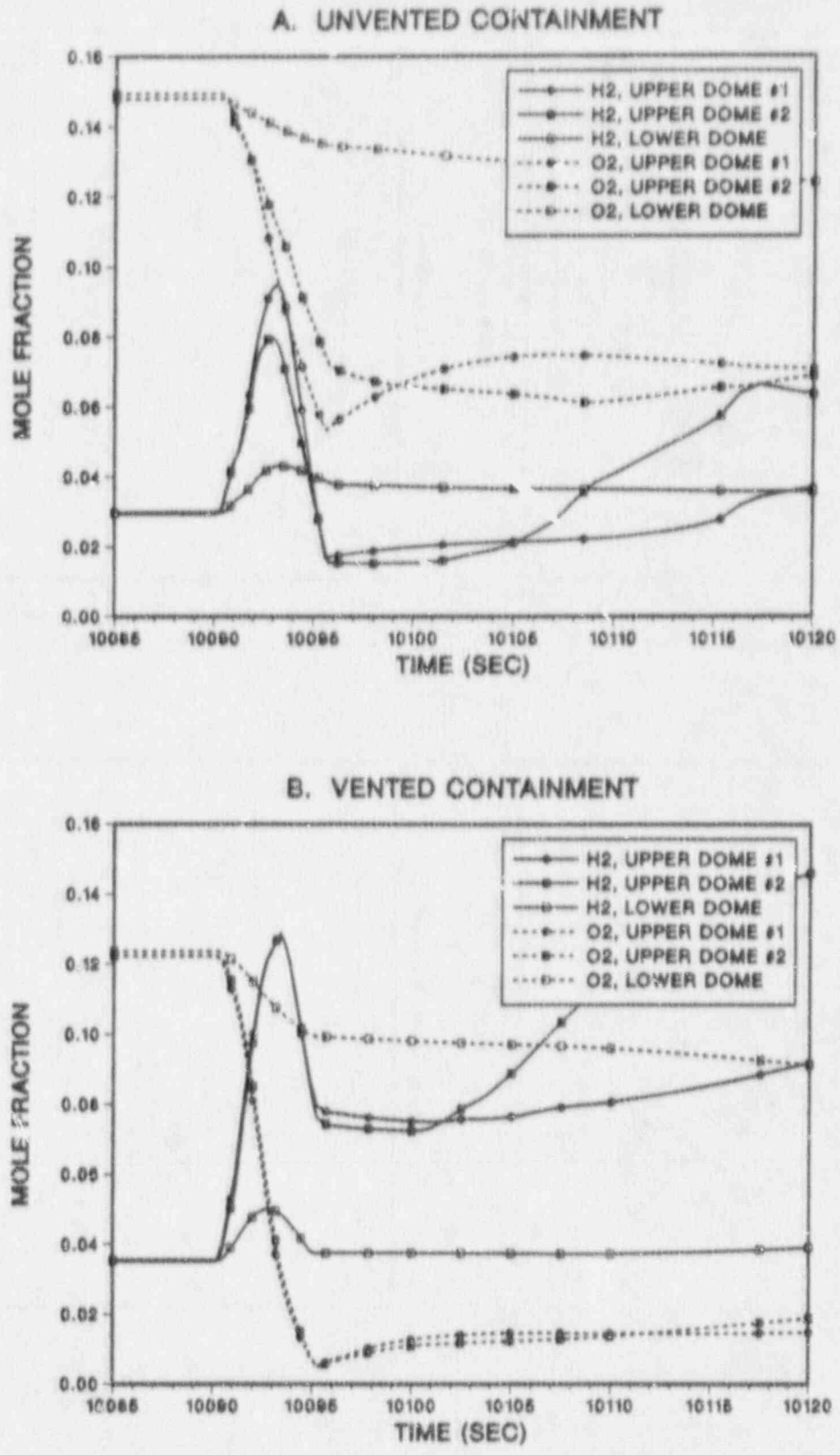

Figure 3.30 H_2 and O_2 concentrations in the upper containment calculated using the 26-cell deck, with and without containment venting.

Prior to VB, time scales are sufficiently long so that natural convection generally keeps the gases well mixed in these calculations, and the gas concentrations for all three upper containment cells are similar until VB at 10090 s. At this point, there is a rapid influx of hydrogen-rich gas from the upper plenum into both the upper dome cells, but not into the lower dome cell. Burns begin in the two upper dome cells once the ignition threshold of 7% is exceeded and the oxygen concentrations begin a rapid decline; hydrogen concentrations also decline rapidly once the rate of hydrogen influx drops below the rate of hydrogen combustion. Flammable concentrations do not develop in the lower dome cell and no burn occurs there. Gas concentrations in the lower dome cell do not vary rapidly; evidently, the calculated mixing rates between the upper and lower dome cells are too low to be effective on the time scales of interest.

In the unvented case, there is a considerable excess of oxygen in the upper dome and the hydrogen burns there are not oxygen-limited. However, some hydrogen does remain unburned in the lower dome cell. (In interpreting these results, it should be noted that the calculated temperatures of the upper dome cells reach 1500-1600 K while the lower dome temperature remains under 800 K; hence, the fraction of the total atmospheric mass residing in the lower dome cell is greater than the cell volumes given above would suggest.)

In the vented case, the behavior is similar except for one important difference: since considerable oxygen was purged from the containment during the time of venting, the burns in the upper dome cells are now oxygen-limited. In addition to the unburned hydrogen in the lower dome cell, there is now considerable unburned hydrogen remaining in the upper dome cells. At the same time, there is a large amount of oxygen remaining in the lower dome cell, adequate to consume the unburned hydrogen in the upper dome if mixing had been sufficiently rapid.

These results explain why hydrogen combustion immediately following VB is less in the 26-cell calculations than in the 6-cell results, and they explain why the effect is largest in the vented case. What they do not answer is the question as to which behavior is actually the more realistic. The elevation at which the hydrogen flows enter the upper containment from the upper plenum is about 5 meters higher than the boundary dividing the upper and lower dome cells in these calculations. As a result of the combustion, the upper dome gases quickly become very buoyant relative to the lower dome gases, and it is not at all clear that there should be a large amount of downward mixing into the lower dome volume under these conditions. Thus, the CONTAIN 26-cell results may be quite realistic. On the other hand, it remains true that the CONTAIN modeling does neglect some processes driven by momentum and turbulence effects which could enhance intercell mixing, and the possibility does exist that the CONTAIN calculations underpredict the degree of mixing, and hence underpredict the amount of hydrogen consumed.

The difference between the 6-cell and the 26-cell calculations provides one measure of the uncertainty in the amount of hydrogen combustion following VB, although factors other than those associated with the nodalization differences are also involved. On the other hand, one cannot directly estimate the resulting uncertainty in the pressures by comparing the results obtained with the two decks, since many other effects contribute to the differences in the pressures. (Indeed, the latter differences tend to be in the opposite direction from what one would expect from the hydrogen combustion differences alone.) A useful sensitivity study might be to renodalize the 26-cell deck to represent the entire upper containment with a single cell, but this has not been done in the present work. In the mean time, a bound on the associated

uncertainty in pressure can be estimated from the adiabatic pressure rise for hydrogen combustion that was noted above.

Before leaving this subject, one other factor which may contribute to the reduced hydrogen combustion immediately following VB should be noted. From Figure 3.29, it is evident that, in the cases involving igniters, the 26-cell deck generally indicates more hydrogen combustion prior to VB than do the simpler decks. This combustion occurs in the ice condenser and, sometimes, in the lower containment; except for the depressurized RCS case (Case BM-7), flammable conditions do not develop in the upper containment prior to VB, given operational igniters. The reason for the greater amount of pre-VB combustion in the 26-cell calculations likely involves the improved hydrogen-oxygen mixing in the ice condenser region due to the recirculation flows modeled in this deck. In any event, it is obvious that hydrogen burned off prior to VB cannot contribute to the combustion events following VB. Insofar as this effect contributes to the differences between the 6-cell and the 26-cell calculations, the latter are considered to be the more realistic.

3.3.3 Comparison of Ice Condenser Responses

The ice condenser plays an important role in the calculations performed for this work. By condensing superheated steam, and by serving as an effective heat sink, it substantially mitigates the maximum loads that would otherwise be calculated in DCH events [Wi87]. On the other hand, steam condensation in the ice condenser generally prevents steam inerting of the upper containment and thus favors hydrogen combustion events. Since ice condenser response can be affected by recirculation flows that can be studied only with the 26-cell deck, it is of interest to compare ice condenser response as evaluated with the various decks. Two questions will be considered here: the dependence upon nodalization of the total amount of ice melted, and the degree of nonuniformity of ice melting as evaluated with the more detailed deck.

Total Ice Melted. In Figure 3.31a, the height of the remaining ice column (proportional to ice mass remaining unmelted) is plotted as a function of time for Cases BM-1 and BM-2 in Table 3.3. In the figure, curves calculated using the same deck have the same line type while curves calculated for the same scenario are plotted with the same plot symbol. For the 26-cell deck, the values plotted are the average of the heights of the four ice columns used to represent the ice condenser. Figure 3.31b gives equivalent information for Cases BM-5 and BM-6.

In all cases, there are three periods of relatively rapid ice depletion, separated by periods in which ice melt is slower. The first two periods of rapid ice melt reflect periods of rapid steam influx from the primary system (see Figure 2.4), while the third results from the DCH event itself. During the second period of high steam influx, at around 9500 s, there is also a strong hydrogen source. When igniters are operational, hydrogen burns in the ice condenser augment the ice melting somewhat (compare BM-1 with BM-2).

Ice melt calculated by the 4-cell and the 6-cell decks are fairly similar for those cases in which both decks were run. In Cases BM-1 and BM-2, the amount of ice melted as calculated by the 26-cell deck is substantially greater than the amount calculated using the simpler decks. On the other hand, differences between the decks are very minor for Cases BM-5 and BM-6, as well as for the other cases listed in Table 3.3.

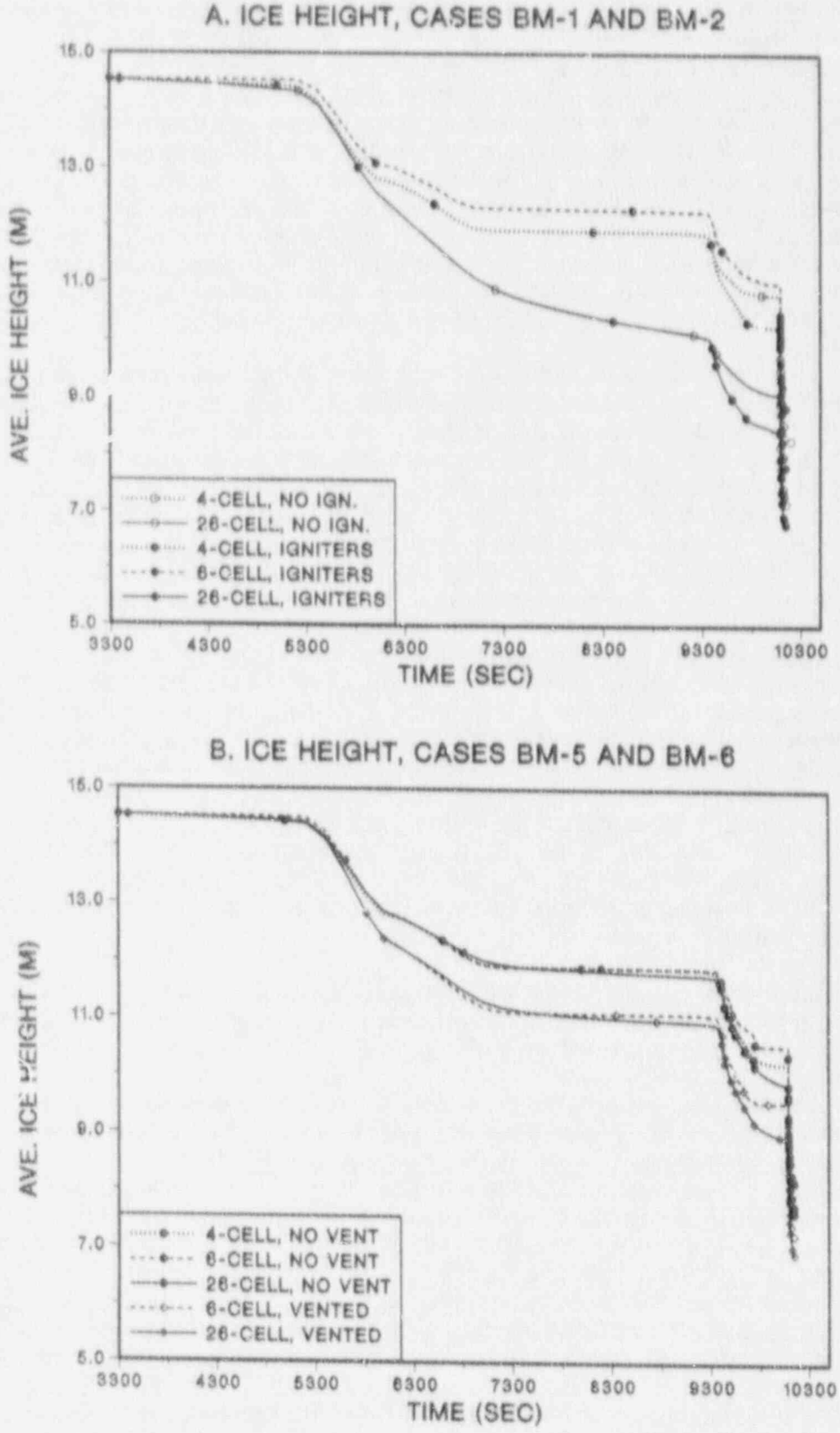

Figure 3.31 Comparison of ice melting rates for the 4-, 6-, and 26-cell decks in selected cases.

These differences reflect differences in the way the lower plenum ice condenser doors were modeled. In Cases BM-1 and BM-2, the doors were modeled as being (approximately) 50% reversible and 50% irreversible flow paths, as in Table 2.2. Once partially opened during periods of high steam flow, they would only reclose until the opening was about 50% of the maximum opening previously achieved; further closure would not occur. With the doors remaining partially open, considerable recirculation was calculated to occur between the ice condenser, the lower plenum, and the lower containment in the 26-cell calculation. The recirculation accelerated the transport of steam from the lower containment to the ice condenser and thereby reduced steam condensation on the lower-containment heat sinks and enhanced it in the ice condenser, much as if the air return fans had been operating (Section 3.2.3). This recirculation flow cannot be modeled with the simpler decks.

In the other cases listed in Table 3.3, the door modeling was changed to that described in Table 2.4, so that the lower plenum doors would almost fully reclose in the absence of a forward pressure, which largely eliminated the recirculation flows between the lower plenum and the lower containment. With the 26-cell deck, recirculation was still calculated to occur within the plena and the ice condenser, but this recirculation had little effect upon the amount of steam transported into the ice condenser and, hence, had little effect upon the total amount of ice melted. As a result, the total ice melt calculated using the 26-cell deck did not differ significantly from that calculated using the simpler decks.

Uneven Ice Melting. Additional insight is obtained by examining the amount of ice melted in each of the four columns used to represent the ice condenser in the 26-cell deck. Results for the 26-cell calculation in Case BM-2 are given in Figure 3.32a. The solid curves represent the ice column height in each of the four columns, while the dashed and dotted curves give, respectively, the average height for the 26-cell calculation and the 6-cell ice column height. In this case, the 26-cell calculation not only gives substantially greater total ice melting, but also gives a quite uneven distribution in the ice melting. The recirculation patterns varied from case to case, but the general tendency was for warm, steam-laden gas to rise into the center columns and chilled gas to descend in the end columns, thereby producing the preferential melting of the center columns.

Figure 3.32b gives equivalent information for Case BM-5. Even though the recirculation flows do not result in increased total ice melting for this case, they still produce a quite uneven pattern of ice melting.

At the time of vessel breach, the central two ice columns are over 50% melted in both the cases considered in Figure 3.32, while the end columns are almost unscathed. It is possible that such an uneven pattern to the ice melt prior to VB could significantly reduce the ability of the ice condenser to mitigate DCH pressure rises. Indeed, this effect may be one reason why the 26-cell deck does not show lower DCH pressures than the 6-cell deck, even though the contribution of hydrogen combustion following VB is smaller for the 26-cell deck (Section 3.3.2). Sensitivity studies could be defined to investigate this question further, but no such studies were performed in the present work. In their absence, conclusions concerning the importance of the uneven ice melting to DCH loads remain rather speculative.

Some additional details of the recirculation flows are discussed in Section 6 of this report, in connection with their effects upon gas distributions and the detonation issue.

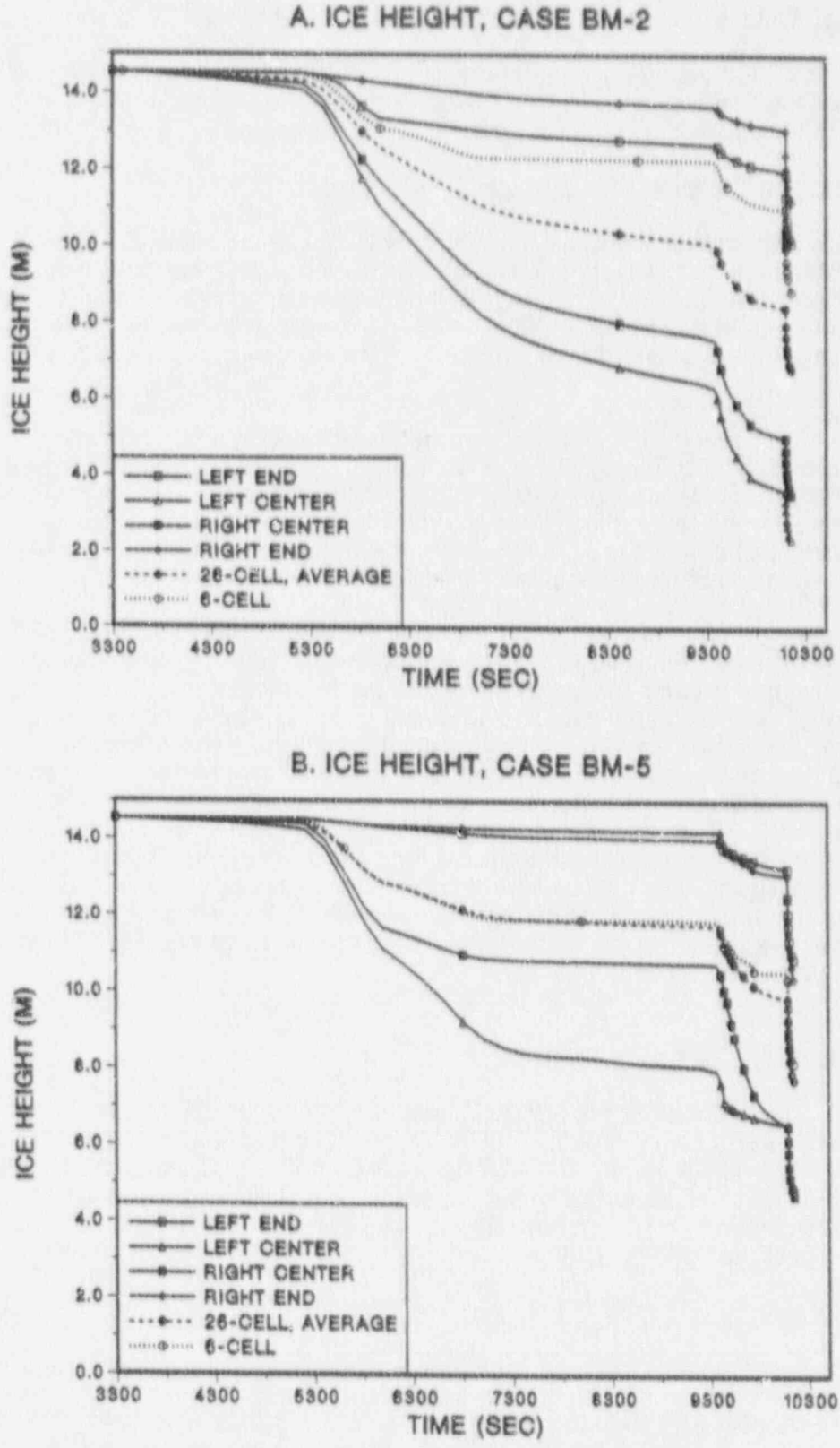

Figure 3.32 Distribution of ice melting calculated by the 26-cell deck in selected cases, illustrating the unevenness in the melting.

In Ref. Di85, some HECTR code analyses of the Sequoyah plant were reported for selected accident sequences. In that work, the ice condenser was nodalized vertically as well as azimuthally, with a total of 16 ice condenser cells being used. Uneven ice melt patterns qualitatively very similar to those observed here were reported in that work also, with essentially the same reasons being involved.

3.3.4 Summary, "Benchmarking" of the Simpler Decks

Where comparable scenarios have been analyzed with both decks, the differences in pressures calculated using the 6-cell and the 26-cell decks were quite small (< 10%). Pressures calculated using the 4-cell deck were somewhat greater, but were still not large enough to substantially affect any of the conclusions that might be drawn from the results concerning the effectiveness of the various mitigation schemes considered.

Despite the generally-reassuring pressure comparisons, a more detailed examination of the 6-cell and the 26-cell calculations reveals significant differences in such output parameters as total hydrogen burned following VB and ice melt behavior. In principle, at least, these differences could have impacts upon the calculated pressures somewhat larger than the pressure differences that were actually observed. Partial cancellation of opposing effects may be involved.

When the primary parameter of interest is the maximum containment pressure calculated, it is concluded that use of the simpler 6-cell deck is justified in view of the substantially greater computational expense of the 26-cell deck, as well as the greater complexity of evaluating the results. Somewhat more caution is required in interpreting the results than might be assumed based upon a consideration of only the pressure differences summarized in Table 3.3. It should also be remembered that the 26-cell results have their own uncertainties and are not necessarily superior in all respects to the 6-cell results. The 4-cell deck is believed to be inferior to the other two and was little used in this work once the latter became available. Nonetheless, use of the improved decks has not revealed any reasons for rejecting conclusions offered concerning the mitigation schemes that were originally assessed using the 4-cell deck; hence, these assessments were not repeated using the improved decks, other than for the spot checks considered in this section.

3.4 Results of 26-Cell Calculations

Maximum containment pressures calculated applying the 26-cell deck to the fully-pressurized scenario are summarized in Table 3.4. The meaning of the various column heads is as described in connection with previous tables. The discussion here will generally be kept brief, since the major use of the 26-cell calculations was to assess hydrogen distribution and detonation threats, and discussion of these questions is deferred to Section 5 of this report.

3.4.1 25% Corium Participation Fraction

The first eleven cases in Table 3.4 assume a 25% corium participation fraction. The present work represents the first time that decks larger than a few cells have been used with the CONTAIN code to analyze ice condenser plants, and many of the 25% cases summarized in Table 3.4 represent exploratory runs carried out to gain understanding of the code response using this deck and the potential effects of such features as the details of ice condenser door modeling and convective flow modeling.

Table 3.4

Results of 26-Cell Calculations, Fully Pressurized RCS

Case No.	Corium Fraction	Igniters Powered	Other	Max. P (MPa)
1	25%	None	Note a	0.47
2	25%	All	Note a	0.43
3	25%	---	No hydrogen burns, Note a	0.34
4	25%	All	Note b	0.42
5	25%	All	Note c	0.45
6	25%	All	Note d	0.41
7	25%	None	All doors fully reversible	0.46
8	25%	None	Note b	0.45
9	25%	None	5 m/s flame speed, Note b	0.46
10	25%	None	Note d	0.47
11	25%	None	Note e	0.46
12	50%	None	Note e	0.70
13	50%	Existing	Note e	0.68
14	50%	Exist + l.p.	Note e	0.65
15	50%	All	Note e	0.66
16	50%	Existing	Fans, Note e	0.73
17	50%	Existing	Vented, Note e	0.58
18	50%	All	Vented, Note e	0.55
19	50%	Existing	Fans, Vented, Note e	0.64

Notes:
[a] Doors modeled as in Table 2.2. Where not otherwise noted, doors were modeled as in Table 2.4.
[b] Lower plenum doors reversible except for an area of 2.2 m^2.
[c] Cells connected center-to-center in calculating gravitational heads.
[d] Lower plenum doors fully reversible.
[e] 5 m/s flame speed used in upper containment and lower containment, default model flame speed in the ice condenser.

Some of the cases involving ice condenser door modeling were found to have significant impacts upon hydrogen distribution and will be discussed in more detail in Section 5. Other cases involve somewhat arcane features of the CONTAIN code whose detailed explanation would involve more verbiage than value; they are listed in Table 3.4 to show that they had little impact upon the calculated pressures and will otherwise receive little discussion.

In general, the pressures reported in Table 3.4 are similar to those reported for the 25% corium cases calculated using the 6-cell deck in Table 3.2, albeit tending to lie near the lower end of the latter range. Comparison of otherwise-similar cases with and without igniters (Case 1 vs 2, 4 vs 8, and 6 vs 9) shows that installing powered igniters in all cells would not result in large benefits here, in agreement with previous results. Imposing a flame speed of 5 m/s in place of the default model correlations for flame

speed had no significant effect (Case 8 vs Case 9). Impacts of the other variations considered were all quite minor.

Case 3 represents a phenomenological sensitivity study in which the CONTAIN hydrogen burn model was deactivated; not surprisingly, pressures were significantly reduced, although not as much so as in the cases involving full inerting (Section 3.1.5). Disabling hydrogen combustion is not equivalent to inerting, since metal-oxygen reactions and the so-called "hydrogen recombination" feature of the CONTAIN DCH model are still active. The latter feature involves the assumption that hydrogen produced by metal-steam reactions in any cell will immediately react with oxygen if any is available in that cell, independently of the normal hydrogen burn model.

3.4.2 50% Corium Participation Fraction

Cases 12-19 in Table 3.4 were calculated assuming 50% corium participation. In all cases, modeling of the ice condenser doors was as summarized in Table 2.4. In particular, given an adequate back pressure, the lower plenum doors could fully reclose unless they had been forced open to their maximum extent, in which case it was assumed that deformation of the crushable hinges would pin the doors open. In the present calculations, this did not happen until the time of VB in the cases without igniters. In the cases with igniters, pressure surges associated with hydrogen burns did sometimes result in the lower plenum doors being pinned open in this fashion.

Cases 12-15 reflect the impact of different assumptions concerning the availability of igniters. Pressure-time histories are plotted in Figure 3.33 for these cases along with the results for Case 11, which is a 25% corium case otherwise similar (not identical) to Case 12. As in the 25% cases, providing power for the igniters did not confer large benefits, either for the existing igniter system (Case 13) or for possible enhanced igniter systems (Cases 14 and 15). (Large effects on the calculated pressures were not expected for these variations; the motivation for running them was to explore their implications for detonation threats in the ice condenser.) Certainly the effects of igniter operation are quite minor compared with the impact of the uncertainty in the corium participation fraction (25% cases versus the 50% cases).

Cases 16-19 (Figure 3.34) explore the implications of various combinations of mitigation systems involving igniters, air return fans, and containment venting. The most favorable combination found involves venting and operating igniters in all cells (Case 18), although venting combined with power for the existing igniter system (Case 17) is almost as favorable. Even for these cases, the calculated pressures are somewhat higher than the median of the NUREG-1150 uncertainty distribution for the Sequoyah containment failure pressure; thus, the calculated threat to containment integrity remains substantial. Operating the fans tends to increase the maximum loads calculated, not decrease them (Case 16 versus Case 13, Case 19 versus Case 17).

There are a number of factors which could affect the DCH loads when the fans operate. One is enhanced steam condensation which lowers the base pressure (i.e., the pressure at VB); this effect should reduce maximum pressures somewhat. On the other hand, fan operation increases oxygen supply in the lower containment, which could enhance the DCH energy release. Fan operation also enhances ice melt, which will tend to increase the loads.

Unmelted ice remaining is plotted as a function of time for selected cases in Figure 3.35. Operating the existing igniter system (Case 13, Table 3.4) increases ice melt slightly after about 9300 s due to the onset of hydrogen burns in the ice

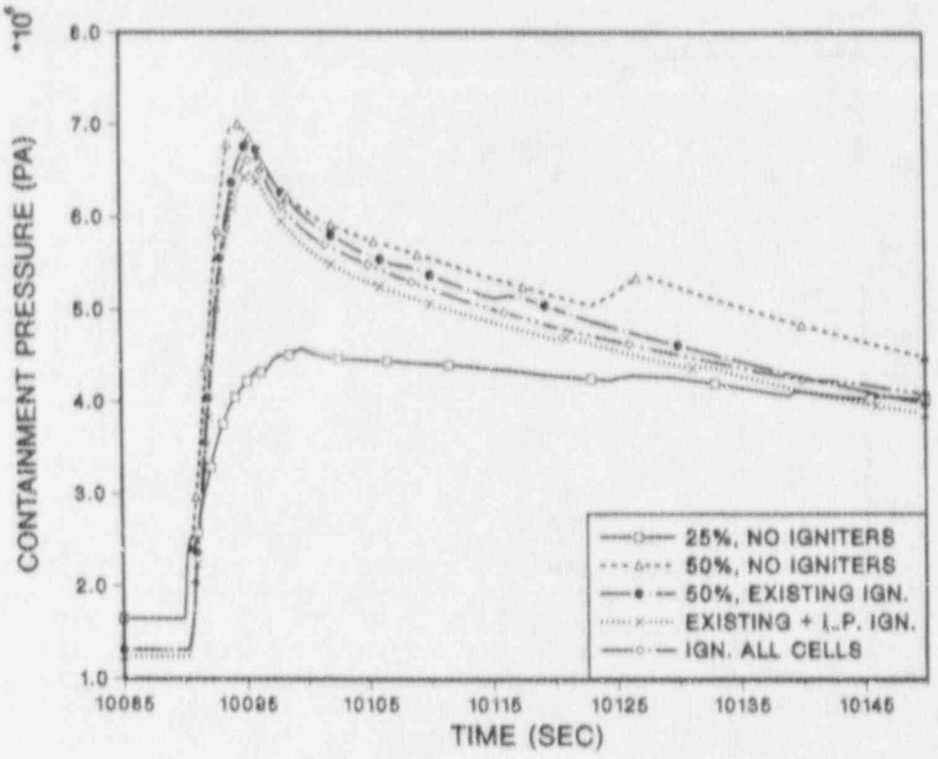

Figure 3.33 Effect of corium participation fraction and effect of igniters on containment pressurization, 26-cell deck.

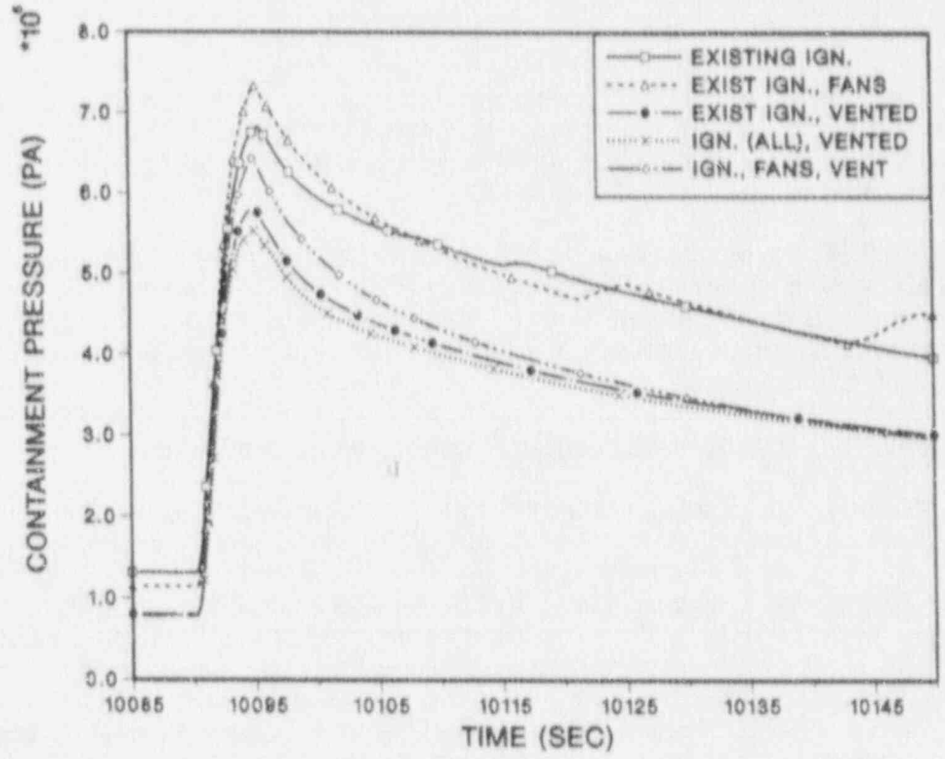

Figure 3.34 Effect of various combinations of igniters, fans, and containment venting, 26-cell deck, 50% corium participation.

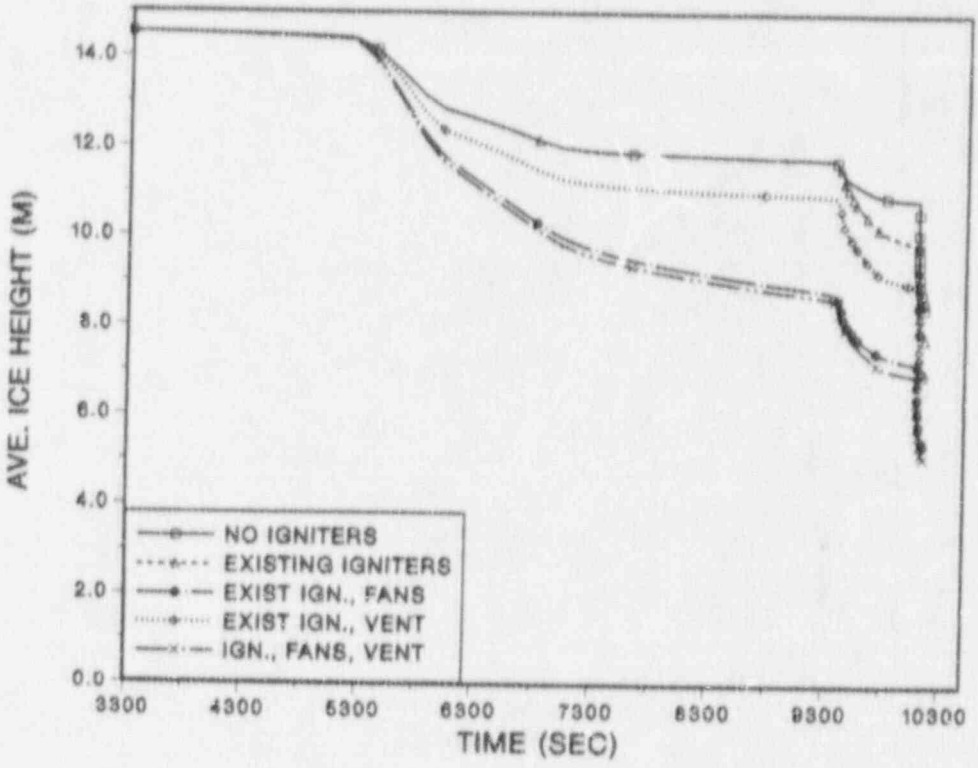

Figure 3.35 Effect of igniters, fans, and venting on rate of ice melting.

condenser, but this effect is minor. Fan operation (Case 16) has a much larger effect. Venting by itself (Case 17) enhances ice melting somewhat, while venting combined with fan operation (Case 19) has about the same effect on ice melting as does fan operation by itself.

In Figure 3.36, the height of each of the four ice columns modeled is plotted for the case with existing igniters and fans operating (Case 16). The ice melting is still quite uneven; evidently, the forced flow produced by the fans is not sufficient to overcome the recirculation flows in the ice condenser. Similar conclusions were reached in Ref. Di85.

3.5 Hydrogen Mass Balance and Post-DCH Containment Conditions

The calculations discussed in this work were not extended out beyond one to two minutes after vessel breach. In terms of assessing the immediate threats of the DCH event itself, this is more than ample, since this time is well past the time of maximum containment pressures. However, the CONTAIN-DCH calculations predict that DCH events may be accompanied by the generation of very large amounts of hydrogen, and much of this hydrogen remains unburned at the time these calculations were terminated. Detailed study of the fate of this hydrogen would involve a substantial effort and it has not been included in this work. It is, however, worth considering the conditions which exist at the time the calculations are terminated in order to gain some insight as to the various possibilities.

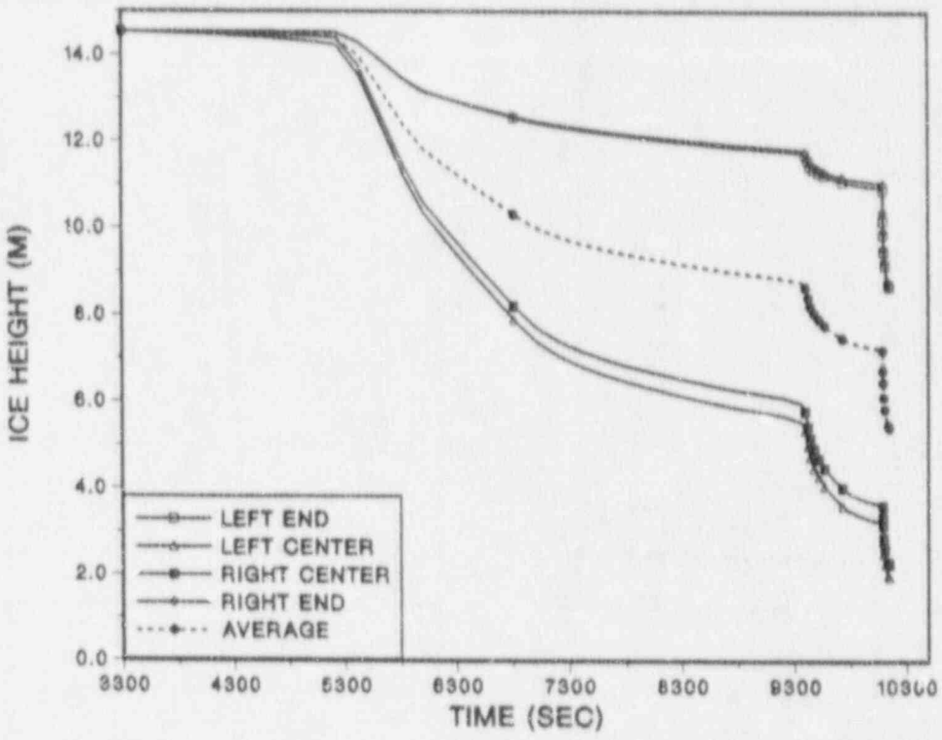

Figure 3.36 Distribution of ice melting calculated with fans and igniters operating.

The case to be considered is Case 8 of Table 3.2, the 6-cell calculation with 50% corium participation and with existing igniters operating. In the present discussion, we assume that the containment survives the DCH event itself. Pressure and temperature histories for this case have already been given in Figures 3.25 and 3.26, respectively. Steam, hydrogen, and oxygen concentrations are plotted in Figures 3.37a-3.37c for all cells except the cavity cell, which is too small to matter; ice remaining is plotted in Figure 3.37d. As might be expected, oxygen is largely limited to the upper containment, while hydrogen is heavily concentrated in the ice condenser. The vessel blowdown lasts longer than the period of metal-steam reactions during DCH, and the continuing blowdown moves much of the hydrogen produced into the ice condenser, where the steam condenses and the hydrogen remains at high concentrations. Even at the time the calculation ends, slightly over half the original ice mass remains unmelted in the ice condenser, and it is still quite effective in condensing steam.

Hydrogen mass balance information is plotted in Figure 3.38, along with the oxygen mass remaining in the atmosphere (right-hand axis). The hydrogen quantities plotted are the total hydrogen mass in the containment atmosphere, the cumulative amount produced by metal-steam reactions during DCH, the cumulative amount burned (including that burned before VB), and the amount entering from the vessel during the blowdown following VB.

During the DCH event, over 1000 kg of hydrogen is produced, almost all of it within the first 5 seconds following VB. At the end of the calculation, there is still a very large amount of unburned hydrogen, about 1200 kg, remaining in the containment. Over half of this resides in the ice condenser, and most of the remainder is in

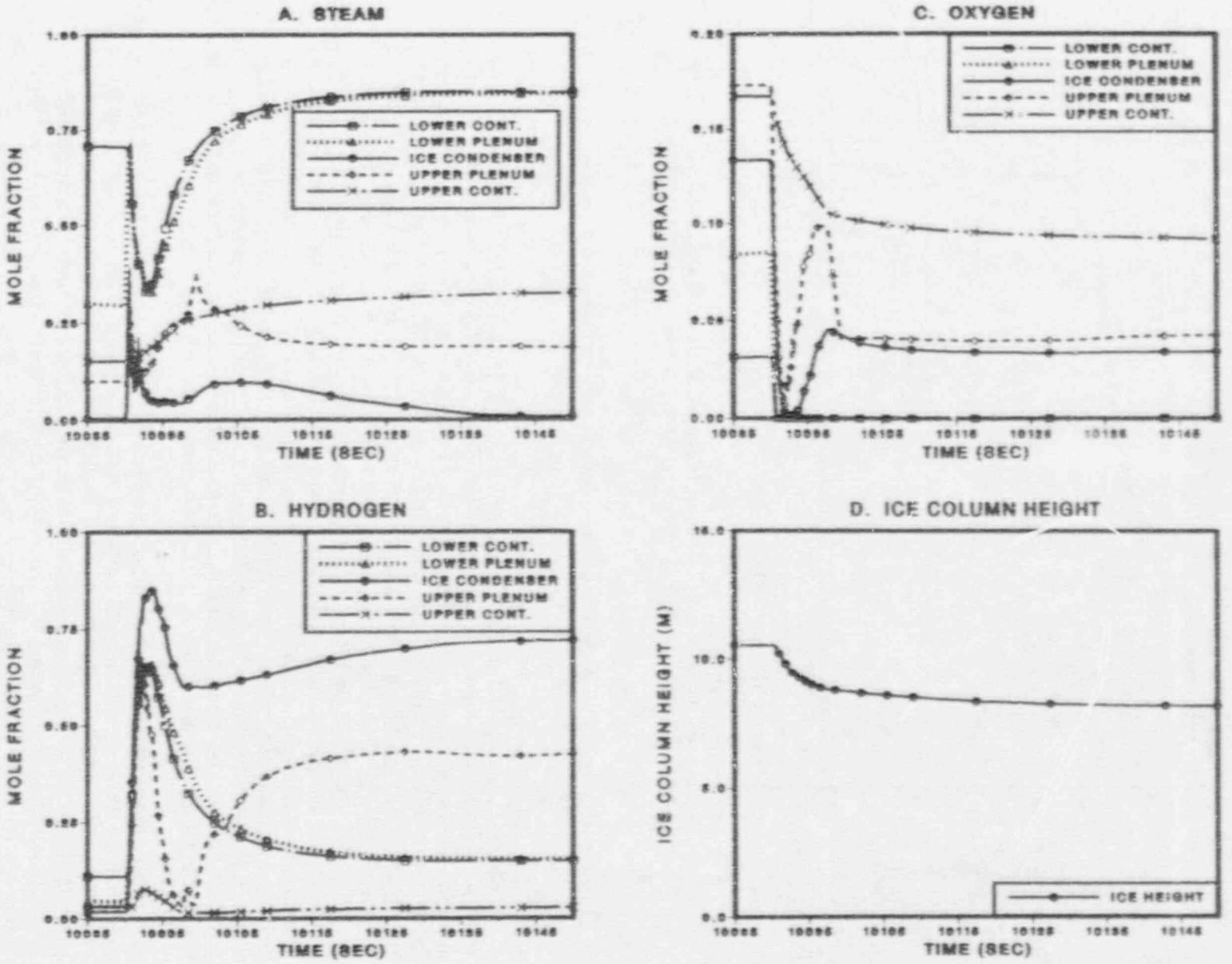

Figure 3.37 Atmospheric compositions and ice remaining following a DCH event with 50% corium participation, 6-cell deck, igniters operating.

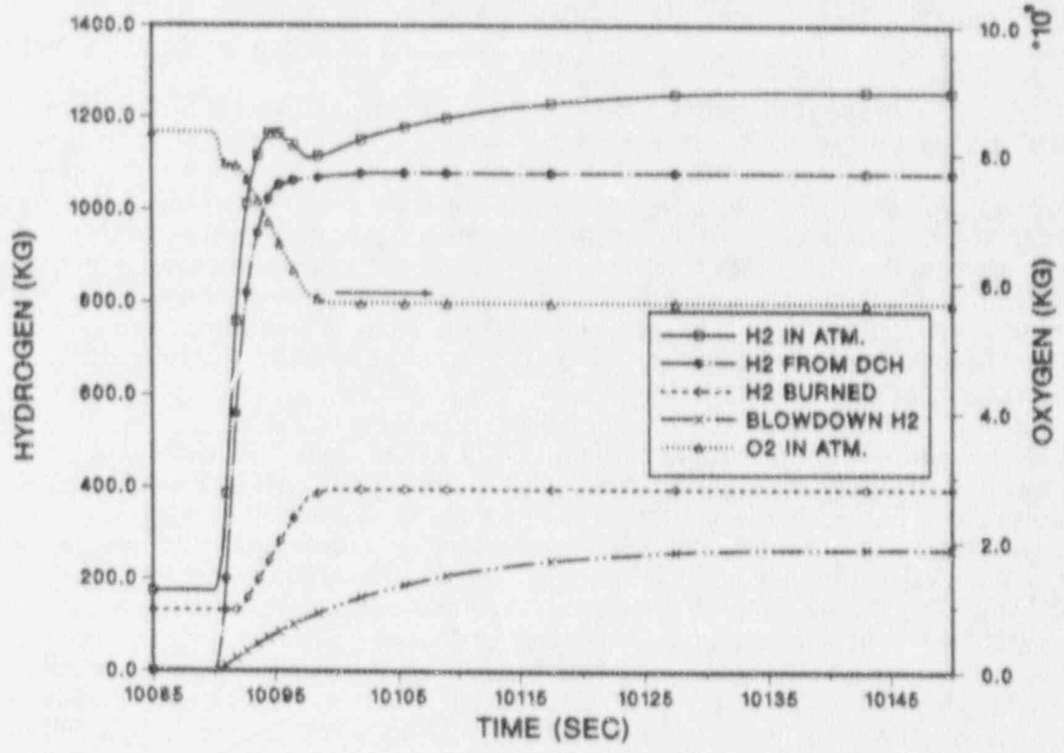

Figure 3.38 Hydrogen mass balance and oxygen inventories, during and immediately after the DCH event of Figure 3.37.

the lower containment. At the end of the calculation, temperatures in the lower containment and the ice condenser plena have recovered to the 400-500 K range, and the ice condenser temperature itself is under 300 K. The upper containment temperature, however, is still over 700 K, reflecting the much lower surface/volume ratio of the upper containment. Containment pressures are therefore still quite high, about 0.47 MPa.

Although the combustion of hydrogen figures prominently in DCH calculations for ice condenser plants, this combustion is actually quite inefficient in the sense that the total consumed during the event, about 260 kg, is under 20% of the total that was potentially available. Containment compartmentalization, with the hydrogen largely kept separate from the oxygen in the upper containment, is the principal reason for this inefficiency.

It might seem surprising that more hydrogen is not transported to the upper containment and burned, but the result is consistent with the sequence of events as calculated by the code. From Figure 3.26, it may be seen that the ice condenser atmospheric temperature goes through a high temperature excursion, but it recovers quite quickly. Pressures in the ice condenser are essentially the same as the containment pressure elsewhere, which is high, up to 0.65 MPa. As the vessel blowdown continues to force the lower containment steam-hydrogen mixture into the ice condenser, the steam is largely condensed. The combination of high pressure,

relatively low temperature, and the ability to condense out the steam allows the ice condenser to act as a fairly effective "trap" for retaining hydrogen, in the short run.

At the end of the calculation, total oxygen in the containment is 5700 kg, about 60% of the inventory prior to any combustion events, with the large majority of it residing in the upper containment. This oxygen is sufficient to burn over 600 kg of the remaining hydrogen. Clearly, a major combustion event could still occur if there were any way to rapidly mix the hydrogen with the remaining oxygen. Note that this conclusion would be true even if, as is likely, the present case turns out to be on the conservative side in connection with the total hydrogen produced during DCH. Since the maximum burn possible is oxygen-limited (by a factor of two), hydrogen production would have to be reduced by a large amount to make a significant reduction in the burn potential.

Vessel blowdown is complete by the time the calculation ends, and no other driving force for rapid mixing is apparent. Thus, mixing on short time scales seems quite unlikely. On the other hand, there are a number of mechanisms for producing mixing on intermediate to long time scales. As the upper containment continues to cool, and pressures decline, some of the hydrogen in the ice condenser will flow upward into the dome region. Furthermore, in the present calculation, the ice condenser intermediate deck and upper plenum doors were forced open beyond the point where they would fully close, although this did not occur to the same extent in all the DCH calculations. If the doors do stay partially open, fairly rapid countercurrent exchanges could mix the gases to some extent because the ice condenser hydrogen concentrations are so high that the ice condenser atmosphere will be less dense than the upper containment atmosphere except when the latter is quite hot.

Over time scales of hours, circulation involving the ice condenser bypass flows could produce substantial mixing (see Section 4.3). Other long-term driving forces for mixing might include steam generated by radionuclide decay heat associated with the dispersed debris in the lower containment, and core-concrete interactions involving the 50% of the core that did not participate in DCH. Sooner or later, mixing of the containment gases is likely to occur.

One key uncertainty complicating the analysis involves the availability of ignition sources during the period of mixing. After the DCH event, it may not be meaningful to equate ignition source availability with availability of operating power for the igniters. Even if the igniters were initially powered, they might not survive the harsh DCH environment. On the other hand, with or without igniters, the DCH event and associated hydrogen burns might start fires within those parts of the containment which still contain oxygen, and some of these fires might smolder for a long time. Given the availability of ignition sources, there would still be important questions concerning the hydrogen combustion mode. For example, it might tend to burn off continuously as it enters the upper containment.

A careful study of the long-term behavior following DCH would be a substantial, though interesting, task. Modeling of decay heat and core-concrete interactions would be needed. The detailed 26-cell deck would be required for at least part of the analysis. One reason is that it is likely that some or all of the ice condenser doors would fail to reclose fully after the DCH event, and recirculation flows through the open doors cannot be modeled without the more detailed deck. As long as ice remains, such recirculation flows would be very important. For example, in Section 5.2, it is shown that recirculation flows through jammed-open lower plenum doors can

be almost as effective as operating the air return fans in re-inerting the lower containment in some situations.

Without additional analyses of the post-DCH behavior, any judgments as to the eventual outcome of this scenario would be little more than unsupported speculation. There are a number of phenomena, ranging from benign combustion modes to containment inerting, which could prevent a significant threat from ever developing. On the other hand, it is clear that a chemical energy source large enough to be potentially dangerous is still present in the containment atmosphere at the point where the analysis performed in the present work is terminated.

4. MITIGATION OF DCH/DEFLAGRATION LOADS WITH RCS DEPRESSURIZATION

4.1 Introduction

In this section, station blackout accidents in which the reactor coolant system (RCS) is depressurized to about 1.5 MPa at vessel breach (VB) will be considered. The specific accident sequence considered is based upon calculations performed at INEL with the SCDAP/RELAP code and involves intentionally latching open the PORV in order to achieve depressurization. However, it is important to bear in mind that, according to the NUREG-1150 analyses, the conditional probability of various thermally-induced RCS boundary failures leading to partial or total RCS depressurization in station blackout sequences is quite high. Thus, understanding the risk profile for ice condenser plants will require understanding the response of the containment to station blackout events with RCS depressurization even if intentional depressurization strategies are never implemented. Many of these accident scenarios are expected to have at least a qualitative resemblance to the cases considered here, and the analyses discussed in this section therefore provide some insight as to how these sequences may behave and how they may differ from those in which the RCS remains at high pressure until vessel breach (VB).

DCH threats can be largely, if not entirely, eliminated by fully depressurizing the primary system prior to VB. However, assuring the capability for complete on-demand depressurization would require substantial primary system hardware modifications. Depressurization using existing systems (i.e., intentionally opening the PORVs) would likely reduce pressures substantially prior to VB, but might not permit achievement of total depressurization. Hence, analysis of depressurization as a mitigation strategy requires treatment of two classes of threats: hydrogen released prior to VB during depressurization, and the residual DCH threat arising when the partially depressurized vessel fails.

In the present study, the residual DCH threat was evaluated assuming that the RCS pressure at VB would be 1.5 MPa. In Section 2.4.2, it was noted that later SCDAP/RELAP analyses suggest that this value may be too high, and that the RCS might even be completely depressurized at VB. If so, the present treatment of the residual DCH threat in the intentionally depressurized sequence is too conservative. However, there are substantial uncertainties in in-vessel melt progression following intentionally opening the PORVs, and it is prudent to allow for the possibility that depressurization may not be complete, as was done in the NUREG-1150 analysis of sequences in which the PORVs unintentionally stick open. In any event, the response of the containment prior to VB is also of interest, and these results would remain applicable even if complete depressurization were to be established by future work.

Reduced primary system pressure actually can mitigate the DCH threat in two quite different ways, and a failure to distinguish between these mitigative effects has caused some confusion in the past. These effects are:

- As the RCS pressure is decreased, the driving force for debris dispersal into the containment is reduced. If the pressure is sufficiently low, the degree of debris dispersal from the cavity and/or the extent of fragmentation of the dispersed debris will be insufficient to generate a significant threat to containment integrity.

- Reducing the RCS pressure reduces the amount of steam that accompanies debris dispersal into the containment. This, in turn, reduces the amount of steam available for thermal and chemical interaction with the debris. Previous calculations [Wi87, Wi88a, Tu89] have indicated that this effect would reduce the resulting DCH loads even if the extent of debris dispersal were unaffected.

Terms such as "DCH low-pressure cutoff" have sometimes been used to refer to these effects, especially the first. Neither effect is a well-defined threshold effect, however, and thus the term "cutoff" can be somewhat misleading.

The first of these effects has been studied in experimental programs at Brookhaven National Laboratories and at Sandia National Laboratories. These investigations have led to correlations for dispersal which are specific to the cavity geometries studied in the experiments; they have not yet resulted in any validated mechanistic models for debris dispersal. The effect of any postulated degree of reduction in debris dispersal can be taken into account in CONTAIN-DCH by adjusting the debris sources input to the code. However, the code itself includes no models for debris dispersal and thus the extent to which debris dispersal will actually be reduced by partial RCS depressurization cannot be analyzed by CONTAIN-DCH. The code does include mechanistic modeling for phenomena governing the effect of the reduced steam supply, and these effects may therefore be analyzed with the code.

In the present study, DCH loads associated with failure of the partially depressurized vessel were analyzed assuming 50% of the total corium mass to be dispersed, as was done in the fully-pressurized scenario. No credit was taken for the reduced corium dispersal that might reasonably be expected to result from the reduced primary system pressure and, hence, only the second of the two mitigative effects noted above was allowed for in these calculations. Thus the analysis of DCH in the partially depressurized scenarios should be considered to be quite conservative, more so than was the case for the fully-pressurized sequence with 50% corium dispersal. Indeed, the 1.5 MPa pressure assumed for the RCS at vessel breach is near the lower bound of the values which could cause significant debris dispersal, based upon the BNL and SNL results. Hence, the degree of conservatism introduced by assuming the same debris mass (and particle size) that was assumed in the fully-pressurized cases may be quite substantial.

In addition to the effect upon DCH, the depressurized sequence, as calculated by SCDAP/RELAP, differs in other important respects from the fully-pressurized scenario. In the depressurized sequence, the accumulators discharge and this water must be boiled off before vessel breach occurs. Partly for this reason, the time between shutdown and vessel breach is substantially lengthened and the steam load on the ice condenser during this time is substantially increased.

Another important difference is that the total hydrogen source to the containment prior to VB is considerably greater in the depressurized sequence, 722 kg versus 307 kg. One reason is that, in the fully-pressurized case, almost half of the hydrogen generated prior to VB still resides in the vessel at the time of VB, according to the MARCH calculation. In addition, there may be some tendency for in-vessel zirconium oxidation to be greater in depressurized sequences [Ha90], although this conclusion must be considered rather tentative. Among other things, the increased hydrogen sources prior to vessel breach contribute to making the loads calculated following VB much more sensitive to assumptions concerning the availability of ignition sources

prior to VB. In the discussion in this section, "ignition sources available" will be equated to "igniters operable", and conversely.

These differences with respect to the fully-pressurized station blackout sequence are also expected to apply to many of the scenarios involving unintentional depressurization due to RCS boundary failures, at least qualitatively.

In the next subsection, calculations illustrating the potential importance of igniter availability and hydrogen combustion uncertainties will be presented. The role of ice condenser bypass flows will be discussed in Section 4.3, along with the question of whether any benefit would result from implementing measures to better control these flows. The effects of providing dedicated power supplies for the air return fans are briefly discussed in Section 4.4, while Section 4.5 will consider selected phenomenological uncertainties involving co-dispersed water and the extent of in-vessel zirconium oxidation. Almost all the calculations to be presented here were performed with the 6-cell deck, because the 26-cell deck proved difficult and expensive to run on this problem; comparison of the 6-cell results with the limited 26-cell results available will be discussed in Section 4.6 as a "benchmarking" exercise for the simpler deck. Consideration of detonation threats in the ice condenser is deferred to Section 5 of this report.

4.2 Effects of Igniters and Hydrogen Phenomenology

The cases involving intentional depressurization that were calculated in this work are summarized in Table 4.1. In the second column, the entry "All" means that igniters were assumed to operate in all cells, while "Existing" means that the existing igniter system was assumed to be powered but that no additional igniters were installed in locations where they are currently absent (e.g., the lower plenum and the ice condenser); "None" implies that no igniters were assumed operational. In the latter cases, ignition sources were assumed to become available in all cells following VB. In some instances, the default burn model correlations for flame speed were overridden by specifying a flame speed of 5 m/s, and entries in the third column indicate for which cells this was done. Other variations (mitigation strategies or phenomenological assumptions) are noted in the fourth column, while the last column gives the maximum pressure calculated for the upper containment.

In Figure 4.1, the pressure history following VB for Case 1 in Table 4.1 is given for the upper containment (solid curve) and the reactor cavity cell (dashed curve). Containment pressures rise to over 0.6 MPa and thus constitute a major threat to containment integrity, despite the depressurization of the RCS. Comparison of the cavity pressures with the fully-pressurized case (Figure 3.25) shows that cavity pressurization is considerably less, but it is still not negligible.

In Figure 4.2, the pressure response is given for several cases in which assumptions concerning igniters and hydrogen burn flame speeds are varied. The solid curve with open symbols (Case 2) gives the results for a calculation analogous to Case 1 (dashed curve, open symbols in Figure 4.2) with igniters assumed to be operating in all cells. In Case 2, the maximum pressure is only 0.42 MPa, a reduction of almost 0.2 MPa with respect to the case without igniters.

As calculated by the default burn model, flame speeds in the burns following VB were low, leading to long burn durations which could be nonconservative in the present context (see Section 2.4.1). Calculations analogous to Cases 1 and 2 were run

Table 4.1

Results of Calculations for the RCS Depressurization Strategy
(6-Cell Deck Used Except in Case 16)

Case No.	Igniters Powered	5 m/s Flame[a]	Other	Max. P (MPa)
1	None	None	---	0.61
2	All	None	---	0.42
3	None	1,2,5,6	---	0.88
4	All	1,2,5,6	---	0.49
5	Existing	1,2,5,6	---	0.41
6	None	1,2,5,6	No Debris (No DCH)	0.70
7	None	1,2,5,6	(Deck Leakage)/10[b]	0.83
8	All	1,2,5,6	(Deck Leakage)/10[b]	0.32
	None	1,2,5,6	(All Bypass)/10[c]	0.80
	All	1,2,5,6	(All Bypass)/10[c]	0.53
	All	None	Fans Operate	0.49
	All	2,5,6	Fans Operate	0.52
13	All	1,2,5,6	20000 kg RCS Water[d]	0.65
14	All	1,2,5,6	20000 kg Cavity Water[d]	0.64
15	Existing	1,2,5,6	High Zr Case	0.45
16	Existing	l.c., u.c.[e]	26-Cell Deck	0.41

[a] 5 m/s burn propagation speed assumed in the specified cells; default model flame speed assumed in all other cells.
[b] Deck leakage bypass flow area reduced by factor of 10.
[c] All bypass flow areas reduced by factor of 10.
[d] Water assumed to be co-dispersed with debris, and to undergo efficient thermal interaction with debris.
[e] 5 m/s flame speed assumed in lower containment and upper containment cells, default model flame speed elsewhere.

with the flame speed specified to be 5 m/s except in the ice condenser and the lower plenum (Cases 3 and 4, respectively; curves with closed symbols in Figure 4.2). For the case without igniters, this change resulted in a large increase in the peak pressure, to a value of almost 0.9 MPa. The sensitivity to the flame speed was considerably less for the case with igniters. The change from the default flame speed to the 5 m/s assumption can have a large impact in the depressurized scenario because the steam concentrations in the upper containment were high, due to the effects of the bypass flows discussed further in Section 4.3.

Case 5 in Table 4.1 was calculated assuming only the existing igniter system was powered. It appears that the existing igniters are sufficient to obtain the benefits of igniters, in terms of the maximum pressures calculated (it will be seen in Section 5 that this is not necessarily true when detonation threats are considered, however).

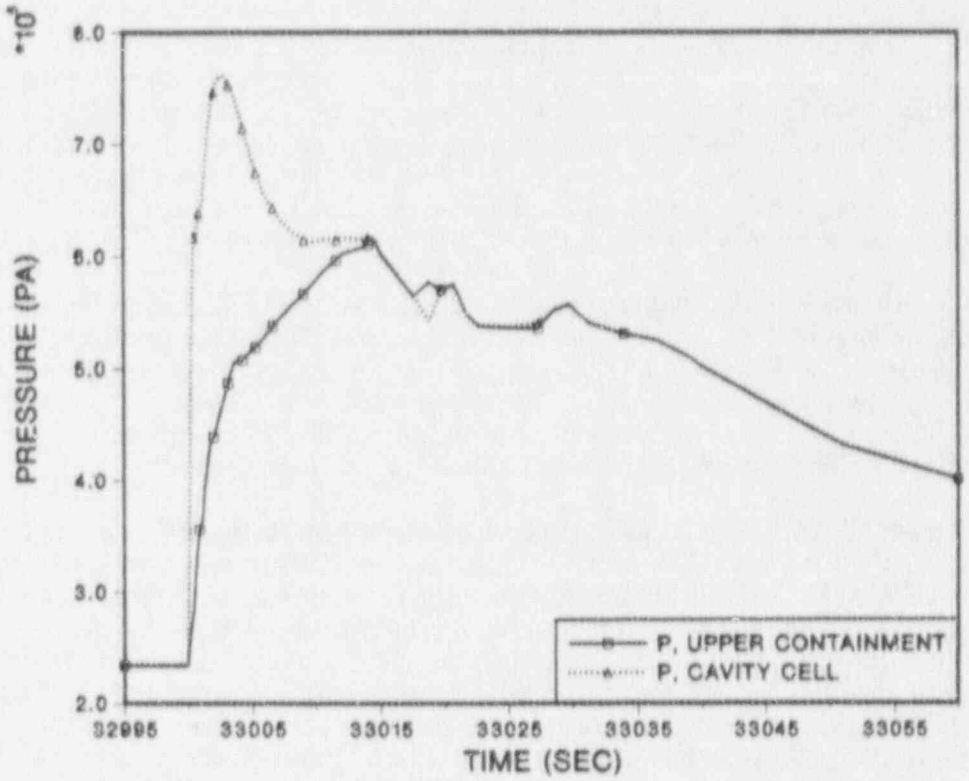

Figure 4.1 Containment pressures following VB in the depressurized scenario, 6-cell deck, 50% corium participation, no igniters operating.

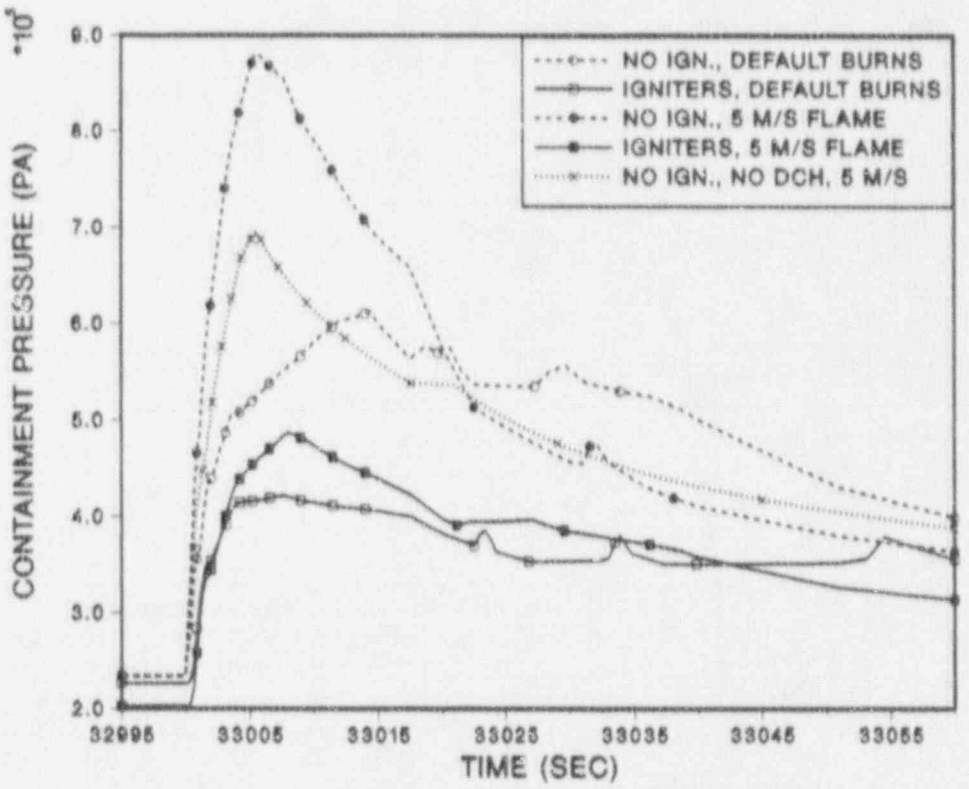

Figure 4.2 Effect of igniter operation prior to VB and of hydrogen burn rate upon containment pressures after VB in the depressurized scenario.

Comparison of these results with those discussed in Section 3 indicates that the station blackout sequence with RCS depressurization benefits much more from having igniters available prior to VB than does the sequence with a fully-pressurized RCS. One reason is that much larger quantities of hydrogen are released prior to VB in the depressurized case, and controlled burning of this hydrogen confers large benefits. Another reason is that the impact of the DCH event itself, for which igniters are ineffective, is considerably less when the RCS is depressurized to 1.5 MPa.

The importance of the hydrogen released prior to VB is illustrated by Case 6 (dotted curve, Figure 4.2), which was calculated as was Case 3 (no igniters) except that all debris sources, and hence all DCH-related phenomena, were deleted from the problem. Following vessel breach, the hydrogen burn by itself gives a severe load, about 0.7 MPa. Obviously, no amount of mitigation of DCH phenomenology is going to be of much help if nothing is done to control the hydrogen threat.

In Figure 4.3, the cumulative hydrogen consumption is plotted as a function of time prior to VB for Cases 2, 4, and 5 of Table 4.1. All three cases include operational igniters in at least some cells and, as a result, the hydrogen is consumed in a number of relatively small burns. Much of this hydrogen combustion, though not all of it, occurs in the ice condenser. In any event, no single large burn occurs and, as a result, no containment-threatening pressures are calculated to result from any of the hydrogen burns occurring prior to VB. This result was quite general in the calculations performed in the present work: in no case for which igniters were assumed to be operating did hydrogen burns result in a significant threat to containment prior to VB.

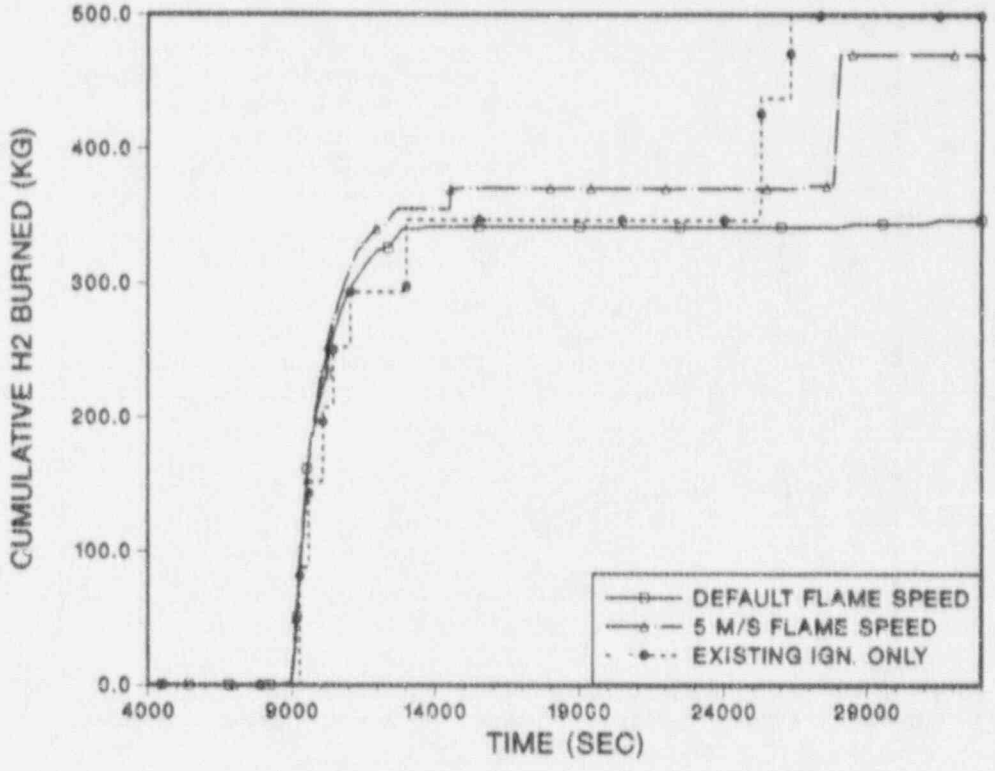

Figure 4.3 Cumulative H_2 consumption prior to VB for selected cases with igniters operating.

By comparing the present results with those calculated for 50% corium participation in Section 3, it is apparent that depressurization of the RCS offers the potential for substantial mitigation if and only if it is combined with providing power for the igniter systems. This result is hardly surprising, since it is generally recognized that hydrogen control is important in ice condenser containments, quite independently of DCH concerns.

4.3 Effects of Ice Condenser Bypass Flows

In Section 2.3.2, it was noted that flow paths between the upper and lower containment that allow for bypass of the ice condenser could play a significant role in calculations of accident sequences of long duration, even though these flow paths are small (< 0.5 m^2 total) compared with the flow paths through the ice condenser (almost 100 m^2, if doors are fully open). The bypass behavior can be quite complex, and has not been fully analyzed for all the calculations. It will be discussed in detail here only for cases which do not involve igniters operating prior to VB, since the cases with igniters operating are more complicated due to the pressure surges resulting from hydrogen burns. The bypass flow behavior can be sensitive to assumptions made concerning the behavior of the lower plenum doors under low pressure differentials. In all calculations for the depressurized station blackout accident, the doors were modeled as described in Table 2.4.

4.3.1 General Principles Governing the Bypass Flows

In understanding the calculated bypass behavior and its consequences, it is helpful to start with the simplified containment representation sketched in Figure 4.4. In the figure, only the upper containment, lower containment, and the ice condenser are represented; the plena are not represented separately. In addition, the flow path designated "deck leakage" will be assumed to be of the same elevation as the elevation of the entrance from the lower containment to the ice condenser (h_2 in the figure); in reality, these elevations are slightly different. The elevation of the refueling canal drains and the elevation of the exit from the top of the ice condenser are designated h_1 and h_3, respectively. The values of h_2 and h_3 indicated in the figure must be taken as being quite approximate, in view of the simplifications to the actual containment geometry that have been made here. The densities of the gases in the lower containment, the ice condenser, and the upper containment are designated ρ_1, ρ_2, and ρ_3, respectively.

When the ice condenser lower plenum doors are open at all, they offer a flow area that is generally of the order of 2 m^2 or greater. In considering convective flow loops involving the bypass paths, one can, as a first approximation, treat the two paths as being independent, with the ice condenser providing the return path in both cases. When the doors are fully closed, their leakage area (0.004 m^2) is too small to be significant, and any recirculation involving the bypass paths must be up through one of the paths and down through the other. Throughout this discussion, it is assumed that pressure heads associated with flows generated by steam (or other) sources into the containment can be neglected in comparison with the heads associated with the buoyancy effects. Since the ice condenser lower plenum doors open so easily, this is not a bad approximation when source rates are low.

When flow through either, or both, of the bypass paths is upward, steam (and hydrogen) can enter the upper containment without passing through the ice condenser.

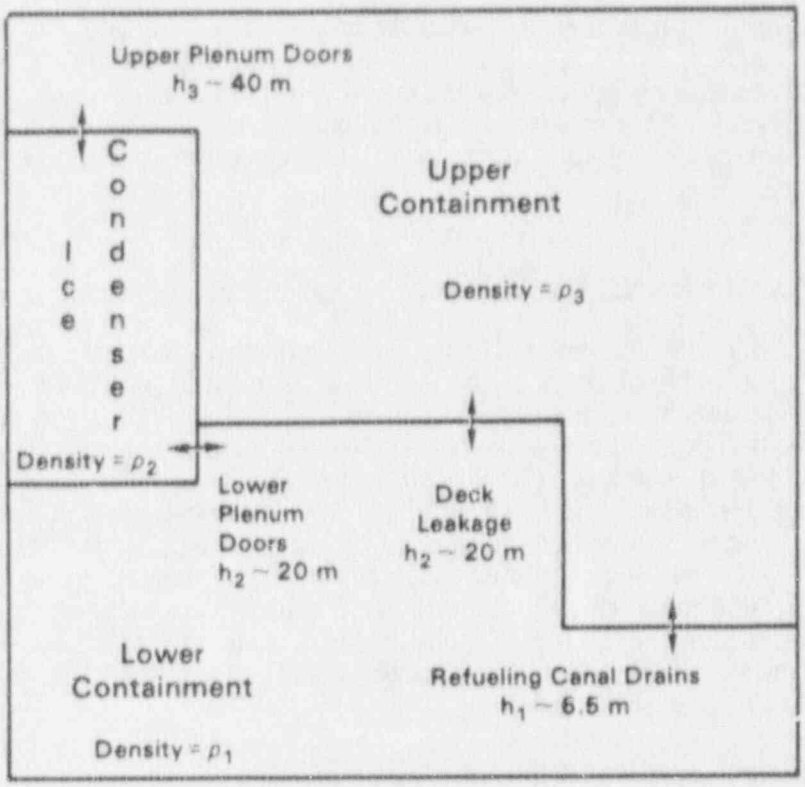

Figure 4.4. Simplified containment geometry for analyzing recirculation flows involving ice condenser bypass paths.

On the other hand, flow downward through the bypass paths has less serious implications; indeed, it acts somewhat as if the air return fans were operating at a very low level. From Figure 4.4, it is apparent that the net pressure head for flow upward through the deck leakage path is

$$\Delta P = g(\rho_2 - \rho_3)(h_3 - h_2). \tag{4.1}$$

The net head for upward flow through the refueling canal drains is given by

$$\Delta P = g[\rho_1(h_2 - h_1) + \rho_2(h_3 - h_2) - \rho_3(h_3 - h_1)]. \tag{4.2}$$

Usually, the densities will be such that $\rho_1 < \rho_3 < \rho_2$. Hence, ΔP in Eq. 4.1 will usually be positive, favoring upward flow through the deck leakage path, if it is at the elevation that was assumed here.

The situation is more complicated for the flow through the refueling canal drains. Sources of steam (and hydrogen) from the RCS enter the lower containment, which therefore tends to heat up rapidly. The high temperatures and high steam mole fractions which develop tend to result in values of ρ_1 that are much less than either ρ_2 or ρ_3. On the other hand, the upper containment, though obviously warmer than the ice condenser, does not heat up nearly as much as the lower containment, at least

initially; hence, ρ_3 generally does not differ from ρ_2 nearly as much as it does from ρ_1. Under these condition, ΔP in Eq. 4.2 will tend to be negative, and flow through the refueling canal drains will be downward from the upper containment to the lower containment. However, if sufficiently high temperatures and/or elevated steam concentrations develop in the upper containment for any reason, the resulting decreases in ρ_3 can cause ΔP to become positive, yielding upward flow through the refueling canal drains.

It is interesting to note that this simple model predicts that, if only the refueling canal drain path were to be available, the system can exhibit bistable behavior. That is, so long as the upper containment remains reasonably cool, the flow through the refueling canal drains will tend to be in the downward direction, and no tendency for the upper containment to heat up will result from this flow. However, if the upper containment does heat up for any reason and the flow reverses, the steam entering the upper containment via the refueling canal drains will tend to keep temperatures in the upper containment high, and thus maintain the conditions favorable to the upward flow.

4.3.2 Bypass Flows in the Unmodified Plant

To return to the actual calculations, Figures 4.5a, 4.5b, and 4.5c give atmospheric compositions and temperatures for the lower containment, the ice condenser, and the upper containment, respectively, for Case 3 in Table 4.1 (a case without igniters). As would be expected, both temperatures and steam mole fractions in the lower containment rise rapidly, while they remain quite low in the ice condenser. In the upper containment, however, the steam mole fractions and temperatures also rise to elevated values, although the rise is considerably slower than in the lower containment. As a result, the containment pressure (Figure 4.5d) exhibits a parallel rise. Since neither temperatures nor steam concentrations in the ice compartment ever reach elevated values, it is evident that flows taking the normal path through the ice condenser cannot be responsible for these results.

The response of the upper containment described in Figure 4.5c can be understood in terms of the flow rates plotted in Figure 4.6. The solid curve gives the flow rate from the lower containment through the lower plenum doors, while dashed curves give the bypass flows. The lower plenum flow is driven largely by the steam and hydrogen sources to containment and it reflects the irregular behavior of these sources. (To some extent, the zig-zag appearance of the curve is an artifact of spacing of output points on the CONTAIN plot file that was too coarse to capture all the details of the flow variations.) For all the flows, positive flow in the figure corresponds to upward flow, out of the lower containment into either the upper containment or the ice condenser.

During most of the time of interest, the flow through deck leakage path is positive, as would be expected from Eq. 4.1 and the associated discussion. On the other hand, the flow through the refueling canal drains is initially downward. At about 18000 s into the accident, the flow reverses and is upward until about 23000 s. This behavior reflects the rising temperatures and steam mole fractions in the upper containment, which reduce ρ_3 relative to ρ_1 and ρ_2 and thereby favor upward flow through the refueling canal drains, as predicted by Eq. 4.2.

Flow through the lower plenum doors is initially positive due to the sources of steam and hydrogen into the lower containment. As these sources fall to low levels

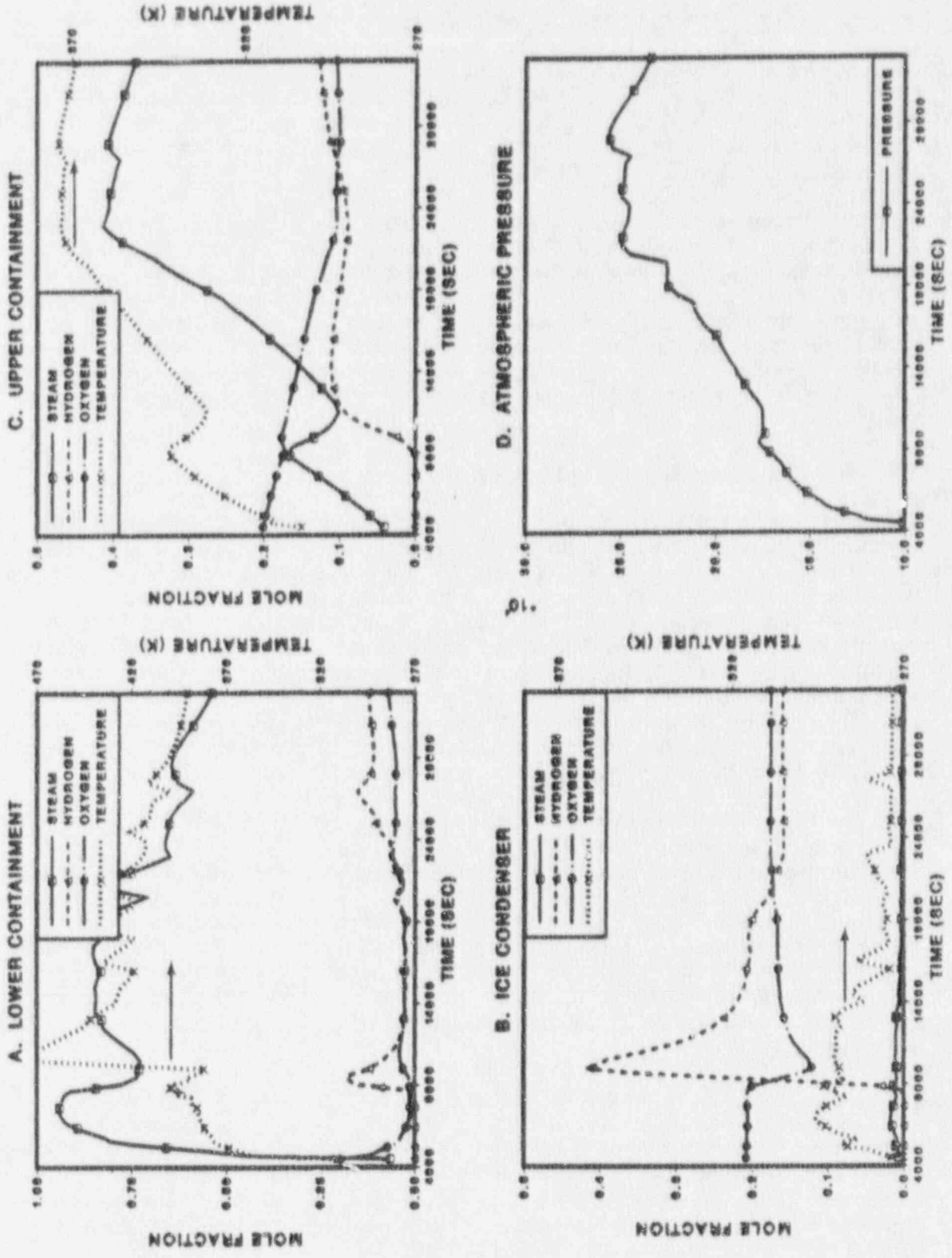

Figure 4.5 Atmospheric compositions, temperatures, and pressures prior to VB, depressurized scenario without igniter operation.

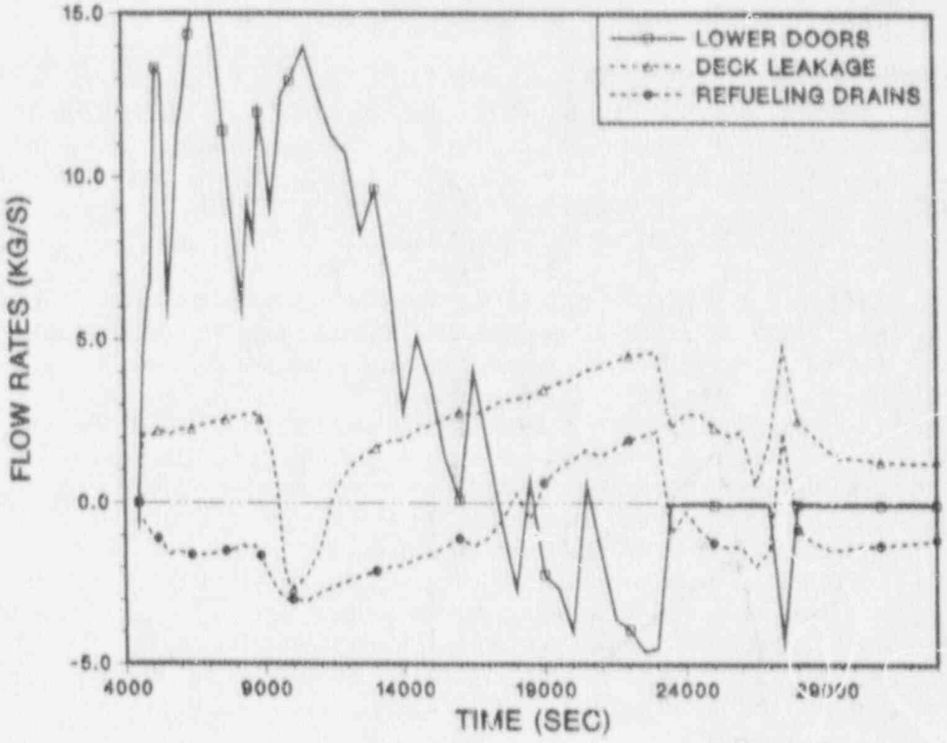

Figure 4.6 Recirculation flow rates involving flow paths that bypass the ice condenser.

(Figure 2.5), flow through the doors reverses and is predominantly negative after about 17000 s into the accident. During this period, the plenum doors are in effect providing the return path for the upward flow through the bypass paths. The reverse flow through the doors implies a reverse pressure differential, which tends to close the doors as they are modeled here (Table 2.4), and any tendency toward door closure can increase the reverse pressure differential associated with the flow. As the reverse flow increases, an instability develops and the doors abruptly close completely at about 23000 s, and remain shut during most of the remaining time prior to VB at 33000 s. Once they close completely, leakage through them is too small to have any significant effect upon the problem. Hence, after 23000 s, recirculation is through the bypass paths alone, and is upward through the deck leakage path and downwards through the refueling canal drains.

The absolute magnitudes of the bypass flows are generally in the range of 1 to 5 kg/s, and the total mass of the upper containment atmosphere is typically of the order of 30000 - 40000 kg in this scenario. Hence, the integrated flow into the upper containment over time periods of the order of 10000 s is comparable to the total atmospheric inventory of the upper containment. It is evident, therefore, that the bypass flows are sufficient to have a large effect upon containment conditions over the relatively long time scales involved in the depressurized sequence considered here.

Around 10000 s after shutdown, there is an interval of time lasting about 2000 s during which even the deck leakage flow is negative. No flows of steam and hot gas are entering the upper containment during this interval, and the temperatures and

steam concentrations in the upper containment therefore begin to decline (Figure 4.5c). The time in question is near the time when hydrogen sources entering the containment are at their maximum (Figure 2.5), and hydrogen concentrations in the ice condenser reach high values (up to 40%; see Figure 4.5b). With hydrogen concentrations this high, the gas density in the ice condenser is actually less than that in the upper containment, even though the temperatures in the ice condenser are considerably lower. As a result, ΔP in Eq. 4.1 is negative, and flow through the deck leakage is downward rather than upward at this time.

Effects of Hydrogen Burns. If igniters or other ignition sources are available, hydrogen burns produce pressure surges and temperature transients which complicate the behavior described here. In addition to their direct effects, the burns can alter the behavior of the ice condenser lower plenum doors. In some calculations, the pressure surges closed the doors, so that they were closed for a larger portion of the transient than was the case in Figure 4.6; in other cases, pressure surges in the forward direction forced the doors fully open. When the latter happened, the doors were assumed to remain fully open in the present calculations (Section 2.3.3 and Table 2.4). This did not have a large effect upon the 6-cell calculations because counter-current recirculation flows through the open doors (represented by a single flow path) cannot be modeled with this deck. In calculations performed using the 26-cell deck (and in reality), counter-current flows through the open doors would be expected to have substantial effects upon the containment response prior to vessel breach if the doors remained fully open (see Section 5).

The containment pressure and steam mole fractions in the upper containment for Case 2 (with igniters) and Case 3 (without igniters) are compared in Figure 4.7. The case with operational igniters has pressures comparable to the case without igniters, while steam mole fractions are somewhat higher. This result was fairly typical of the other cases with operating igniters that were considered. Qualitatively, the overall effect of the bypass flows is quite similar for the two cases.

It is interesting to note that the maximum pressures prior to VB in Figure 4.7, about 0.25 MPa, are significantly higher than the pressure calculated to result from a design basis large break LOCA (10.8 psig or 0.176 MPa, from Ref. TVA74). In the latter scenario, flow rates are very large, the lower plenum doors open fully, buoyancy pressure heads are negligible compared with the other driving pressures involved, and virtually all the flow passes through the ice condenser where the steam is condensed, effectively controlling the pressure rise. The bypass flows have only a minor impact upon this scenario. Indeed, they would not be expected to have an important effect upon any accident sequence within the design basis. For rapid blowdowns, the ice condenser will act as it does for the large LOCA; for prolonged accidents within the design basis, at least one train of air return fans and/or containment sprays would be operating, and either would effectively prevent the containment pressurization due to bypass flows that is calculated to occur here.

4.3.3 Effects of Reduced Bypass Flow

Since the bypass flows have significant effects in these calculations, it is reasonable to consider whether any substantial benefits would result from reducing the bypass flows. It is also worth performing calculations with the deck leakage reduced as a sensitivity study for the unmodified plant because the area and flow resistance assumed here for this flow path are based upon the FSAR analyses [TVA74], which were stated there to be conservative. Actual leakage might be substantially smaller.

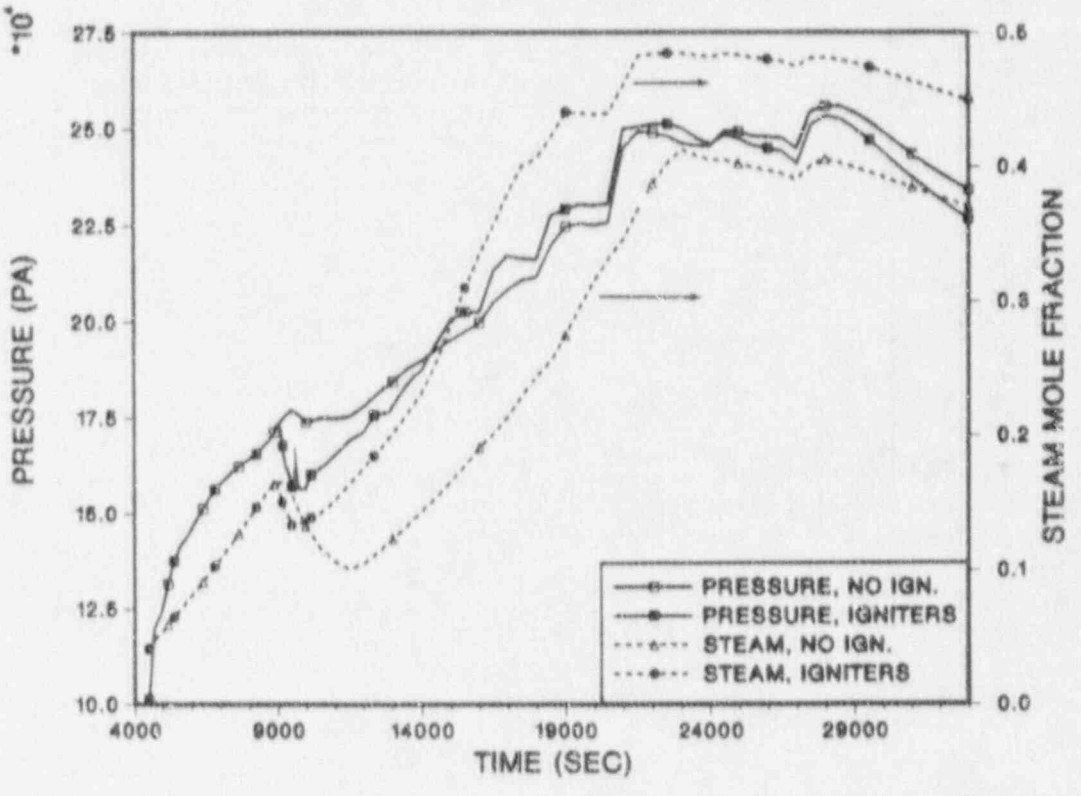

Figure 4.7 Pressures and steam mole fractions in the upper containment, with and without igniters.

In addition, no information was given there as to the elevation of the leakage flow paths. The elevation assumed here (20.6 m) is purely an assumption made for the sake of the present work. No sensitivity studies were performed concerning this elevation. If it were to be substantially lower, flow through this path would behave more as does the flow through the refueling canal drains. Substantially higher elevations for this flow path are not possible, since the elevation assumed here is already at the top of the lower containment.

Cases 7 and 8 in Table 4.1 were run with and without igniters, respectively, and with the deck leakage bypass flow path area reduced by a factor of ten. Cases 9 and 10 are analogous cases with both the deck leakage and the refueling canal drain paths reduced by a factor of ten. The maximum pressures calculated for Cases 7 and 9 (without igniters) still exceed 0.8 MPa, indicating that no significant improvements result in terms of maximum loads calculated, if igniters are not available.

The cases with igniters are a little more interesting. Containment pressure responses after vessel breach are plotted for these cases in Figure 4.8a, along with the response of the analogous calculation with the unmodified bypass (Case 4). The calculation with both bypass paths reduced (Case 10) shows no mitigation; if anything, the loads are somewhat higher than for the cases with unmodified bypass. On the other hand, the calculation with only the deck leakage reduced (Case 8) shows fairly significant mitigation, with a maximum containment pressure of only 0.32 MPa.

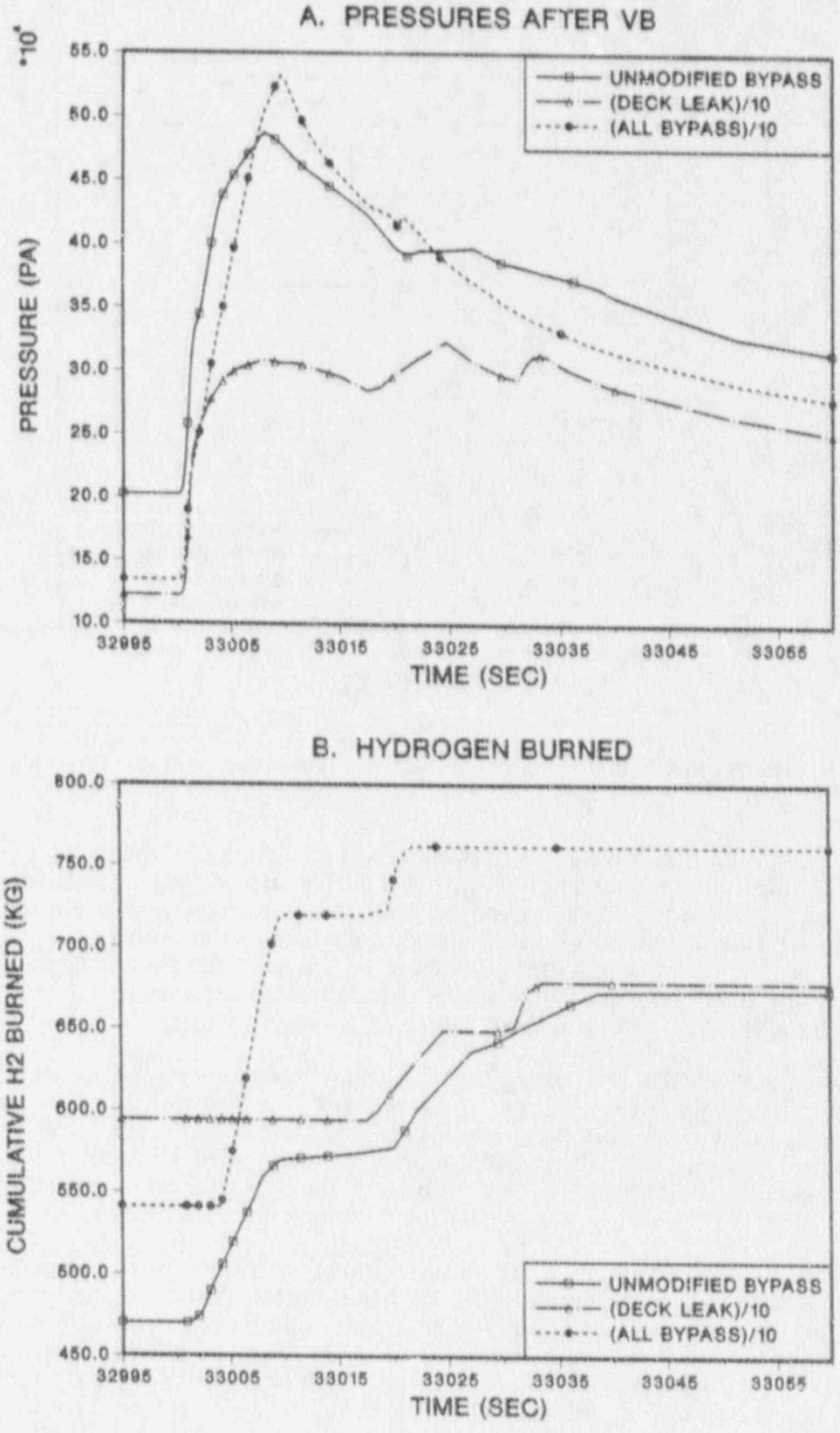

Figure 4.8 Containment pressures and hydrogen burned following VB for cases with modified ice condenser bypass flow paths.

Hydrogen burned following VB is plotted in Figure 4.8b for these cases, and it is apparent that the extent of hydrogen combustion at this time is considerably smaller for Case 8 than for Case 10.

These results are not fully understood, and may in part reflect chance factors concerning the hydrogen burns that follow VB, but the results are sufficiently intriguing that some additional details of the behavior prior to VB are worth discussing. We consider first the results obtained for the cases without igniters, since the abrupt, short-lived transient responses associated with the numerous hydrogen burns render an intelligible display of the long-term behavior with igniters virtually impossible. As with the calculations for the unmodified bypass flows, operation of the igniters did not appear to greatly alter the effects of the bypass flows themselves in these analyses.

Pressures, temperatures, and steam concentrations in the upper containment are displayed in Figures 4.9a, 4.9b, and 4.9c respectively, for Cases 1, 7, and 9. Both the case with only the deck leakage reduced and the case with all bypass reduced show only very limited temperature increases in the upper containment and virtually no increase in steam concentrations; there is very little difference between the two cases. Both of the reduced bypass cases do show some pressurization of the containment, but it is substantially less than for the unmodified case. This pressurization results from compression of the air due to displacement by steam of air initially in the lower containment, plus the addition of hydrogen to the atmosphere.

In Figure 4.9d, the bypass flows for Case 7 (reduced deck leakage) are compared with the bypass flows for Case 1 (unmodified bypass). (Bypass flows in the calculation with all bypass paths reduced by a factor of ten are too small to have a significant effect and they are not plotted for the sake of clarity.) In Case 7, the deck leakage flow is very small, as would be expected. The refueling canal drain flow is significant, but it is always in the downward direction. It therefore does nothing to heat the upper containment or increase steam concentrations there. With the deck leakage flow largely eliminated, nothing acts to heat the upper containment prior to VB and the flow through the refueling canal drains shows no tendency to reverse, as it did in the unmodified bypass case. Since the flow through the refueling canal drains is always in the downward direction, eliminating most of this flow (Case 9) has little additional effect upon the conditions in the upper containment.

As Figure 4.8b shows, the difference in maximum pressures calculated for Case 8 and Case 10 appears to be related to the difference in the amounts of hydrogen combustion calculated for these cases. In Case 8, no burn occurs until 19 seconds after VB, and this burn initiates in the upper plenum and propagates into the upper containment when the hydrogen concentration there is only about 5%; the resulting burn is very weak and incomplete. In Case 10, a burn initiates directly in the upper containment only 4 seconds following VB with the hydrogen concentration equal to 7%, which gives a considerably stronger, more complete burn. One possible reason for this difference is that, in Case 8, less hydrogen was available in the lower containment at VB and more time was required to generate and transport sufficient hydrogen to the upper containment to produce a burn there. The reduced hydrogen inventory in the lower containment reflects the effects of the downward flow through the refueling canal drains; thus, in this particular case, the flow through the drains may have had a beneficial effect. Chance factors may also have been involved, however.

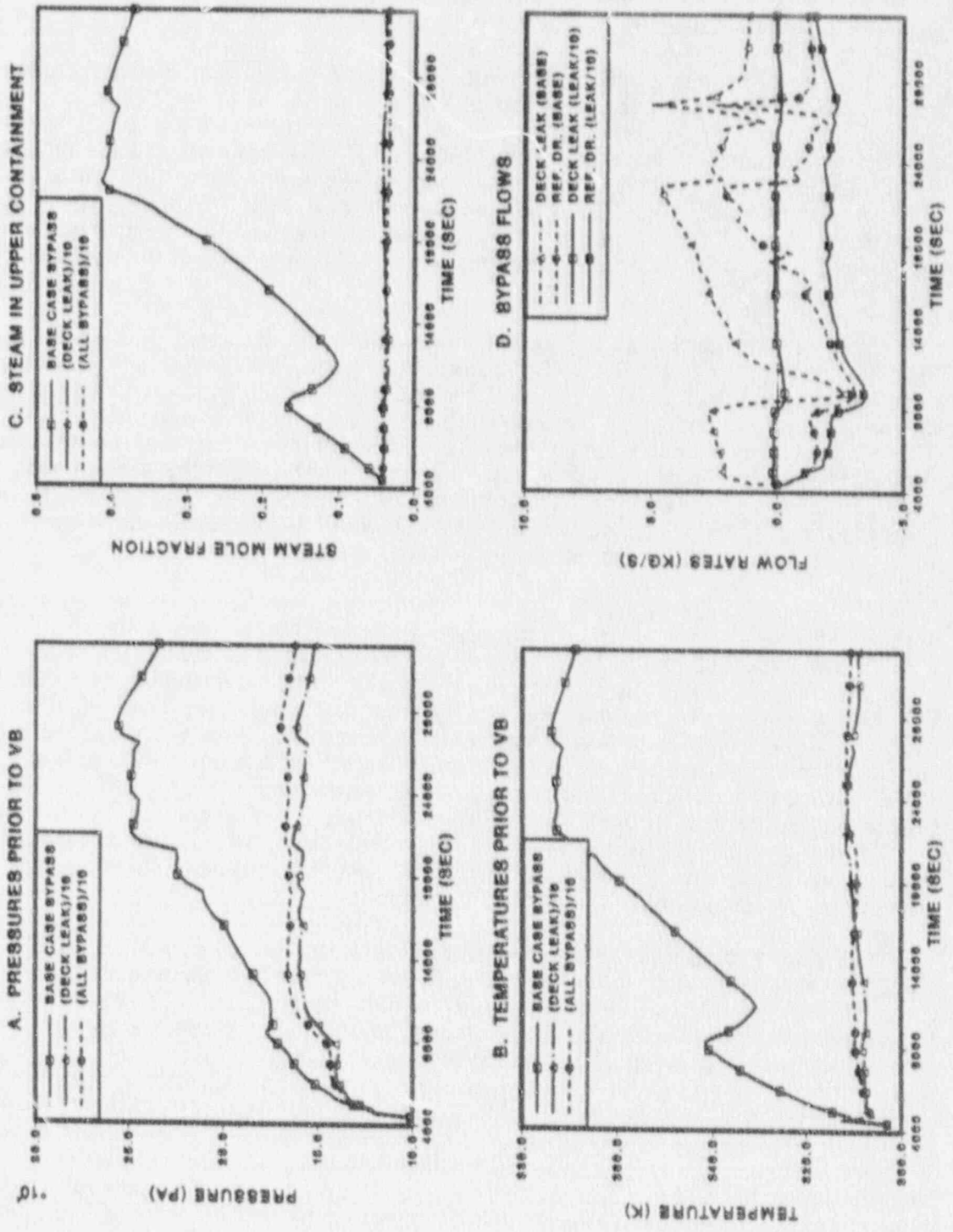

Figure 4.9 Effect of modified ice condenser bypass flows upon selected containment parameters prior to VB.

Changes to the bypass flows also result in changes in the amount of ice melted. This subject is discussed in Section 4.4.2, along with the effects of the air return fans on ice melting.

Based upon the results discussed here, it appears that flows between the lower and upper containments can have some fairly significant effects, but it is also clear that the bypass flow behavior is sensitive to many details which are themselves quite uncertain: location and magnitude of the various flow paths; atmospheric temperatures and compositions in the lower containment, the ice condenser, and the upper containment; details of the response of the lower plenum doors, including their response to the pressure surges caused by hydrogen burns. Many of these parameters will, in turn, be sensitive to the details of the sources of steam and hydrogen from the primary system. Gas stratification effects in the upper and/or lower containments, which were not modeled here, could also alter the bypass flows.

In the absence of more detailed study of these uncertainties, care must be taken not to overgeneralize from the results of the calculations presented here. However, some tentative conclusions can be offered concerning some of the behaviors calculated which may be reasonably general. The results suggest that any deleterious effects of the bypass paths may be limited to the deck leakage. In the cases considered, flow through the refueling drains was not itself deleterious because it was generally downward from the upper containment to the lower, except when other factors (e.g., the deck leakage) caused substantial heating of the upper containment. Indeed, this flow may have beneficial effects, although more detailed study would be required to confirm this.

In one respect, the case with reduced deck leakage but unmodified refueling drains may be quite unrealistic. The refueling drains are expected to be blocked (flooded) under some circumstances, including accidents with sprays operating and any accident in which the volume of water in the lower containment sumps exceeds about 750 m^3 [Ca84]. Sprays were not operating in any of the scenarios considered, but water volumes in the lower containment generally exceeded 750 m^3 later than about 12000 to 15000 s after shutdown. Drain blockage was not modeled in this work, however. Drain blockage would not have a large impact upon the calculations with unmodified bypass flows, because the effects of bypass flows were dominated by the deck leakage. In the case with reduced deck leakage, drain blockage would in effect convert the scenario into the case with all bypass reduced. However, if further study did confirm that flows of a few kg/s from the upper to the lower containment actually are beneficial, it would be possible to provide an equivalent flow by other means, e.g., by using low-capacity air return fans.

4.4 Dedicated Power for the Air Return Fans

It would be reasonable to expect that operation of the air return fans might have a substantial effect upon containment conditions in the depressurized station blackout sequence. For one thing, recirculation of the upper containment atmosphere through the ice condenser would be expected to largely eliminate the effects of the bypass flows discussed in the previous section, since the fans produce a flow of the order of 50 to 100 kg/s, and the bypass flows were generally under 5 kg/s. Calculations were therefore performed to assess the benefits, if any, of fan operation. The fans were modeled as described in Section 2.4.3. Only cases with igniters operating in all cells were considered.

4.4.1 Effect on Maximum Pressures and Hydrogen Burns

Case 11 in Table 4.1 was calculated with air return fans operating using the default burn model flame speed, while Case 12 was calculated assuming the 5 m/s flame speed in the upper and lower containment. For this calculation, there was little dependence upon the flame speed. Comparison with the analogous calculations without the fans (Cases 2 and 4, respectively) suggest the fans offer little benefit. Indeed, the calculations with the fans give slightly higher pressures, although the differences are too small to be considered very significant.

Since fans have been suggested as a means of controlling detonation threats, it is worth considering their effects in a little more detail, even though they may not offer much promise for reducing the maximum pressures following vessel breach. In Figure 4.10, Cases 4 and 12 are compared with respect to pressures before and after VB, steam mole fraction in the upper containment before VB, and hydrogen burned following VB. It is apparent that the fans do initially keep the pressures and steam mole fractions lower than in the case without fans, although their effectiveness declines later in the accident due to melting of the ice.

With the fans operating, more hydrogen is burned prior to VB than without the fans (Figure 4.10d). Most of this hydrogen is burned in the upper and lower containment rather than in the ice condenser itself, while the reverse is true of the cases without the fans. This effect is a consequence of the mixing action of the fans. The fact that these burns occur in the larger volumes of the containment, rather than in the relatively small ice condenser, results in individual burns that are larger than in the case without fans. Hence, the burns prior to VB develop higher pressures with the fans running, up to about 0.33 MPa. The threat to containment integrity from any burns prior to VB is still quite minor, however.

After vessel breach, the pressure curve for the case with fans shows two peaks, and comparison of Figures 4.10b and 4.10d shows that the second peak is the result of a hydrogen burn. The initial pressure rise results from the DCH event itself, without benefit of a hydrogen burn. Total hydrogen combustion following VB is greater in the case without fans, but the burn with fans operating is more coherent.

4.4.2 Effects of Fans and Bypass on Ice Melting

Ice remaining unmelted for Cases 4 (no fans) and 12 (fans operate) are compared in Figure 4.11. Also shown in the figure are the ice inventories for the two cases involving reduced bypass with igniters operating (Cases 8 and 10). Both the air return fans and the bypass modifications affect ice melting by affecting the flow through the ice condenser, and it is therefore convenient to discuss these scenarios together.

The results in Figure 4.11 are easily understood. Case 4 (no fans, unmodified bypass) has the least ice melt because substantial steam bypasses the ice condenser, while the case with fans has the most rapid ice melt because the fans rapidly move the steam to the ice condenser, reducing the amount of steam that condenses on other containment heat sinks before reaching the ice condenser. The cases with reduced bypass exhibit an intermediate behavior. Of the two, the case with reduced deck leakage but unmodified refueling canal drains (Case 8) shows the greater ice melt, because the downward flow through the drains acts somewhat as if the fans were on at a low level.

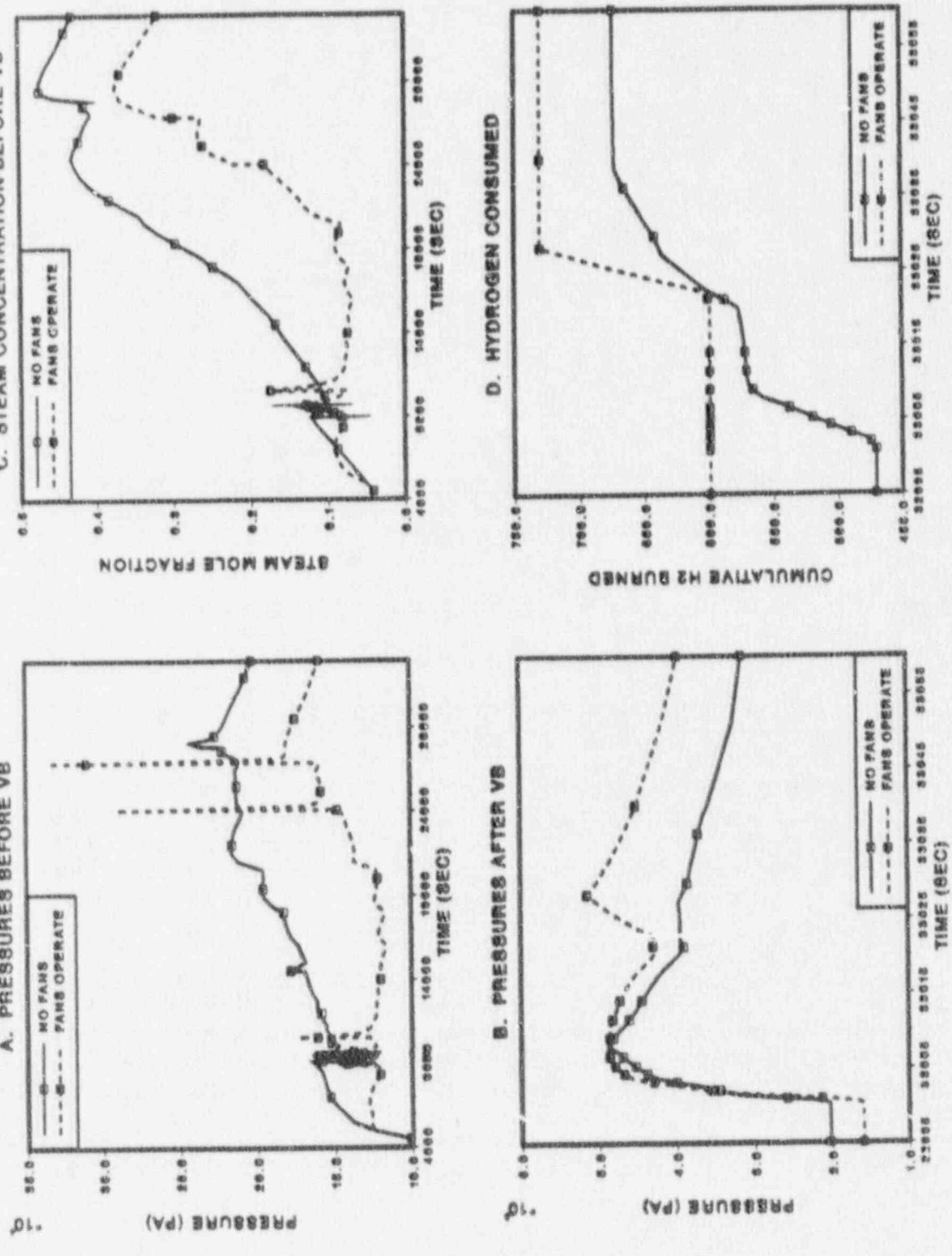

Figure 4.10 Effect of fan operation upon selected containment parameters.

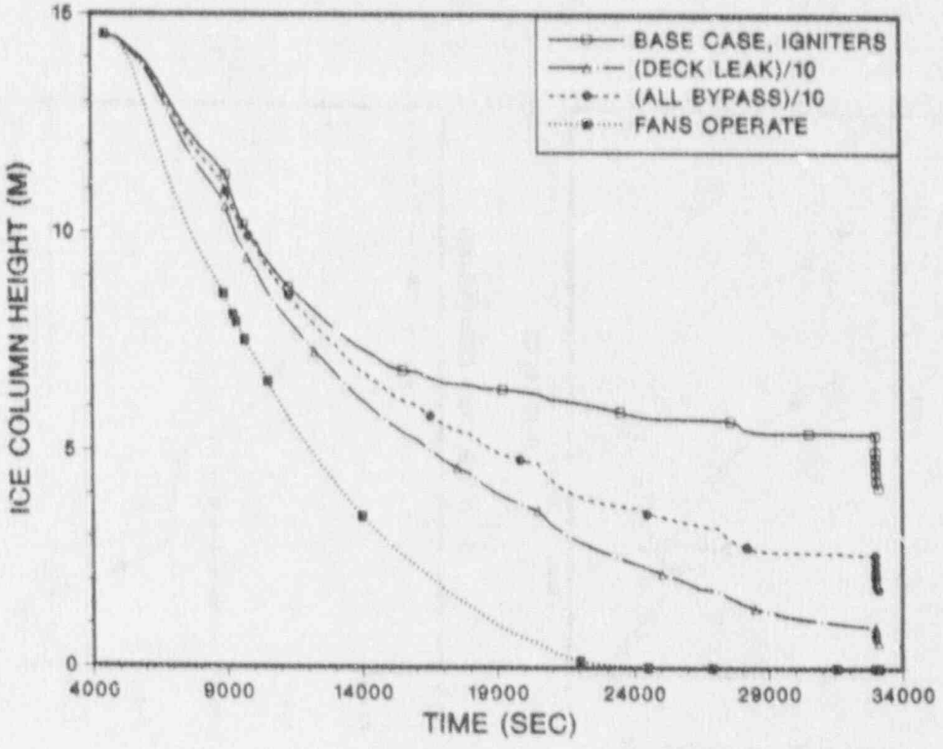

Figure 4.11 Effect of fans and modifications to the bypass flow paths upon the rate of ice melting.

Perhaps the most important result displayed in Figure 4.11 is the large amount of ice melt that has occurred by the time of vessel breach. Even in the calculation with unmodified bypass and no fans, almost two thirds of the ice has been melted. With fans running, the ice is totally depleted well before VB. The total depletion of the ice may be one reason why operating the fans does not mitigate the pressure rise that follows vessel breach. However, it should be noted that the case with reduced deck leakage and unmodified refueling drains (Case 8) exhibits almost total ice depletion, yet this case yielded an especially low degree of containment pressurization after VB. Not all the reasons for these results have been identified.

The fan modeling used here corresponds to both trains of fans operating at full power. It is interesting to note that Case 8 involves a qualitatively similar, but quantitatively much weaker, downward flow through the refueling drains, and this case has a considerably more favorable response in terms of the maximum pressure calculated. These results invite speculation that it could be beneficial to operate the air return fans at something much less than full power. In view of the sensitivity of these calculations to minor variations, it is obvious that no conclusions concerning this possibility can be drawn at present, but additional study might be of interest in future work.

4.5 Selected Phenomenological Sensitivities

In Section 2.5 of this report, it was pointed out that there are many phenomenological modeling uncertainties and uncertainties in the accident sequence

description that could affect the calculations performed in this work. Detailed study of their affects was not attempted in this work, but two uncertainties that were briefly considered are the possible effects of water co-dispersed with the debris and the influence of the zirconium content of the melt.

4.5.1 Water Co-Dispersed With the Debris

If moderate amounts of water are co-dispersed with the debris in such a way that there is effective thermal interaction between the debris and the water, the rapid steam generation that results can enhance DCH loads. On the other hand, a very large amount of water could quench the debris, reducing the loads. The general principles involved in the trade-off between the enhanced steam effect and the quenching effect were discussed in more detail in Ref. Wi87 and Wi88.

In the present study, it was assumed that 20000 kg of water would be co-dispersed with the debris and would thermally (and chemically) interact with it. The purpose of the calculations was to investigate whether co-dispersed water could enhance the DCH loads, and the amount was therefore chosen to lie in the range for which enhancement would be expected. The particular quantity assumed is otherwise arbitrary.

Two cases were considered. In the first (Case 13 in Table 4.1), the water was assumed to represent water remaining in the primary system that could be ejected along with the debris at the time of vessel breach. In the second (Case 14), it was assumed that the co-dispersed water represented water in the cavity. The cases differ only in that the initial enthalpy of the primary system water is higher, and somewhat less energy is therefore required to vaporize it. Both cases are otherwise similar to Case 4.

Containment pressurization in Cases 13 and 14 are compared with Case 4 in Figure 4.12. The co-dispersed water cases yield substantially higher calculated pressures than does the dry-cavity case. There is little difference between Cases 13 and 14, however.

There are important uncertainties in the analysis of DCH with co-dispersed water. Some of these were discussed in Section 2.5, and the caveats given there should be heeded before basing judgments on the present results. However, these results do indicate that there is at least a potential for co-dispersed water to enhance the loads, and this effect must be considered in any accident sequence for which there could be water in the cavity and/or primary system water could be ejected from the vessel at approximately the same time that the debris is ejected.

4.5.2 Zirconium Content of the Melt

A SCDAP/RELAP calculation that involved a high degree of in-vessel zirconium oxidation (about 72%) was deliberately chosen to provide the primary system sources in this work, in order to be "conservative" with respect to the pre-VB hydrogen sources. However, this means that only 6300 kg of unoxidized zirconium remained at VB, and only half of this was assumed to be participate in DCH, in the 50% corium cases.

The zirconium-steam reaction is a potentially important source of energy. It also generates hydrogen, although total hydrogen generated is not very sensitive to zirconium content in these calculations because all the cases considered included large amounts of iron. The iron-steam reaction is an effective source of hydrogen, although

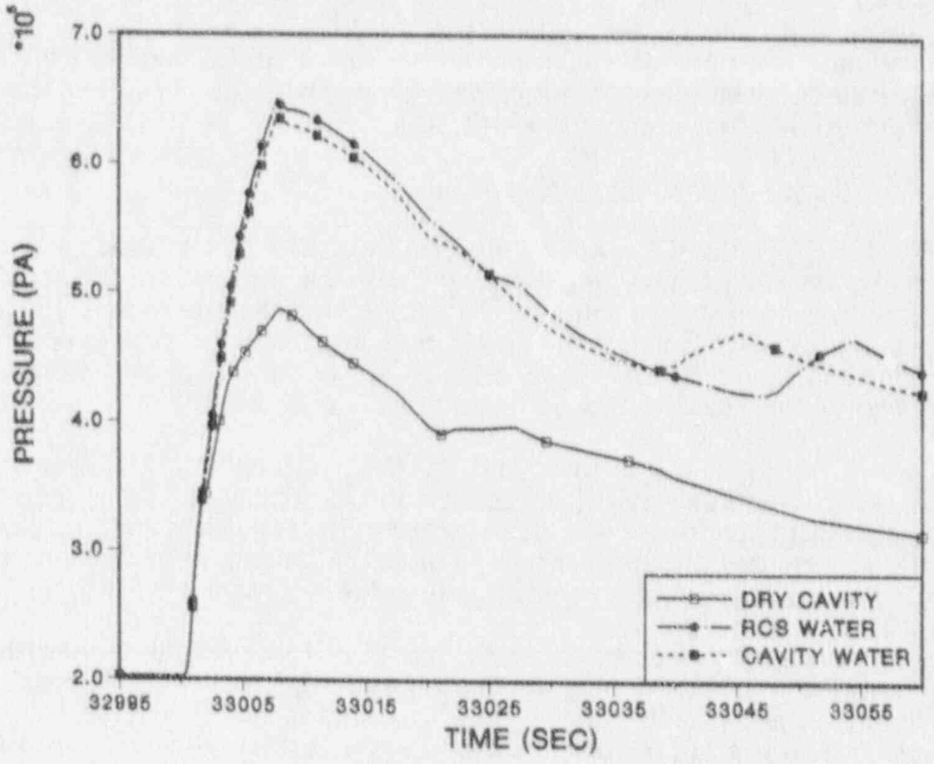

Figure 4.12 Effect of co-dispersed water upon containment pressurization.

it generates relatively little energy. Thus, the principal impact of zirconium is expected to be upon the chemical energy released, not upon the hydrogen generated.

A "high Zr" calculation (Case 15 of Table 4.1) was defined, based upon a SCDAP/RELAP calculation in which the in-vessel zirconium oxidation was about 45%, leaving 12500 kg unoxidized. The hydrogen source prior to VB was reduced so that the total hydrogen released was equivalent to this amount of in-vessel zirconium oxidation. Since zirconium melts at temperatures much lower than the oxidic components, especially when eutectic formation is taken into account, it was assumed that all the zirconium would be in the 50% of the core that was molten and that could participate in DCH. Hence, in the "high Zr" case, the zirconium content of the debris was increased to 12500 kg, almost a factor of four higher than the base case. The ZrO_2 content of the debris source was reduced in proportion to the in-vessel oxidation, while the other debris constituents were left unchanged. All other input was as in Case 5 of Table 4.1 (existing igniters operate).

In Figure 4.13, the pressure response of Cases 5 and 15 are compared. Also shown are the temperatures in the lower containment (Cell 2 of Figure 2.2). The enhanced energy release in the high-Zr case has a substantial effect upon the temperatures in the lower containment, but the effect upon the containment pressure is not large. One reason is that, in the depressurized scenario, the steam supply in the lower containment is limited, which means that the atmospheric heat capacity is less than that of the airborne debris; hence, even after local debris-gas equilibration

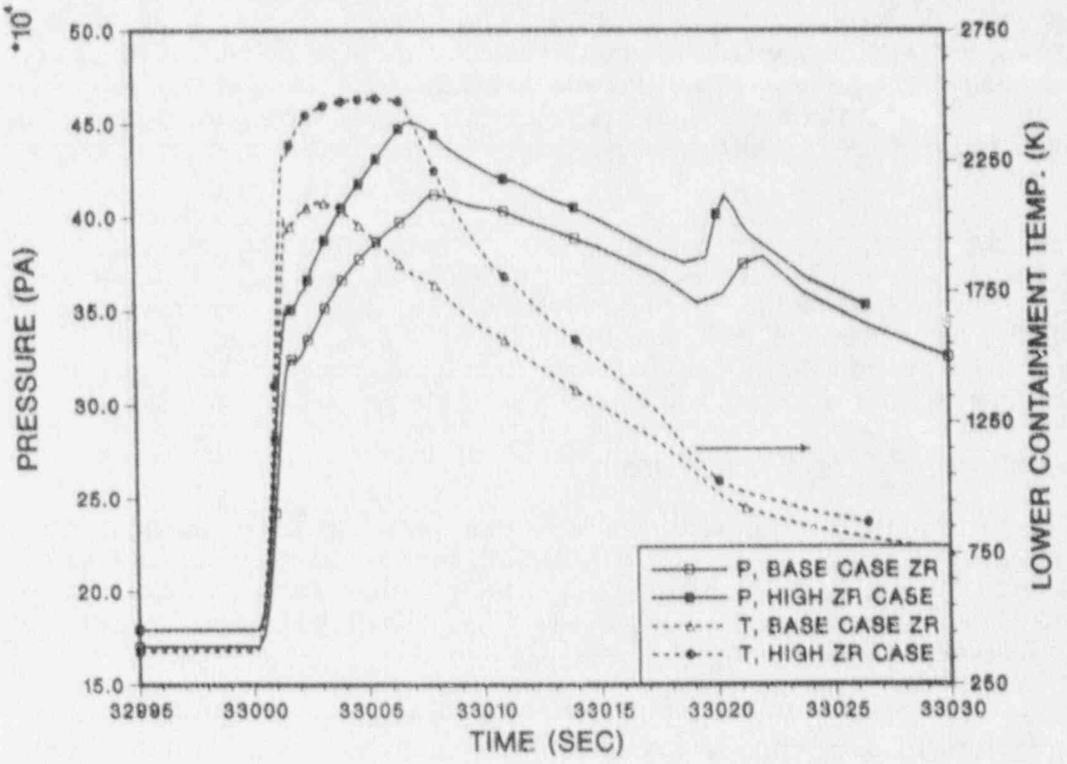

Figure 4.13 Effect of increased zirconium in the melt upon containment pressurization and temperatures in the lower containment.

occurs, much of the energy remains in the debris. Another factor is that, with limited steam supply, the extreme temperatures developed result in very rapid radiant energy transfer to lower-containment heat sinks, and energy is lost from the system more rapidly than it is transported to the upper containment, which contains the main reservoir of atmospheric heat sink. These effects are described in more detail in Refs. Wi87 and Wi88.

Once again, this result should not be overgeneralized. With larger steam supplies, the enhanced zirconium content might be more effective in increasing containment pressurization, especially if co-dispersed water is involved. However, a low steam supply may be fairly typical of station blackout sequences with RCS depressurization. In this event, the results described here do indicate that, for the depressurized scenario with no co-dispersed water, the containment pressures are not expected to be very sensitive to the zirconium content of the melt.

4.6 Benchmark Comparisons of 6-Cell and 26-Cell Results

Only one complete calculation was run for the depressurized station blackout sequence using the 26-cell deck. This case is entered into Table 4.1 as Case 16; it includes the assumption that existing igniters operate and the hydrogen burn flame speed is 5 m/s in the upper and lower containment volumes. In assessing the effects of

the refined nodalization, it may be compared with Case 5 of Table 4.1. An otherwise-analogous case with fans operating was also calculated out to 25000 s, at which point it encountered computational difficulties and was terminated. A number of other 26-cell cases were also run in order to study hydrogen distributions during the period of high hydrogen influx at around 9000 s. These cases were terminated at about 11000 s into the transient.

The conclusions that were offered earlier in this section concerning the depressurized station blackout sequence are based upon the 6-cell calculations. It is therefore of considerable interest to benchmark this simpler deck against the 26-cell results where the latter are available. In making these comparisons, only the 26-cell calculations with and without fans that were mentioned above will be considered, since the others were not carried out sufficiently far to be very useful for this purpose.

4.6.1 Comparison Case Without Fans

From a practical point of view, the most important quantity calculated is the containment pressure response after VB. Results for this parameter are compared for the 6-cell and 26-cell decks in Figure 4.14a. The agreement between the results given by the two decks is excellent, better than was the case for calculations of the sequence with a fully-pressurized primary system.

There was also generally good agreement between the two decks for pressures and temperatures in the upper containment prior to VB, except that transient pressure and temperature spikes associated with hydrogen burns came at different times and had different intensities. Dangerous pressurization events did not occur prior to VB with either deck. The numerous sharp temperature and pressure spikes gave the plot package used here fits, and curves for these parameters are therefore not presented.

Steam mole fractions in the upper containment calculated for the two decks are compared in Figure 4.14b. There are obviously some quantitative differences, and the agreement is not quite as good as that obtained for the pressure and temperature comparisons. Nonetheless, the overall behaviors are qualitatively quite similar and reflect the same basic phenomena, i.e., the ice condenser bypass flows.

Cumulative hydrogen combustion calculated before and after VB is plotted in Figures 4.14c and 4.14d, respectively. The calculated quantities of hydrogen consumed prior to VB are very similar for the two decks. The same is true for the period immediately following VB except that the 6-cell deck yielded a second burn during this period while the 26-cell deck did not give a second burn of any significance. The second burn calculated using the 6-cell deck resulted in a secondary peak in the pressure trace (Figure 4.14a), but it came too late to add to the maximum pressure calculated.

4.6.2 Comparison Case With Fans Operating

The "comparison case" with fans operating actually does not provide a fully valid comparison, because the 26-cell calculation was performed assuming only existing igniters were available, while the most nearly comparable 6-cell calculation (Case 12, Table 4.1) included the assumption that igniters were operating in all cells. Despite this difference, Figure 4.15a shows that the amounts of hydrogen consumed as a function of time were very nearly the same for the two calculations. As in the case without fans, the two decks gave generally good agreement as to pressures and temperatures in the upper containment; although the 26-cell deck gave somewhat

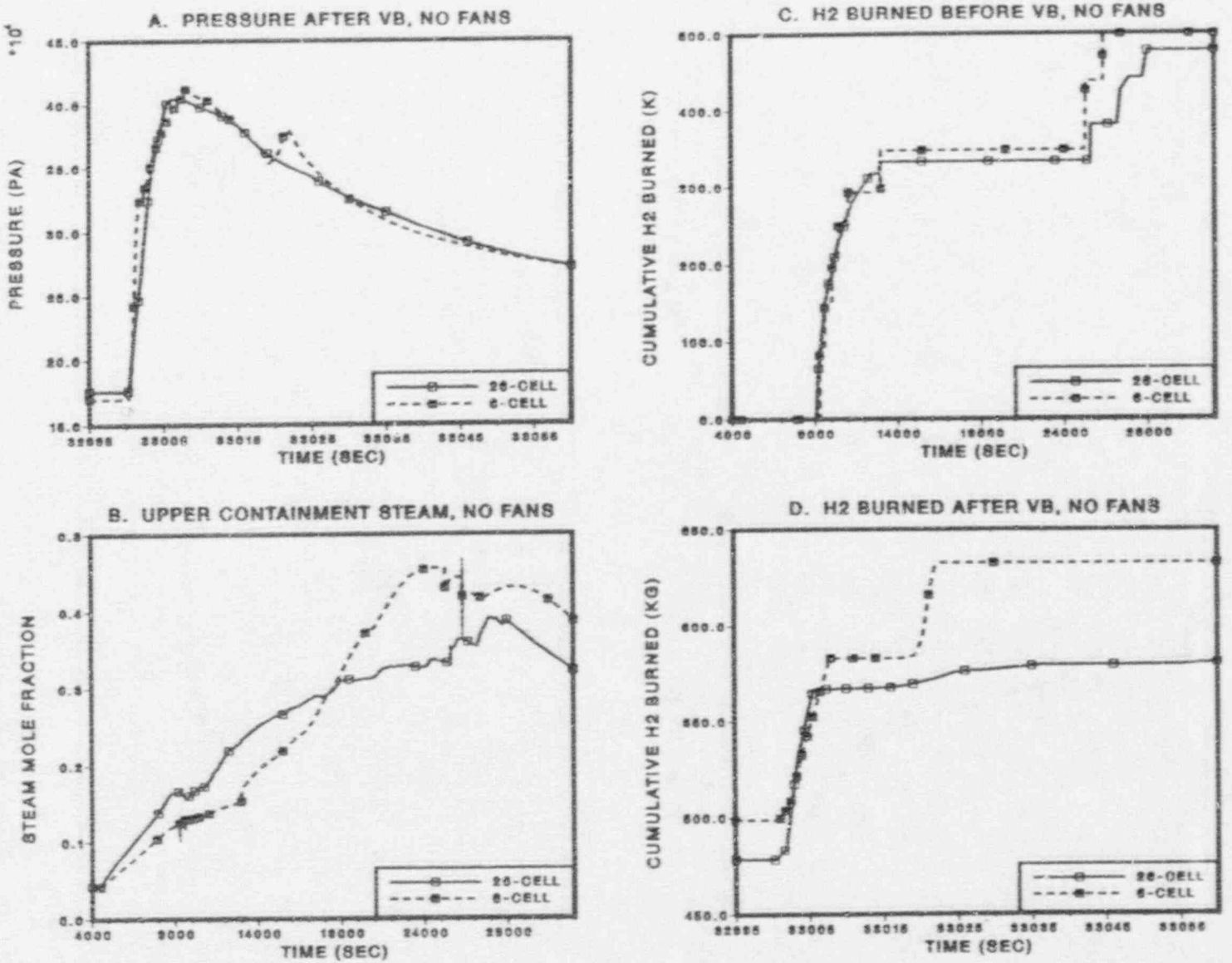

Figure 4.14 Comparison of 6-cell and 26-cell results, fans not operating.

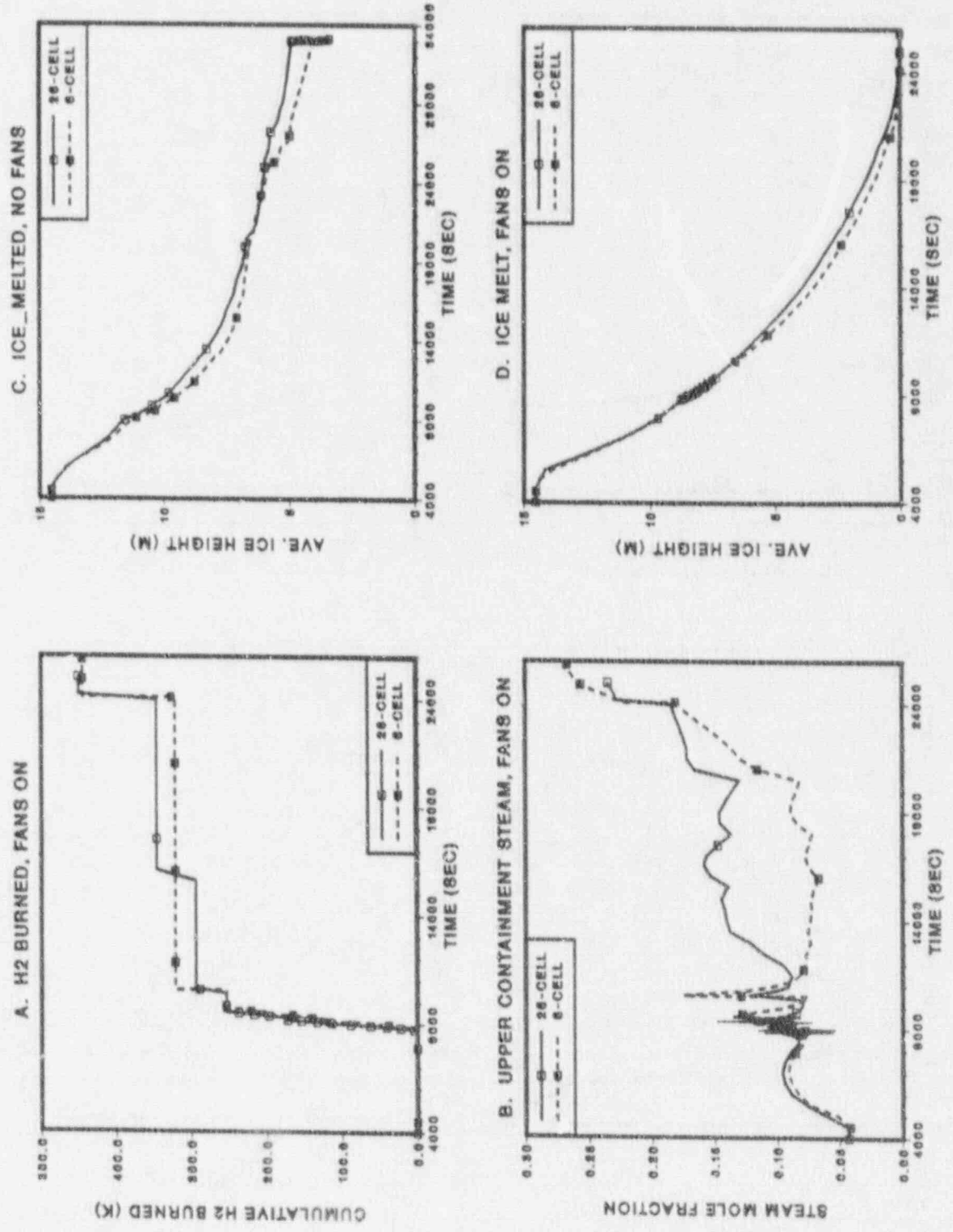

Figure 4.15 Comparison of 6-cell and 26-cell results for selected parameters, with and without fans operating.

higher values at times, the differences did not exceed 0.01 MPa and 10-15 K, respectively, except for transients associated with hydrogen burns.

Upper containment steam mole fractions from the two calculations are compared in Figure 4.15b. Initially, the agreement is excellent, and the behaviors are again quite similar near the end of the calculation. During the interval from about 12000 to 23000 s into the accident, the 26-cell deck is calculating somewhat higher steam fractions. This difference is due to the uneven ice melting calculated by the 26-cell deck.

4.6.3 Comparison of Ice Condenser Behavior

In Figure 4.15c, the height of the remaining ice column as a function of time calculated using the 6-cell deck is compared with the average ice column height in the 26-cell calculation, for the case without fans operating. In Figure 4.15d, a similar comparison is made for the case with fans operating. In both instances, the total amounts of ice remaining as a function of time are very similar for the two decks.

The agreement between the two decks found for the total ice remaining is potentially misleading, because the ice melt calculated using the 26-cell deck is very uneven. The height of the ice column remaining in each of the four ice columns of the 26-cell deck is plotted in Figure 4.16a for the case without fans, and in Figure 4.16b for the case with fans. Also shown is the average ice height.

The irregularity of the ice melting in the case without fans is especially striking. The right center quadrant (Cell 20 in Figure 2.3) melts out much more rapidly than any of the others. This pattern differs from what was calculated for the fully-pressurized scenario (see Section 3.3.3), for which the ice melting was approximately left-right symmetric even though it also was quite uneven, with the central quadrants melting much more rapidly than the end quadrants. In the present case, the recirculation flows were such as to concentrate the upward steam flow in the right center quadrant.

One reason for the asymmetric ice condenser response is that, after about 9700 s, hydrogen burns blow open the intermediate deck and upper plenum doors to their maximum extent on the two right hand quadrants, after which they do not fully reclose as they are modeled here (see Table 2.4). The doors on the left side are never opened to the point of irreversibility. With these doors remaining partially open, the asymmetric ice melt is accentuated; note the abrupt increase in the rate of melt of the right end quadrant at this time. However, the tendency for the right center quadrant to melt more rapidly begins well before any hydrogen burns and is, in fact, the likely cause of the more forceful burns in the right quadrants of the ice condenser.

The reason for the initial asymmetry, and why it differs from the other cases studied, is not known. It is clear, however, that any tendency for the steam flow to concentrate more in some sections than in others produces changes in the ice condenser and the door response that tends to accentuate the initial tendency. The steam from the primary system enters the lower containment in the central compartment (Cell 9, in Figure 2.3) and this leads to greater initial steam flows into the central quadrants of the ice condenser. The positive feedbacks noted subsequently amplify this tendency. The behavior calculated is no doubt sensitive to many modeling uncertainties and assumptions concerning the scenario details, and large quantitative uncertainties must be allowed for in the results. However, the qualitative behavior predicted seems quite reasonable, physically.

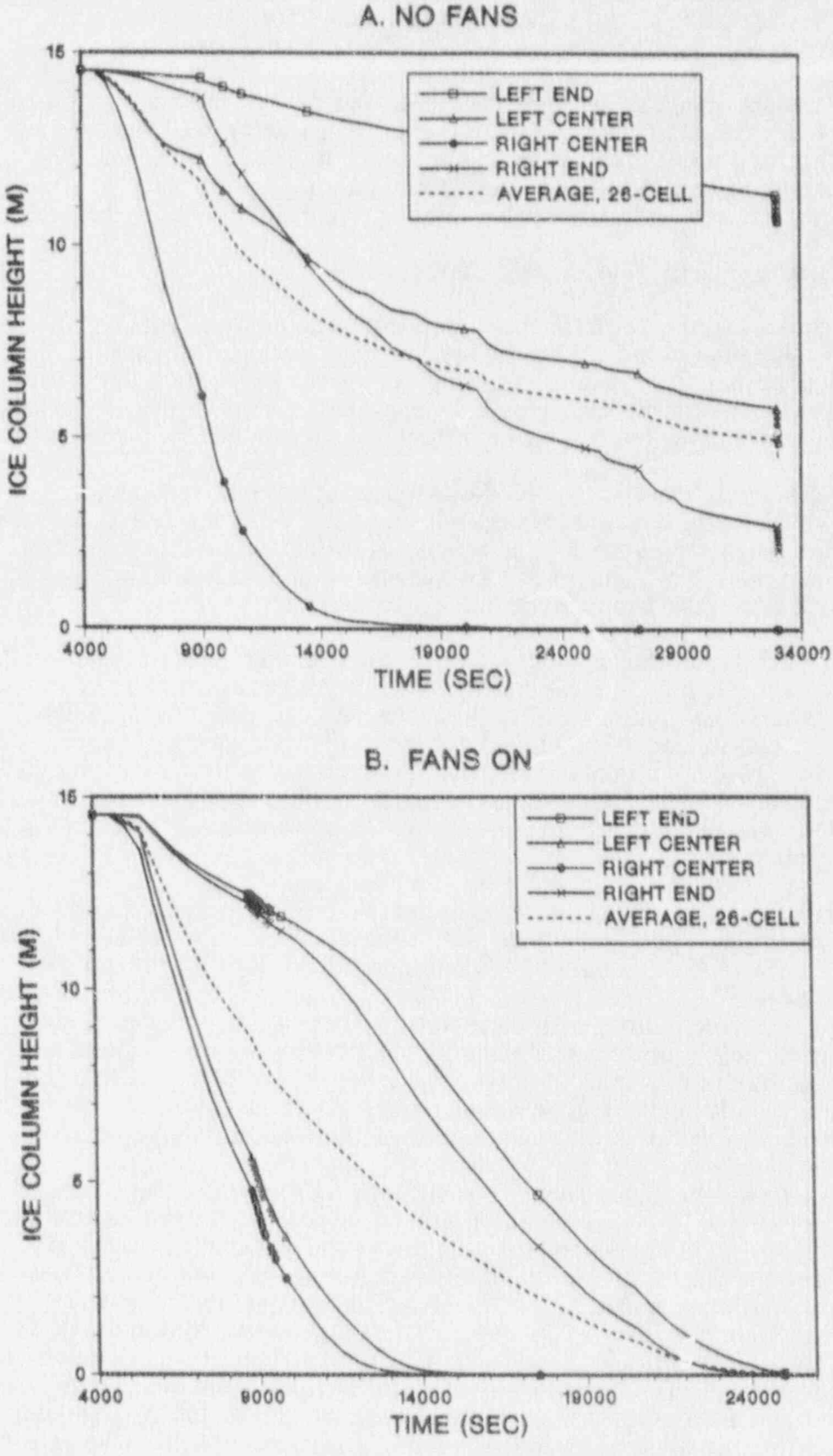

Figure 4.16 Distribution of ice melting and total ice melt, with and without fans operating (26-cell calculations).

With the fans running, the ice melt pattern is more symmetric but it is still quite uneven. One consequence of the uneven melting is that more steam reaches the upper containment, which explains the somewhat higher steam concentrations calculated by the 26-cell deck during the interval 11000-23000 s in Figure 4.15b. Note that the interval with significant differences in steam concentrations begins at about the time the ice in the two central quadrants is almost completely melted, and ends at about the time that all ice is melted in both calculations.

In view of the very uneven ice melting patterns, it might seem surprising that the total ice remaining as a function of time is so similar for the two decks. Similar results were obtained for the fully-pressurized sequence in Section 3.3.3, except for the cases in which the lower plenum doors were assumed to remain open to a large degree. The reason appears to be that there is enough recirculation within the ice condenser so that most of the steam which initially enters one of the heavily depleted quadrants circulates into one of the other quadrants and is condensed before it can leave the ice condenser.

The total quantity of ice melted is proportional to the amount of energy removed from the containment atmosphere. The fact that the unevenness of the ice melt does not greatly affect this quantity is an indication that ice condenser efficiency is not seriously impaired by the uneven ice melt for the scenario considered here. However, this may not always be true; if flow rates into the ice condenser are much greater, the extent to which steam and/or hot gas initially entering a depleted quadrant will reach an ice-filled quadrant before leaving the ice condenser may be less. It is plausible, at least, that uneven ice melting could compromise the effectiveness of the ice condenser in mitigating a DCH event. There is little sign of this in the pressure responses compared in Figure 4.14a, but the depressurized sequence considered here represents a rather weak DCH event. In the fully-pressurized calculations, there was some indication that uneven ice melt did reduce mitigation somewhat, even though the extent of ice melting was considerably less than that calculated for the depressurized sequence. Some additional sensitivity studies to investigate these questions may be warranted.

5. HYDROGEN DISTRIBUTION ISSUES: DETONATION THREATS

5.1 Introduction

Scope and Limitations of the Analysis. The 4-cell and 6-cell containment representations are inadequate to study detonation threats, in part because of the intrinsically low resolution and also because the level of detail is insufficient to model complex natural circulation patterns which can have important effects upon the gas distributions. Hence, only 26-cell results will be cited here.

The CONTAIN code does not include a detonation model, and it cannot, therefore, either predict the occurrence of detonations or calculate their consequences. It can, however, calculate atmospheric compositions at various locations and times, and these compositions may then be compared with available information on sensitivity to detonation as a function of gas composition, thereby permitting judgments as to whether detonations are at least possible. Even within this context, the code has certain limitations which should be kept in mind:

1. Within a given cell, the atmosphere is assumed to be well mixed; hence, no information is obtained as to the formation of detonable gas pockets on a subcell scale. It should be noted, however, that detonation of sufficiently small gas pockets would present little threat to containment integrity. Additional analysis would be needed to estimate the maximum size of a gas volume which could detonate without seriously endangering the containment.

2. When igniters are assumed to operate in a given cell, combustion is assumed to initiate as soon as flammable concentrations are reached, which usually automatically precludes detonable concentrations ever developing within that cell, in the calculation. Exceptions could arise during times of very rapid inflow into the cell, e.g., as when hydrogen is replenished more rapidly than it is consumed, which sometimes might happen during the calculation of a DCH event. However, the modeling is insufficiently detailed to reliably evaluate this situation. Hence, cases with igniters assumed to operate in all cells will not be considered here, nor will the conditions that develop following VB be assessed for potential detonation threats.

3. CONTAIN is a lumped-parameter, control volume code, and the degree to which codes of this type (or any other codes) can predict complex gas distributions is a subject of ongoing study. The comparison between PNL ice condenser experimental results and CONTAIN simulations, which is being performed as part of the CPI program, does suggest that CONTAIN can give a qualitatively reasonable description of the recirculation patterns involved, including those in the ice condenser region [Ru90]. Quantitatively, both these results and the results of other studies (e.g., code validation exercises performed at the German HDR facility) show that there are important uncertainties in the calculations of gas distributions (Section 2.4.1). In particular, the tendency toward gas stratification can be substantially underestimated under some conditions, especially when study of gas stratification within open volumes is attempted. Hence, no attempt will be made to consider the latter type of stratification in the present work.

Both the present work and previous analyses [Di85] indicate that detonable gas compositions are most likely to arise in the ice condenser region. The ice condenser

represents a relatively distinct physical volume, separated from the rest of the containment by the various door systems. Buoyant flows enter this region from the bottom, which is not the situation most likely to lead to stratification effects of the type that the code cannot handle. Hence, assessments of the detonation hazards in the ice condenser are not expected to be invalidated by the limitations noted here, though no doubt some quantitative uncertainty will be introduced. It is our judgment that these uncertainties are likely less than those associated with the uncertainties in the sources from the primary system, although there is no proof that this is the case.

Finally, it is important to remember that it has not even been established that detonations in the ice condenser constitute a significant threat to containment integrity. There is little doubt that, given detonation propagation through a free space of several meters or more, containment-threatening dynamic loads could be generated. However, the ice condenser is a very "busy" volume, with free unobstructed spaces being considerably less than a meter in much of this volume. Multiple shock reflections would occur at the ice basket surfaces and at other structure interfaces, and deformation of these structures could be an important energy absorption mechanism. Detailed analyses would be required in order to determine whether, and under what circumstances, detonations could actually threaten containment integrity, and no such analysis has been done. In the mean time, it is assumed here that the occurrence of detonable mixtures is something one would prefer to avoid.

Dependence of Detonation Sensitivity upon Composition. It is common to speak of "detonable compositions" as if detonability exhibited sharp thresholds as a function of the composition variables, but this is an oversimplification; it is more accurate to speak of detonation sensitivity as a function of these variables. Only a very brief discussion of this subject is given here; it is based upon information summarized in Ref. Ti90.

A useful measure of the detonation sensitivity is the detonation cell size, λ. Conservatively, detonations should be considered possible when λ/d is of the order of unity or smaller, where d is a "characteristic dimension" of the system (typically the diameter of a tube or a minimum wall separation in a rectangular duct). Note that this measure implies detonations are more likely to occur at large scale than at small scale, a trend which has been established experimentally.

Even given ignition of a mixture with $\lambda/d << 1$, it is by no means certain that a detonation will result. It is noteworthy, however, that turbulence and the presence of obstacles in the flame propagation path tend to favor flame acceleration and deflagration to detonation transition (DDT). Both turbulence and obstacles are likely to be available in the containment during severe accidents. Detonations can also be initiated directly by strong shocks and by hot jets entering the mixture. The latter initiation mode may be of interest at the time of vessel breach and HPME/DCH onset.

A combination of experimental data and semi-empirical predictions, taken from Ref. Ti90, concerning λ as a function of composition for steam-air-hydrogen mixtures is summarized in Figure 5.1. In the figure, λ is plotted against the equivalence ratio, Φ, for several different values of the steam concentration. The equivalence ratio is the ratio of the actual amount of hydrogen present to that required to form a stoichiometric ratio with the oxygen available; it is equal to $0.5\ X(H_2)/X(O_2)$, where the X's are the mole fractions.

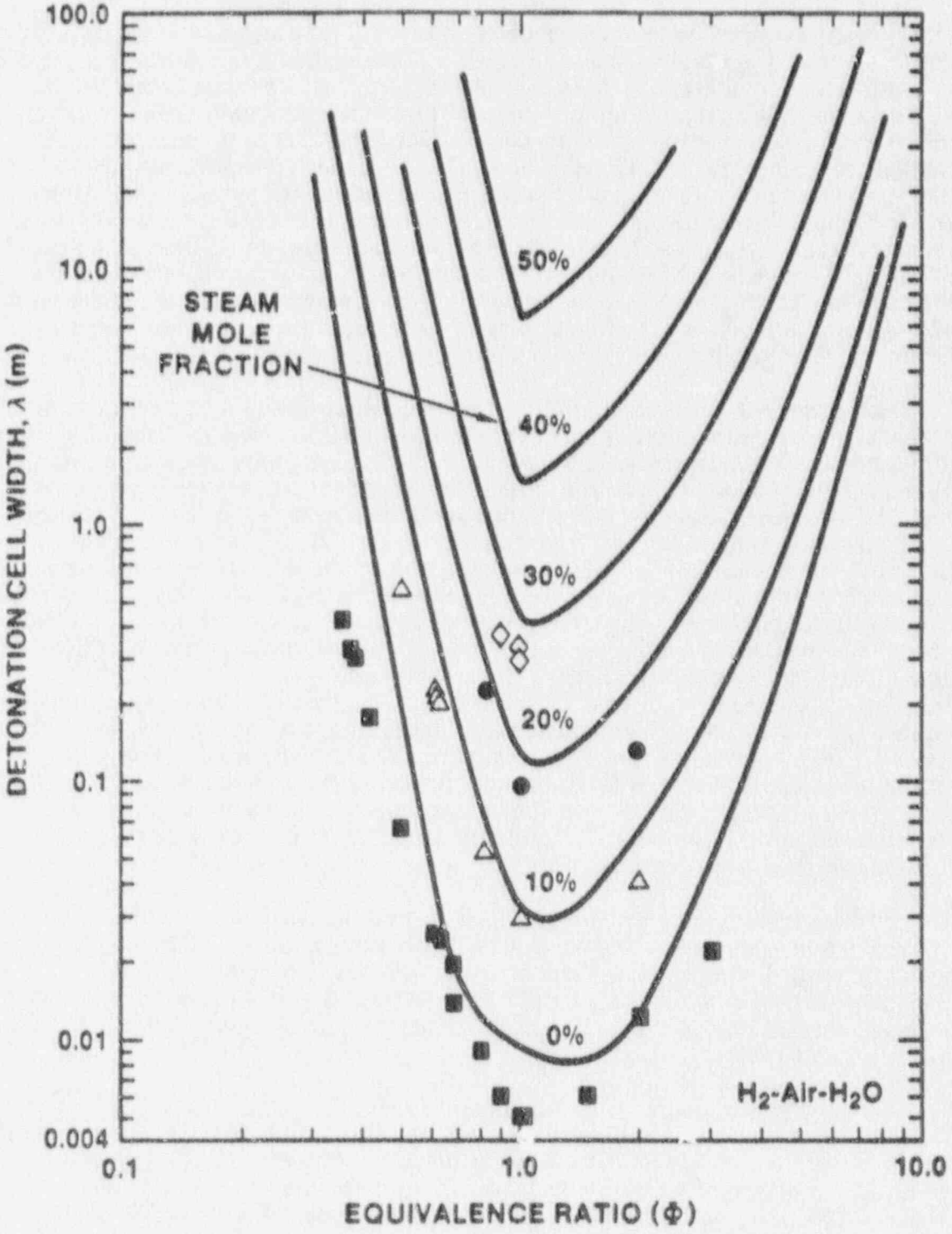

Figure 5.1 Some detonation cell width data and predictions from Ref. St90 (H_2-air-steam, ρ_{air} = 1.184 kg/m^3, T = 100 °C for data; T = saturation for prediction). Adapted from Ref. Ti90.

Figure 5.1 indicates that detonation sensitivity is a strong function of the gas composition, with the sensitivity decreasing (λ increasing) rapidly as Φ deviates substantially in either direction from unity. The sensitivity also decreases rapidly as the steam mole fraction increases. In addition, the sensitivity is a function of pressure and, especially, temperature; there is some reason to believe that λ decreases substantially with increasing temperature for those mixture compositions which are relatively insensitive at lower temperatures. Thus, at higher temperatures, the U-shaped curves in Figure 5.1 are expected to both broaden and move closer together [St90]. It should be remembered that these expectations are based largely upon semi-empirical models that involve assumptions which may not be valid for conditions far removed from those characterizing the available data base. In addition, the figure is meaningful only when the initial conditions are approximately equal to those stated in the caption. The figure also applies only when oxygen and nitrogen are in the normal atmospheric ratio; once oxygen has been partially depleted by previous hydrogen burns, λ will be greater than Figure 5.1 implies, sometimes by large factors.

The preceding systematics apply to the detonation sensitivity, or ease with which a detonation may be initiated. They do not directly tell how severe a detonation will be if one occurs. From a practical point of view, the loads parameters of greatest interest are usually the maximum dynamic pressure and the detonation impulse, with the impulse sometimes being the more important in determining the response of large structures such as nuclear power plant containments. In fully-developed detonations, these parameters will both be proportional to the initial pressure P_0 and the impulse will be proportional to the detonation propagation distance, other things being equal. The detonation loads will also increase as the chemical energy release per unit volume of gas increases, although the dependence upon this parameter is not so simple. At a given total gas pressure, this energy release is proportional to $\mathrm{Min}(X(O_2),X(H_2)/2)/T_0$, where T_0 is the initial temperature. Hence, mixtures with equivalence ratios far from unity will result in less severe detonations as well as being more difficult to initiate, other things being equal. Detonation loads are a very complex subject, however, with many other dependencies in addition to those noted here. Among these is the effect of shock reflection and interaction, which is highly dependent upon the containment geometry, the location where the detonation initiates, its direction of propagation, etc.

Still another concern is that highly accelerated flames may develop at hydrogen concentrations below those for which true detonations are believed to be possible; for example, in air-hydrogen mixtures, accelerated flames may be possible for concentrations of the order of 10% [Ti90]. The peak dynamic pressures associated with accelerated flames will be less than for true detonations, but the total impulse may be comparable.

Primary System Sources. In the fully-pressurized station blackout sequence, the source of hydrogen input to the containment from the primary system is insufficient to result in a detonation threat except during the last 1000 s prior to VB (Figure 2.4). In contrast, the period of maximum hydrogen input in the depressurized scenario occurs at about 10000 s, long before VB, although there is a second, smaller influx of hydrogen at about 25000 s.

In general, detonable gas compositions are most likely to arise during or shortly after the periods of most rapid hydrogen influx. Hence, attention will be focused on the time interval from 9200 s to vessel breach (at 10090 s) in the fully-pressurized sequence, and the time interval from 8500 s to 11000 s for the depressurized sequence. Sources of steam and hydrogen for these intervals are displayed in Figure 5.2. For the

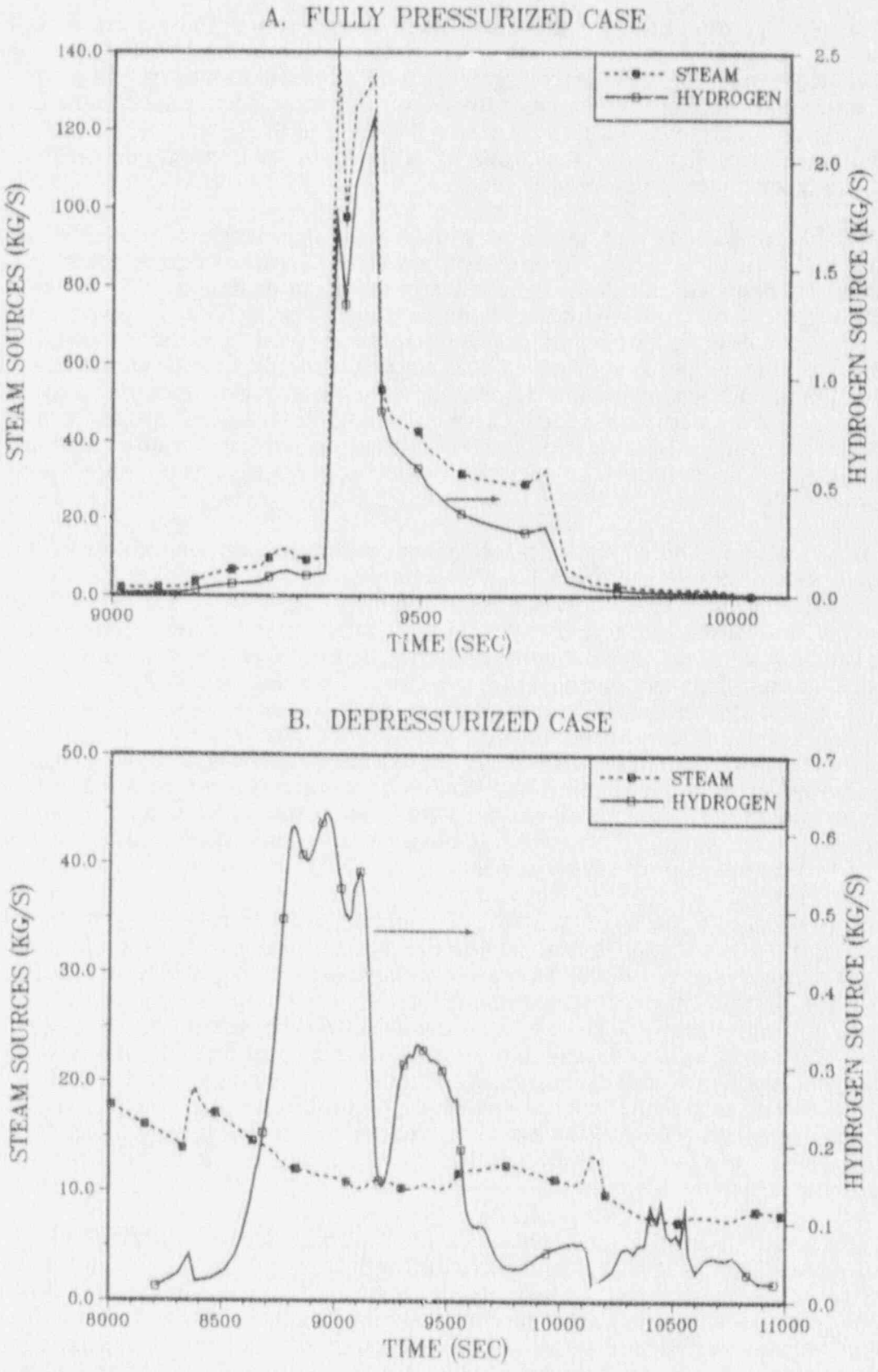

Figure 5.2 Sources of steam and hydrogen from the primary system during periods of highest influx, pressurized and depressurized scenarios.

fully-pressurized case, both the steam and the hydrogen source show a strong peak at about 9400 s, which corresponds to the time of core slump in the MARCH calculation. For the depressurized case, the hydrogen source is somewhat more spread out in time, and the time at which it is the strongest does not correspond to a time at which the steam source is particularly strong. These differences in the sources will be seen to have important implications for the severity of the detonation threat in several of the scenarios to be discussed in this section.

The magnitude of these sources as a function of time depends intimately upon the details of the in-vessel meltdown progression, which is an area of gross uncertainty; the containment response calculated is sensitive to these source details. When these uncertainties are combined with the phenomenological uncertainty involved in the containment modeling, one might suppose that the uncertainty in the results of the CONTAIN calculations is enormous. This conclusion might be valid if one viewed the goal of the calculations to be determining the atmospheric composition at a specific location and at a specific time during a specific accident sequence. However, the goal of the present work is best viewed as an effort to explore the spectrum of containment responses possible, and how this spectrum responds to the various mitigation schemes considered.

In this context, the strong time-dependence and sequence-dependence of the primary system sources used here is actually beneficial. We know of no reason to believe that the variations involved are outside the range of what is credible for severe accidents. Furthermore, there is every likelihood that these sources are realistic in at least two respects: they vary strongly as a function of time, and they are quite different for different accident sequences. Thus, the range of containment behaviors calculated should represent a reasonable subset of the range of behaviors possible in reality, even though it is obviously impossible to rule out still other, quite different, behaviors for accident scenarios not studied. In effect, the variability of the sources to be expected "washes out" some of the effects of the various uncertainties involved when one considers the range of the responses calculated, rather than the behavior obtained for a particular time and place. In assessing possible mitigation schemes, it is this range of behaviors that one needs to keep in mind.

Presentation of the Results. In the calculations of DCH-related quasi-static loads discussed in Sections 3 and 4, a single number, the maximum pressure calculated in the upper containment, sufficed to represent the result of the greatest practical interest. The problem of presenting the results is more complicated here, since a variety of flow patterns and gas compositions at a variety of times and places may be of interest. There is, in fact, no way to present all the information that might possibly be relevant. Only a representative sampling of results can be given, with the examples selected chosen to indicate results of greatest practical importance and/or to illustrate important phenomenological behavior. In most cases, the results given include information on the gas composition at the time and place for which the detonation hazard appears to be the greatest.

Cases to be discussed are listed in Table 5.1. The cases with the RCS fully pressurized correspond to the cases discussed in Section 3.4 in the context of DCH-induced pressures, and they are assigned the same case numbers as in Table 3.4 of that section. Some numbers are skipped, corresponding to cases that need not be discussed here. For reference purposes, the maximum hydrogen concentration calculated for the ice condenser is given in the next to last column of the table, although it should be apparent that these scenarios cannot be satisfactorily described in terms of this single

Table 5.1

Calculations Performed for the Assessment of Detonation Threats

Case No.	RCS P (MPa)	Igniters Powered	Other	Max. $X(H_2)^*$	P_0 (MPa)
1	16.6	None	Note a	0.29	0.145
12	16.6	None	---	0.30	0.178
13	16.6	Existing	---	0.25	0.174
14	16.6	Existing + l.p.[b]	---	0.24	0.174
16	16.6	Existing	Fans Powered	0.14	0.128
17	16.6	Existing	Containment Vented	0.29	0.112
19	16.6	Existing	Fans; Vented	0.18[c]	0.092
20	1.5	None	---	0.35	0.176
21	1.5	Existing	---	0.17	0.168
22	1.5	Existing +l.p.[b]	---	0.09	0.171
23	1.5	Existing	Fans Operate	< 0.08	0.125
24	1.5	Existing	Surge Line Break	0.17	[illegible]
25	1.5	Existing	Fans; Surge Break	0.13[c]	[illegible]

Notes:
* Max. H_2 in ice condenser, not including times for which O_2 and/or H_2O concentrations are incompatible with combustion.
[a] Doors modeled as in Table 2.2. In all other cases, doors were modeled as in Table 2.4.
[b] Igniters installed and operated in the lower plenum, in addition to existing igniter systems.
[c] Occurred at a time of significant oxygen depletion due to previous hydrogen burns.

number alone. In the last column, the containment pressure at the time of the maximum hydrogen concentration is given; this pressure would be "P_0" if a detonation actually initiated at this time.

5.2 Response of the Unmodified Plant

5.2.1 Recirculation Flow Patterns

The density of the gas in the ice condenser is normally considerably greater than that in the lower containment, and gas from the latter enters the ice condenser at the bottom. Hence it is only to be expected that natural convection circulation patterns can be important. The patterns change with time and with the scenario, and only a few illustrative examples will be given here. The flows are especially complex when operating the igniters results in numerous small hydrogen burns, and the flow patterns will be discussed in detail here for only some cases without igniters.

Figure 5.3 portrays the flow pattern calculated for Case 1 of Table 5.1 for two representative times of interest in the sequence with the RCS fully pressurized. The first time is at 9400 s, during the time of strong hydrogen and steam input to the

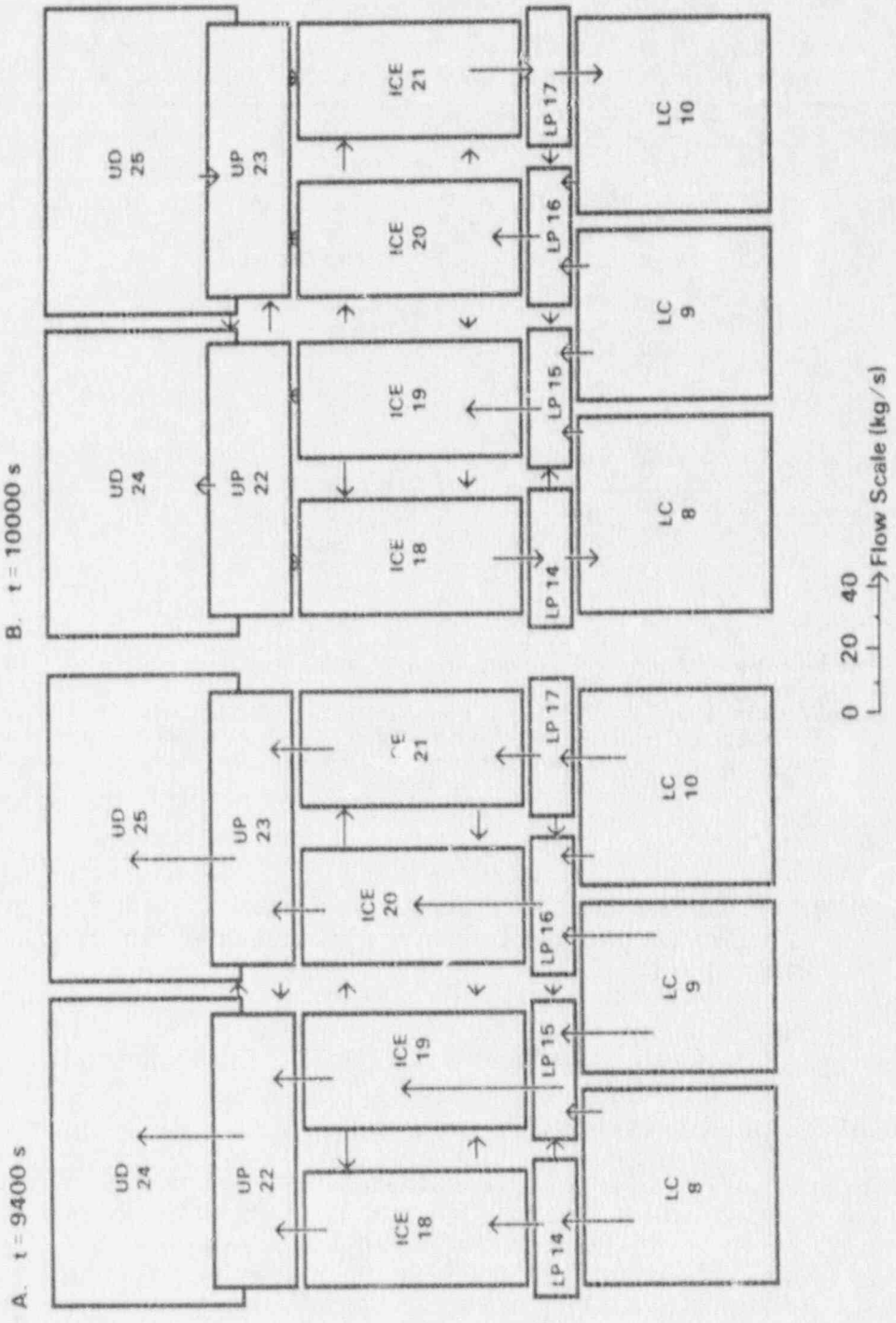

Figure 5.3 Flow patterns in the ice condenser region with the lower plenum doors remaining partially open.

containment. The second is at about 10000 s, shortly before VB, when sources to the containment are much smaller. In the figure, the various boxes represent the computational cells describing the lower containment inside the crane wall ("LC", Cells 8-10), the lower plenum ("LP", Cells 14-17), the ice condenser ("Ice", Cells 18-21), the upper plenum ("UP", Cells 22 and 23), and the upper dome region ("UD", Cells 24 and 25). The figure is not to scale, but the relative elevations of the lower plenum, the ice condenser, and the upper plenum are approximately to scale. On the other hand, the lower plenum is actually at the same elevation as the upper portion of the lower containment and flow from the latter into the plenum is radially outward, not directly upward as suggested by the two-dimensional representation of Figure 5.3. The lengths of the arrows in the figure are proportional to the flow rates, in kg/s, between the indicated cells. In addition to the flows indicated, there are substantial convective interchanges between the lower containment cells, and between the upper containment cells. These flows are not represented in the diagrams of Figure 5.3. Except for these instances, the absence of an arrow connecting any two adjacent cells in the diagram means that the flow was too small to represent on the scale used, i.e., < 1 kg/s.

In Case 1 of Table 5.1, the ice condenser doors were modeled as summarized in Table 2.2. In this representation, the lower doors were treated as being (approximately) half reversible and half irreversible. In the calculation, strong steam and primary system water sources at about 5000-6000 s into the transient (see Figure 2.4) were calculated to open the doors substantially, and all the doors remained about one third open after this time. The geometric relation between the lower containment and the lower plenum cells is such that six separate flow paths are involved, with their areas being approximately in the ratios 3:1:2:2:1:3. Approximately the same fraction of the total door area is open for all six segments at the times for which Figure 5.3 is drawn.

At 9400 s, the forced flow resulting from the strong sources entering the containment is the dominant factor governing the flow patterns. Nonetheless, a substantial natural convective pattern is superimposed upon the forced flow pattern. Flow upward into the ice condenser is concentrated in the two central sections, there is lateral flow toward the end sections in the upper part of the ice condenser, and lateral flow toward the center in the lower portion of the ice condenser and in the lower plenum.

In both the fully-pressurized sequence and the depressurized sequence, steam and hydrogen enter the containment from the pressurizer quench tank, which is located in Cell 9. Cell 9 tends to have somewhat higher temperatures and steam mole fractions than either Cell 8 or Cell 10, which probably contributes to the initial tendency for flows and ice melting to be greatest in the central portion of the ice condenser. At later times, such as those for which the figures are drawn, the unequal ice distribution itself reinforces this tendency.

Figure 5.3b shows that the flow pattern at 10000 s, when the sources are weak, is quite different from the pattern obtained when the sources are strong. The flow pattern within the ice condenser and the plena is completely dominated by the recirculation flow; there is hardly any net flow. Though the absolute magnitudes of the flows are less than in Figure 5.3a, they are still of the order of a few tens of kilograms per second. Perhaps the most striking feature of the flow pattern is that there is a large amount of convective interchange between the lower containment and the lower plenum (and hence the ice condenser). This exchange amounts to about 30 kg/s. Since the mass of the atmosphere in the entire lower containment is about

10000 kg at this time, the convective exchange through the partially open doors is sufficient to have a large effect upon lower containment conditions on time scales of a few hundred seconds.

In the remainder of the calculations listed in Table 5.1, the doors were modeled as in Table 2.4, which is believed to be more realistic. In this representation, the lower plenum doors were assumed to be fully reversible unless they were forced open to the maximum extent possible, in which case deformation of crushable hinges was assumed to hold them open (see Appendix A). In the present scenario, the flows prior to VB were not strong enough to cause this to happen, and hence the doors largely reclosed when the sources were small (complete closure requires a small back pressure). However, the flow patterns with doors open are still of interest, since some other scenarios might have sources strong enough to jam the doors open. Indeed, this sometimes happened as the result of pressure surges associated with hydrogen burns in the cases calculated with igniters assumed to operate.

Case 12 in Table 5.1 was calculated using the reversible representation of the doors, again without igniters operating. The recirculation patterns at 9400 s and 10000 s for this case are diagrammed in Figure 5.4a. The patterns differ significantly from the previous case. At 9400 s, the tendency of the flow to concentrate in the central part of the ice condenser is much stronger than in the previous case. Indeed, the flow in the two end segments of the ice condenser is actually downward, in the lower portion. Overall, the modification of the forced flow pattern by the natural circulation pattern is considerably greater than in Figure 5.3a.

One reason for this difference is that the lower door panels entering the two central cells of the lower plenum (Cells 15 and 16) are open about 5 to 10 times as wide as are the doors entering the two end cells. This reflects the fact that the ice condenser cold head is less in the central region than in the colder end region. The steam and gas entering the lower plenum therefore meets less resistance in forcing open the doors near the center. The difference in temperature and in atmospheric composition for the different segments of the ice condenser are sufficient to produce differences in the cold head of up to a few tens of pascals. This is enough to have a substantial impact upon the degree to which the doors open (see Table 2.4). Hence, the door response provides another positive feedback that amplifies any initial tendency toward nonuniform flow and nonuniform ice melting in the ice condenser.

When the sources to containment are weak (Figure 5.4b), the lower plenum doors almost completely close, and there is very little flow in either direction between the lower plenum and the lower containment. With little steam (and energy) entering the ice condenser, there is less driving force for convective circulation within the ice condenser region than there was for the analogous case with the doors partly open. Nonetheless, the convective flows within the ice condenser and the plena are still significant.

The flow patterns displayed here are only a few examples out of many that might be offered. For example, in the depressurized sequence without fans operating, the upward flow, and hence the ice melt, was disproportionately concentrated in the right center section of the ice condenser, as was discussed in Section 4.6. In calculations with the fans running, the flow patterns tended to be qualitatively similar to those illustrated at 9400 s in Figures 5.3a and 5.4a: the net pattern was the result of a fairly strong forced flow field superimposed upon a recirculation pattern of comparable strength. For all cases examined in this work, the recirculation flow was always significant except for the period of extremely strong forced flows immediately

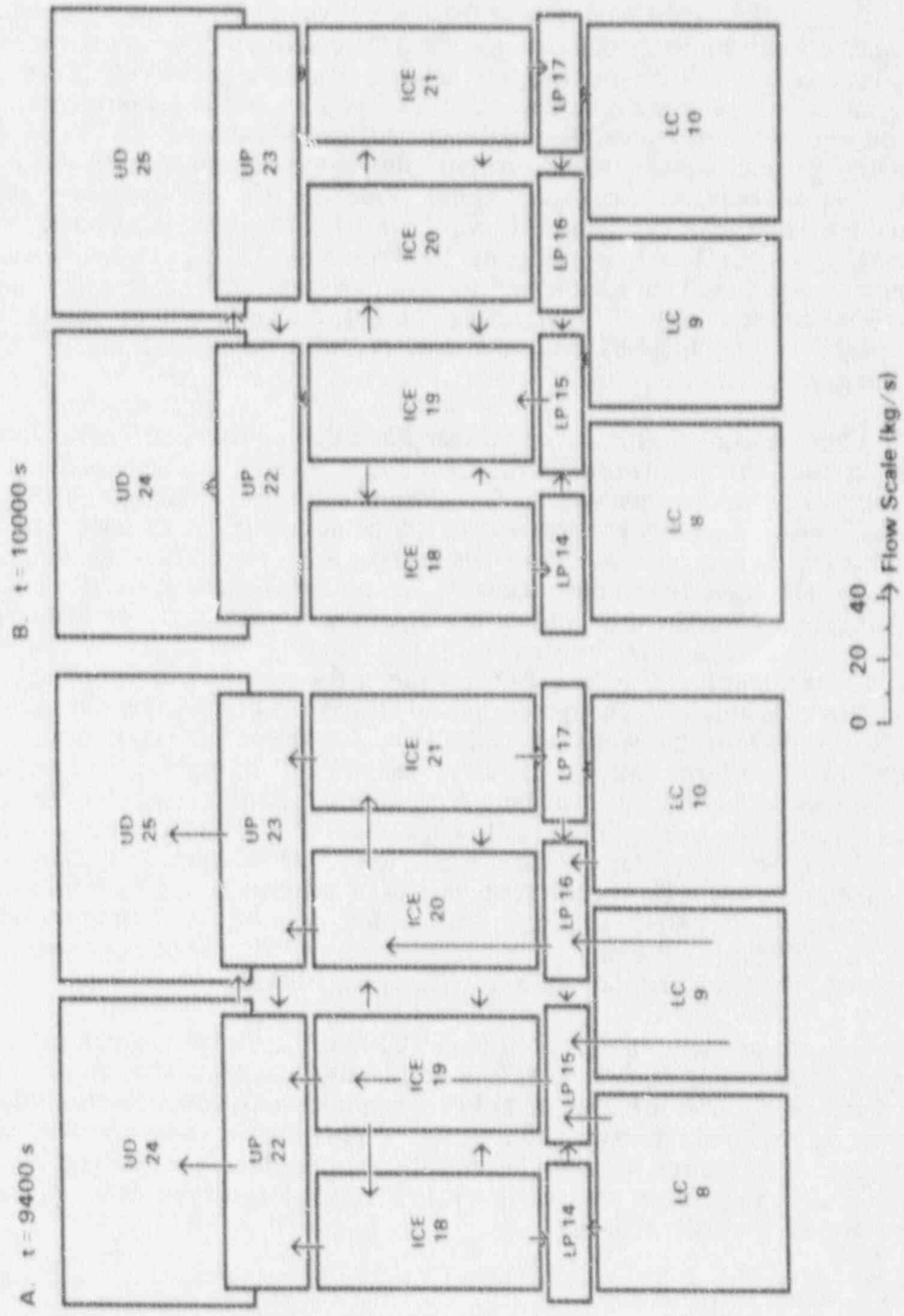

Figure 5.4 Flow patterns in the ice condenser region with the lower plenum doors reversible.

following vessel breach and DCH onset. In all cases, the distribution of ice melt prior to VB was very uneven.

In addition to uncertainties in the sources driving the flow patterns calculated here, there are some significant modeling uncertainties. Some are related to limitations in the flow modeling which were discussed previously (Section 2.4.1; also, Section 5.1). There are also uncertainties in such input parameters as the flow turbulent loss coefficients used to describe flow resistance in CONTAIN. Even the physical geometry parameters were no always entirely clear from the available information sources. However, it is not likely that any of these uncertainties would alter the qualitative behavior observed, even if some quantitative uncertainty does result. In HECTR code calculations for Sequoyah [Di85], sensitivity studies were performed in which ice condenser flow coefficients and heat transfer coefficients were varied over wide (order-of-magnitude) ranges; the recirculation patterns calculated showed little sensitivity to these parameters and were quite similar to those calculated in the present work.

There is one other modeling uncertainty that could conceivable have a qualitative impact upon the results obtained, and it has to do with the coarseness of the ice condenser nodalization used. In the present work, the recirculation flow pattern always involved some variation on the theme of upward flows concentrated in the central region and downward flow, or at least less upward flow, in the end regions. This pattern resulted in unevenness in the ice melting and in the door responses, which provided reinforcement for the initial tendency in this direction. Physically, it seems very reasonable that instabilities of this general type would exist. However, this general argument says little as to the scale of the resulting instabilities and associated circulation patterns. Although the nodalization used here does not exactly force the particular pattern that was observed, it obviously does permit only large-scale instabilities and flow patterns to be represented. If, in reality, the instabilities were to be dominated by flow patterns on a considerably smaller scale than those permitted by the present nodalization, the results might be rather different. For example, the overall impact on the large-scale distribution of ice melting, and upon ice condenser performance, might be considerably less than implied here. It would be interesting to perform sensitivity studies using a finer nodalization of the ice condenser, although it is not clear whether the physics modeled is adequate to permit a completely definitive answer to this question, however fine the nodalization.

Despite this possibility, it remains true that the steam sources enter the containment in Cell 9. It is therefore reasonable to expect that there would be a tendency of the upward flow, and of the ice melting, to concentrate in the central region, as the calculations predict. It is also reasonable to expect that once established, this imbalance will be self-amplifying. It seems likely, therefore, that the CONTAIN calculations are qualitatively correct, despite the limitations inherent in the coarse nodalization used.

5.2.2 Gas Distributions

Lower Doors Partially Open. Information on the steam and hydrogen distributions in the lower containment and in the ice condenser for Case 1 of Table 5.1 is provided in Figure 5.5. Oxygen concentrations may be inferred by noting that the only gases in the problem are steam, hydrogen, and oxygen and nitrogen in the normal atmospheric ratio, since no hydrogen burns that would deplete the oxygen occur prior to VB in this calculation. The cell numbering scheme is: Cells 8-10, lower containment inside the crane wall; Cells 11-13, lower annulus (between the crane wall

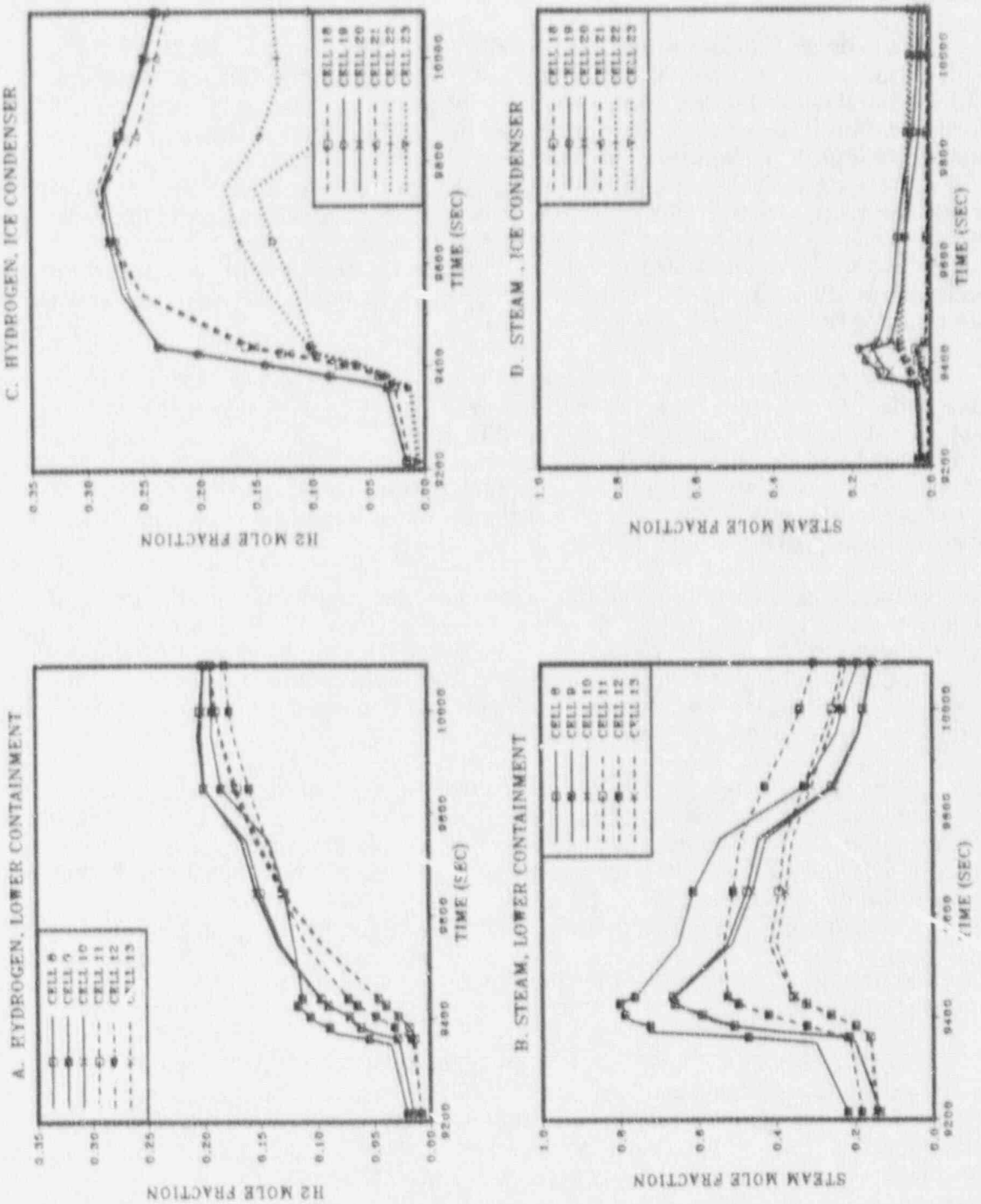

Figure 5.5 Hydrogen and steam concentrations in the lower containment and in the ice condenser, lower plenum doors remain partially open.

and the containment pressure boundary); Cells 18-21, the ice condenser; and Cells 22 and 23, the upper plenum.

The primary system sources enter in Cell 9, and this cell has the highest steam concentrations of the lower containment cells. However, the convective exchange with Cells 8 and 9 is substantial, and steam concentrations in these cells track the Cell 9 concentration fairly closely. Exchange with the annulus cells is slower, and concentrations in these cells therefore show a greater lag in following the concentrations in the lower containment inside the crane wall. Steam concentrations inside the crane wall are high enough to produce steam inerting during the time of strong primary system sources, but they fall quite rapidly and are about 20% or somewhat less at the time of VB. This decline is primarily due to the convective recirculation flows between the lower containment and the ice condenser, which was discussed in the preceding subsection.

Hydrogen concentrations in the lower containment at VB are about 20%, and this atmosphere is not only highly flammable but detonable. With steam and hydrogen concentrations of 20% each, $\Phi = 0.75$, and Figure 5.1 indicates that λ would be of the order of 0.1 to 1 m. Since this is an order of magnitude smaller than typical lower containment dimensions, occurrence of a global detonation involving much of the lower containment at VB is difficult to rule out in this scenario, assuming there are no ignition sources prior to vessel breach.

In the ice condenser, equivalence ratios are only slightly less than unity, and steam fractions are low, ≤ 0.1 during the time of interest. Detonation cell sizes may be estimated from Figure 5.1 as being in the range 0.01-0.1 m. Such gas mixtures must be considered to be quite sensitive to detonation. Flammable compositions develop in the upper plenum also, and detonation sensitivity, though much lower than in the ice condenser, is not completely negligible.

Lower Doors Reversible. Gas compositions in the lower containment and in the ice condenser are displayed for Case 12 of Table 5.1 in Figure 5.6. In this case, there is little recirculation flow between the lower containment and the ice condenser (Figure 5.4) and steam mole fractions in the lower containment are 0.6 or higher, high enough to inert the atmosphere against combustion. Hence, operating the existing igniters would not be expected to burn off this hydrogen in the lower containment. On the other hand, there is probably little detonation hazard in the lower containment at the time of vessel breach, even allowing for the possible effects of the sudden heating of the atmosphere at this time.

In the ice condenser, however, the situation is very different. Even more than in the previous case, hydrogen equivalence ratios are close to unity, and steam concentrations range from small to negligible. These atmospheric compositions correspond to detonation sensitivities that are close to the maximum possible. Detonation sensitivity in the upper plenum is higher than in the calculation with the lower plenum doors partially open, though not quite as high as in the ice condenser.

Depressurized Sequence. In Figure 5.7, results for the depressurized station blackout sequence, without igniters, are displayed (Case 20, Table 5.1). As in all the cases other than Case 1, the reversible lower plenum door model (Table 2.4) was used. Atmospheric compositions are similar to those displayed in Figure 5.6 for Case 12: the lower containment is steam inerted, while ice condenser conditions are close to the maximum possible detonation sensitivity. Indeed, equivalence ratios are slightly higher than unity, but not enough higher to significantly reduce detonation sensitivity.

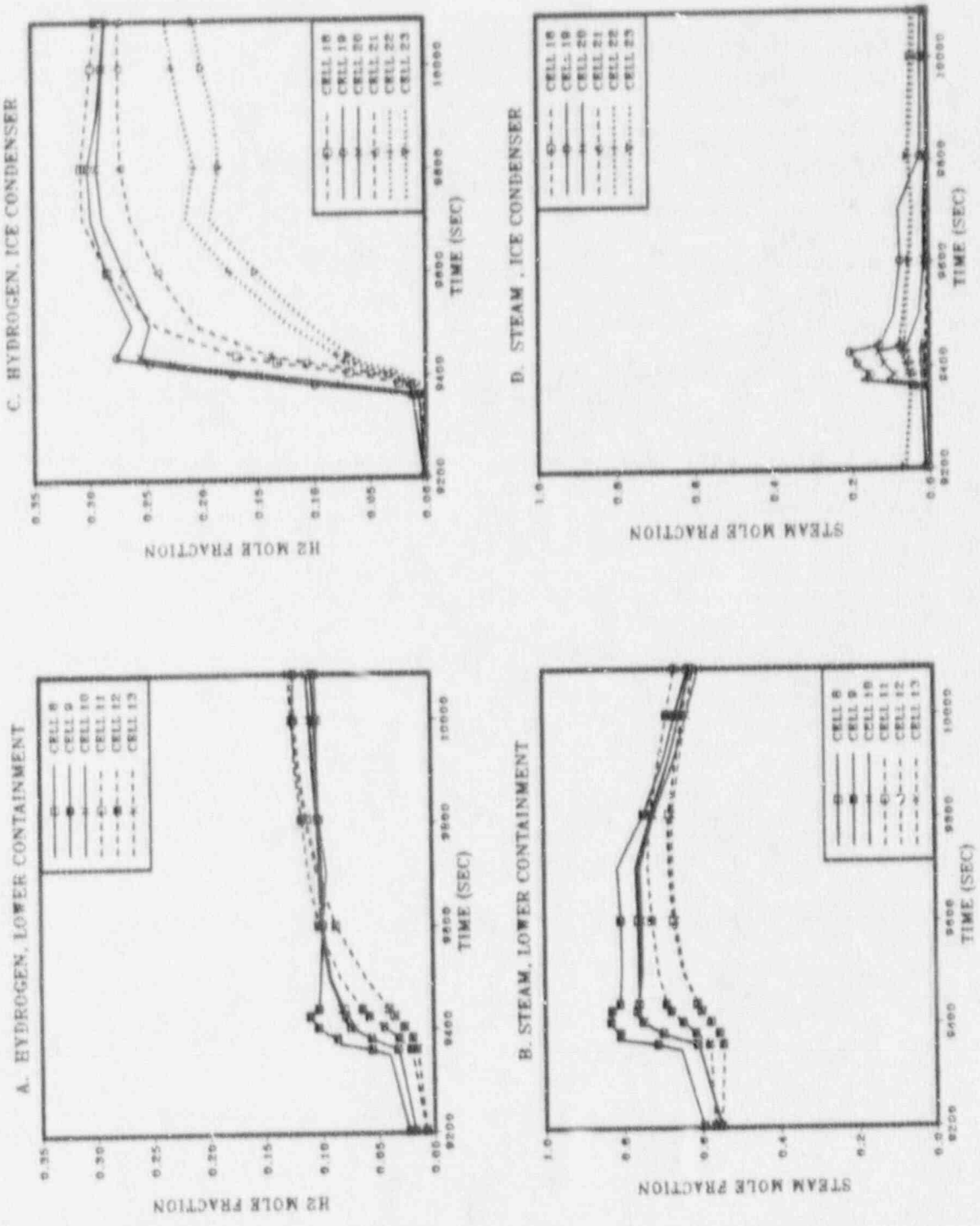

Figure 5.6 Hydrogen and steam concentrations in the lower containment and in the ice condenser, lower plenum doors reversible.

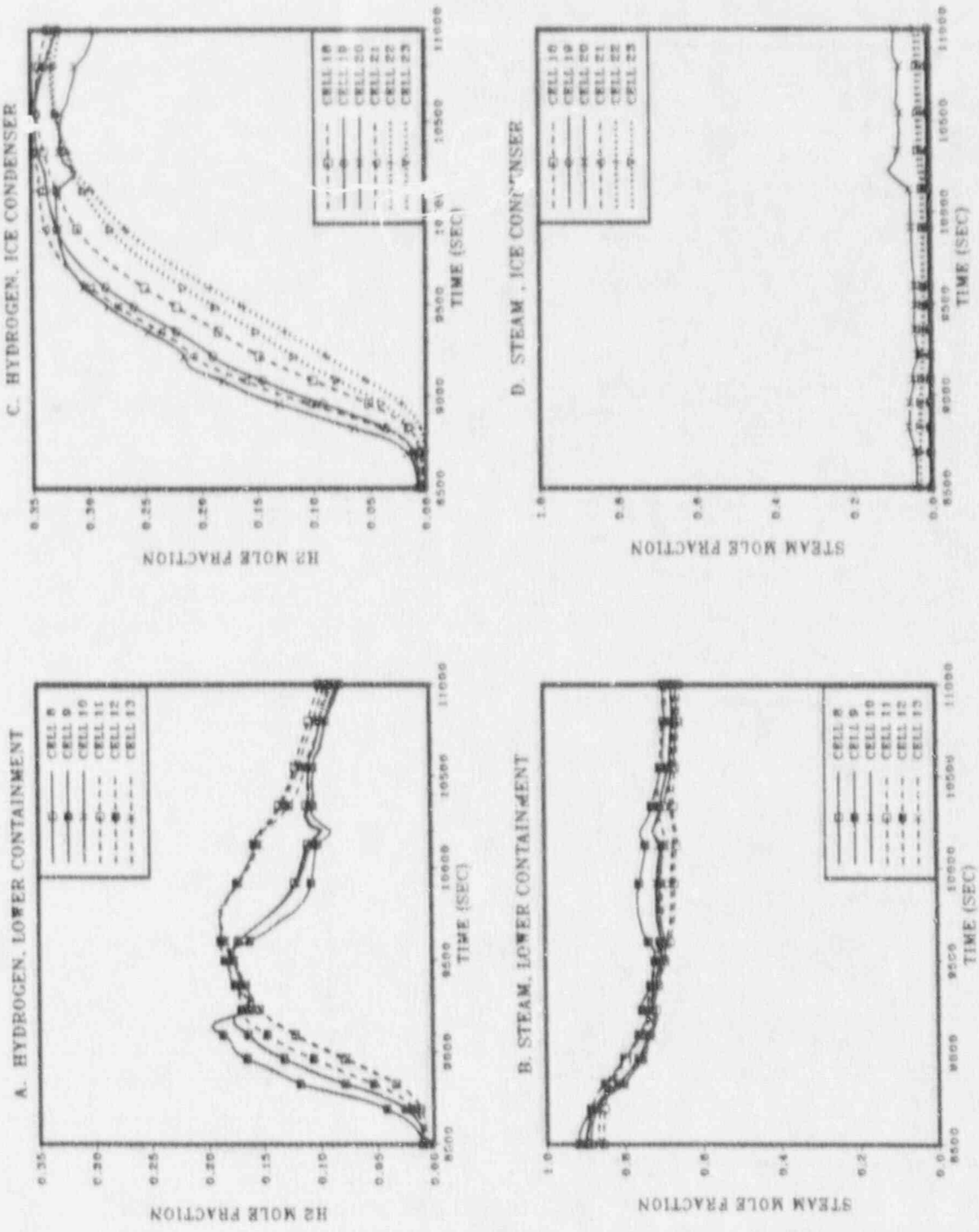

Figure 5.7 Hydrogen and steam concentrations in the lower containment and in the ice condenser, doors reversible, depressurized scenario.

In this calculation, the upper plenum atmosphere eventually becomes as detonable as is the ice condenser atmosphere.

In the fully-pressurized cases considered, the plots end at the time of VB, when an ignition source is essentially guaranteed. In the depressurized scenario, VB does not occur until times much later than those displayed in the figure (this calculation was not carried out beyond 11000 s). Hence, highly detonable mixtures might develop without ignition occurring. However, it should be noted that the spark energy required to ignite near-stoichiometric mixtures at low steam concentrations is extremely small, of the order of 0.02 millijoules [Ti90]. It may be very difficult to rule out the chance occurrence of ignition of highly sensitive mixtures such as these. Once ignited, the available experimental data suggest that near-stoichiometric mixtures are likely to undergo DDT except, possibly, in the absence of obstacles in the flame propagation path [Sh89]. The latter situation does not apply here.

Summary, Detonation Hazards w/o Igniters. Gas distributions and detonation potential are expected to be sensitive to assumptions concerning the behavior of the lower plenum doors, as well as sensitive to the steam and hydrogen sources input to the containment. The calculations described here involve substantial variation in these parameters. Despite these variations, the results are strikingly consistent in one crucial respect: gas compositions having near-maximum detonation sensitivity develop in the ice condenser in all cases. The only reasonable conclusion is that the development of highly detonable mixtures in the ice condenser must be considered quite likely, if ignition sources are absent; given ignition of such a mixture, actual detonations must also be considered quite plausible.

Detonable conditions also tended to develop in the upper plenum, although the detonation sensitivity varied more than it did in the ice condenser. In the lower containment, conditions tended to remain steam inerted when the lower plenum doors were allowed to close. Flammable and/or detonable conditions developed only when the doors remained open to a substantial degree, thereby permitting convective interchange with the ice condenser to condense much of the steam.

5.3 Effects of Igniters

In view of the results just described, it is clear that hydrogen control is needed if detonation threats are to be avoided during station blackout sequences, with or without RCS depressurization. One obvious means of hydrogen control to consider is igniters, and these will be analyzed in the present section. With igniters operating, hydrogen burns produce numerous abrupt variations in gas composition, which creates a problem in presenting the results; plots such as those in Figures 5.5-5.7 would be quite unintelligible in many cases. Graphical presentations of gas compositions, etc, will therefore be limited to displays of the behavior at selected times and locations of special interest.

Igniter operation will produce transient pressure surges (and hence flow surges) due to hydrogen burns. There also may be more persistent effects upon the convective recirculation patterns discussed in Section 5.2.1. The situation is quite complex and has not been assessed in detail. Based upon the pattern of ice melting resulting, it appears that in some cases, hydrogen burns associated with igniter operation merely accentuate the pattern that had already been established. In other cases, the pattern changes somewhat; that is, the relative depletion rates of the various ice columns change after the onset of the hydrogen burns. One factor involved is that pressure

surges associated with the burns can force some or all of the various ice condenser doors to open beyond the point of irreversibility, so that they remain partially or totally open. The open doors can then have substantial effects upon the circulation patterns. The times and locations at which this happens varies from case to case, and this effect likely explains at least some of the variability observed in the patterns of ice melt that result.

5.3.1 Existing Igniter Systems

Case 13 of Table 5.1 is the same as Case 12 except that the existing igniter systems were assumed to be powered. Hence, the gas distributions given in Figure 5.6 apply to this case also up until the time that the first hydrogen burns occur. Since the lower containment is steam inert, and since the lower plenum and the ice condenser do not have igniters, the first burns initiate in Cell 22 (in the upper plenum), at 9427 s into the transient. Concentrations of oxygen, hydrogen, and steam in Cell 22 at the time of interest are plotted in Figure 5.8a. The abrupt changes in gas concentrations signal the onset of the hydrogen burn. In this and subsequent figures, note that steam concentration is plotted against the right-hand axis.

Once combustion is initiated in the upper plenum, it propagates down into the ice condenser, where hydrogen concentrations are much higher, up to 25% in Cell 19 (Figure 5.8b). These gas compositions are well into the range that would be considered detonable, even allowing for steam concentrations of up to about 20%. It appears, therefore, that merely operating the existing igniters may not be very effective in protecting against detonations in the ice condenser, because hydrogen concentrations there may rise well into the detonable range by the time concentrations in the upper plenum, where the igniters are located, reach the normal flammability limits. Similar results have been observed in calculations for Sequoyah using the HECTR code [Di85].

Calculations were also run for the depressurized case with existing igniters assumed to operate (Case 21 of Table 5.1). Up until the onset of hydrogen burns, this calculation is identical to the case without igniters (Case 20 and Figure 5.7). Combustion first initiates in the right-hand side of the upper plenum (Cell 23) because the upward flow through the ice condenser tends to concentrate in the right center quadrant, as was discussed previously. Gas compositions in Cells 23 and 20 are given in Figures 5.8c and 5.8d, respectively. The response is similar to the fully-pressurized scenario except that the hydrogen concentrations in the ice condenser at the time of combustion onset are not as high. They are not low enough to be considered safe with respect to detonations, however.

After the initial combustion event, there is a long, complicated series of burns associated with the continuing influx of hydrogen into the ice condenser region. Only a small part of this series is represented in Figure 5.8. At no time, however, did potentially detonable atmospheres accumulate to the degree they did at the start of this series. This result appeared to be fairly general: in most of the calculations involving igniters, the highest hydrogen concentrations in the ice condenser were at the time of the first hydrogen burns, if concentrations were ever high enough to be of any concern at all. In one case involving containment venting (Section 5.4.2), somewhat higher concentrations did develop later in the scenario, but oxygen had been substantially depleted and detonation threats probably would have been negligible.

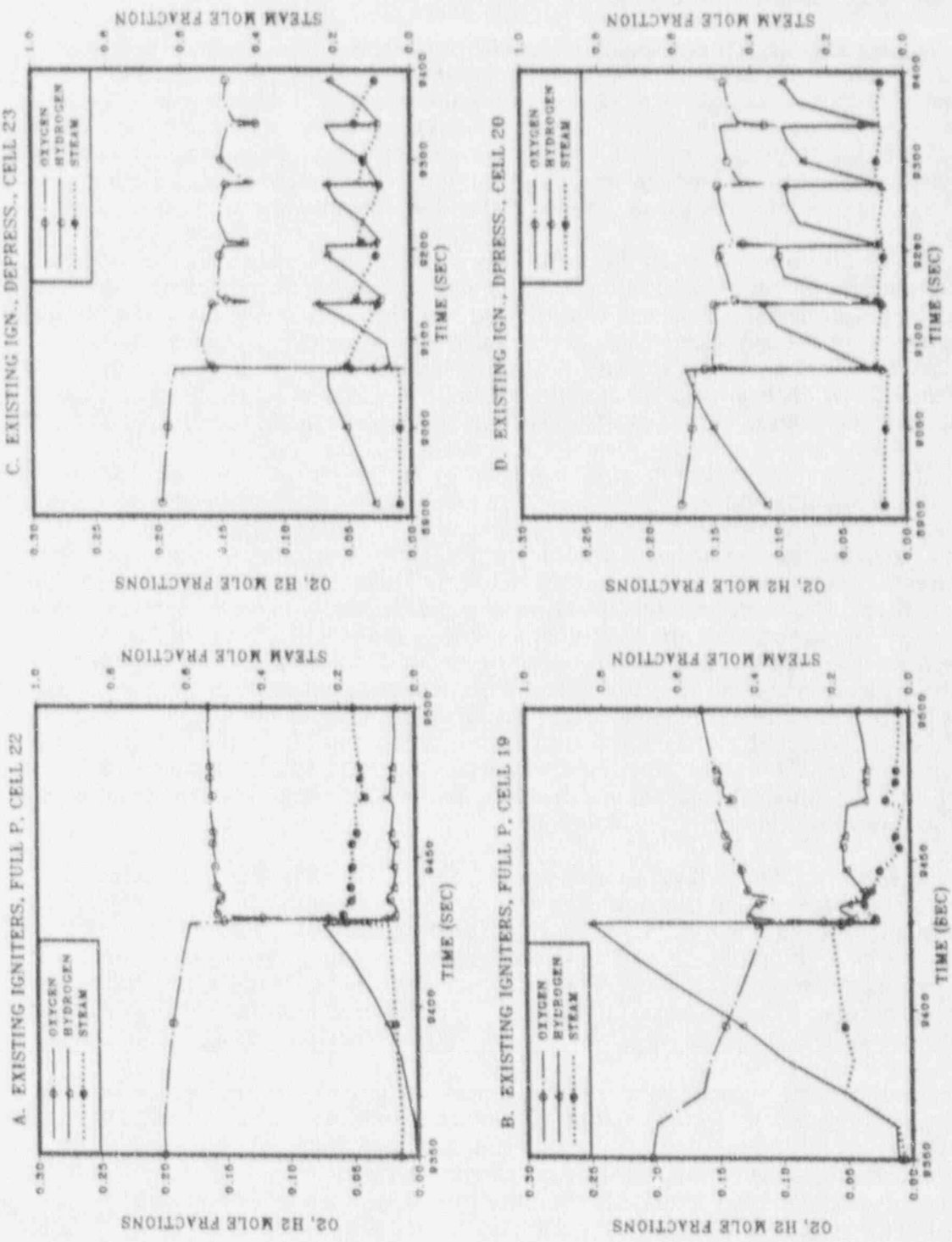

Figure 5.8 Atmospheric compositions at selected locations, pressurized and depressurized scenarios, existing igniters powered.

5.3.2 Augmented Igniter Systems

Igniters in the Lower Plenum. Since hydrogen enters the ice condenser from below, igniters in the lower plenum might prevent the buildup of detonable concentrations in the ice condenser were it not for the problem of steam inerting. In the 6-cell calculations, the lower plenum tended to be steam inert when the air return fans were not running. In the 26-cell calculations, however, the convective exchanges between the ice condenser and the lower plenum sometimes prevented steam inerting. Hence, the possible benefits of igniters in the lower plenum are worth considering.

Calculations were run for both the fully pressurized sequence and the depressurized sequence in which it was assumed that all existing igniter systems were operating and, in addition, it was assumed that igniters had been installed in the lower plenum, but not in the ice condenser itself. Some gas compositions of interest are given in Figure 5.9. In the fully-pressurized sequence, compositions for Cells 22 and 19 are not given because, if they were, they would be almost the same as those given in Figures 5.8a and 5.8b; that is, installing the lower plenum igniters made very little difference.

The reason for these results is suggested by the gas compositions plotted in Figures 5.9a and 5.9b for Cells 14 and 15 in the lower plenum. Hydrogen concentrations in Cell 15 do rise above the 7% ignition level relatively early, at 9370 s; at this time the hydrogen concentration in the ice condenser is still very low (Figure 5.8b). However, steam concentrations in Cell 15 are well above the steam inerting limit, and the igniters have no effect. In Cell 14, steam concentrations are lower, but so are the hydrogen concentrations; the flammability limit is not reached until about 9425 s, which is almost the same time that the burn initiated in the upper plenum in the previous scenario. Hence, by the time a burn does start in the lower plenum, it is too late to prevent detonation-sensitive gas compositions from developing in the ice condenser. The high steam concentrations in Cell 15 result from the fact that the strong hydrogen source to containment is concurrent with a strong steam source (Figure 5.2a), plus the fact that the flow into the lower plenum is heavily concentrated in the central portion (Figure 5.4a).

In Figures 5.9c and 5.9d, gas concentrations in Cells 16 and 20 are plotted (depressurized case). Here the strategy works as intended: Cell 16 is the lower plenum cell which first reaches flammable hydrogen compositions and it is not steam inerted. Small burns originate in this cell and propagate upward into the ice condenser while the hydrogen concentrations there are still harmless. Note, however, that the steam concentrations in Cell 16 are quite high, of the order of 40% or higher; major changes to the scenario description might not be required to produce inerting in this case also.

These results suggest that the effectiveness of the lower plenum igniters can be reduced by the fact that the locations of the lower plenum which receive the greatest hydrogen influx, and therefore first achieve potentially flammable hydrogen concentrations, are also the locations receiving the highest steam influx, which can cause inerting. It seems likely that the strategy will work for some scenarios, but it may fail for others. Unless it can be shown that scenarios in the latter category are implausible, relying on igniters in the lower plenum to prevent detonation threats in the ice condenser appears to be rather chancy.

Igniters in the Ice Condenser. In the assessments of DCH-related pressurization, some calculations were run with igniters in all cells, including the ice condenser. There is little point discussing these results in detail here because invoking the default

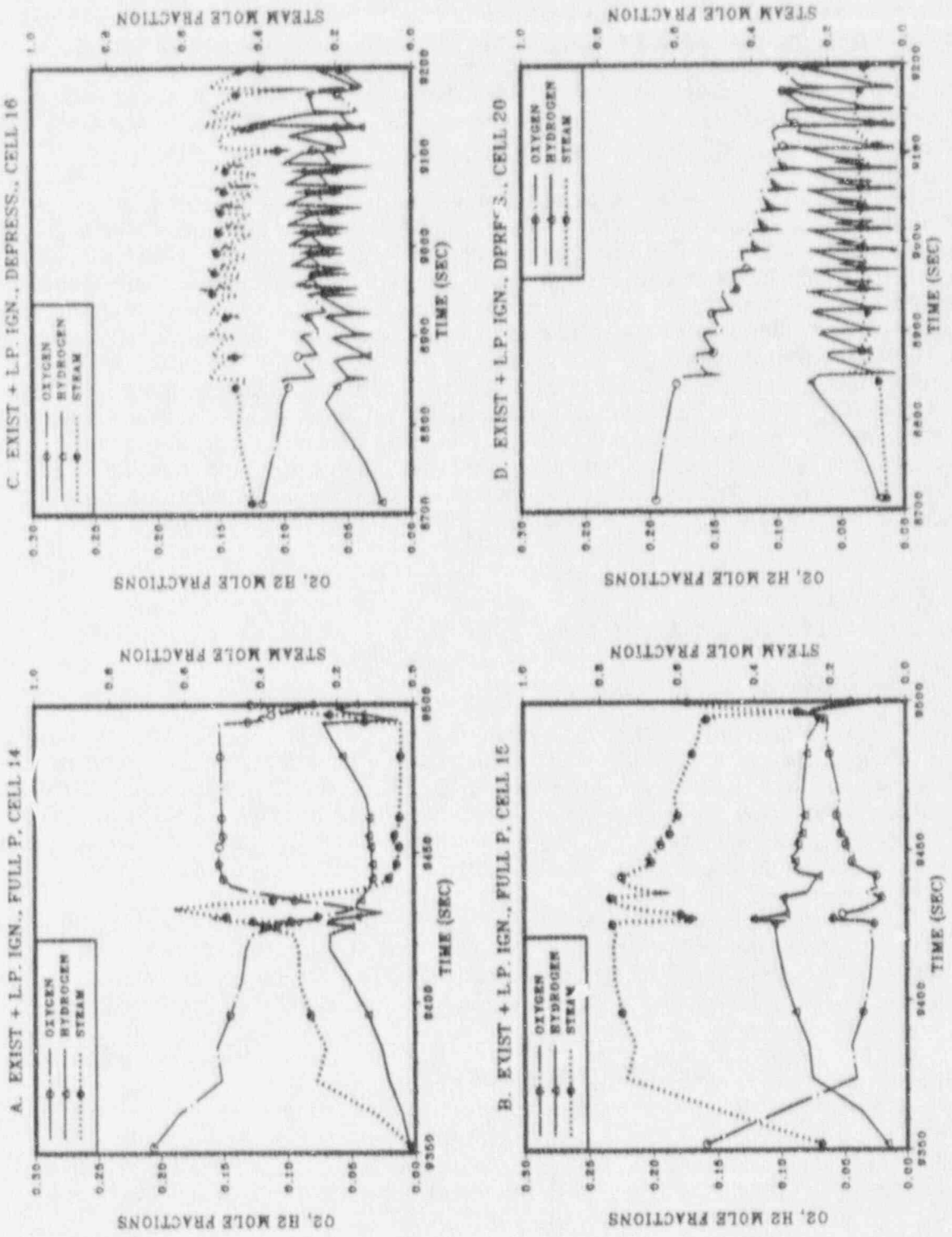

Figure 5.9 Atmospheric compositions at selected locations, pressurized and depressurized scenarios, existing igniters powered and additional igniters installed in the lower plenum.

burn model assures that detonable concentrations cannot develop in the calculation, subject to the limitations noted in the introduction to Section 5. The flow patterns calculated in this work indicate that it would be important to have good igniter coverage in the central regions of the ice condenser, where hydrogen concentrations are calculated to build up the most rapidly. Beyond this observation, the nodalization of the ice condenser used here is too coarse to justify more detailed recommendations concerning igniter placement.

In addition to the gas composition and distribution questions addressed by the present work, there are a number of other issues which should be considered in evaluating the desirability of installing igniters in the ice condenser. One issue is the question noted earlier of whether a detonation in the ice condenser actually would seriously threaten containment integrity. Another question is whether igniters in the ice condenser environment could be counted on to perform reliably. For example, the present calculations indicated that very high water aerosol (fog) densities could develop in the ice condenser in some scenarios. These high fog densities might impair igniter performance. This question is not considered in detail here because it is known that the present model involves certain limitations which could considerably overestimate the water aerosol densities under ice condenser conditions. CONTAIN 1.11 will include major upgrades to the aerosol/steam condensation modeling which would be very useful here, if it is desired to pursue this question further in future studies.

5.4 Air Return Fans and Containment Venting

5.4.1 Air Return Fans

The air return fans produce flow rates of about 50 m^3/s, if both trains of fans are operating. Hence, the fans can produce substantial atmospheric mixing on time scales of minutes to a few tens of minutes. This mixing would be expected to reduce or eliminate detonation hazards except, possibly, when source rates are sufficiently high so that dangerous concentrations of hydrogen can develop on time scales shorter than the fan mixing time scales.

Calculations assuming that independent power was available for both trains of fans were performed for both the fully pressurized and the depressurized station blackout sequences (Cases 16 and 23, Table 5.1). The existing igniter system was assumed to be operating, but installation of additional igniters was not considered.

For the fully-pressurized case, the initial hydrogen burn events showed the same pattern as that exhibited previously: ignition in the upper plenum, followed by propagation downward into the ice condenser. Atmospheric compositions are plotted for Cells 22 and 19 in Figure 10a and Figure 10b, respectively. At the same time, a virtually identical sequence of burns was taking place in Cells 23 and 20; with fans operating, flows through the ice condenser were quite symmetrical, although they continued to be strongly concentrated in the two center quadrants.

Although the scenario is qualitatively similar to those calculated for the fully pressurized sequence without fans operating, the maximum hydrogen concentrations in the ice condenser are significantly less than without the fans, about 14% versus 25%. With the calculated steam concentrations of about 20%, this atmospheric composition would be expected to have a low detonation sensitivity, although a detonation might not be strictly impossible. However, there are substantial

uncertainties in the numerical concentrations calculated for the time of ignition. When these uncertainties are allowed for, detonations cannot be ruled out unless it can be shown that the scenario analyzed here is a quite conservative one in terms of the potential detonation threat. Even at 14% hydrogen, the possible effects of accelerated flames may also require consideration.

In this analysis, the first hydrogen burns occurred in the upper plenum rather than in the lower containment because the large steam source entering along with the hydrogen both diluted the hydrogen and kept steam concentrations close to the 55% inerting limit, despite the operation of the fans. Atmospheric compositions for Cell 9 in the lower containment are shown in Figure 5.10c. At the time of ignition in the upper plenum, hydrogen concentrations would permit a burn in the lower containment but the steam concentrations are too high. In the adjacent parts of the lower containment (Cells 8 and 10, not plotted), steam concentrations are slightly lower, below the inerting limit, but the hydrogen concentrations are also below the flammability limit. Hence, no burns occur in the lower containment at this time. Later, burns do occur there, but by then, the sequence of initial burns in the upper plenum and the ice condenser has already taken place. Since some of the steam and hydrogen concentrations are close to the flammability limits involved, the sequence of events would be sensitive to minor changes in the modeling and/or the sources input to the containment.

Conditions in Cell 9 are displayed in Figure 5.10d for the depressurized station blackout sequence with fans and existing igniters operating. In this calculation, the response of the lower containment is quite different. The fans keep steam concentrations well below the inerting threshold, numerous small hydrogen burns are initiated by the igniters, and these burns have no difficulty propagating into the ice condenser, keeping concentrations there at safe levels. In this case, the combination of fans and the existing igniters works exactly as one would hope. At no time or place within the containment did hydrogen concentrations rise significantly above the flammability threshold of 7%, and detonation threats are nonexistent in this calculation.

In both the calculations with fans operating, containment pressures were about 25-30% lower at the time of burn initiation than in the analogous cases without fans (Table 5.1). If a detonation did occur, the lower initial pressure would yield proportionately lower dynamic loads, other parameters being equal.

The results obtained here indicate that supplying power for the a.. return fans plus the existing igniter system may not be a complete panacea for detonation threats; depending upon the steam and hydrogen sources to the containment, dangerous hydrogen concentrations might still develop in the ice condenser before a flammable atmosphere developed at any locations where igniters are present. On the other hand, the fans would certainly mitigate a number of scenarios that would be dangerous without them. In a probabilistic risk assessment, therefore, these calculations indicate that substantial credit could be taken for reduced detonation threats if both the fans and the igniters were operating, even though the detonation probabilities likely could not be set to zero.

5.4.2 Containment Venting

Containment venting was considered in this work primarily as a means of mitigating DCH-related containment pressurization, but its implications for

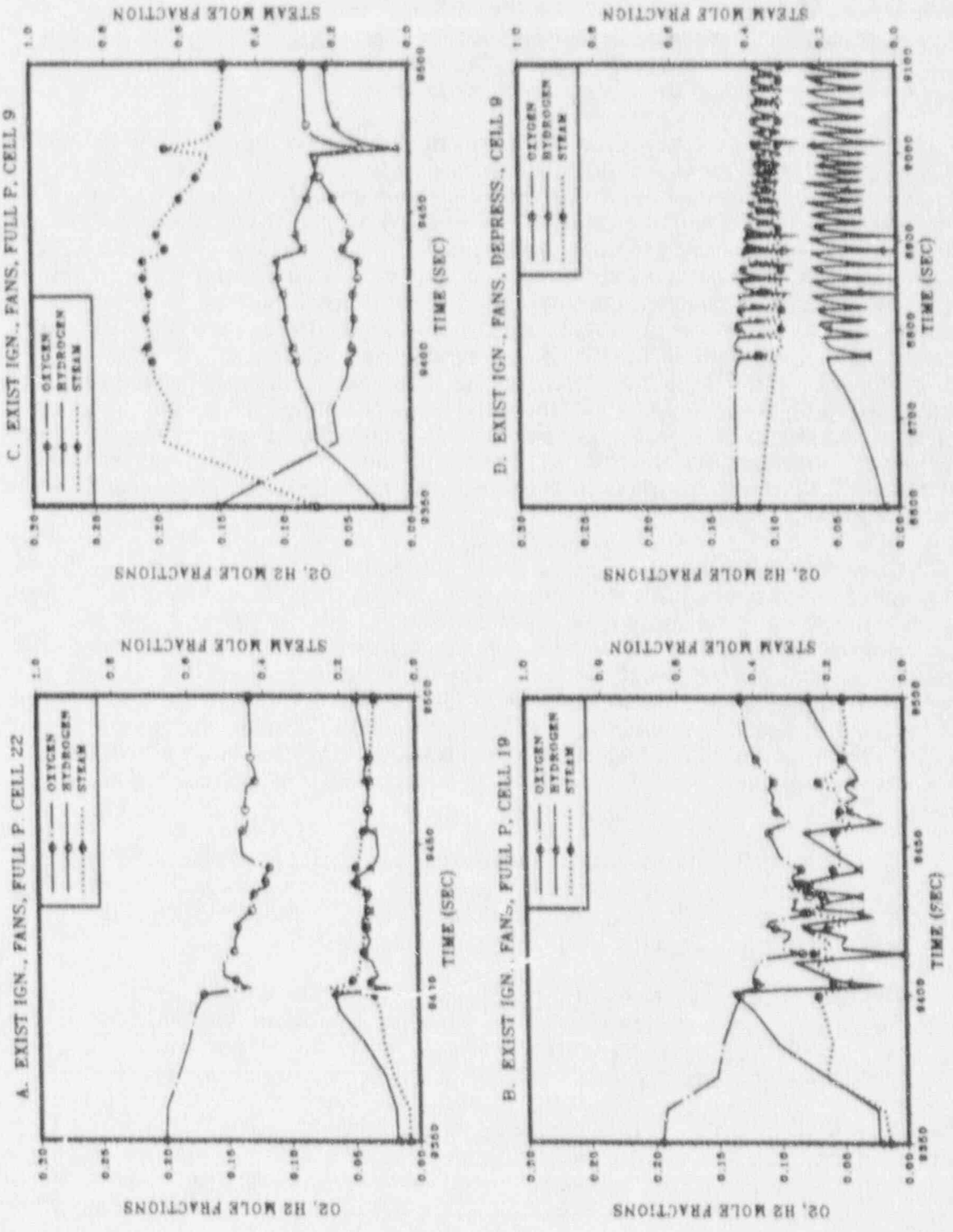

Figure 5.10 Atmospheric compositions at selected locations, pressurized and depressurized scenarios, existing igniters and fans powered.

detonation threats prior to VB should be briefly considered. Venting calculations were performed only for the station blackout sequence with fully pressurized RCS. Calculations were performed with and without dedicated power supplies for the air return fans, and in both cases the existing igniter systems were assumed to be powered.

In both calculations, the hydrogen combustion events showed the now-familiar pattern of initiating in the upper containment and propagating down into the ice condenser. The gas compositions in the upper plenum and in the part of the ice condenser with the highest hydrogen concentration are plotted in Figures 5.11a and 5.11b for the case without fans, and for the case with fans in Figures 5.11c and 5.11d. Both cases closely resemble their unvented analogues, although the hydrogen concentrations are slightly higher in the vented case. Presumably this difference reflects the loss of noncondensible gases other than hydrogen during the period of venting. (Since the vents were assumed to be closed off at the onset of core degradation, no hydrogen would have been vented.)

Figure 5.11d shows that, in the case with fans operating, the first burn in the ice condenser was not the one which initiated at the highest hydrogen concentration, unlike all the other cases considered in this work. However, at the time of the burn with the highest hydrogen concentration, oxygen had been substantially depleted by prior burns, and this burn would probably present less of a detonation threat than would the first burn. The latter would itself be at most a marginal threat, for the conditions calculated here.

In the case without fans, the lower containment was strongly steam inerted at the time of greatest interest here, while it was marginally inerted in the calculation with fans. Steam concentrations in the lower containment tended to be slightly higher than in the unvented cases; again this difference probably reflects the loss of noncondensible gas during the period of venting. On the positive side, P_0 is somewhat lower in the vented cases.

In general, the effects of venting on hydrogen detonation threats do not appear to be large. A decision as to whether to implement mitigation strategies involving containment venting should be based primarily upon factors other than the impact upon detonation risks.

5.5 Surge Line Failure (Depressurized Scenario)

The SCDAP/RELAP calculations for the "early" depressurization scenario which were used here indicated that the surge line would get sufficiently hot so that it could fail during this accident sequence. The nominal time of failure was 9545 s. Sources to the containment following the surge line failure were generated by CONTAIN blowing down the primary system cell at the postulated time of failure (Section 2.4.2). Substantial vessel depressurization had already occurred by this time, and the vessel pressure was taken to be about 3.5 MPa, based upon the SCDAP/RELAP analyses.

Two cases were considered, one without the air return fans operating and one with the fans. In both cases, the existing igniter system was assumed to be powered.

In the cases without surge line failure, hydrogen burns commence at around 9000 s or earlier, well before the time of the postulated failure. Hence, the initial burn histories in the present calculations are identical to those described previously for the depressurized sequence with existing igniters operating. In the case without fans, the

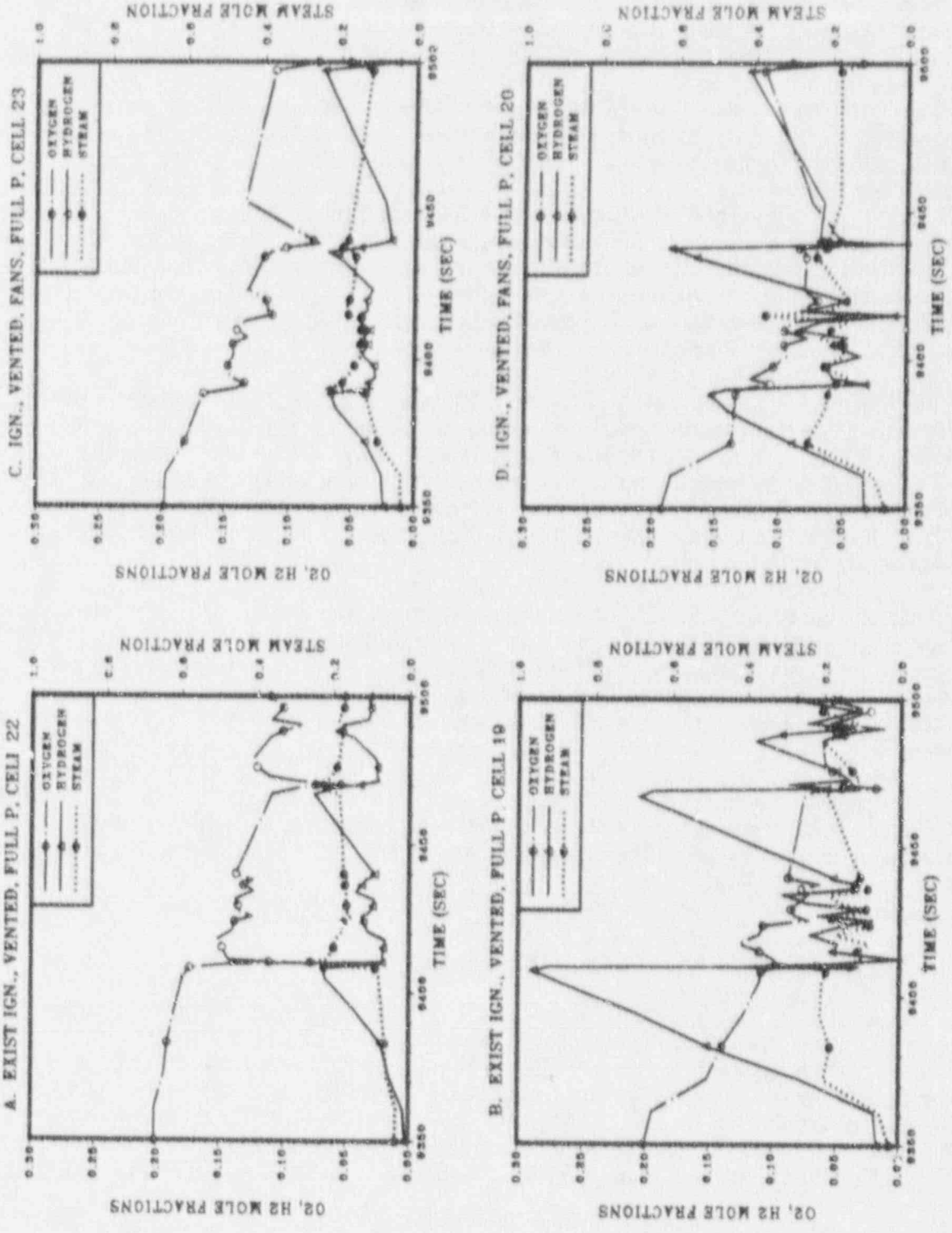

Figure 5.11 Atmospheric compositions at selected locations, pressurized scenario, vented containment, igniters powered, with and without fans powered.

lower containment is strongly steam-inerted at the time of surge line failure and all ice condenser burns originate in the upper plenum. However, the maximum hydrogen concentrations in the ice condenser following surge line failure, about 15%, were somewhat less than those existing at the time of the first burn, prior to surge line failure (17%). Furthermore, in the burns following the failure, oxygen concentrations had been reduced by prior burns. Any combustion threats following the surge line failure therefore appear to be minor compared with those associated with the initial burn.

In the case with air return fans operating, steam concentrations in the lower containment were initially well below the inerting limit, but quickly rose until the lower containment was at least partially inerted (the exact concentrations calculated are not to be trusted because of uncertainties in the mixing rates under these conditions). However, this did not happen until some hydrogen burns initiated in the lower containment, and these were calculated to propagate into the ice condenser. The burn history was rather complex and the various interrelationships were not entirely clear; burns in the upper plenum could also have propagated into the ice condenser if lower-containment burns had been absent. In any event, the maximum hydrogen concentration achieved in the ice condenser prior to ignition was about 13% This value is higher than the value calculated for the analogous case without surge line failure (< 8%). However, at the time of the burns, oxygen concentrations were low (< 10%) due to prior burns and steam concentrations were relatively high (~ 30%). This event does not seem to be very threatening.

After the calculations had been completed it was discovered that, due to an input error, the flow from the failed surge line had been directed to the cavity cell (Cell 1), not Cell 9 in the lower containment as had been intended. However, Cell 1 is quite small and the principal flow path out of it is to Cell 9. Hence, the steam from the surge line break would flow out of Cell 1 into Cell 9, where it should have been directed, with very little delay (less than a second). The effect of this error is expected to be very minor, and the calculations were not repeated.

Even after allowing for the various uncertainties in the containment modeling, it would not appear that the surge line failure scenario would present a very severe threat to containment <u>provided</u> one could be certain that the in-vessel portion of the scenario would proceed as assumed in the calculations used to generate the steam and hydrogen sources input to the containment calculations. However, there are large uncertainties in the details of the surge line failure scenario (it is even quite uncertain as to whether the surge line will fail). Some of these uncertainties could substantially alter the assessment of detonation threats following the failure. For example, the surge line might fail at a time when the primary system pressure was higher, and/or the vessel contained more hydrogen, and/or the lower containment hydrogen concentrations were higher. In this event, the situation might more closely resemble the fully pressurized scenario in which strong steam and hydrogen sources entered the containment simultaneously. As we have seen, detonation hazards are considerably more difficult to control in that scenario than in the depressurized scenario.

There may be one feature of the surge line failure scenario which will tend to mitigate detonation threats generally. Surge line failure is the result of strong heating by hot gases flowing into the pressurizer from the reactor vessel during core degradation. It is likely to occur only after substantial core degradation has taken place and, hence, after substantial hydrogen generation has already occurred. In the case analyzed here, this sequence of events meant that, when hydrogen burns associated with surge line failure did occur in the ice condenser, oxygen levels there

had already been significantly depleted by previous hydrogen burns, provided at least the existing igniter systems were operating. If this behavior is general to surge line failure scenarios, it may be that detonation threats following surge line failure will be secondary to the threats associated with the first hydrogen combustion events to take place in the ice condenser. However, in the absence of more detailed study, and/or better definition of the surge line failure scenarios, this suggestion must be regarded as being rather speculative at present.

6. Sensitivity Studies Using the NUREG-1150 Methodology

6.1 Introduction

This chapter discusses the effects of various containment improvements on the potential risks associated with the Sequoyah plant. The risk profiles associated with severe accidents are provided. The accident definitions and frequencies, as well as the accident progression and source term models, associated with the NUREG-1150 analysis [NRC89] were applied to sensitivity studies involving the containment improvements. Section 6.2 is provided as a summary of the methods, models, results and insights for the Sequoyah NUREG-1150 analysis; this section provides the background material necessary to understand the probabilistic framework of this study, as well emphasizing the important features of the modeling and risk results (which subsequently led to the formulation of the sensitivity studies). Section 6.3 describes the sensitivity studies that were performed in support of the CPI program. The risk integration method developed for this program is described in Section 6.4. Section 6.5 provides the base case and sensitivity study results. Section 6.6 summarizes the results of the CPI sensitivity studies.

6.2 Summary of NUREG-1150 Analysis for Sequoyah, Unit 1

The United States Nuclear Regulatory Commission (NRC) has recently completed a major study to provide a current characterization of severe accident risks from light water reactors (LWRs). This characterization is derived from integrated risk analyses of five plants, one of which is the Sequoyah Nuclear Station, Unit 1.

The risk assessments on which NUREG-1150 is based can generally be characterized as consisting of four analysis steps, an integration step, and an uncertainty analysis step:

1. Accident frequency analysis: the determination of the likelihood and nature of accidents that result in the onset of core damage.

2. Accident progression analysis: an investigation of the core damage process, both within the reactor vessel before it fails and in the containment afterwards, and the resultant impact on the containment.

3. Source term analysis: an estimation of the radionuclide transport within the reactor coolant system and the containment, and the magnitude of the subsequent releases to the environment.

4. Consequence analysis: the calculation of the offsite consequences, primarily in terms of health effects in the general population.

5. Risk integration: the assembly of the outputs of the previous tasks into an overall expression of risk.

6. Uncertainty analysis: the propagation of the uncertainties in initiating events, failure events, accident progression branching ratios and parameters, and source term parameters through the first three analyses above, and the determination of which of these uncertainties contributes the most to the uncertainty in risk.

The modeling of physical phenomena in the first four steps is performed in a global manner; i.e., if any models are used, they are very simple. The results of complex modeling, however, are used as inputs for the first four steps. The first step is documented in NUREG/CR-4550, Volume 5 [Bt90] and the last five steps are documented in NUREG/CR-4551, Volume 5 [Gr90]. The methodology for the analyses is described in NUREG/CR-4550, Volume 1 [Er90] and NUREG/CR-4551, Volume 1 [Bg90]. The CPI study involves Steps 1 through 3 and the propagation of the uncertainties described in Step 6. Changes to the analysis due to proposed containment improvements were implemented only for Step 2. Due to time and budget constraints, it was not possible to perform the full consequence analysis and risk integration, so an approximate integration method for determining risk potential was developed as described in Section 6.3. The unmodified NUREG-1150 analysis for internal initiators utilizing the approximate integration methods adopted for this study is referred to as the "base case" for the CPI.

The steps described above may be summarized in the risk equation:

$$RISK_k = \Sigma_i \Sigma_j FREQ_i * CRMP_{i,j} * CONS_k (FP_{i,j}); \qquad \text{(Eq. 6.1)}$$

where:

$RISK_k$	=	the risk associated with consequence measure k
$FREQ_i$	=	the frequency of accident sequence i
$CRMP_{i,j}$	=	the probability of containment release mode j, given accident sequence i
$FP_{i,j}$	=	the fission product source term for containment release mode j of accident sequence i
$CONS_k$	=	the magnitude of consequence k, given fission product source term (FP) for sequence i,j

There are uncertainties associated with each of the inputs to the risk equation. The focus of the NUREG-1150 analysis was upon the identification of the input areas that carried with them the largest uncertainties and that had the potential to contribute significantly to the risk magnitudes. Uncertainty distributions were provided in large part by expert panels as described in [Ha90]; some uncertainty distributions were obtained from a generic data base or were developed internally by the project staff. Over 200 variables (~ 110 independent variables) were sampled in the Sequoyah NUREG-1150 analysis. Examples of variables that were sampled include initiating event frequencies, component failure rates, pressure rise in containment at vessel breach, containment failure pressure, and a number of parameters governing the source term, including the decontamination factor for the ice condenser. The Latin hypercube sampling approach [Im84] was used to incorporate the uncertainty distributions into the analysis. Latin hypercube sampling is a stratified Monte Carlo sampling technique. The sample size for the Sequoyah analysis was 200. Each sample element or observation might be thought of as representing a single risk assessment with each uncertain variable set at a fixed value. The integrated risk estimates have associated distributions; for the most part, only mean values are reported for this study.

6.2.1 Accident Frequency Analysis

Event tree and fault tree techniques are used in the accident frequency analysis to investigate the manner in which various initiating events can lead to core damage and

the frequency of various types of accidents. Experimental data, past observational data, and modeling results are combined to produce frequency estimates for the minimal cut sets that lead to core damage. A minimal cut set is a unique combination of initiating event and individual hardware or operator failures. The minimal cut sets are grouped into plant damage states (PDSs), where all minimal cut sets in a PDS state provide a similar set of initial conditions for the subsequent accident progression analysis. Thus, the PDSs form the interface between the accident frequency analysis and the accident progression analysis. The outcome of the accident frequency analysis is a frequency for each PDS or group of PDSs for each observation in the sample. Internally initiated accidents at Sequoyah are placed into five PDS groups:

- PDS Group 1: Loss of offsite power (LOSP), which includes long-term and short-term station blackouts (SBOs).
- PDS Group 2: Anticipated transient without scram (ATWS).
- PDS Group 3: Transient initiated events other than LOSP and ATWS.
- PDS Group 4: Loss-of-coolant accidents (LOCAs).
- PDS Group 5: Bypass events, including interfacing systems LOCA (V-Sequence) and accidents initiated by a steam generator tube rupture (SGTR).

The mean core damage (CD) frequency for internally initiated events at Sequoyah for each PDS Group and the percentage of the total mean core damage frequency (TMCDF) per reactor-year (R-yr) associated with each group is provided in Table 6.1.

6.2.2 Accident Progression Analysis

The accident progression analysis uses large, complex event trees to determine the possible ways in which an accident might evolve from each plant damage state. The definition of each plant damage state provides enough information to define the initial conditions for the accident progression event tree (APET) analysis. Past

Table 6.1

Sequoyah Mean Core Damage Frequency for Internal Initiators

PDS Group	Mean CD Frequency (1/R-yr)	%TMCDF
1, Long-Term SBO	5.0E-06	9
1, Short-Term SBO	9.6E-06	17
2, ATWS	1.9E-06	3
3, Transients	2.5E-06	4
4, LOCAs	3.6E-05	63
5, V-sequence	6.5E-07	1
5, SGTR	1.7E-06	3

observations, experimental data, mechanistic code calculations, and expert judgment were used in the development of the model for accident progression that is embodied in the APET and in the selection of the branch probabilities and parameter values used in the APET. Due to the large number of questions in the Sequoyah APET and the fact that many of these questions have more than two outcomes, there are far too many paths through the APET to permit their individual consideration in subsequent source term and consequence analysis. Therefore, the paths through the trees are grouped into accident progression bins (APBs), where each bin is a group of paths through the event tree that define a similar set of conditions for source term analysis. The properties of each accident progression bin define the initial conditions for the estimation of a source term. The result of the accident progression analysis is a probability for each APB, conditional on the occurrence of a PDS, for each observation in the sample.

Treatment of Hydrogen Phenomenology in NUREG-1150. For the Sequoyah APET, the hydrogen threat to containment is treated during the core degradation process, at the time of vessel breach and also during and after the bulk of core-concrete interaction (CCI) has occurred. During core degradation, accumulation of hydrogen can occur in the ice condenser when igniters and fans are inoperable (typical station blackout scenario). Local concentrations of hydrogen in the ice condenser can reach detonable levels. Hydrogen deflagrations can also be of sufficient magnitude to fail the containment. The distribution of hydrogen within containment during core degradation, the frequency of ignition of the hydrogen, and the subsequent static and dynamic loading of containment for the NUREG-1150 analysis were provided by an expert panel. Another group of experts addressed the structural response of the Sequoyah containment and provided distributions for failure pressures and impulses, and the corresponding modes of failure.

At the time of vessel breach, containment loads from hydrogen burns are coupled with loads from direct containment heating (DCH). The loads at vessel breach for the NUREG-1150 analysis were provided by an expert panel. The distributions the experts provided were based upon the consideration of various phenomena including: ex-vessel steam explosions, vessel blowdown, hydrogen combustion, and DCH. The higher ends of the distributions are governed by loads due to the combustion of pre-existing hydrogen, hydrogen created at vessel breach, and DCH events.

At late times during a station blackout accident, the hydrogen that is in containment becomes a threat to containment, when power, and subsequently sprays, are recovered. When the ice is melted at late times in the accident, the containment atmosphere becomes steam-inerted. If sprays are then initiated, the atmosphere becomes flammmable due to reduction of the steam concentration.

Core Damage Arrest. For some of the accident sequences, the potential exists for arresting the core damage process and preventing vessel breach. This is possible when recovery of injection has occurred before core degradation has progressed too far. Injection is recovered either because power is recovered in a blackout sequence, or because a low pressure injection system is enabled due to a decrease in the the reactor coolant system (RCS) pressure. For all accident sequences except the V-sequence, arrest of core damage can occur. Overall, the frequency-weighted average indicates that core damage is arrested about 40% of the time.

RCS Depressurization. During the core degradation phase of an accident, there are several mechanisms that can create a reduction in the RCS pressure. The pressure reduction is important in two respects. First, as mentioned above, a decrease in RCS

pressure may enable available low pressure injection systems to operate, potentially averting vessel breach. Second, if the accident proceeds to vessel breach, the reduction in RCS pressure reduces the DCH threat at vessel breach. There are five mechanisms by which the RCS can be depressurized prior to vessel breach:

- Temperature-induced hot leg or surge line failure,
- Power-operated relief valves (PORVs) or safety relief valves (SRVs) stick open (temperature related),
- Temperature-induced reactor coolant pump seal failure,
- Temperature-induced SGTR, and
- Deliberate opening of the PORVs by the operators (not possible during station blackout accidents in the unmodified plant).

The first four mechanisms are temperature-related and inadvertent; i.e., they are assumed to occur with neither deliberate intervention by the operators nor by automatic actuation of a safety system. These four mechanisms are induced by temperatures (sometimes in conjunction with high system pressures) higher than those of normal operating conditions. The first three mechanisms are predicted to occur frequently for most accidents. Considering these means for depressurization acting together, there are very few accidents that proceed through vessel breach at system pressure.

Accident Progression Results. For each of the five PDS groups listed in Table 6.1, the major paths through the Sequoyah APET are presented in Table 6.2. This table shows the mean values of the probability of an accident progression bin (APB) conditional upon the occurrence of the PDS group. There is actually a distribution associated with each of the mean values. There can be several accident progression bins that occur for a given PDS group; therefore, the accident progression bins have been defined in a certain order. This means that if an accident fits into a bin, then it will automatically be excluded from a subsequent bin. The ordering of the accident progression paths and the label descriptor of each row in Table 6.2 follows:

1) bypass of containment (Bypass);
2) no vessel breach, but isolation failure or containment failure during core degradation (No VB, Very Early CF);
3) no vessel breach and no containment failure (No VB, No CF);
4) vessel breach, and isolation failure or containment failure during core degradation (VB, Very Early CF);
5) alpha mode failure of containment at vessel breach - an energetic in-vessel steam explosion fails both the vessel and containment (VB, alpha, Early CF);
6) containment failure at vessel breach, RCS pressure greater than 200 psia (VB, hi RCS P, Early CF);
7) containment failure at vessel breach, RCS pressure less than 200 psia (VB, lo RCS P, Early CF);
8) vessel breach and containment failure late, by hydrogen burn (VB H_2 burn, Late CF);
9) vessel breach and very late containment failure, by basemat melt-through or overpressure (VB, BMT or V Late OP); and
10) vessel breach and no containment failure or no bypass (VB, No CF).

Table 6.2

Mean Frequency of Accident Progression Bins
for PDS Groups

APB	PDS Group: LOSP	ATWS	Transients	LOCAs	Bypass	All Accidents
Bypass	0.001	0.130	0.006		1.000	0.056
No VB, Very Early CF	0.038	0.001	0.005	0.002		0.011
No VB, No CF	0.384	0.171	0.785	0.367		0.371
VB, Very Early CF	0.014	0.003		0.002		0.005
VB, alpha, Early CF	0.002	0.003		0.002		0.002
VB, hi RCS P, Early CF	0.064	0.023	0.014	0.031		0.035
VB, lo RCS P, Early CF	0.054	0.020	0.004	0.014		0.023
VB, H_2 burn, Late CF	0.150	0.001		0.001		0.038
VB, BMT or V Late OP	0.065	0.150	0.039	0.260		0.170
VB, No CF	0.200	0.470	0.130	0.300		0.260

Early failures involving hydrogen burns and detonations occur with the highest conditional frequency for the SBO accidents, due to unavailability of the hydrogen igniters and the air return fans. SBO accidents also involve the most frequent occurrence of containment failures by DCH coupled with hydrogen burns and late failures due to ignition of combustible gases generated during CCI. The late failure scenario occurs because power is recovered late, the steam is condensed from the containment atmosphere, and the combustible gases are ignited. Containment bypass is caused in PDS groups other than the bypass PDS group by temperature-induced SGTRs. As mentioned above, vessel breach is averted quite frequently because core damage is arrested. There are some arrested sequences in which containment failure

occurs during the core degradation process because of hydrogen burns or detonations. Most of the very late failures involve basemat melt-through for the LOSP, ATWS and Transient PDS Groups. For the LOCAs, the very late failures involve long-term overpressure failures due to early failure of the containment spray systems.

The columns in Table 6.2 do not necessarily total 1.0 because some of the paths through the tree are truncated if the path frequency, conditional on occurrence of the plant damage state, is less than 1.0E-05. The truncation does not occur for risk significant pathways with greater frequency than for nonsignificant pathways. Thus, it is expected that the effect of the truncation of very low frequency pathways in the accident progression analysis is minimal (the accident pathway frequency must be multiplied by the PDS frequency for each sample observation in order to obtain the absolute frequency of each bin for each sample observation).

6.2.3 Source Term and Consequence Analyses

A source term is calculated for each APB with a non-zero conditional probability for each observation in the sample by a fast-running parametric computer model. The computer model is not designed to model the fission product transport, physics, and chemistry from first principles. Instead, it utilizes the integrated results of many detailed codes (e.g., CONTAIN, MELCOR, STCP, MAAP) and the conclusions of many experts. Most of the parameters that calculate fission product release fractions in the computer model are sampled from distributions provided by an expert panel [Ha90].

The number of APBs for which source terms are calculated is so large that it is not computationally practical to perform a consequence calculation for every source term. As a result, the source terms had to be combined into source term groups. Each source term group is a collection of source terms that result in similar consequences. The process of mapping APBs to source term groups is called partitioning. This process considers the potential of each source term group to cause early fatalities and latent cancer fatalities. The result of the source term calculation and subsequent partitioning is that each APB for each sample observation is assigned to a source term group. A consequence analysis is performed for each source term group, generating both mean consequences and distributions of consequences. Since each APB is assigned to a source term group, the consequences are known for each APB of each observation in the sample.

6.2.4 Risk Estimates

Public risk estimates are obtained by integration of the accident frequency analysis, the accident progression analysis, the source term analysis, and the consequence analysis. The risk results are obtained in the form of distributions of frequency for various consequence measures. There are many statistical representations of the risk results; this report will supply limited information and focus on two consequence measures: early fatalities and latent cancer fatalities.

The sample for the Sequoyah analysis included 200 observations, i.e., there are 200 members in the statistical sample that is used to incorporate the uncertain variables in the analysis. The histograms indicated in Figure 6.1 (from [Gr90]) show the uncertainty distributions for the annual risks from internally initiated events at Sequoyah for early fatality and latent cancer fatality risks. Each histogram is formed from the annual risk values of the 200 sample members. The annual risk is determined by averaging over

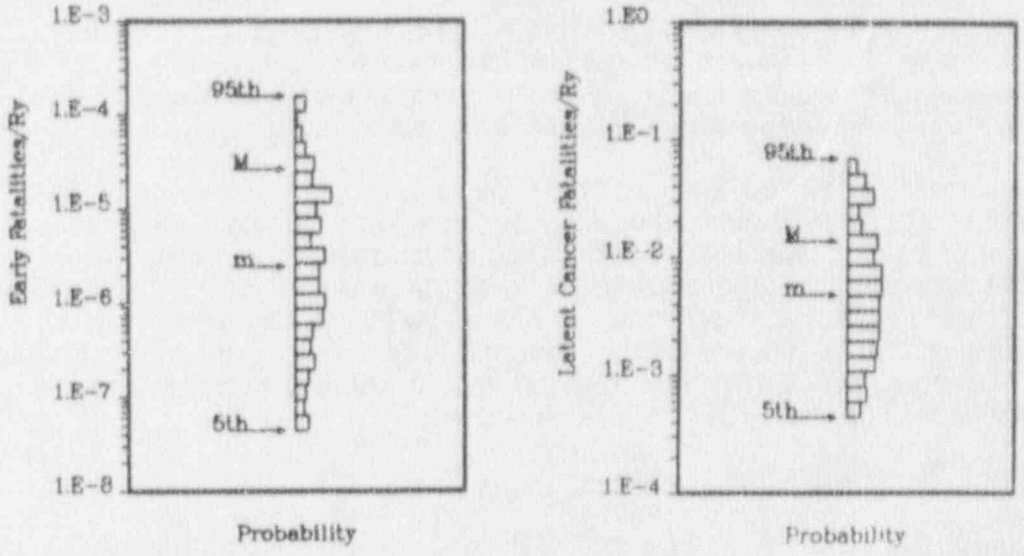

Figure 6.1 Early and latent cancer fatality distributions for Sequoyah - internal initiators.

the different weather states as well as over the different types of accidents that can occur. For the distributions in Figure 6.1, the fifth, fiftieth (m), and ninety-fifth percentiles as well as the mean (M) values are indicated. The mean value of the distribution for early fatality risk is 2.6E-05 per reactor year, and the mean value of the distribution for latent cancer fatality risk is 1.4E-02 per reactor year.

Significant Contributors to Mean Risk Estimates. One method for computing the contribution to risk is denoted the fractional contribution to mean risk (FCMR). The FCMR is obtained by dividing the mean risk due to a given contributor by the total mean risk. For the PDS groups noted above, the FCMR for early and latent cancer fatalities is presented in Table 6.3. Note that the mean early fatality risk is dominated by the V-sequence; another significant contributor is the LOSP group. The largest contributors to latent cancer fatalities are the LOSP and SGTR groups.

Table 6.4 shows the fractional contribution to the mean risk of the APBs defined in Table 6.2. The bypass bin has been divided between its V-sequence and SGTR constituents. Note that most of the station blackout contribution to risk in Table 6.3 is associated with failures at vessel breach, involving containment failure due to hydrogen combustion events, DCH, and liner melt-through. The contribution due to bypass is greater than in Table 6.3, because some SGTRs occur during the accident progression and are not classified as SGTR accident initiators. The failures of containment at vessel breach when the RCS is at low pressure, are due to hydrogen combustion events, and contribute quite significantly to both mean early fatality and mean latent cancer risks. There is risk associated with some accident progressions in which the vessel is not breached, because the containment was not isolated or failed during core degradation due to hydrogen burns or detonations.

The risk estimates in Tables 6.3 and 6.4 were based on consequence calculations in which it was assumed that 99.5% of the population in the emergency planning zone are evacuated. The remaining 0.5% of the population does not evacuate and continues normal activity. The emergency planning zone extends from the plant site out to a 10 mile radius. Details of the methods and assumptions used to incorporate

Table 6.3

Fractional Contribution of PDS Groups
to Mean Risk Measures (99.5% Evacuation)

	Early Fatalities	Latent Cancer Fatalities
Mean Risk/R-yr	2.6E-05	1.4E-02
PDS Group	FCMR	FCMR
LOSP	0.23	0.41
ATWS	0.02	0.04
Transients	0.00	0.01
LOCAs	0.02	0.14
Bypass, V-sequence	0.68	0.10
Bypass, SGTR	0.05	0.30

Table 6.4

Fractional Contribution of Accident Progression
Bins to Mean Risk Measures (99.5% Evacuation)

	Early Fatalities	Latent Cancer Fatalities
Mean Risk/R-yr	2.6E-05	1.4E-02
APB	FCMR	FCMR
Bypass, V-sequence	0.68	0.10
Bypass, SGTR	0.07	0.35
No VB, Very Early CF	0.01	0.05
No VB, No CF	0.00	0.00
VB, Very Early CF	0.02	0.04
VB, alpha, Early CF	0.00	0.01
VB, hi RCS P, Early CF	0.08	0.23
VB, lo RCS P, Early CF	0.14	0.17
VB, H_2 burn, Late CF	0.00	0.04
VB, BMT or V Late OP	0.00	0.02
VB, No CF	0.00	0.00

the consequence results for the source term groups into the integrated risk analysis are given in [Bg90].

In support of the NUREG-1150 effort, there were complete risk calculations performed with the assumption that there was no evacuation of the population. The risk profiles were reported in [NRC89], and the results will be presented here to facilitate comparison to the CPI risk integration method that is described in Section 6.4. Latent cancer fatality risk is almost independent of evacuation assumptions, and highly dependent upon release magnitudes. The early fatality risk, however, is very sensitive to the assumptions made about evacuation with respect to the timing of the releases.

Tables 6.5 and 6.6 report the results for the calculations when it is assumed that the population does not evacuate (the mitigative actions of sheltering, crop and land interdiction, etc. are still assumed). Tables 6.5 and 6.6 illustrate that the mean early fatality risk is increased by a factor of 1.3 and the event contributions to the mean risk have changed. In particular, the contribution from the V-sequence has shifted to the SGTR accidents. In general, the SGTR accidents involve very large releases, but the releases occur after most of the population has evacuated because the SGTR accidents are of very long duration, and ample warning is given. When it is assumed that none of the population evacuates, the releases associated with an SGTR accident can cause many early fatalities. The changes in the mean latent cancer risk and fractional contribution of PDS groups and APBs are very minor, and in fact cannot be discerned when comparing Tables 6.5 and 6.6 to Tables 6.3 and 6.4.

6.3 CPI Sensitivity Studies

As noted in the previous section, accidents involving bypass of the containment are dominant contributors to the risk at Sequoyah. Early failures of containment also

Table 6.5

Fractional Contribution of PDS Groups
to Mean Risk Measures (0% Evacuation)

	Early Fatalities	Latent Cancer Fatalities
Mean Risk/R-yr	3.5E-05	1.4E-02
PDS Group	FCMR	FCMR
LOSP	0.16	0.41
ATWS	0.01	0.04
Transients	0.00	0.01
LOCAs	0.02	0.14
Bypass, V-sequence	0.33	0.10
Bypass, SGTR	0.49	0.30

Table 6.6

Fractional Contribution of Accident Progression
Bins to Mean Risk Measures (0% Evacuation)

	Early Fatalities	Latent Cancer Fatalities
Mean Risk/R-yr	3.5E-05	1.4E-02
APB	FCMR	FCMR
Bypass, V-sequence	0.33	0.10
Bypass, SGTR	0.50	0.35
No VB, Very Early CF	0.01	0.05
No VB, No CF	0.00	0.00
VB, Very Early CF	0.01	0.04
VB, alpha, Early CF	0.00	0.01
VB, hi RCS P, Early CF	0.05	0.23
VB, lo RCS P, Early CF	0.08	0.17
VB, H_2 burn, Late CF	0.01	0.04
VB, BMT or V Late OP	0.00	0.02
VB, No CF	0.00	0.00

contribute significantly to the risk profile. There were five sensitivity studies performed for the CPI involving containment improvements that are expected to reduce risk potential by reducing the frequency of occurrence of early containment failure. The five sensitivity studies that were run are:

- Sensitivity 1, DCH Mitigation by Partial Depressurization of the RCS. The primary system is assumed to be depressurized by intentional opening of the PORVs by the operators. The study was performed by modification of the base case accident progression event tree (APET), to incorporate depressurization by the operators at all times.

- Sensitivity 2, DCH Mitigation by Partial Depressurization of the RCS, Back-up Power Supply for Fans and Igniters. The primary system is assumed to be depressurized by intentional opening of the PORVs by the operators. It is also assumed that the fans and igniters are supplied power by a back-up system. The same value as the base case for frequency of operator failure to initiate the igniters (0.01) is assumed. The same value as the base case for fan failure upon demand (0.001) is assumed.

- Sensitivity 3, DCH Mitigation by Partial Depressurization of the RCS, Back-up Power Supply for Igniters. The primary system is assumed to be depressurized by intentional opening of the PORVs by the operators. It is assumed that the igniters, but not the fans, are supplied power by a back-up

system. The same value as the base case for frequency of operator failure to initiate the igniters (0.01) is assumed.

- Sensitivity 4, Containment Strength Increased. The containment failure pressure and impulsive failure criteria were increased to correspond to estimated criteria for the Watts Bar plant. The fifth, fiftieth, and ninety-fifth percentiles of the failure pressure, and the impulsive failure criteria in the ice condenser (IC) and the upper plenum (UP) of the ice condenser for the base case and this study are:

	Base Case			Sensitivity 4		
	5th	50th	95th	5th	50th	95th
Failure Pressure (kPa)	3.6	5.4	7.6	9.5	11.3	13.4
IC Impulse Load (kPa-s)	2	21	46	6	50	110
UP Impulse Load (kPa-s)	2	9	38	5	25	103

- Sensitivity 5, Elimination of Direct Contact Failure Mode. For Sequoyah, the containment might fail shortly after the vessel is breached due to accumulation of molten core debris at the steel containment wall. The hypothetical scenario involves the ejection of molten debris from the vessel at high pressure. Subsequent pressurization of the cavity fails the seal table and some debris enters the instrumentation room in which the seal table is located. The debris accumulates on the floor against the containment liner and eventually melts through the liner. This mode of containment failure was eliminated from the APET for this sensitivity study.

6.4 CPI Method for Risk Integration

In order to estimate the risk significance of the sensitivity studies, a simplified method was developed for risk integration. The integration must be done in a manner that gives an indication of public risk, for various combinations of event tree pathways and accident sequences. The MELCOR Accident Consequence Code System (MACCS) is used to perform radiological consequence calculations. Full consequence calculations could not be performed for each sensitivity study because an inordinate amount of computational time is involved with the MACCS calculations. The method used for presenting the base case and sensitivity study results for the CPI program utilizes early and latent cancer fatality "potentials" that are based on release magnitudes and timing, but do not account for such factors as release energies, evacuation, and other mitigative actions.

6.4.1 Source Term Partitioning

The method developed for risk integration utilizes partitioned source terms, which involves the grouping of similar source terms. The partitioning procedure was developed for and utilized in the NUREG-1150 analyses, is documented in [Im89], and is summarized here. For partitioning, the radionuclide releases assigned in the source term portion of the analysis are assigned "effects weights". The effects weights include the early fatality weight (EFW) and the chronic fatality weight (CFW), and are measures of the radiological potential of a source term to cause consequences in the absence of any emergency response mitigating effects except hot spot and 24-hour

relocation. The EFW is a measure of the radiological potential of a source term to cause early fatalities, and the CFW is a measure of the radiological potential of a source term to cause latent cancer fatalities.

To obtain the EFW, the radionuclide release for each source term is converted to an equivalent I-131 release. The basis of equivalency is for an 8 hour bone marrow dosage from three exposure pathways: cloudshine, inhalation, and groundshine. The MACCS consequence code is run for I-131 releases of various sizes. The MACCS calculations involve the actual site weather and demographic data for the Sequoyah plant. There is no evacuation or sheltering of the population, the release duration is minimal, and the release is at ground-level elevation with no plume rise. This tends to overestimate the number of early fatalities that would occur for most situations; however, the purpose of assigning health effects weights is to assess the radiological potential for the health effects. If full radiological consequence calculations are required, the MACCS calculations are then performed for the partitioned source term groups with appropriate timing, emergency response, and plume rise assumptions. The relationship between early fatalities and equivalent I-131 releases is shown in Figure 6.2 (from [Gr90]). The curve in Figure 6.2 relates released activity, in becquerels (Bq), for I-131 to a corresponding mean number of early fatalities predicted by a full MACCS calculation for the Sequoyah site.

The relationship of latent cancer fatalities to release magnitudes is much more linear than for early fatalities. Equivalent doses are therefore not required to obtain the CFW. MACCS calculations are run for a fixed release of each of the 60 radionuclides included in the NUREG-1150 consequence calculations, utilizing the Sequoyah site weather and demographic data. As with the EFW calculations, there are no mitigative actions assumed for the CFW calculations. The results of these calculations and the assumed linear relationship between the amount released and cancer fatalities for each radionuclide are then used to estimate the total number of chronic fatalities associated with a source term. This estimated number of chronic fatalities is the CFW.

The site-specific MACCS calculations that underlie the early and chronic health effect weights were performed with very conservative assumptions with respect to the energy and timing of the releases and also with respect to the emergency responses taken. As a result, these weights should be regarded as a measure of the potential of a source term to cause early and chronic fatalities rather than as an estimate of the fatalities that would actually result from a source term.

6.4.2 Base Case Results Utilizing Risk Potential Integration Method.

For the CPI risk integration of the NUREG-1150 results, the frequency-weighted source terms are assigned EFWs and CFWs. The risk equation, Eq. 6.1, is therefore transformed to the equation for risk potential:

$$R\text{-}POT_k = \Sigma_i \Sigma_j FREQ_i * CRMP_{i,j} * FW_k (FP_{i,j}); \qquad \text{(Eq. 6.2)}$$

where:

$R\text{-}POT_k$ = the risk potential associated with consequence measure k (where k is either early fatality or latent cancer fatality risk potential)

$FREQ_i$ = the frequency of accident sequence i

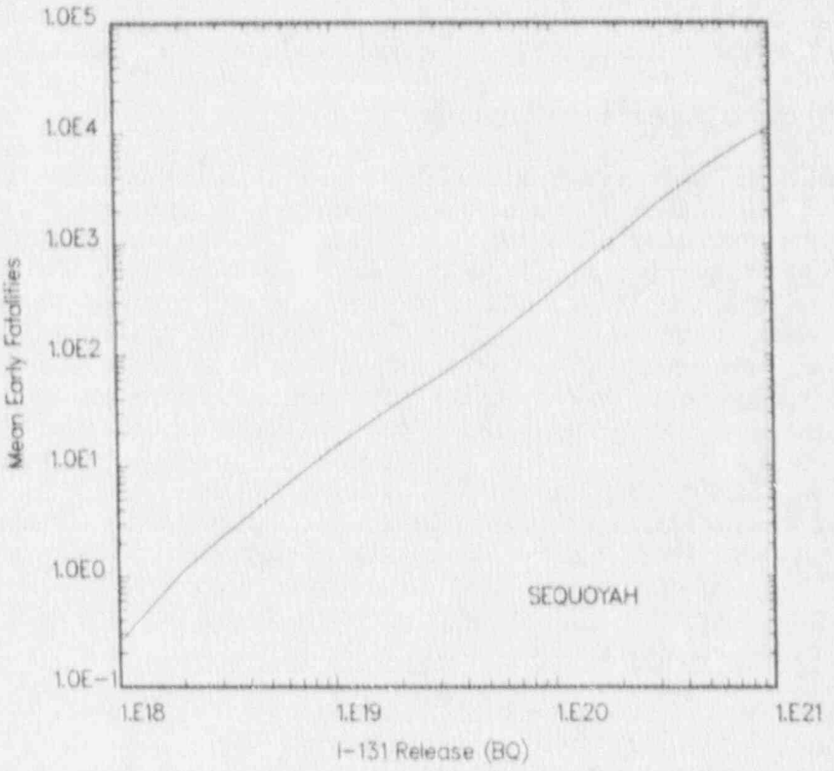

Figure 6.2 Mean early fatalities versus I-131 released activity for Sequoyah

$CRMP_{i,j}$	=	the probability of containment release mode j, given accident sequence i
$FP_{i,j}$	=	the fission product source term for containment release mode j of accident sequence i
FW_k	=	the fatality weight assigned to the fission product source term (FP) for sequence i,j

The result is a distribution of 200 risk potential estimates. Mean risk potentials and fractional contributions of APBs to mean risk potentials can then be extracted.

The results in Tables 6.4 and 6.6 for the NUREG-1150 early fatality risk and fractional contributions are presented in Table 6.7, along with the mean early fatality risk potential and the fractional contributions as calculated for the CPI base case. The base case results for all accident sequences is 8.2E-05 per reactor year in terms of the early fatality potential. This value is about three times greater than when 99.5% evacuation is assumed and more than twice as great as when no evacuation is assumed for the actual risk calculations. The risk potentials are more conservative estimates of risk than when no evacuation is assumed because mitigative actions and release energy are not considered as they are when the MACCS consequence calculations are performed.

When considering the fractional contributions of APBs to mean risk, however, there is fairly good agreement between the calculation for no evacuation and the CPI potential. The contribution of early containment failures is less for the risk estimates

Table 6.7

Fractional Contribution of Accident Progression Bins to Mean Early Fatality Risk

	99.5% Evac	0% Evac	CPI Base Case Potentials
Mean Risk/R-yr	2.6E-05	3.5E-05	8.2E-05
APB	FCMR	FCMR	FCMR
Bypass, V-sequence	0.68	0.33	0.28
Bypass, SGTR	0.07	0.50	0.31
No VB, CF during CD	0.01	0.01	0.03
No VB, no CF, no bypass	0.00	0.00	0.00
VB, CF during CD	0.02	0.01	0.04
CF at VB, Alpha-mode	0.00	0.00	0.01
CF at VB, Hi RCS Pr.	0.08	0.05	0.16
CF at VB, Lo RCS Pr.	0.14	0.08	0.16
VB, Late CF	0.00	0.01	0.01
VB, Very Late CF	0.00	0.00	0.00
VB, no CF, no bypass	0.00	0.00	0.00

than for the potential estimates because consideration of sheltering and the release energy is important (recall that these are considered for the no-evacuation risk calculation). A large portion of the early containment failures involve energetic releases, causing lofting of the plume, and less early fatalities.

The results in Tables 6.4 and 6.6 for the NUREG-1150 latent cancer risk and fractional contributions are presented in Table 6.8, along with the mean risk latent cancer risk potential and the fractional contributions as calculated for the CPI base case. The base case results for all accident sequences is 1.1E-01 per reactor year in terms of the latent cancer fatality potential. This value is about an order of magnitude greater than for the actual risk calculations. For latent cancer fatalities, the mitigative measures assumed for the MACCS calculations are very important for the actual risk calculations. In particular, food interdiction decreases the consequences by as much as factor of five for large releases. Large releases dominate the upper ends of the risk distributions and thus influence the mean risk value. When considering fractional contributions of APBs to mean risk for latent cancer fatalities, there is rather good agreement between the actual risk calculations and the CPI potential.

These comparisons show that the early fatality and latent cancer fatality risk potentials can be useful in the estimation of risk if some important points are kept in mind. The potential estimates are conservative with respect to a full risk estimate which takes into account plume lofting and gives credit for evacuation and emergency response mitigating effects. For early fatality potential, evacuation, sheltering, and

Table 6.8

Fractional Contribution of Accident Progression Bins to Mean Latent Cancer Fatality Risk

	99.5% and 0% Evac	CPI Base Case Potentials
Mean Risk/R-yr	1.4E-02	1.1E-01
APB	FCMR	FCMR
Bypass, V-sequence	0.10	0.10
Bypass, SGTR	0.35	0.43
No VB, CF during CD	0.05	0.04
No VB, no CF, no bypass	0.00	0.00
VB, CF during CD	0.04	0.04
CF at VB, Alpha-mode	0.01	0.01
CF at VB, Hi RCS Pr.	0.23	0.20
CF at VB, Lo RCS Pr.	0.17	0.17
VB, Late CF	0.04	0.02
VB, Very Late CF	0.02	0.00
VB, no CF, no bypass	0.00	0.00

release energy are particularly important; for latent cancer fatality potential, crop and land interdiction are important. The fractional contributions to the mean risk potential estimates are qualitatively adequate in indicating trends; in particular, the FCMRs for the latent cancer potential estimates show very good agreement with the full risk calculation estimates. The fractional contributions of particular bins can be used to determine potentially risk-significant accident pathways.

6.5 Sensitivity Study Results for the CPI

The mean risk potentials (per reactor-yr) for the base case and sensitivity studies as defined in Section 6.3 are given in Table 6.9. The percentage reduction in mean risk from the base case is provided for the sensitivity studies.

Note that the greatest reductions in mean early fatality and latent cancer risk potentials occurs for Sensitivities 2, 3 and 4. The reduction in risk potential is relatively minor for Sensitivities 1 and 5 for both risk measures. Deliberate depressurization of the RCS alone has little effect on the potential risk profile. One reason is that hydrogen deflagrations and detonations can still cause early containment failure. Another is that there are unintentional mechanisms that in many cases depressurize the system, thereby sufficiently reducing the DCH threat without necessitating deliberate depressurization. As will be seen in the following section, the occurrence of containment failure at vessel breach with the system at high pressure is reduced for Sensitivity 1, but failures from other phenomena such as hydrogen events

Table 6.9

Mean Early Fatality and Latent Cancer
Risk Potentials (1/R-yr)

Conseq.	Base	Sens. 1	Sens. 2	Sens. 3	Sens. 4	Sens. 5
Early Fat.	8.2E-05	8.0E-05	5.6E-05	6.1E-05	5.3E-05	8.0E-05
Reduction		2%	32%	26%	35%	2%
Latent Can.	1.1E-01	1.1E-01	7.1E-02	7.8E-02	6.5E-02	1.1E-01
Reduction		3%	37%	31%	41%	3%

alone are increased. For Sequoyah, the largest reduction in risk potential is for situations in which hydrogen ignition and hydrogen distribution through containment is assured during station blackouts by assuming that back-up power is available for the igniters and air return fans. When the containment is assumed to be similar to the Watts Bar containment, the reduction in risk potential is greater than in any of the other sensitivity studies.

A more detailed presentation of the results is provided in Tables 6.10, 6.11 and 6.12. Table 6.10 provides the mean frequencies of the defined accident pathways. Table 6.11 provides the mean early fatality potentials for the defined accident pathways, and Table 6.12 provides the mean latent cancer fatality potentials for the defined pathways. The frequencies of the pathways defined here are absolute frequencies (they are not conditional upon various PDS groups). Unlike the method of binning for Tables 6.4 and 6.5 the pathways presented here are not mutually exclusive; i.e., if a scenario fits more than one definition, it will be included in more than one pathway. The pathways chosen for Tables 6.10, 6.11 and 6.12 and the label descriptors for each row are:

- All core damage accidents (Total Core Damage).
- The V-sequence in which no credit is given for scrubbing by area fire sprays in the auxiliary building (Dry V-Sequence).
- The V-sequence in which credit is given for scrubbing by area fire sprays in the auxiliary building (Wet V-Sequence).
- SGTR sequences in which the secondary SRV recloses (SGTR, SRV Recloses).
- SGTR sequences in which the secondary SRV sticks open (SGTR, SRV Sticks Open).
- Pathways in which containment failure occurs during core degradation; these include failure to initially isolate the containment (CF During CD).

- Pathways in which containment failure occurs at, or shortly after vessel breach (Total CF at VB).

- Pathways in which containment failure occurs at, or shortly after vessel breach, and the RCS pressure is less than 200 psia (CF at VB, Low RCS Pr.).

- Pathways in which containment failure occurs at, or shortly after vessel breach, and the RCS pressure is greater than 200 psia. This case includes events involving DCH (CF at VB, Hi RCS Pr.).

- Pathways in which containment failure occurs at, or shortly after vessel breach, and the mode of containment failure is a catastrophic rupture, i.e., there gross rupture of containment with extensive structural failure (CF at VB, Cat. Rupt.).

- Pathways in which containment failure occurs at, or shortly after vessel breach, and the mode of containment failure is a rupture, nominally 1 ft^2 (CF at VB, Rupture).

- Pathways in which containment failure occurs at, or shortly after vessel breach, and the mode of containment failure is a leak, nominally 0.1 ft^2 (CF at VB, Leak).

- Pathways in which containment failure occurs at, or shortly after vessel breach, and an SGTR has also occurred (CF at VB, SGTR). (Pathways in which containment fails and an interfacing systems LOCA occurred are of negligible frequency, and thus were not binned separately as were containment failures that occur during an SGTR accident.)

In Table 6.10, the V-sequence frequencies are the same for the base case and the sensitivity studies because there were no sensitivity studies performed that involved the V-sequence. Temperature-induced SGTRs are SGTRs with reclosing SRVs. For Sensitivities 1, 2 and 3, temperature-induced SGTRs are eliminated because they cannot occur at intermediate or low pressure; thus, the occurrence of SGTRs with reclosing SRVs is decreased slightly for these sensitivity studies.

The occurrence of CF during core degradation (see sixth row of Table 6.10) increases slightly for Sensitivity 1. This is because less hydrogen is retained in the RCS when the system is at lower pressures, resulting in more failures from hydrogen burns during core degradation. For hydrogen control back-up power systems involved in Sensitivities 2 and 3, and for the stronger containment assumed for Sensitivity 4, the occurrence of CF during CD for the base case is decreased substantially, about 80%. Not all CF during CD can be eliminated because failures to isolate containment are included in this category.

The occurrence of CF at vessel breach decreases for every sensitivity study. For Sensitivity 1, the base case occurrence of CF at VB is decreased by 41%, due to a 75% reduction in CF when the system is at high or intermediate pressure (for intentional depressurization, 80% of the depressurized sequences are at low pressure and 20% are at intermediate pressure). For Sensitivity 1, however, CF at VB when the system is at low pressure increases, due to CF by hydrogen burns at vessel breach.

Table 6.10

Mean Frequency of Occurrence of Defined
Accident Progression Pathways

Accident Progression Pathway	Mean Frequencies					
	Base	Sens. 1	Sens. 2	Sens. 3	Sens. 4	Sens. 5
Total Core Damage	5.5E-05	5.5E-05	5.5E-05	5.5E-05	5.5E-05	5.5E-05
Dry V-Sequence	1.3E-07	1.3E-07	1.3E-07	1.3E-07	1.3E-07	1.3E-07
Wet V-Sequence	5.2E-07	5.2E-07	5.2E-07	5.2E-07	5.2E-07	5.2E-07
SGTR, SRV Recloses	5.6E-07	5.5E-07	5.5E-07	5.5E-07	5.6E-07	5.6E-07
SGTR, SRV Sticks Open	1.4E-06	1.4E-06	1.4E-06	1.4E-06	1.4E-06	1.4E-06
CF During CD	1.1E-06	1.2E-06	2.4E-07	2.3E-07	2.1E-07	1.1E-06
Total CF at VB	3.9E-06	2.3E-06	1.3E-06	1.4E-06	1.5E-06	3.4E-06
CF at VB, Low RCS Pr.	1.3E-06	1.6E-06	1.2E-06	1.1E-06	5.2E-07	1.1E-06
CF at VB, Hi RCS Pr.	2.7E-06	6.4E-07	1.3E-07	3.1E-07	9.8E-07	2.3E-06
CF at VB, Cat. Rupt.	1.5E-06	1.0E-06	4.0E-07	3.5E-07	1.9E-07	1.5E-06
CF at VB, Rupture	1.2E-06	5.6E-07	3.7E-07	5.1E-07	1.7E-07	1.2E-06
CF at VB, Leak	1.2E-06	6.9E-07	5.3E-07	5.3E-07	1.1E-06	6.9E-07
CF at VB, SGTR	2.9E-07	1.8E-07	1.8E-07	1.8E-07	7.2E-08	2.3E-07

For Sensitivities 2 and 3, the base case occurrence of CF at VB is decreased by about 65%. CF at VB with the RCS at low pressures still occurs with low but not insignificant frequency for these sensitivities. These failures are associated with the upper ends of the distributions for the loads at vessel breach and are attributable to the quasistatic pressure rise from steam explosions from fuel-coolant interactions; hydrogen burns and/or steam spikes from quenching of debris can also contribute to the loading. For Sensitivities 4 and 5, the base case occurrence of CF at VB is decreased by about 60% and 14%, respectively. For the stronger containment assumed in Sensitivity 4, the failures at VB are not totally eliminated because the direct contact mode of failure still occurs for the times when the RCS pressure is elevated at vessel failure. However, for this type of CF, the failure mode is assumed to be a leak because of the decontamination effects of the shield building, thereby decreasing the source term and in turn affecting the risk potential. For rupture failures of containment (the most frequent failure mode), the shield building is also assumed to rupture.

In Table 6.11, the mean early fatality potential associated with the bypass sequences is relatively large and is essentially unchanged for the sensitivity studies. For SGTRs, the risk potential varies slightly between the sensitivity studies because containment failure can also occur during the SGTR accidents, and the release is increased when this occurs.

Table 6.11

Mean Early Fatality Potentials for Defined
Accident Progression Pathways

Accident Progression Pathway	Mean Early Fatality Potentials					
	Base	Sens. 1	Sens. 2	Sens. 3	Sens. 4	Sens. 5
Total Core Damage	8.2E-05	8.1E-05	5.6E-05	6.1E-05	5.3E-05	8.1E-05
Dry V-Sequence	1.2E-05	1.2E-05	1.2E-05	1.2E-05	1.2E-05	1.2E-05
Wet V-Sequence	1.2E-05	1.2E-05	1.2E-05	1.2E-05	1.2E-05	1.2E-05
SGTR, SRV Recloses	8.5E-06	8.4E-06	8.4E-06	8.4E-06	8.4E-06	8.5E-06
SGTR, SRV Sticks Open	1.7E-05	1.6E-05	1.6E-05	1.6E-05	1.4E-05	1.6E-05
CF During CD	5.2E-06	6.3E-06	8.6E-07	8.[illegible]E-07	3.8E-07	5.2E-06
Total CF at VB	3.4E-05	3.0E-05	1.2E-05	1.7E-05	7.4E-06	3.2E-05
CF at VB, Low Pr.	1.7E-05	1.8E-05	9.8E-06	8.9E-05	5.4E-06	1.5E-05
CF at VB: Hi RCS Pr.	1.7E-05	1.2E-05	1.8E-06	7.7E-06	2.0E-06	1.7E-05
CF at VB, Cat. Rupt.	1.9E-05	1.7E-05	6.5E-06	5.8E-06	3.7E-06	2.0E-05
CF at VB, Rupture	8.1E-06	8.2E-06	2.1E-06	7.8E-06	1.0E-06	8.3E-06
CF at VB Leak	6.5E-06	5.0E-06	3.0E-06	2.9E-06	2.6E-06	4.0E-06
CF at VB, SGTR	6.2E-06	4.6E-06	4.6E-06	4.6E-06	1.2E-06	5.4E-06

The mean early fatality potential associated with CF during CD for the base case is increased by 20% for Sensitivity 1, because occurrence of CF during CD has increased, as discussed earlier for Table 6.10. For Sensitivities 2 and 3, the base case mean early fatality potential associated with CF during CD is decreased by about 85%. For Sensitivity 4, there is more than an order of magnitude decrease in early fatality risk potential associated with containment failures during core degradation, and no change in risk potential for Sensitivity 5. The base case mean early fatality potential associated with CF at VB is decreased for all sensitivity studies: 12% for Sensitivity 1, 65% for Sensitivity 2, 50% for Sensitivity 3, 80% for Sensitivity 4, and 6% for Sensitivity 5.

In Table 6.12, the mean latent cancer fatality potential associated with the bypass sequences is essentially unchanged for the sensitivity studies. The mean latent cancer fatality potential associated with CF during CD for the base case is increased by 28% for Sensitivity 1, due to the increase in the occurrence of CF during CD. For Sensitivities 2 and 3, the base case mean latent cancer fatality potential associated with CF during CD is decreased by about 80%. As with early fatality risk potential, there is more than an order of magnitude decrease in latent cancer fatality risk potential associated with containment failures during core degradation for Sensitivity 4, and no change in risk potential for CF during CD in Sensitivity 5.

Table 6.12

Mean Latent Cancer Fatality Potentials for Defined Accident Progression Pathways

Accident Progression Pathway	Mean Latent Cancer Fatality Potentials					
	Base	Sens. 1	Sens. 2	Sens. 3	Sens. 4	Sens. 5
Total Core Damage	1.1E-01	1.1E-01	7.1E-02	7.8E-02	6.5E-02	1.1E-01
Dry V-Sequence	6.0E-03	6.0E-03	6.0E-03	6.0E-03	6.0E-03	6.0E-03
Wet V-Sequence	5.5E-03	5.5E-03	5.5E-03	5.5E-03	5.5E-03	5.5E-03
SGTR, SRV Recloses	9.8E-03	9.6E-03	9.6E-03	9.6E-03	9.8E-03	9.8E-03
SGTR, SRV Sticks Open	3.7E-02	3.7E-02	3.7E-02	3.7E-02	3.4E-02	3.7E-02
CF During CD	8.6E-03	1.1E-02	1.6E-03	1.5E-03	6.8E-04	8.6E-03
Total CF at VB	5.4E-02	4.7E-02	2.0E-02	2.7E-02	1.1E-02	5.0E-02
CF at VB: Low RCS Pr.	2.7E-02	2.9E-02	1.7E-02	1.6E-02	7.4E-03	2.4E-02
CF at VB: Hi RCS Pr.	2.7E-02	1.8E-02	2.5E-03	1.1E-02	3.8E-03	2.6E-02
CF at VB, Cat. Rupt.	3.1E-02	2.6E-02	1.2E-02	1.1E-02	4.9E-03	3.1E-02
CF at VB, Rupture	1.2E-02	1.3E-02	3.4E-03	1.2E-02	1.5E-03	1.2E-02
CF at VB, Leak	1.2E-02	8.4E-03	4.4E-03	4.2E-03	4.8E-03	6.8E-03
CF at VB, SGTR	1.2E-02	8.4E-03	8.4E-03	8.4E-03	2.4E-03	1.0E-02

The base case mean latent cancer fatality potential associated with CF at VB is decreased for all sensitivity studies: 13% for Sensitivity 1, 63% for Sensitivity 2, 50% for Sensitivity 3, 80% for Sensitivity 4, and 7% for Sensitivity 5.

6.6 Summary

In this chapter, the NUREG-1150 methodology has been used to study the effects of various containment improvements on the potential risk profile for the Sequoyah plant. Accidents in which the containment is bypassed and those in which containment fails early are the main contributors to the potential risks. For the sensitivity studies involved in this work (which do not address bypass accidents), the results indicate that containment improvements involving a backup power supply for the igniters and fans, as well as depressurization of the primary system, provide the largest reduction in potential risks.

Bypass accidents are significant contributors to the Sequoyah potential risk profile. Mitigation of the releases from the bypass sequences would probably significantly reduce the estimated risks. However, prevention measures for bypass accidents could prove more cost effective than installation of mitigative systems.

The accidents that involve hydrogen events or that proceed to vessel breach at high pressure are also significant contributors to potential risk at Sequoyah. At present, it appears that many sequences that are initiated at high pressure will be depressurized by inadvertent temperature-induced mechanisms. Depressurization of high pressure sequences is important in two respects: 1) the DCH threat is reduced, and 2) core damage arrest can occur before the vessel is breached. The sensitivity results indicate that intentional depressurization by itself has little impact upon either the frequency of containment failure or the risk potential. If the frequency of inadvertent depressurization is less than assumed in the NUREG-1150 models, the results will be more sensitive to intentional depressurization.

The sensitivity results indicate that primary system depressurization and assured operation of the igniters and fans decreases the risk potentials significantly. There was not much difference between the results for depressurization with operation of both systems and depressurization with operation of the igniters only. These results are consistent with the CONTAIN results noted in Section 4. The CONTAIN results, however, did indicate that fan operation was beneficial in reducing detonation threats (Section 5).

The increase in failure criteria for quasistatic pressure rises and dynamic pressure loads to correspond to the Watts Bar containment resulted in the largest reductions for risk potential for both early fatalities and latent cancer fatalities. The reductions were due to a significant decrease in early containment failures. The stronger containment made more difference than did any of the mitigation strategies considered when the latter were applied to the weaker containment, thus emphasizing the importance of plant-specific considerations.

7. Conclusions

It is difficult to define mitigation strategies for DCH scenarios in ice condenser plants that offer large benefits if the RCS remains at system pressure up until the time of vessel breach. Of all the strategies considered here, only containment inerting reduced the maximum pressures calculated sufficiently to have a large effect upon containment failure probability. Independent power supplies for the igniters, containment venting, and a subatmospheric containment offered some modest benefits. Combinations of certain improvements (notably igniters plus containment venting) offered some further improvement, but the effect was still less than that of certain phenomenological uncertainties such as the amount of corium that might participate in a DCH event. Hence, no combination of improvements considered, other than those including inerting, seems likely to substantially reduce the probability of early containment failure as assessed in a PRA which attempts to take into account phenomenological uncertainty, e.g., as was done in the NUREG-1150 study.

Partially depressurizing the RCS (to 1.5 MPa) was assessed as a mitigation strategy and was found to have little to offer unless it is combined with providing independent power supplies for the igniters, in which case substantial benefits were obtained. Augmenting existing igniter systems with additional igniters in, e.g., the ice condenser did not give any substantial additional reductions in the maximum pressures calculated following vessel breach. As in the fully-pressurized scenario, operating the air return fans did not give any further reductions in the DCH pressures. With igniters operating, calculated maximum pressures for the hydrogen deflagrations occurring prior to VB were small and posed no threat to containment.

The preceding assessments do not allow for the possible occurrence of detonations. Detonation threats were evaluated by performing calculations of gas distributions using a relatively detailed 26-cell deck representing the Sequoyah containment. If igniters were not operating, there was a strong tendency to develop highly detonable gas mixtures in the ice condenser for all cases considered in both the fully pressurized and the depressurized station blackout sequences. Depending upon the circumstances, detonable concentrations could also develop in the upper plenum and even in the lower containment. Providing independent power for the existing igniter systems resulted in only limited improvements in the ice condenser, although it largely eliminated detonation threats in the upper plenum insofar as the present analyses could determine. If independent power was also provided for the air return fans, benefits were greater but it was still not clear that detonation in the ice condenser could be completely ruled out, due in part to the large uncertainties in the sources from the primary system. The present study was limited only to considering when and where detonable gas concentrations might arise; it is not known whether occurrence of a detonation in the ice condenser would actually threaten containment integrity.

Sensitivity studies were performed using the NUREG-1150 event trees and related modeling to determine the effect of some of the containment improvements considered upon the Sequoyah risk profile. Depressurization combined with independent power for both igniters and fans offered the largest benefits of those strategies considered; it reduced risks associated with early containment failures by about a factor of three. The impact of a stronger containment, corresponding to the estimated failure pressure of the Watts Bar plant, was assessed and found to be greater than the effect of any of the mitigation strategies assessed for the Sequoyah plant. The general agreement between the implications of the NUREG-1150

sensitivity studies and the implications of the CONTAIN calculations is noteworthy, in view of the fact that the former involved much less detailed modeling than the latter, and the CONTAIN calculations were not available until after the NUREG-1150 work had been completed.

There are many uncertainties in the analyses performed here, and there are large uncertainties in such quantities as the absolute magnitudes of the containment pressures calculated for any specific scenario. However, the assessments of the effectiveness of the various mitigation strategies considered are based upon comparisons of analyses performed for the unmodified plant with otherwise-similar analyses for the plant with the postulated improvements in place. Although caution is always warranted, it is not believed that the uncertainties in the analysis are such as to invalidate these comparisons.

REFERENCES

Al87 K. Almenas, "Natural Circulation Currents in a Post-LOCA Containment," Proceedings of the National Heat Transfer Conference, Pittsburg, Pa, pp. 175-181, 1987.

Bg90 E. G. Bergeron, et al., "Evaluation of Severe Accident Risks: Methodology for the Accident Progression, Source Term, Consequence, Risk Integration and Uncertainty Analyses," NUREG/CR-4551, Vol. 1, Draft Rev. 1, SAND86-1309, Sandia National Laboratories, Albuquerque, NM, to be published. *

BNL90 "Assessment of Ice Condenser Containment Performance Issues," NUREG/CR-5589, Brookhaven National Laboratory, Upton, New York, to be published.*

Bt90 R. C. Bertucio and S. R. Brown, "Analysis of Core Damage Frequency From Internal Events, Sequoyah Unit 1," NUREG/CR-4550, Vol. 5, Rev. 1, SAND86-2084, Sandia National Laboratories, Albuquerque, NM, April 1990.

Ca84 A. L. Camp, V. L. Behr, and F. E. Haskin, "MARCH-HECTR Analysis of Selected Accidents in an Ice-Condenser Containment", NUREG/CR-3912, SAND83-0501, Sandia National Laboratories, Albuquerque, NM, December 1984.

Ch88 Rosanna Chambers, D. J. Hanson, R. J. Dallman, and F. Odar, "Depressurization to Mitigate Direct Containment Heating," 16th LWR Safety Information Meeting, Gaithersberg, MD, October 1988.

De86 R. S. Denning, et al., "Radionuclide Release Calculations for Selected Severe Accident Scenarios," Vol. II, NUREG/CR-4624, BMI-2139, Battelle Columbus Laboratories, Columbus, Ohio, May 1986.

Di85 S. E. Dingman and A. L. Camp, "Pressure-Temperature Response in an Ice-Condenser Containment for Selected Accidents," in Proceedings of the 13th Water Reactor Safety Research Information Meeting, Gaithersburg, Md, October 22-26 1985.

Di86 S. E. Dingman, et al., "HECTR Version 1.5 User's Manual," NUREG/CR-4507, SAND86-0101, Sandia National Laboratories, Albuquerque, NM, April 1986.

Er90 D. M. Ericson, et al., "Analysis of Core Damage Frequency: Internal Events Methodology," NUREG/CR-4550, Vol. 1, Rev. 1, SAND86-2084, Sandia National Laboratories, January 1990.

Gi84 J. A. Gieseke, et al., "Radionuclide Release Under Specific LWR Accident Conditions," Vol. IV, BMI-2104, Battelle Columbus Laboratories, Columbus, Ohio, July 1984.

*Available in the NRC Public Document Room, 2120 L Street, NW.Washington, DC.

Go89 D. W. Golden, et al., "Depressurization as an Accident Management Strategy to Minimize the Consequences of Direct Containment Heating (Draft)," NUREG/CR-5447, EGG-2574, Idaho National Engineering Laboratory, Idaho Falls, Idaho, September 1989.

Gr90 J. J. Gregory, et al., "Evaluation of Severe Accident Risks: Sequoyah Unit 1," NUREG/CR-4551, Vol. 5, Part 1, SAND86-1309, Sandia National Laboratories, Albuquerque, NM, to be published.*

Ha90 F. T. Harper, et al., "Evaluation of Severe Accident Risks: Major Input Parameters," NUREG/CR-4551, Vol. 2, Draft Rev. 1, SAND86-1309, Sandia National Laboratories, to be published.*

He89 T. S. Heames and R. C. Smith, "Integrated MELPROG-TRAC Analyses of a PWR Station Blackout," ANS Proceedings of the 1989 National Heat Transfer Conference, Philadelphia, PA, August 6-9, 1989.

Im84 R. L. Iman and M. J. Shortencarier, "A FORTRAN 77 Program and User's Guide for the Generation of Latin Hypercube and Random Samples for Use with Computer Models," NUREG/CR-3624, SAND83-2365, Sandia National Laboratories, 1984.

Im89 R. L. Iman, et al., "A User's Guide for PARTITION: A Program for Defining the Source/Term Consequence Analysis Interface in the NUREG-1150 Probabilistic Risk Assessments," NUREG/CR-5253, SAND88-2940, Sandia National Laboratories, May 1990.

Ke87 J. E. Kelly, R. J. Henninger, and J. F. Dearing, "MELPROG-PWR/MOD1 Analysis of a TMLB' Accident Sequence," NUREG/CR-4742, SAND86-2175, Sandia National Laboatories, NM, January 1987.

La89 J. Langhans, "Comparison of CONTAIN-Results with Experimental PHDR Data," Gesellschaft fur Reaktorsicherheit (GRS) wbH, Koln, FRG. Paper presented at SMIRT-10, Anaheim, CA, August 14-18, 1989.

Le88 M. T. Leonard, et al., "Supplemental Radionuclide Release Calculations for Selected Severe Accident Scenarios," NUREG/CR-5062, BMI-2160, Battelle Columbus Laboratories, Columbus, Ohio, February 1988.

Mo78 K. V. Moore, et al., "RETRAN -- A Program for One-Dimensional Transient Thermal-Hydraulic Analysis of Complex Fluid Flow Systems," CCM-5, Vol. 1, p. III-92, Energy Incorporated, Idaho Falls, Idaho, December 1978.

Mu83 K. K. Murata, et al., "CONTAIN: Recent Highlights in Code Testing and Validation," Cambridge Conference, Cambridge, MA, August 28 - September 1, 1983.

Mu88 K. K. Murata and D. L. Y. Louie, "Parametric CONTAIN Calculations of the Containment Response of the Grand Gulf Plant Due to Reactor Pressure Vessel Failure at High Pressure," Fourth Workshop on Containment Integrity, Washington, D.C., June 14-17, 1988; K. K. Murata and D. L. Y. Louie, Internal Memorandum to NUREG-1150 Expert Panel Members, Sandia National Laboratories, February 15, 1988.

*Available in the NRC Public Document Room, 2120 L Street NW., Washington, DC.

Mu89 K. K. Murata, D. E. Carroll, K. E. Washington, F. Gelbard, G. D. Valdez, D. C. Williams, and K. D. Bergeron, "User's Manual for CONTAIN 1.1, A Computer Code for Severe Nuclear Reactor Accident Containment Analysis," NUREG/CR-5026, SAND87-2309, Sandia National Laboratories, Albuquerque, NM, 1989.

NRC75 "Reactor Safety Study -- An Assessment of Accident Risks in U.S. Commercial Nuclear Power Plants," WASH-1400 (NUREG-75/014), U.S. Nuclear Regulatory Commission, Washington, D.C., 1975.

NRC87 U.S. NRC, "Reactor Risk Reference Document," (Draft for Comment), NUREG-1150, U.S. Nuclear Regulatory Commission, Washington, DC, February 1987.

NRC89 U.S. NRC, "Severe Accident Risks: An Assessment for Five U.S. Nuclear Power Plants," (Second Draft for Peer Review), NUREG-1150, U.S. Nuclear Regulatory Commission, Washington, DC, June 1989.

Pi85 M. Pilch and W. W. Tarbell, "High Pressure Ejection of Melt From a Reactor Pressure Vessel: The Discharge Phase," NUREG/CR-4383, SAND85-8512, Sandia National Laboratories, Albuquerque, NM, September 1985.

Ru90 N. A. Russell and D. C. Williams, "Comparison of CONTAIN Code Simulations to Experimental Ice Condenser Data," SAND89-3096C, to be published in the Proceedings of the Second International Conference on Containment Design and Operation, Toronto, Canada, October 14-17, 1990.

Sh89 M. P. Sherman, S. R. Tieszen, and W. B. Benedick, "FLAME Facility -The Effect of Obstacles and Transverse Venting on Flame Acceleration and Transition to Detonation for Hydrogen-Air Mixtures at Large Scale," NUREG/CR-5275, SAND85-1264, Sandia National Laboratories, Albuquerque, NM, April 1989.

St90 D. W. Stamps, W. B. Benedick, and S. R. Tieszen, "Hydrogen-Air-Diluent Detonation Study for Nuclear Reactor Safety Analysis," Sandia National Laboratories, Albuquerque, NM, September 1990.

Ta86 W. W. Tarbell, et al., "Pressurized Melt Ejection Into Scaled Reactor Cavities," NUREG/CR-4512, SAND86-0153, Sandia National Laboratories, Albuquerque, NM, October 1986.

Ta88 W. W. Tarbell, et al., "Direct Containment Heating and Aerosol Geberation During High Pressure Melt Ejection Experiments," Proceedings of the Thermal Hydraulics Division, 1988 ANS/ENS Winter Meeting, Washington, DC, October 31 - November 4 1988.

Ti90 S. R. Tieszen, et al., "Hydrogen Distribution and Combustion," Chapter 6 in Ex-Vessel Severe Accident Review for the Heavy Water New Production Reactor, Draft for Comment, SAND90-0234, Sandia National Laboratories, Albuquerque, NM, February 1990.

Tu87 N. K. Tutu, et al., Chapter 3 in "Safety Research Programs Sponsored by the Office of Nuclear Regulatory Research: Quarterly Progress Report January 1 - March 31, 1987", NUREG/CR-2331, BNL-NUREG-51454, Vol. 7, No. 1, Brookhaven National Laboratory, Upton, NY.

Tu89 N. K. Tutu, C. K. Park, C. A. Grimshaw, and T. Ginsberg, "Estimation of Containment Pressure Loading Due To Direct Containment Heating for the Zion Plant" (Draft), NUREG/CR-5282, BNL-NUREG-52181, Brookhaven National Laboratory, Upton, NY, June 1989.

TVA74 "Sequoyah Nuclear Plant Final Safety Analysis Report," Tennessee Valley Authority, 1974, with subsequent amendments.

TVA81 "Containment Response to Degraded Core Events for the Sequoyah Plant," Attachment 3 to Letter dated 12/1/81 from L. M. Mills (Manager of Nuclear Regulation and Safety, TVA) to Director of Nuclear Reactor Regulation, USNRC (attention Ms. E. Adensam, Chief, Licensing Branch No. 4, Div. of Licensing)

TVA88 S. A. White, "Response to Questions from EI Services on Sequoyah Nuclear Plant (SQN) Containment Design (Dated April 22, 1988)," Tennessee Valley Authority, letter w. enclosure to J. L. Tills (Jack Tills & Associates), dated July 1, 1988.

WC74 "Final Report Ice Condenser Full Scale Section Test at the Waltz Mill Facility," WCAP-8211, Appendix (Non-Proprietary), May 1974.

Wi87 D. C. Williams, K. D. Bergeron, D. E. Carroll, R. D. Gasser, J. L. Tills, and K. E. Washington, "Containment Loads Due to Direct Containment Heating and Associated Hydrogen Behavior: Analysis and Calculations With the CONTAIN Code," NUREG/CR-4896, SAND87-0633, Sandia National Laboratories, Albuquerque, NM, May 1987

Wi88a D. C. Williams and D. L. Y. Louie, "CONTAIN Analyses of Direct Containment Heating in the Surry Plant," Proceedings of the Thermal Hydraulics Division, 1988 ANS/ENS Winter Meeting, Washington, DC, October 31 - November 4 1988.

Wi88b D. C. Williams, "Proposed Matrix for CONTAIN Ice Condenser Parametric Calculations," Sandia National Laboratories, letter report to J. Hulman, USNRC, May 2, 1988.

Wi88c D. C. Williams, "CONTAIN Calculations for the Ice Condenser Parametrics Program: Potential for Mitigation of DCH Scenarios in Ice Condenser Containments," Letter Report to NRC/DSIR, October 25, 1988.

APPENDIX A

Description of the CONTAIN Sequoyah Deck Used in the Containment Performance Improvements Program

The purpose of this Appendix is to present the CONTAIN deck used to represent the Sequoyah containment. The emphasis in the discussion is on the description of the plant itself; e.g., compartment volumes, interconnections, heat sink structures, etc. The phenomenological modeling assumptions used are not discussed, nor is description given of input specific to a particular accident scenario (e.g., sources of steam and gas to the containment from the primary system). The most important of these features of the input are discussed in the main report. An example of the complete input for the 26-cell Sequoyah deck is provided on microfiche in the pocket on the inside cover of this report. The example provided is the deck for Case 19 of Table 3.4, which involves a station blackout accident with fully-pressurized RCS, backup power provided for fans and the existing igniter system, and containment venting up until the time of onset of core degradation.

All CONTAIN input is in SI units. In the input deck, anything to the right of a double ampersand (&&) is treated as a comment and is ignored by the computer.

The configuration of the deck is diagrammed schematically in Figure 2.3 of the main text. The identities of the various cells are as follows:

Cell 1:	Cavity region below the vessel, including instrument tunnel and keyway
Cells 2-5:	Steam generator doghouses
Cell 6:	Upper cavity region, i.e., above the vessel
Cell 7:	Pressurizer doghouse
Cells 8-10:	Lower containment inside the crane wall
Cells 11-13:	Annulus region between the crane wall and the containment shell below the ice condenser inlet plenum
Cells 14-17:	Ice condenser inlet plenum
Cells 18-21:	Ice condenser. The ice condenser is subdivided azimuthally, with each segment representing the full height of the ice condenser
Cells 22-23:	Ice condenser upper plenum
Cells 24-25:	Upper containment dome region
Cell 26:	Lower portion of the upper containment, including the refueling canal space
Cell 27:	Extra cell used to provide a source of blowdown steam and hydrogen at the time of vessel breach

Cell 28: Extra cell used to represent the environment

This deck is derived from HECTR input decks used in various analyses of the Sequoyah containment at Sandia [Ca84, Di85] which employed the HECTR code, supplemented by information derived from the FSAR [TVA74], and additional information provided by TVA [TVA81, TVA88]. Tracing the ultimate source of all the plant data used here could prove to be a difficult and time-consuming task. A detailed review of the deck by knowledgable plant personnel would have been desirable, but it did not prove possible to arrange such a review for the present project. The lack of such a review is one major motivation for providing this Appendix; i.e., so that any specific features of the plant representation that may be of interest to the reader may be checked.

CONTAIN input is divided into two major portions, global and cell-level, with global input being given first. Global input refers to input parameters which apply to the entire problem, while cell-level input refers to parameters which apply only to the individual cell for which they are specified. The latter parameters must be specified separately for each cell for which they are relevant. Input parameters for physics models not used in a given cell need not be specified for that cell. The description of the CONTAIN input structure that follows, together with the comments in the deck itself, may be adequate for some purposes; the CONTAIN 1.1 User's Manual [Mu89] should be consulted for additional information.

Global Input: Flow Paths

The only global input requiring consideration in the present review is that which describes the flow paths between cells. CONTAIN has two types of flow path which are used here: "regular" flow paths and "engineered vent" flow paths. The distinction between the two is actually largely arbitrary and has more to do with the history of code development and the code architecture than it does with any difference in the applications of the two types of flow paths. One practical difference is important, however: direct parallel "regular" flow paths between two cells are not permitted, while two cells may be connected by any number of engineered vents. Hence, if any two cells are to be directly connected by two or more flow paths, only one may be a regular flow path and all others must be engineered vents. (The engineered vents also offer some other improvements over the regular flow path options which are less important for present purposes; see Ref. Mu89 for details.)

CONTAIN input is largely keyword-driven, of a form "keyword=value", where "keyword" is the prescribed keyword and "value" is the numerical value to be assigned to the variable identified by "keyword". Flow input is described in Section 3.2.3 of the User's Manual. The quantities directly related to the plant configuration, and hence of greatest importance to the present review, are as follows for the regular flow paths:

area(i,j) = cross sectional area of the flow path from cell i to cell j

avl(i,j) = ratio of flow path area to flow path length

cfc(i,j) = flow loss coefficient (see below)

elevfp(i,j) = elevation of end of flow path attached to cell j

elevcl(i) = elevation of center of mass of cell i (this information is input as part of the flow block, since it is used in calculating gravitational heads for buoyancy-driven flows)

dp(i,j) = pressure difference required to open a pressure-sensitive flow path that is initially closed; need not be specified for normal flow paths that require no pressure differential to open them.

The flow loss coefficient is related to the flow coefficient C and the resistance coefficient K used in the Crane Handbook [Cr79] by cfc = $1/(2C^2)$ and cfc = K/2, respectively.

For engineered vents, the analogous input is of the form:

from=i to=j: identifies a flow path connecting cell i to cell j

varea = flow path area

vavl = ratio of flow path area to flow path length

vcfc = flow loss coefficient

velevb = elevation of flow path at end attached to cell i

velevf = elevation of flow path at end attached to cell j

CONTAIN does not have a model for counter current flows within a single flow path. Such flow could be important when adjacent cells are connected by large flow paths and natural circulation is expected to be important to the overall flow patterns which determine gas distributions. In order to simulate countercurrent flows between adjacent cells, the flow path is divided into a lower portion and an upper portion in some cases. In all instances where this has been done, the lower portion is modeled as a regular flow path with an elevation of h - L/4, where h is the elevation of the center of the flow path and L is a characteristic dimension, in the vertical direction, of the flow path opening. The upper portion is modeled as an engineered vent with an elevation of h + L/4. The comment "&& recirculation flow simulated" is inserted in the deck wherever this has been done. Note that, in these cases, each of the two flow paths is assigned half the flow area corresponding to the total physical opening area. In general, this technique is applicable only when the cells in question are at approximately the same elevation; using it for cells located one above the other introduces spurious circulation effects and is therefore not done.

Proper definition of the following flow paths deserves special attention:

1. Flows out of the cavity region (Cell 1), including alterations in the flow paths that are likely to result from the extreme temperatures and pressures that may develop in the cavity during a high pressure melt ejection (HPME) event.

2. Flow paths between the lower and upper containment regions which bypass the ice condenser.

3. Flow representation within the ice condenser and the plena: flow areas and flow resistances. These are important because of the importance of recirculation flows in some of the CONTAIN calculations.

4. The ice condenser doors. The doors are modeled as flow paths with areas that are functions of pressure. For the enclosed deck, these areas are as was described in Section 2.3 of the main report.

Because of their importance, the ice condenser doors merit some additional discussion. Partially irreversible behavior for the intermediate and upper deck doors is allowed for because it is assumed that, if the panels are fully opened, some of them could fall over backwards, after which they could not reclose. (Here, "reversible" means that the door will tend to reclose when the pressure difference across the door falls; "irreversible" means that the flow path can increase in area as the pressure rises, but it will never decrease.)

For the intermediate deck and upper plenum doors, the area versus pressure parameters were taken from the HECTR decks noted above, and the values used there were taken from CLASIX input for analyses performed in support of earlier assessments of hydrogen control problems at Sequoyah [TVA81]. Based upon information obtained more recently from TVA [TVA88], plus information in the FSAR [TVA74], the representation of the lower plenum doors used in the later stages of this study was the following:

Pressure (Pa)	Area (m^2)
$\leq$ - 14.0	0.00403
0.0	2.0
4.788	2.6
9.576	3.75
19.15	6.23
28.73	20.24
38.30	44.6
$\geq$ 46.92	78.0

Door areas are assumed to vary reversibly and linearly with pressure between the values given. The rationale for this representation is as follows:

- In Ref. TVA88, it is stated that, under zero pressure differential, the doors will be at a neutral point corresponding to a "gap of approximately 1-2 inches between each pair of doors", implying an opening of about 2 m^2 total for the 24 pairs of doors. (It should be noted, however, that the FSAR implies a neutral point gap of only 3/8 $\pm$ 1/8 inch.)
- The residual opening of 0.004 m^2 under negative pressure differential corresponds approximately to the design basis leakage of 50 cfm under the ice condenser cold head pressure [TVA88]. The value at which the doors are assumed to begin to open, -14 Pa, corresponds to approximately half the ice condenser cold head.
- The pressure-area curve for positive pressure differences is based upon Figure 6.5-19 of the FSAR [TVA74].

Ref. TVA88 states that once the doors are opened during a DBA, the door hinge assemblies are designed to deform, preventing reclosure. The pressure required to do

this is not given (door momentum, in addition to static pressure, is presumably involved in producing this deformation). It is also indicated that, if the doors open under conditions insufficiently severe to deform the hinges, they can reclose, at least to the neutral point. It is not entirely clear whether they are expected to reclose fully in the event that a reverse pressure is re-established (e.g., if the ice condenser cold head is re-established).

In the present study, it was assumed that the lower plenum doors normally would reclose fully, given the necessary reverse pressure (i.e., 14 Pa). The exception was that, if the doors were once fully opened, it was assumed that they would remain fully open, in order to simulate the deformable hinge behavior noted above. A minor code modification was required to simulate this behavior; the modification is activated by the keyword "pinup" in the input stream defining the lower plenum doors.

Some aspects of the containment response have been found to be quite sensitive to lower plenum door behavior (see Section 5.2 of the main report). If additional refinements to these calculations prove desirable in the future, the following questions should be addressed:

- What conditions are required in order to cause a degree of hinge deformation that would prevent door reclosure?
- If hinge deformation does not occur, will the doors reclose completely or would they reclose only partially (e.g., to the neutral point), even in the presence of a negative pressure differential?
- What is the best available approximation for the complete pressure vs area curve?

Cell-Level Input

Input for each cell is initiated by the input line "cell=n", where 'n' is the cell number. The next three input blocks ("control", "geometry", and "atmos") are mandatory; the remaining cell-level input is optional. The input of interest to the present review is discussed next.

Cell geometry. The keyword "geometry" is followed by the cell volume (m^3) and the cell height (m), i.e., its dimension in the vertical direction.

Heat-transfer structures. The input block describing the various containment structures that can act as heat sinks in each cell is introduced by the keyword "struc". Information is then entered for each structure in the current cell. Structures may be modeled as slabs, half-cylinders, and hemispheres; in the present deck, they are modeled as slabs. A structure may also be identified as a "roof", "wall", or "floor", depending upon its orientation with respect to the vertical. The heat and mass transfer correlations used can depend upon the orientation.

For present purposes, the important input parameters (and the keywords introducing them) are as follows:

type = roof, wall, or floor

nslab = number of nodes used in the thermal conduction calculation within the structure

chrlen = characteristic structure dimension, used in the heat and mass transfer correlations (sensitivity to this parameter is slight)

slarea = area of the structure surface in contact with the atmosphere

compound = material for each of the 'nslab' structure nodes; materials are taken from the CONTAIN materials library or from user-defined materials tables

x = positions of the interface nodes (nslab + 1 values). The interface with the atmosphere corresponds to x = 0 for slab structures, and the last value gives the structure thickness.

The parameters of greatest interest for the present review are the structure materials, surface areas, and thicknesses. In interpreting the latter, it should be noted that most internal structures (i.e, those with both surfaces inside containment) have been modeled as half structures with adiabatic outer boundary conditions. This treatment permits reproduction of the total structure surface area in each cell and the total material volume, but does not permit calculation of heat transfer from one cell to another through an intervening structure. The crane wall between the upper containment and the ice condenser has been modeled as a structure in the upper containment with the full wall thickness and an adiabatic outer boundary condition, since the interface with the ice condenser is insulated.

The containment shell is also modeled with an adiabatic outer boundary condition. Thus, there is no treatment of heat transfer through the shell to the atmosphere of the shield building and to the outer concrete wall of the latter. In part, this treatment reflects the fact that the version of CONTAIN used in this work cannot treat heat transfer through a structure separating two cells in a fully realistic fashion. This limitation was largely removed by recent code enhancements and the importance of this question could be examined in future studies if desired.

Lower-Cell Modeling. Lower-cell modeling is introduced by the keyword "low-cell" and is used for a variety of purposes in CONTAIN, including modeling of coolant pools. Only limited use was made of the lower cell models in this study and the calculations were not sensitive to the lower cell modeling that was used; it will not be discussed in detail here.

Ice Condenser Modeling. Cells 18, 19, 20, and 21 each represent one fourth of the ice condenser. In these cells, the ice condenser input begins following the keyword "engineer". Parameters related to system design follow; numbers in ( ) are the values in the deck.

hitici = initial height of ice bed (14.53 m)

tmsici = initial mass of ice (2.775×10^5 kg)

citice = initial temperature of ice (264 K)

citlex = temperature at which melted ice and condensed steam are assumed to leave the ice chest (335 K)

ciarfl = cross-sectional flow area through the ice chest (41.75 m^2)

arhtin = initial area of ice available for heat transfer (6200 m^2)

The values given above are for each of the four ice condenser cells; thus, the values given for tmsici, ciarfl, and arhtin would be multiplied by four to apply to the entire ice condenser.

There are, of course, structures other than the ice bed in the ice condenser cells, and the representation of these structures in the present deck is not complete. No structure corresponding to the ice baskets is allowed for. In the CONTAIN model, adding structure to represent ice basket surface area would tend to double count the total heat transfer area when ice is present. As the ice melts, the empty portions of the ice baskets probably should be explicitly modeled as a structure; however, the code does not currently have the capability to add basket structure as a function of ice melting.

Other Modeling. There are many input blocks in addition to those briefly discussed here. Most of these have more to do with phenomenological modeling and the accident sequence definition than they do with the description of the plant. Brief comments included in the deck generally give some indication of what these input blocks represent; the User's Manual [Mu89] may be consulted for details. However, the manual contains no allusion to any inputs related to direct containment heating (DCH), since DCH modeling is not yet available in the released versions of the code.

References

Ca84 A. L. Camp, V. L. Behr, and F. E. Haskin, "MARCH-HECTR Analysis of Selected Accidents in an Ice-Condenser Containment", NUREG/CR-3912, SAND83-0501, Sandia National Laboratories, Albuquerque, NM, December 1984.

Cr79 "Flow of Fluids Through Valves, Fittings, and Pipes," Technical Paper No. 410, Crane Co., New York, NY, 1979.

Di85 S. E. Dingman and A. L. Camp, "Pressure-Temperature Response in an Ice-Condenser Containment for Selected Accidents," in Proceedings of the 13th Water Reactor Safety Research Information Meeting, Gaithersburg, Md, Oct. 22-26 1985.

Mu89 K. K. Murata, et al., "User's Manual for CONTAIN 1.1, A Computer Code for Severe Nuclear Reactor Accident Containment Analysis," NUREG/CR-5026, SAND87-2309, Sandia National Laboratories, Albuquerque, NM, 1989.

TVA74 "Sequoyah Nuclear Plant Final Safety Analysis Report," Tennessee Valley Authority, 1974, with subsequent amendments.

TVA81 "Containment Response to Degraded Core Events for the Sequoyah Plant," Attachment 3 to Letter dated 12/1/81 from L. M. Mills (Manager of Nuclear Regulation and Safety, TVA) to Director of Nuclear Reactor Regulation, USNRC (attention Ms. E. Adensam, Chief, Licensing Branch No. 4, Div. of Licensing)

TVA88 S. A. White, "Response to Questions from EI Services on Sequoyah Nuclear Plant (SQN) Containment Design (Dated April 22, 1988)," Tennessee Valley Authority, letter w. enclosure to J. L. Tills (Jack Tills & Associates), dated 7/1/88.

DISTRIBUTION

Argonne National Laboratory (3)
9700 Cass Avenue
Argonne, IL 60439
Attn: L. Baker
D. Cho
B. Spencer

Battelle's Columbus Laboratories (3)
505 King Avenue
Columbus, OH 43201
Attn: P. Cybulski
R. S. Denning
A. Fentiman

Brookhaven National Laboratory (5)
Upton, NY 11973
Attn: G. A. Green
T. Ginsberg
N. K. Tutu
T. Pratt
H. Nourbakhsh

Burns & Roe, Inc.
800 Kinderkamack Road
Oradell, NJ 07649
Attn: F. J. Patti

Duke Engineering and Services
P. O. Box 36911
Mail Stop PP 02A
Charlotte, NC 28236
Attn: Roger Wagstaff

EG&G Idaho (3)
P.O. Box 1625
Idaho Falls, ID 83415
Attn: C. Allison
P. D. Bayless
R. Gottula

Electric Power Research Institute (3)
3412 Hillview Avenue
Palo Alto, CA 94303
Attn: E. Fuller
M. Murillo
B. R. Sehgal

Energy, Inc.
P.O. Box 736
Idaho Falls, ID 83402
Attn: John Schroeder

Engineering Planning
and Management, Inc.
Post West Office Center
Three Speen Street
Framingham, MA 01701
Attn: Dan P. Griggs

Fauske & Associates, Inc. (2)
16W070 - 83rd Street
Burr Ridge, IL 60521
Attn: R. Henry
M. G. Plys

Jack Tills & Associates (2)
209 Eubank NE
Albuquerque, NM 87123
Attn: J. Tills
A. Gu

Los Alamos National Laboratory (4)
Los Alamos, NM 87545
Attn: R. J. Henninger
P. Y. Pan
M. Stevenson
P. R. Shire

Massachussettes Institute of Technology
Cambridge, MA 02139 (2)
Attn: M. Golay
M. S. Kazimi

Numerical Applications, Inc.
GESA Building, Suite A
825 Geothals Drive
Richland, WA 99352
Attn: Dr. M. Thurgood

Pacific Northwest Laboratory (3)
Battelle Boulevard
Richland, WA 99352
Attn: P. C. Owczarski
C. Wheeler
W. K. Winegardner

Oak Ridge National Laboratories (6)
P.O. Box Y
Oak Ridge, TN 37830
Attn: S. Greene
S. A. Hodge
A. Malinauskas
C. Hyman
T. S. Kress
M. L. Tobias

New York Power Authority
120 Main Street
White Plains, NY 10601
Attn: R. E. Deem

Renssellaer Polytechnic Institute
Department of Nuclear Engineering
Troy, NY 12180-3590
Attn: Prof. Richard Lahey

Risk Management Associates
2309 Dietz Farm Road
Albuquerque, NM 87107
Attn: P. Bieniarz

Science & Engineering Associates
2500 Louisiana NE, Suite 610
Albuquerque, NM 87110
Attn: Frank [illegible]

Stone & Webs
P.O. Box 2325
Boston, MA 02107
Attn: A. Drozd
J. Metcalf
E. Warman

Technology for Energy Corporation (2)
One Energy Center
Pellissippi Parkway
Knoxville, TN 37922
Attn: J. Carter
H. A. Mitchell

U.S. Department of Energy
Office of Nuclear Safety Coordination
Washington, DC 20545
Attn: R. W. Barber

U.S. Department of Energy
RRT/DOE
NE 530
Washington, DC 20545
Attn: H. Alter

U.S. Department of Energy (2)
Albuquerque Operations Office
P.O. Box 5400
Albuquerque, NM 87185
Attn: J. R. Roeder, Director
Transportation Safeguards
D. L. Krenz, Director
Energy Research Technology
For: C. B. Quinn
R. N. Holton

U.S. Nuclear Regulatory Commission (29)
Office of Nuclear Regulatory Research
Washington, DC 20555
Attn: B. Agrawal
E. Beckjord
W. Beckner
Y. S. Chen
E. Chow
M. Cunningham
F. Eltawila
J. Han
M. Khatib-Rahbar
T. King
[illegible]ine (5)
G. Marino
R. Meyer
W. Minners
J. Mitchell
B. Morris
C. W. Nilsen
Z. Rosztoczy
B. Sheron
T. Speis
C. G. Tinkler
T. J. Walker
P. Worthington
R. W. Wright
N. Zuber

U.S. Nuclear Regulatory Commission (3)
Office of Nuclear Reactor Regulation
Washington, DC 20555
Attn: R. Barrett
T. Murley
R. L. Palla

University of California at
Los Angeles (2)
Nuclear Energy Laboratory
405 Hilgard Avenue
Los Angeles, CA 90024
Attn: I. Catton
W. Kastenburg

University of California at
Santa Barbara
Department of Chemical and
Nuclear Engineering
Santa Barbara, CA 93106
Attn: Professor T. Theofanous

University of Maryland
Department of Nuclear Engineering
College Park, MD 20742
Attn: Professor Kazys Almenas

University of Missouri
Nuclear Engineering Department
Columbia, MO 65211
Attn: Professor S. Loyalka

University of Wisconsin
Department of Nuclear Engineering
153 Engineering Research Building
1500 Johnson Drive
Madison, WI 53706
Attn: Professor M. Corradini

Westinghouse Electric Corporation
PO Box 355
Pittsburg, PA 15230
Attn: N. Liparulo

Westinghouse Hanford Company (3)
P.O. Box 1970
Richland, WA 99352
Attn: G. R. Armstrong
J. Martin
L. D. Muhlestein

Westinghouse Savannah River
Woodside Executive Park
1359 Silver Bluff Rd.
Aiken, SC 29808-0001
Attn: Kevin O'Kula

AEE Winfrith (2)
Dorchester Dorset
DT2 8DH
UNITED KINGDOM
Attn: R. Potter
P. N. Smith

AERE Harwell
Didcot
Oxfordshire OX11 ORA
UNITED KINGDOM
Attn: J. Gittus, AETB

Atomic Energy of Canada, Ltd.
Whiteshell Nuclear Research
Establishment
Pinawa, Manitoba ROE 1 LO,
CANADA
Attn: Dr. D. J. Wren

Battelle Institute e.V. (3)
Am Romerhof 35
D-6000 Frankfurt am Main 90
FEDERAL REPUBLIC OF GERMANY
Attn: K. Fischer
D. T. Kanzleiter
L. Wolf

Catedra de Tecnologia Nuclear
E.T.S. INGENIEROS INDUSTRIALES
UNIVERSIDAD POLITECNICA
C/ Jose Gutierrez Abascal, 2
28006-MADRID
SPAIN
Attn: Professor A. Alonso

Culham Laboratory
Culham
Abingdom
Oxfordshire OX14 3DB
UNITED KINGDOM
Attn: F. Briscoe

Departimento di Costruzioni
Meccaniche e Nucleari
Facolta di Ingengneria
via Diotisalvi 2
56100 Pisa ITALY
Attn: Professor M. Mazzini

ENEA-DISP
DISP/ALCO/PROCS
Via Vitaliano Brancati, 48
00144 Roma, ITALY
Attn: Dr. Maurizio Colagrossi

Gesellschaft fur
Reaktorsicherheit mbH
Postfach 101650
Glockengasse 2
D-5000 Koln 1
FEDERAL REPUBLIC OF GERMANY
Attn: J. Langhans

Japan Atomic Energy Research Institute
Division of Nuclear Safety Research (2)
Nuclear Safety Research Center
Tokai Research Establishment
Tokai, Ibaraki-ken 319-11
JAPAN
Attn: K. Muramatsu
K. Soda

Joint Research Center (JRC)
21020 ISPRA (Varese), ITALY
Attn: Dr. Antonio Markovina

Kernforschungszentrum Karlsruhe (3)
Postfach 3640
D-7500 Karlsruhe 1
FEDERAL REPUBLIC OF GERMANY
Attn: G. Heusener
W. Scholtyssek
W. Schoeck

Netherlands Energy Research
Foundation (ECN)
Postbus 1
1755 ZG Petten,
THE NETHERLANDS
Attn: Henk M. van Rij

OEC
200 Rue de la Loi
1049 Brussels
BELGIUM
Attn: E. Della-Loggia, SdM2/77

Power Reactor and Nuclear Fuel
Development Corporation (2)
Fast Breeder Reactor Development
Project
9-13, 1 Chome, Akasaka
Minato-ku, Tokyo
JAPAN
Attn: T. Aoki
A. Watanabe

Power Reactor and Nuclear Fuel
Development Corporation (3)
Oarai Engineering Center
4002 Narita, Oarai-machi
Ibaraki-ken, 311-13 JAPAN
Attn: Y. Himeno
H. Hiroi
O. Miyake

RISO National Laboratory
Department of Energy Technology
Post Box 49
DK-4000
Roskilde, DENMARK
Attn: Dr. Kurt Lauridsen

Statens Vattenfallsverk
Avd. BVK 4
S-16287 Vaellingby
SWEDEN
Attn: Wiktor Frid

Technische Universitat Munchen
Forschungsgelande
8046 Garching
FEDERAL REPUBLIC OF GERMANY
Attn: Prof. Dr. Ing. Helmut Karwat

UKAEA Safety & Reliability Directorate
Culcheth (6)
Wigshaw Lane
Warrington WA3 4NE
Cheshise
UNITED KINGDOM
Attn: F. Abbey
P. N. Clough
J. F. Collier
I. H. Dunbar
S. Ramsdale
R. L. D. Young

Sandia Distribution:

3141 S. A. Landenberger (5)
3151 W. I. Klein
6400 D. J. McCloskey
6410 D. A. Dahlgren
6412 A. L. Camp
6412 S. E. Dingman
6413 F. T. Harper
6420 W. B. Gauster
6422 D. A. Powers
6422 M. D. Allen
6422 M. Pilch
6424 K. D. Bergeron
6424 J. J. Gregory (3)
6424 D. C. Williams (3)
6429 K. E. Washington (20)
6429 R. G. Gido
6429 R. O. Griffith
6429 N. A. Russell
6460 J. V. Walker
6463 M. Berman
6470 D. L. Berry
6473 W. A. von Riesemann
8524 J. A. Wackerly

NRC FORM 335 (2-89) NRCM 1102, 3201, 3202

U.S. NUCLEAR REGULATORY COMMISSION

BIBLIOGRAPHIC DATA SHEET

(See instructions on the reverse)

1. REPORT NUMBER (Assigned by NRC, Add Vol., Supp., Rev., and Addendum Numbers, if any.)

NUREG/CR-5586
SAND90-1102

2. TITLE AND SUBTITLE

Mitigation of Direct Containment Heating and Hydrogen Combustion Events in Ice Condenser Plants: Analyses With the CONTAIN Code and NUREG-1150 PRA Methodology

3. DATE REPORT PUBLISHED

MONTH: October
YEAR: 1990

4. FIN OR GRANT NUMBER

A1838

5. AUTHOR(S)

D. C. Williams
J. J. Gregory

6. TYPE OF REPORT

Technical

7. PERIOD COVERED (Inclusive Dates)

8. PERFORMING ORGANIZATION – NAME AND ADDRESS (If NRC, provide Division, Office or Region, U.S. Nuclear Regulatory Commission, and mailing address; if contractor, provide name and mailing address.)

Sandia National Laboratories
P. O. Box 5800
Albuquerque, NM 87185

9. SPONSORING ORGANIZATION – NAME AND ADDRESS (If NRC, type "Same as above"; if contractor, provide NRC Division, Office or Region, U.S. Nuclear Regulatory Commission, and mailing address.)

Division of Safety Issue Resolution
Office of Nuclear Regulatory Research
U.S. Nuclear Regulatory Commission
Washington, DC 20555

10. SUPPLEMENTARY NOTES

11. ABSTRACT (200 words or less)

Using Sequoyah as a representative plant, calculations have been performed with a developmental version of the CONTAIN computer code to assess the effectiveness of various possible improvements to ice condenser containments in mitigating severe accident scenarios involving direct containment heating (DCH) and/or hydrogen combustion. Mitigation strategies considered included backup power for igniters and/or air return fans, augmented igniter systems, containment venting, containment inerting, subatmospheric containment operation, reduced ice condenser bypass, and primary system depressurization. Various combinations of these improvements were also considered. Only inerting the containment or primary system depressurization combined with backup power supplies for the igniter systems resulted in large decreases in the peak pressures calculated to result from DCH events. Potential hydrogen detonation threats were also assessed; providing backup power for both the igniter systems and the air return fans would significantly reduce the potential for detonations but might not totally eliminate it. Sensitivity studies using the NUREG-1150 PRA methodology indicated that primary system depressurization combined with backup power for both igniters and fans could reduce the contribution to the mean risk potential of the class of events considered by about a factor of three.

12. KEY WORDS/DESCRIPTORS (List words or phrases that will assist researchers in locating the report.)

reactor containment, ice condenser, containment performance improvement, mitigation, severe accidents, direct containment heating, hydrogen combustion, detonation, CONTAIN 1.1, PRA, NUREG-1150, risk profiles, PRA sensitivity studies

13. AVAILABILITY STATEMENT

Unlimited

14. SECURITY CLASSIFICATION

(This Page) Unclassified
(This Report) Unclassified

15. NUMBER OF PAGES

16. PRICE

NRC FORM 335 (2-89)

THIS DOCUMENT WAS PRINTED USING RECYCLED PAPER.

*U.S. GOVERNMENT PRINTING OFFICE: 1990-276-323

UNITED STATES
NUCLEAR REGULATORY COMMISSION
WASHINGTON, D.C. 20555

NUREG/CR-5586

Copy of fiche

BEGIN JOB

RUN SEQUENCE NUMBER 7

LASER PRINTER QUFUE ualasers

JOB IDENTIFICATION an4ua5 JOBCOM= e00019899 900717151258

PROCESSED BY ONODE Tue Jul 17 15:22:01 1990

USER TITLE

SEND TO: BDX 603 GWBOLLI GWBOLLI

```
cray
&& ----- 26 cell ice condenser model for sequoyah: january 1989 ------
&& ----------<global input>-----------------------------------
control  ncells=26  ntit1=3  ntzone=11 nsectn=10 nac=1
nuntbg=28 maxtbg=111 nengv=32 mududn=5000
eoi
&& ----material names-----------------------------------------
material compound
  n2 o2 h2o h2ol h2ov fe h2 conc
  userdef fed zrd feod zrold uo2d insul
&& cernames big small rcs  && no solid aerosols
&& -----edit times-------------------------------------------
times 7250. 3300.0
 2.5  202.5 9350.0
 1.0   11.0  9440.0
  2.5 102.5 10085.0
  2.5   5.0 10090.0
0.025 0.225 10092.0
0.025 0.225 10094.0
0.025 0.225 10096.0
0.05 0.45 10098.0
0.10 0.50 10110.0
 0.5 1.5 10130.0
 1.0  3.0 10150.0
&& ------------------------------------------------------------
1.00 1.00 1.00 1.00 1.00 1.00   1.00 1.00 1.00 1.00 1.00 1.00
1.00 1.00 1.00 1.00 1.00 1.00   1.00 1.00 1.00 1.00 1.00 1.00
1.00 1.00 1.00 1.00 1.00 1.00   1.00 1.00 1.00 1.00
trestart 17 4000. 6000. 8000. 9000. 9500. 10000.
           10090. 10092.5 10095. 10100. 10105. 10110.
           10120. 10130. 10140. 10150. 10500.
  && edmult=5
    longedt=10
     shortedt=5
title
46ici: 26-cell sequoyah dch on 'xda4g2u': counter-current flow; 4 ice cells;
(eng. v. & reg.) (int. & upper) doors, fully rev. fsar eng. v. with 'pinup'
for i.p. doors; vent & exist ign. & fans; 50% bni-2104_corium, fp; dts=2.5 s
&& --------aerosols-------------------------------------------
aerosol tgas2= 2500. pgas2= 1.7e7 && nocond=1 28 && nocond in rcs (aerosol runs)
          h2ol   1.0e-6  0.695
&& debug 3 engice dcontm cnvnos 9400.0 9400.61
&& -------intercell flow conditions-------------------------

flows && flow path definition block
implicit 27

elevcl(1)=0.0   &&  cell 1 (cavity) flow data

  area(1,6)=1.0  avl(1,6)=0.1  cfc(1,6)=4.0
    elevfp(1,6)=12.97  elevfp(6,1)=2.97    && reactor vessel annulus

  area(1,9)= 3.3  avl(1,9)= 1.43  cfc(1,9)= 1.0
   elevfp(1,9)=8.53 elevfp(9,1)=8.53    && cavity to lower compartment

  area(1,12)=1.80 avl(1,12)=1.4 cfc(1,12)=1.0 dp(1,12)=1.e7 close(1,12)
    elevfp(1,12)=10.27  elevfp(12,1)=10.27  && seal table

  area(1,27)=0.0 avl(1,27)=1.5 cfc(1,27)=0.7 topen(1,27)=0.0 && primary system
    contract(1,27)=0.7815 elevfp(1,27)=1.3 elevfp(27,1)=1.3 && bloudoun

elevcl(2)=27.0  && sg 1 & 2 doghouse (1st half)

  area(2,3)=16.5 avl(2,3)=5.0 cfc(2,3)=0.7
    elevfp(2,3)=32.0 elevfp(3,2)=32.0  && intra-doghouse connection

  area(2,8)=16.9 avl(2,8)=3.1 cfc(2,8)=0.71 fpcosn(2,8)=-1.0
    elevfp(2,8)=29.6 elevfp(8,2)=29.6  && connection to lower containment
```

```
elevcl(3)=27.0  && sg 1 & 2 doghouse (2nd half)

  area(3,8)=16.0 avl(3,8)=3.1 cfc(3,8)=0.69 fpcosn(3,8)=-1.0
    elevfp(3,8)=20.0 elevfp(8,3)=20.0  && connection to lower containment

elevcl(4)=27.0  && sg 3 & 4 doghouse (1st half)

  area(4,5)=16.5 avl(4,5)=5.0 cfc(4,5)=0.7
    elevfp(4,5)=32.0 elevfp(5,4)=32.0  && intra-doghouse connection

  area(4,10)=16.0 avl(4,10)=3.1 cfc(4,10)=0.71 fpcosn(4,10)=-1.0
    elevfp(4,10)=20.0 elevfp(10,4)=20.0  && connection to lower containment

elevcl(5)=27.0  && sg 3 & 4 doghouse (2nd half)

  area(5,10)=16.3 avl(5,10)=3.1 cfc(5,10)=0.69 fpcosn(5,10)=-1.0
    elevfp(5,10)=20.0 elevfp(10,5)=20.0  && connection to lower containment

elevcl(6)=16.0  &&  reactor space ("upper cavity", above the vessel)

  area(6,8)=7.5 avl(6,8)=6.7 cfc(6,8)=2.
    elevfp(6,8)=19.5 elevfp(8,6)=19.5  && paths to lower containment

  area(6,9)=7.4 avl(6,9)=6.7 cfc(6,9)=2.
    elevfp(6,9)=19.5 elevfp(9,6)=19.5  && paths to lower containment

  area(6,10)=7.4 avl(6,10)=6.7 cfc(6,10)=2.
    elevfp(6,10)=19.5 elevfp(10,6)=19.5  && paths to lower containment

elevcl(7)=27.0  &&  pressurizer doghouse

  area(7,9)=8.6 avl(7,9)=1.5 cfc(7,9)=0.7 fpcosn(7,9)=-1.0
    elevfp(7,9)=20.0 elevfp(9,7)=20.0  &&  no recirculation flows

elevcl(8)=12.3  &&  lower containment # 1

  area(8,9)=23.5 avl(8,9)=1.5 cfc(8,9)=0.7 && to low. cont. #2
    elevfp(8,9)=10.6 elevfp(9,8)=10.6 && recirculation flow simulated

  area(8,10)=9.0 avl(8,10)=2.0 cfc(8,10)=1.0  &&  this junction should close
    elevfp(8,10)=5.0 elevfp(10,8)=5.0          &&  when lower cont. floods

  area(8,11)=4.5 avl(8,11)=0.75 cfc(8,11)=0.7 && to lower annulus #1
    elevfp(8,11)=11.55 elevfp(11,8)=11.55 && recirculation flow simulated

  area(8,26)=0.0967 avl(8,26)=0.161 cfc(8,26)=1.25
    elevfp(8,26)=20.92 elevfp(26,8)=20.32  &&  deck bypass leakage

elevcl(9)=12.3  &&  lower containment # 2

  area(9,10)=23.5 avl(9,10)=1.5 cfc(9,10)=0.7 && to low. cont. #3
    elevfp(9,10)=10.6 elevfp(10,9)=10.6 && recirculation flow simulated

  area(9,12)=4.4 avl(9,12)=0.75 cfc(9,12)=0.7 && to lower annulus #2
    elevfp(9,12)=11.55 elevfp(12,9)=11.55 && recirculation flow simulated

  area(9,26)=0.0967 avl(9,26)=0.161 cfc(9,26)=1.25
    elevfp(9,26)=20.92 elevfp(26,9)=20.32  &&  deck bypass leakage

elevcl(10)=12.3  &&  lower containment # 3

  area(10,13)=4.95 avl(10,13)=0.75 cfc(10,13)=0.7 && to lower annulus #3
    elevfp(10,13)=11.55 elevfp(13,10)=11.55 && recirculation flow simulated

  area(10,26)=0.0967 avl(10,26)=0.161 cfc(10,26)=1.25
    elevfp(10,26)=20.92 elevfp(26,10)=20.32  &&  deck bypass leakage
```

```
elevcl(11)=12.3  && lower annulus #1. Elev. increased to i.c. elev.

  area(11,12)=1.5 avl(11,12)=0.67 cfc(11,12)=1.0
    elevfp(11,12)=12.3 elevfp(12,11)=12.3       && to lower annulus #2

elevcl(12)=12.3  && lower annulus #2

  area(12,13)=1.5 avl(12,13)=0.67 cfc(12,13)=1.0
    elevfp(12,13)=12.3 elevfp(13,12)=12.3       && to lower annulus #3

elevcl(13)=12.3  && lower annulus #3

elevcl(14)=19.0  && lower plenum #1

  area(14,15)=2.1 avl(14,15)=0.77 cfc(14,15)=1.5
    elevfp(14,15)=19.0 elevfp(15,14)=19.0  && to lower plenum #2

  area(14,18)=22.9 avl(14,18)=2.68 cfc(14,18)=0.7 fpcosn(14,18)=1.0
    elevfp(14,18)=20.4 elevfp(18,14)=20.4  && to ice chest #1

elevcl(15)=19.0  && lower plenum #2

  area(15,16)=2.1 avl(15,16)=0.77 cfc(15,16)=1.5
    elevfp(15,16)=19.0 elevfp(16,15)=19.0  && to lower plenum #3

  area(15,19)=22.9 avl(15,19)=2.68 cfc(15,19)=0.7 fpcosn(15,19)=1.0
    elevfp(15,19)=20.4 elevfp(19,15)=20.4  && to ice chest #2

elevcl(16)=19.0  && lower plenum #3

  area(16,17)=2.1 avl(16,17)=0.77 cfc(16,17)=1.5
    elevfp(16,17)=19.0 elevfp(17,16)=19.0  && to lower plenum #4

  area(16,20)=22.9 avl(16,20)=2.68 cfc(16,20)=0.7 fpcosn(16,20)=1.0
    elevfp(16,20)=20.4 elevfp(20,16)=20.4  && to ice chest #3

elevcl(17)=19.0  && lower plenum #4

  area(17,21)=22.9 avl(17,21)=2.68 cfc(17,21)=0.7 fpcosn(17,21)=1.0
    elevfp(17,21)=20.4 elevfp(21,17)=20.4  && to ice chest #4

&& ice condenser - - - - - -
elevcl(18)=27.7  && ice chest #1

  area(18,19)=3.95 avl(18,19)=1.25 cfc(18,19)=1.5  && to ice chest #2
    elevfp(18,19)=24.05 elevfp(19,18)=24.05 && recirculation flow simulated

  area(18,22)=0.0 avl(18,22)=1.79 cfc(18,22)=0.7 fpcosn(18,22)=1.
    pdaflag(18,22)=1 elevfp(18,22)=35.0 elevfp(22,18)=35.0 && interned. doors
    var-area(18,22) flag=2
      var-x=delta-p x=4  -1.e+7    2e3.     28498.    1.e+7
      var-y=area    y=4   0.465    0.465   17.56   17.56
    eoi

elevcl(19)=27.7  && ice chest #2

  area(19,20)=3.95 avl(19,20)=1.25 cfc(19,20)=1.5  && to ice chest #3
    elevfp(19,20)=24.05 elevfp(20,19)=24.05 && recirculation flow simulated

  area(19,22)=0.0 avl(19,22)=1.79 cfc(19,22)=0.7 fpcosn(19,22)=1.
    pdaflag(19,22)=1 elevfp(19,22)=35.0 elevfp(22,19)=35.0 && interned. doors
    var-area(19,22) flag=2
      var-x=delta-p x=4  -1.e+7    2e3.     28498.    1.e+7
      var-y=area    y=4   0.465    0.465   17.56   17.56
    eoi

elevcl(20)=27.7  && ice chest #3
```

```
    elevfp(20,21)=24.05 elevfp(21,20)=24.05 && recirculation flow simulated

  area(20,23)=0.0 avl(20,23)=1.79 cfc(20,23)=0.7 fpcosn(20,23)=1.
    pdaflag(20,23)=1 elevfp(20,23)=35.0 elevfp(23,20)=35.0 && interned. doors
    var-area(20,23) flag=2
      var-x=delta-p x=4  -1.e+7    263.      28498.     1.e+7
      var-y=area    y=4   0.465     0.465    17.56   17.56
    eoi

elevcl(21)=27.7  && ice chest #4

  area(21,23)=0.0 avl(21,23)=1.79 cfc(21,23)=0.7 fpcosn(21,23)=1.
    pdaflag(21,23)=1 elevfp(21,23)=35.0 elevfp(23,21)=35.0 && interned. doors
    var-area(21,23) flag=2
      var-x=delta-p x=4  -1.e+7    263.      28498.     1.e+7
      var-y=area    y=4   0.465     0.465    17.56   17.56
    eoi

elevcl(22)=37.6  &&  upper plenum #1

  area(22,23)=6.2 avl(22,23)=1.0 cfc(22,23)=0.7  &&  to upper plenum #2
    elevfp(22,23)=36.3 elevfp(23,22)=36.3  &&  recirculation flows simulated

  area(22,24)=0.0 avl(22,24)=4.70 cfc(22,24)=0.7 fpcosn(22,24)=1.
    pdaflag(22,24)=1 elevfp(22,24)=40.2 elevfp(24,22)=40.2 && upper doors
    var-area(22,24) flag=2
      var-x=delta-p x=4  -1.e+7    263.      4441.     1.e+7
      var-y=area    y=4   0.93      0.93     46.95    46.95
    eoi

elevcl(23)=37.6  &&  upper plenum # 2

  area(23,25)=0.0 avl(23,25)=4.70 cfc(23,25)=0.7 fpcosn(23,25)=1.
    pdaflag(23,25)=1 elevfp(23,25)=40.2 elevfp(25,23)=40.2 && upper doors
    var-area(23,25) flag=2
      var-x=delta-p x=4  -1.e+7    263.      4441.     1.e+7
      var-y=area    y=4   0.93      0.93     46.95    46.95
    eoi

elevcl(24)=44.2  &&  upper dome #1

  area(24,25)=296.5 avl(24,25)=16.7 cfc(24,25)=0.7 && to upper dome #2
    elevfp(24,25)=39.9 elevfp(25,24)=39.9 && recirculation flow simulated

  area(24,26)=182.  avl(24,26)=11.1 cfc(24,26)=0.7 fpcosn(24,26)=-1.0
   &&  elevfp(24,26)=35.0 elevfp(26,24)=35.0 && to lower dome; no recirc.

  area(24,28)=0.1 avl(24,28)=0.1 cfc(24,28)=0.7 pdaflag(24,28)=1
    elevfp(24,28)=40.2 elevfp(28,24)=40.2 tclose(24,28)=8144.  && vent
    var-area(24,28) flag=1
      var-x=delta-p x=3 -1.e+7 0.0 1.e+7
      var-y=area    y=3  0.0   0.1 0.1
    eoi

elevcl(25)=44.2  &&  upper dome #2

  area(25,26)=182.  avl(25,26)=11.1 cfc(25,26)=0.7 fpcosn(25,26)=-1.0
  &&  elevfp(25,26)=35.0 elevfp(26,25)=35.0 && to lower dome; no recirc.

elevcl(26)=26.0  && lower dome region and refueling space

elevcl(27)=5.0  &&  primary system

elevcl(28)=44.2  &&  the great outdoors

&& Sequoyah bloudown, fully pressurized RCS, 50% corium case
var-area,1,27 flag=1
```

```
var-x=time
x=111
   1.0089997e+04  1.0090000e+04  1.0090017e+04     1.0090033e+04  1.0090050e+04
   1.0090068e+04  1.0090088e+04  1.0090108e+04     1.0090131e+04  1.0090154e+04
   1.0090181e+04  1.0090208e+04  1.0090238e+04     1.0090271e+04  1.0090306e+04
   1.0090340e+04  1.0090375e+04  1.0090409e+04     1.0090444e+04  1.0090479e+04
   1.0090514e+04  1.0090549e+04  1.0090583e+04     1.0090618e+04  1.0090652e+04
   1.0090688e+04  1.0090722e+04  1.0090757e+04     1.0090791e+04  1.0090826e+04
   1.0090860e+04  1.0090896e+04  1.0090930e+04     1.0090965e+04  1.0090999e+04
   1.0091034e+04  1.0091069e+04  1.0091104e+04     1.0091139e+04  1.0091173e+04
   1.0091208e+04  1.0091242e+04  1.0091277e+04     1.0091312e+04  1.0091347e+04
   1.0091381e+04  1.0091416e+04  1.0091450e+04     1.0091485e+04  1.0091520e+04
   1.0091555e+04  1.0091592e+04  1.0091630e+04     1.0091669e+04  1.0091710e+04
   1.0091753e+04  1.0091798e+04  1.0091845e+04     1.0091894e+04  1.0091945e+04
   1.0091999e+04  1.0092056e+04  1.0092115e+04     1.0092179e+04  1.0092245e+04
   1.0092315e+04  1.0092391e+04  1.0092471e+04     1.0092556e+04  1.0092647e+04
   1.0092746e+04  1.0092852e+04  1.0092967e+04     1.0093092e+04  1.0093229e+04
   1.0093380e+04  1.0093547e+04  1.0093733e+04     1.0093944e+04  1.0094186e+04
   1.0094464e+04  1.0094791e+04  1.0095184e+04     1.0095669e+04  1.0096276e+04
   1.0096883e+04  1.0097489e+04  1.0098098e+04     1.0098709e+04  1.0099321e+04
   1.0099938e+04  1.0100556e+04  1.0101177e+04     1.0101801e+04  1.0102427e+04
   1.0103057e+04  1.0103688e+04  1.0104324e+04     1.0104962e+04  1.0105603e+04
   1.0106247e+04  1.0108196e+04  1.0111508e+04     1.0116277e+04  1.0121924e+04
   1.0127789e+04  1.0131569e+04  1.0137808e+04     1.0147621e+04  1.0155374e+04
   1.0160292e+04
y=111
     0.00000e+00    3.04522e-03    1.14144e-02       1.94361e-02    2.74412e-02
     3.52986e-02    4.30676e-02    5.07338e-02       5.83036e-02    6.57726e-02
     7.31375e-02    8.03934e-02    8.75352e-02       9.43734e-02    1.00530e-01
     1.06103e-01    1.11168e-01    1.15789e-01       1.20017e-01    1.23896e-01
     1.27465e-01    1.30758e-01    1.33802e-01       1.36622e-01    1.39241e-01
     1.41677e-01    1.43947e-01    1.46067e-01       1.48049e-01    1.49905e-01
     1.51647e-01    1.53282e-01    1.54820e-01       1.56269e-01    1.57635e-01
     1.58924e-01    1.60142e-01    1.61295e-01       1.62386e-01    1.63421e-01
     1.64402e-01    1.65334e-01    1.66220e-01       1.67063e-01    1.67866e-01
     1.68630e-01    1.69359e-01    1.70055e-01       1.70719e-01    1.71364e-01
     1.72003e-01    1.72638e-01    1.73267e-01       1.73890e-01    1.74508e-01
     1.75121e-01    1.75729e-01    1.76330e-01       1.76926e-01    1.77517e-01
     1.78101e-01    1.78680e-01    1.79253e-01       1.79819e-01    1.80380e-01
     1.80935e-01    1.81483e-01    1.82024e-01       1.82560e-01    1.83088e-01
     1.83610e-01    1.84124e-01    1.84632e-01       1.85132e-01    1.85624e-01
     1.86109e-01    1.86585e-01    1.87052e-01       1.87511e-01    1.87960e-01
     1.88399e-01    1.88827e-01    1.89243e-01       1.89637e-01    1.89915e-01
     1.90128e-01    1.90293e-01    1.90423e-01       1.90529e-01    1.90615e-01
     1.90687e-01    1.90747e-01    1.90798e-01       1.90841e-01    1.90878e-01
     1.90911e-01    1.90939e-01    1.90964e-01       1.90986e-01    1.91005e-01
     1.91053e-01    1.91106e-01    1.91151e-01       1.91181e-01    1.91201e-01
     1.91210e-01    1.91220e-01    1.91231e-01       1.91234e-01    1.91234e-01
     1.91234e-01
eoi

engvent && engineered vents for (a) recirc. flow between adjacent cells;
          && (b) ice condenser doors

from=8 to=9 varea=23.5 vavl=1.5 vcfc=0.7 && low cont. #1 to #2
    velevb=14.0 velevf=14.0 eoi    && recirculation flow simulated

  from=8 to=11 varea=4.5 vavl=0.75 vcfc=0.7 && low cont. #1 to annulus #1
    velevb=13.05 velevf=13.05 eoi    && recirculation flow simulated

  from=8 to=14 vcfc=0.7 velevb=19.0 velevf=19.0 && lower doors (rev.)
    pinup
    rvarea-p flag=2          && lower cont. #1 to lower plenum #1
       x=10 -1.0e+7  -14.0  0.0 4.788 9.576   19.15 28.73 38.30 46.92 46.9201
       y=10 .00101 .00101 0.500 0.650 0.938   1.56  5.06  11.16 19.51 19.51
    eoi
  eoi
```

```
  from=8 to=15 vcfc=0.7 velevb=19.0 velevf=19.0 && lower doors (rev.)
    pinup
    rvarea-p flag=2           && lower cont. #1 to lower plenum #2
       x=10 -1.0e+7  -14.0  0.0 4.788 9.576   19.15 28.73 38.30 46.92 46.9201
       y=10 3.61e-4 3.61e-4 .179 .233 0.336   0.558 1.81  3.99  6.98  6.98
    eoi
  eoi

  from=8 to=26 varea=0.0875 vavl=0.062 vcfc=0.75
    velevb=6.47 velevf=7.69 eoi  && refueling drain

from=9 to=10 varea=23.5 vavl=1.5 vcfc=0.7 && low cont. #2 to #3
    velevb=14.0 velevf=14.0 eoi    && recirculation flow simulated

  from=9 to=12 varea=4.4 vavl=0.75 vcfc=0.7 && low cont. #2 to annulus #2
    velevb=13.05 velevf=13.05 eoi    && recirculation flow simulated

  from=9 to=15 vcfc=0.7 velevb=19.0 velevf=19.0 && lower doors (rev.)
    pinup
    rvarea-p flag=2           && lower cont. #2 to lower plenum #2
       x=10 -1.0e+7  -14.0  0.0 4.788 9.576   19.15 28.73 38.30 46.92 46.9201
       y=10 6.46e-4 6.46e-4 .321 .417 0.601   0.999 3.25  7.15  12.51 12.51
    eoi
  eoi

  from=9 to=16 vcfc=0.7 velevb=19.0 velevf=19.0 && lower doors (rev.)
    pinup
    rvarea-p flag=2           && lower cont. #2 to lower plenum #3
       x=10 -1.0e+7  -14.0  0.0 4.788 9.576   19.15 28.73 38.30 46.92 46.9201
       y=10 6.46e-4 6.46e-4 .321 .417 0.601   0.999 3.25  7.15  12.51 12.51
    eoi
  eoi

from=10 to=13 varea=4.95 vavl=0.75 vcfc=0.7 && low cont. #3 to annulus #3
    velevb=13.05 velevf=13.05 eoi    && recirculation flow simulated

  from=10 to=16 vcfc=0.7 velevb=19.0 velevf=19.0 && lower doors (rev.)
    pinup
    rvarea-p flag=2           && lower cont. #3 to lower plenum #3
       x=10 -1.0e+7  -14.0  0.0 4.788 9.576   19.15 28.73 38.30 46.92 46.9201
       y=10 3.61e-4 3.61e-4 .179 .233 0.336   0.558 1.81  3.99  6.98  6.98
    eoi
  eoi

  from=10 to=17 vcfc=0.7 velevb=19.0 velevf=19.0 && lower doors (rev.)
    pinup
    rvarea-p flag=2           && lower cont. #3 to lower plenum #4
       x=10 -1.0e+7  -14.0  0.0 4.788 9.576   19.15 28.73 38.30 46.92 46.9201
       y=10 .00101 .00101 0.500 0.650 0.938   1.56  5.06  11.16 19.51 19.51
    eoi
  eoi

  from=10 to=26 varea=0.0875 vavl=0.062 vcfc=0.75
    velevb=6.47 velevf=7.69 eoi  && refueling drain

from=18 to=19 varea=3.95 vavl=1.25 vcfc=1.5 && ice chest #1 to #2
    velevb=31.35 velevf=31.35 eoi  && recirculation flow simulated

  from=18 to=22 vavl=0.58 vcfc=0.7 velevb=35.0 velevf=35.0 vcosn=1.0
    rvarea-p flag=2  && intermediate doors, ice chest #1 to up. plenum #1
       x=4   -1.e7  28496.  37910.   1.e+7
       y=4    0.0    0.0   5.698    5.698
    eoi
  eoi

from=19 to=20 varea=3.95 vavl=1.25 vcfc=1.5 && ice chest #2 to #3
    velevb=31.35 velevf=31.35 eoi  && recirculation flow simulated
```

```
  from=19 to=22 vavl=0.56 vcfc=0.7 velevb=35.0 velevf=35.0 vcosn=1.0
    irarea-p flag=2  && intermediate doors, ice chest #2 to up. plenum #1
      x=4   -1.e7  28498.   37910.    1.e+7
      y=4    0.0    0.0    5.698     5.698
    eoi
  eoi

from=20 to=21 varea=3.95 vavl=1.25 vcfc=1.5 && ice chest #3 to #4
    velevb=31.35 velevf=31.35 eoi  && recirculation flow simulated

  from=20 to=23 vavl=0.56 vcfc=0.7 velevb=35.0 velevf=35.0 vcosn=1.0
    irarea-p flag=2  && intermediate doors, ice chest #3 to up. plenum #2
      x=4   -1.e7  28498.   37910.    1.e+7
      y=4    0.0    0.0    5.698     5.698
    eoi
  eoi

from=21 to=23 vavl=0.56 vcfc=0.7 velevb=35.0 velevf=35.0 vcosn=1.0
    irarea-p flag=2  && intermediate doors, ice chest #4 to up. plenum #2
      x=4   -1.e7  28498.   37910.    1.e+7
      y=4    0.0    0.0    5.698     5.698
    eoi
  eoi

from=22 to=25 varea=6.2 vavl=1.0 vcfc=0.7  && upper plenum #1 to #2
    velevb=35.9 velevf=58.9 eoi  && recirculation flow simulated

  from=22 to=24 vavl=9.21 vcfc=0.69 velevb=40.2 velevf=40.2 vcosn=1.0
    irarea-p flag=2  && upper plenum doors to upper done #1
      x=4  -1.e+7   4441.    8619   1.e+7
      y=4     0.0    0.0    46.04  46.04
    eoi
  eoi

from=23 to=25 vavl=9.21 vcfc=0.69 velevb=40.2 velevf=40.2 vcosn=1.0
    irarea-p flag=2  && upper plenum doors to upper done #2
      x=4  -1.e+7   4441.    8619.  1.e+7
      y=4     0.0    0.0    46.04  46.04
    eoi
  eoi

from=24 to=25 varea=296.5 vavl=16.7 vcfc=0.7 && upper done #1 to #2
    velevb=46.5 velevf=46.5 eoi  &&  recirculation flow simulated

 from=24 to=11 && air return fans (first train)
    vflow-t flag=1
      x=3 0.0 5300.0 1.0e7
      y=3 0.0 27.35 27.35
    eoi
  eoi

 from=25 to=13 && air return fans (second train)
    vflow-t flag=1
      x=3 0.0 5300.0 1.0e7
      y=3 0.0 27.35 27.35
    eoi
  eoi

 from=2 to=11       && hydrogen skimmers
    vflow-t flag=1
      x=3 0.0 5300.0 1.0e7
      y=3 0.0 0.177 0.177
    eoi
  eoi

 from=3 to=11       && hydrogen skimmers
    vflow-t flag=1
      x=3 0.0 5300.0 1.0e7
```

```
      y=3 0.0 0.177 0.177
    eoi
  eoi

 from=6 to=11      && hydrogen skimmers
    vflow-t flag=1
      x=3 0.0 5300.0 1.0e7
      y=3 0.0 0.142 0.142
    eoi
  eoi

 from=4 to=13      && hydrogen skimmers
    vflow-t flag=1
      x=3 0.0 5300.0 1.0e7
      y=3 0.0 0.177 0.177
    eoi
  eoi

 from=5 to=13      && hydrogen skimmers
    vflow-t flag=1
      x=3 0.0 5300.0 1.0e7
      y=3 0.0 0.177 0.177
    eoi
  eoi

 from=6 to=13      && hydrogen skimmers
    vflow-t flag=1
      x=3 0.0 5300.0 1.0e7
      y=3 0.0 0.142 0.142
    eoi
eoi

&& ------------print options---------------------------------
prengsys prflow praer prflow-cl preat

&&  --- direct heating input parameters --------
&&   ---- NOTE  NOTE  NOTE  NOTE  NOTE  NOTE ------------
&&  to run dch calculations, it is necessary to:
&&    -- activate the following block
&&    -- provide trapping rates and particle velocites for all cells
&&    -- eliminate BCOUTER subblock input from Cell 1 and 6 STRUC block,
&&       unless new dch executable is made (1/27/89).
&&    -- supply phase 4 (debris) materials

  dheat
   diadrp=0.0005  dendrp=7800.0  thresh=1200.0 rcomb2=on  ieqopt=2
   difo2=1.6      difh2o=1.0     htcmul=1.0    radmul=0.0   radgas=0.8
   radimp=on      htcimp=on      zrrat=0.1599  ferat=0.8401
   liqside 0.0    0.0 0.0 0.0 0.0
  velocity 6.9 6.0 6.0 6.0 6.0   6.9 6.0 6.9 6.9 6.9
           6.5 6.5 6.5 6.5 6.5   6.5 6.5 5.1 5.1 5.1
           5.1 5.1 5.1 5.1 5.1   5.1 5.1 5.1
  traprate 0.2 0.84 0.84 0.84 0.84   0.91 1.18 0.60 0.66 0.69
           0.68 0.68 0.66 2.6 2.6    2.6 2.6 0.96 0.96 0.96
           0.96 1.02 1.02 0.20 0.20  0.20 0.20 0.20
  eoi

&& ---- material properties for debris ----
userdat

     uo2d       debris  4 change to "debris" for DCH
          moleu       2.7007e+02
          temps         44
              3.0000e+02  4.0000e+02  5.0000e+02  6.0000e+02  7.0000e+02
              8.0000e+02  9.0000e+02  1.0000e+03  1.0500e+03  1.1000e+03
              1.1500e+03  1.2000e+03  1.2500e+03  1.3000e+03  1.3500e+03
              1.4000e+03  1.4500e+03  1.5000e+03  1.5500e+03  1.6000e+03
              1.6500e+03  1.7000e+03  1.7500e+03  1.8000e+03  1.8500e+03
```

```
        1.9000e+03  1.9500e-03  2.0000e+03  2.0500e+03  2.1000e+03
        2.1500e+03  2.2000e+03  2.2500e+03  2.3000e+03  2.3500e+03
        2.4000e+03  2.4500e+03  2.5000e+03  2.5500e+03  2.6000e+03
        2.6500e+03  2.7000e+03  2.7500e+03  2.8000e+03
    condt
        8.5417e+00  7.0075e+00  5.9438e+00  5.1651e+00  4.5726e+00
        4.1090e+00  3.7392e+00  3.4400e+00  3.3119e+00  3.1960e+00
        3.0912e+00  2.9964e+00  2.9107e+00  2.8335e+00  2.7639e+00
        2.7016e+00  2.6459e+00  2.5966e+00  2.5531e+00  2.5153e+00
        2.4829e+00  2.4555e+00  2.4331e+00  2.4154e+00  2.4023e+00
        2.3936e+00  2.3892e+00  2.3891e+00  2.3930e+00  2.4011e+00
        2.4131e+00  2.4291e+00  2.4490e+00  2.4727e+00  2.5003e+00
        2.5317e+00  2.5669e+00  2.6058e+00  2.6486e+00  2.6951e+00
        2.7454e+00  2.7994e+00  2.8573e+00  2.9190e+00
    entht
        4.7186e+02  2.5643e+04  5.2865e+04  8.1370e+04  1.1071e+05
        1.4069e+05  1.7121e+05  2.0218e+05  2.1783e+05  2.3358e+05
        2.4942e+05  2.6535e+05  2.8137e+05  2.9749e+05  3.1369e+05
        3.2998e+05  3.4636e+05  3.6283e+05  3.7940e+05  3.9608e+05
        4.1286e+05  4.2977e+05  4.4681e+05  4.6401e+05  4.8139e+05
        4.9897e+05  5.1661e+05  5.3492e+05  5.5337e+05  5.7221e+05
        5.9149e+05  6.1130e+05  6.3172e+05  6.5283e+05  6.7473e+05
        6.9752e+05  7.2134e+05  7.4631e+05  9.8223e+05  1.0131e+06
        1.0439e+06  1.0748e+06  1.1056e+06  1.1365e+06
    rhot
        1.0964e+04  1.0940e+04  1.0915e+04  1.0887e+04  1.0856e+04
        1.0827e+04  1.0795e+04  1.0761e+04  1.0743e+04  1.0725e+04
        1.0707e+04  1.0688e+04  1.0669e+04  1.0649e+04  1.0629e+04
        1.0609e+04  1.0588e+04  1.0567e+04  1.0546e+04  1.0524e+04
        1.0502e+04  1.0479e+04  1.0457e+04  1.0433e+04  1.0410e+04
        1.0386e+04  1.0362e+04  1.0338e+04  1.0313e+04  1.0288e+04
        1.0263e+04  1.0237e+04  1.0211e+04  1.0185e+04  1.0158e+04
        1.0132e+04  1.0105e+04  1.0077e+04  1.0050e+04  1.0022e+04
        9.9942e+03  9.9660e+03  9.9375e+03  9.9088e+03
    spht
        2.3615e+02  2.6395e+02  2.7946e+02  2.8951e+02  2.9683e+02
        3.0263e+02  3.0754e+02  3.1187e+02  3.1389e+02  3.1584e+02
        3.1773e+02  3.1956e+02  3.2136e+02  3.2314e+02  3.2491e+02
        3.2670e+02  3.2851e+02  3.3040e+02  3.3238e+02  3.3450e+02
        3.3682e+02  3.3940e+02  3.4232e+02  3.4566e+02  3.4953e+02
        3.5402e+02  3.5927e+02  3.6540e+02  3.7257e+02  3.8092e+02
        3.9062e+02  4.0184e+02  4.1476e+02  4.2956e+02  4.4643e+02
        4.6556e+02  4.8714e+02  5.1137e+02  6.1704e+02  6.1704e+02
        6.1704e+02  6.1704e+02  6.1704e+02  6.1704e+02
eoi
zrd        debris && change to "debris" for DCH
    moleu        9.1220e+01
    temps         36
        3.0000e+02  4.0000e+02  5.0000e+02  6.0000e+02  7.0000e+02
        8.0000e+02  9.0000e+02  1.0000e+03  1.0500e+03  1.1000e+03
        1.1500e+03  1.2000e+03  1.2500e+03  1.3000e+03  1.3500e+03
        1.4000e+03  1.4500e+03  1.5000e+03  1.5500e+03  1.6000e+03
        1.6500e+03  1.7000e+03  1.7500e+03  1.8000e+03  1.8500e+03
        1.9000e+03  1.9500e+03  2.0000e+03  2.0500e+03  2.1000e+03
        2.1500e+03  2.2000e+03  2.2500e+03  2.3000e+03  2.3500e+03
        2.4000e+03  2.4500e+03  2.5000e+03
    condt
        2.8000e+01  2.8000e+01  2.8000e+01  2.8000e+01  2.8000e+01
        2.8000e+01  2.8000e+03  2.8000e+01  2.8000e+01  2.8000e+01
        2.8000e+01  2.8000e+01  2.8000e+01  2.8000e+01  2.8000e+01
        2.8000e+01  2.8000e+01  2.8000e+01  2.8000e+01  2.8000e+01
        2.8000e+01  2.8000e+03  2.8000e+01  2.8000e+01  2.8000e+01
        2.8000e+01  2.8000e+01  2.8000e+01  2.8000e+01  2.8000e+01
        2.8000e+01  2.8000e+01  2.8000e+01  2.8000e+01  2.8000e+01
        2.8000e+01  2.8000e+01  2.8000e+01
    entht
        5.2300e+02  3.0329e+04  6.1950e+04  9.4810e+04  1.2853e+05
        [illegible]
```

eoi
zr.o2d

Relen
kemps

Depths: 8.8 Check to "Depths" for DCH

sphi

rhot

sphi

rhot

enthi

condi

sphi

rhot

eoi
fed

debris as change to "debris" for DCH

molen
temps
5.56478e+02

cond

enth

rhot

spht

eoi
feed

debris as change to "debris" for DCH

molen
temps
7.18506e+01

cond

```
            6.0000e+00  6.0000e+00  6.0000e+00  6.0000e+00  6.0000e+00
            6.0000e+00  6.0000e+00  6.0000e+00  6.0000e+00  6.0000e+00
            6.0000e+00  6.0000e+00  6.0000e+00  6.0000e+00  6.0000e+00
            6.0000e+00  6.0000e+00  6.0000e+00  6.0000e+00  6.0000e+00
            6.0000e+00  6.0000e+00  6.0000e+00
        entht
            1.3835e+03  7.2485e+04  1.4632e+05  2.2212e+05  2.9957e+05
            3.7848e+05  4.5878e+05  5.4041e+05  5.8171e+05  6.2333e+05
            6.6527e+05  7.0753e+05  7.5009e+05  7.9297e+05  8.3616e+05
            8.7966e+05  9.2347e+05  9.6758e+05  1.0120e+06  1.0567e+06
            1.4367e+06  1.4842e+06  1.5317e+06  1.5791e+06  1.6266e+06
            1.6741e+06  1.7216e+06  1.7691e+06  1.8165e+06  1.8640e+06
            1.9115e+06  1.9590e+06  2.0065e+06  2.0540e+06  2.1014e+06
            2.1489e+06  2.1964e+06  2.2439e+06
        rhot
            5.7000e+03  5.7000e+03  5.7000e+03  5.7000e+03  5.7000e+03
            5.7000e+03  5.7000e+03  5.7000e+03  5.7000e+03  5.7000e+03
            5.7000e+03  5.7000e+03  5.7000e+03  5.7000e+03  5.7000e+03
            5.7000e+03  5.7000e+03  5.7000e+03  5.7000e+03  5.7000e+03
            5.7000e+03  5.7000e+03  5.7000e+03  5.7000e+03  5.4231e+03
            5.3907e+03  5.3582e+03  5.3257e+03  5.2932e+03  5.2607e+03
            5.2282e+03  5.1958e+03  5.1633e+03  5.1308e+03  5.0983e+03
            5.0658e+03  5.0333e+03  5.0008e+03
        spht
            6.9196e+02  7.2646e+02  7.4867e+02  7.6652e+02  7.8193e+02
            7.9614e+02  8.0965e+02  8.2274e+02  8.2917e+02  8.3554e+02
            8.4186e+02  8.4815e+02  8.5440e+02  8.6062e+02  8.6682e+02
            8.7300e+02  8.7916e+02  8.8531e+02  8.9144e+02  8.9756e+02
            9.4964e+02  9.4964e+02  9.4964e+02  9.4964e+02  9.4964e+02
            9.4964e+02  9.4964e+02  9.4964e+02  9.4964e+02  9.4964e+02
            9.4964e+02  9.4964e+02  9.4964e+02  9.4964e+02  9.4964e+02
            9.4964e+02  9.4964e+02  9.4964e+02
    eoi
    insul   solid
      nolew 60.0
      temps 2  300.0 3000.0
      condt 1.454 1.454
      entht 3.375e4 3.409e6
      rhot  2000.0  2000.0
      spht  1250.0  1250.0
    eoi


eoi

&& ------<cell input>-----------------------------------

&&  reactor cavity cell1 --------------
cell=1

control
  nhtm=5 mxslab=12 jconc=10 jint=1 jpool=1 nsopl=1 nsppl=3 nsoatm=6
  nspatm=84
eoi
geometry 396.0   7.04                  && volume & height
atmos=3  1.013e5  311.0                && initial pressure & temperature
o2=.2095  n2=.7905  h2ov=0.01   && initial atmos. composition
source=  6
&& ----------direct heat sources-------------------------
&& ---- calculated using 'gasblow2', 'axcav' tuned to match bnl exp.
&& Sequoyah bloudown, fully pressurized RCS, 50% corium case
    uo2d  84 iflag=1   &&    50500.000 kg
t=
  1.0090000e+04  1.0090066e+04  1.0090065e+04     1.0090103e+04  1.0090131e+04
  1.0090154e+04  1.0090181e+04  1.0090208e+04     1.0090235e+04  1.0090271e+04
  1.0090306e+04  1.0090340e+04  1.0090375e+04     1.0090409e+04  1.0090444e+04
  1.0090479e+04  1.0090514e+04  1.0090549e+04     1.0090583e+04  1.0090618e+04
  1.0090652e+04  1.0090688e+04  1.0090723e+04     1.0090757e+04  1.0090791e+04
```

```
    1.0090826e+04  1.0090860e+04  1.0090896e+04     1.0090930e+04  1.0090965e+04
    1.0090999e+04  1.0091034e+04  1.0091069e+04     1.0091104e+04  1.0091139e+04
    1.0091173e+04  1.0091208e+04  1.0091242e+04     1.0091277e+04  1.0091312e+04
    1.0091347e+04  1.0091381e+04  1.0091416e+04     1.0091450e+04  1.0091485e+04
    1.0091520e+04  1.0091555e+04  1.0091592e+04     1.0091630e+04  1.0091669e+04
    1.0091710e+04  1.0091753e+04  1.0091798e+04     1.0091845e+04  1.0091894e+04
    1.0091945e+04  1.0091999e+04  1.0092056e+04     1.0092115e+04  1.0092179e+04
    1.0092245e+04  1.0092315e+04  1.0092391e+04     1.0092471e+04  1.0092556e+04
    1.0092647e+04  1.0092746e+04  1.0092852e+04     1.0092967e+04  1.0093092e+04
    1.0093229e+04  1.0093380e+04  1.0093547e+04     1.0093733e+04  1.0093944e+04
    1.0094186e+04  1.0094464e+04  1.0094791e+04     1.0095184e+04  1.0095669e+04
    1.0096278e+04  1.0098098e+04  1.0099321e+04     1.0102427e+04
mass=
     2.03769e+03     6.36546e+03     8.34547e+03      1.02763e+04     1.21420e+04
     1.39296e+04     1.56309e+04     1.72366e+04      1.87368e+04     2.00517e+04
     2.10713e+04     2.19103e+04     2.25909e+04      2.31318e+04     2.35496e+04
     2.38592e+04     2.40728e+04     2.42016e+04      2.42563e+04     2.42450e+04
     2.41757e+04     2.40557e+04     2.38910e+04      2.36875e+04     2.34500e+04
     2.31831e+04     2.28909e+04     2.25770e+04      2.22446e+04     2.18967e+04
     2.15358e+04     2.11644e+04     2.07844e+04      2.03979e+04     2.00063e+04
     1.96113e+04     1.92142e+04     1.88162e+04      1.84183e+04     1.80214e+04
     1.76264e+04     1.72340e+04     1.68450e+04      1.64597e+04     1.60787e+04
     1.57030e+04     1.53275e+04     1.49426e+04      1.45491e+04     1.41464e+04
     1.37349e+04     1.33146e+04     1.28860e+04      1.24490e+04     1.20039e+04
     1.15512e+04     1.10911e+04     1.06239e+04      1.01502e+04     9.67045e+03
     9.18517e+03     8.69502e+03     8.20081e+03      7.70333e+03     7.20350e+03
     6.70239e+03     6.20127e+03     5.70144e+03      5.20444e+03     4.71203e+03
     4.22618e+03     3.74912e+03     3.28336e+03      2.83175e+03     2.39752e+03
     1.98430e+03     1.59619e+03     6.60772e+02      6.17613e-10     5.37671e+02
     1.31702e+02     1.29169e+02     7.90865e+01      0.00000e+00
temp    =
     2.55000e+03     2.55000e+03     2.55000e+03      2.55000e+03     2.55000e+03
     2.55000e+03     2.55000e+03     2.55000e+03      2.55000e+03     2.55000e+03
     2.55000e+03     2.55000e+03     2.55000e+03      2.55000e+03     2.55000e+03
     2.55000e+03     2.55000e+03     2.55000e+03      2.55000e+03     2.55000e+03
     2.55000e+03     2.55000e+03     2.55000e+03      2.55000e+03     2.55000e+03
     2.55000e+03     2.55000e+03     2.55000e+03      2.55000e+03     2.55000e+03
     2.55000e+03     2.55000e+03     2.55000e+03      2.55000e+03     2.55000e+03
     2.55000e+03     2.55000e+03     2.55000e+03      2.55000e+03     2.55000e+03
     2.55000e+03     2.55000e+03     2.55000e+03      2.55000e+03     2.55000e+03
     2.55000e+03     2.55000e+03     2.55000e+03      2.55000e+03     2.55000e+03
     2.55000e+03     2.55000e+03     2.55000e+03      2.55000e+03     2.55000e+03
     2.55000e+03     2.55000e+03     2.55000e+03      2.55000e+03     2.55000e+03
     2.55000e+03     2.55000e+03     2.55000e+03      2.55000e+03     2.55000e+03
     2.55000e+03     2.55000e+03     2.55000e+03      2.55000e+03     2.55000e+03
     2.55000e+03     2.55000e+03     2.55000e+03      2.55000e+03     2.55000e+03
     2.55000e+03     2.55000e+03     2.55000e+03      2.55000e+03     2.55000e+03
     2.55000e+03     2.55000e+03     2.55000e+03      2.55000e+03
eoi
    zrd  84 iflag=1    &&      5662.000 kg
t=
    1.0090000e+04  1.0090066e+04  1.0090088e+04     1.0090108e+04  1.0090131e+04
    1.0090154e+04  1.0090181e+04  1.0090208e+04     1.0090238e+04  1.0090271e+04
    1.0090306e+04  1.0090340e+04  1.0090375e+04     1.0090409e+04  1.0090444e+04
    1.0090479e+04  1.0090514e+04  1.0090549e+04     1.0090583e+04  1.0090618e+04
    1.0090652e+04  1.0090688e+04  1.0090722e+04     1.0090757e+04  1.0090791e+04
    1.0090826e+04  1.0090860e+04  1.0090896e+04     1.0090930e+04  1.0090965e+04
    1.0090999e+04  1.0091034e+04  1.0091069e+04     1.0091104e+04  1.0091139e+04
    1.0091173e+04  1.0091208e+04  1.0091242e+04     1.0091277e+04  1.0091312e+04
    1.0091347e+04  1.0091381e+04  1.0091416e+04     1.0091450e+04  1.0091485e+04
    1.0091520e+04  1.0091555e+04  1.0091592e+04     1.0091630e+04  1.0091669e+04
    1.0091710e+04  1.0091753e+04  1.0091798e+04     1.0091845e+04  1.0091894e+04
    1.0091945e+04  1.0091999e+04  1.0092056e+04     1.0092115e+04  1.0092179e+04
    1.0092245e+04  1.0092315e+04  1.0092391e+04     1.0092471e+04  1.0092556e+04
    1.0092647e+04  1.0092746e+04  1.0092852e+04     1.0092967e+04  1.0093092e+04
    1.0093229e+04  1.0093380e+04  1.0093547e+04     1.0093733e+04  1.0093944e+04
    1.0094186e+04  1.0094464e+04  1.0094791e+04     1.0095184e+04  1.0095669e+04
    1.0096278e+04  1.0098098e+04  1.0099321e+04     1.0102427e+04
```

```
mass=
    2.28463e+02    7.13667e+02    9.35684e+02      1.15217e+03    1.36135e+03
    1.56177e+03    1.75252e+03    1.93255e+03      2.10074e+03    2.24817e+03
    2.36249e+03    2.45655e+03    2.53286e+03      2.59351e+03    2.64037e+03
    2.67507e+03    2.69901e+03    2.71348e+03      2.71959e+03    2.71832e+03
    2.71055e+03    2.69709e+03    2.67863e+03      2.65581e+03    2.62918e+03
    2.59926e+03    2.56650e+03    2.53131e+03      2.49404e+03    2.45503e+03
    2.41457e+03    2.37293e+03    2.33033e+03      2.28698e+03    2.24308e+03
    2.19880e+03    2.15426e+03    2.10965e+03      2.06504e+03    2.02054e+03
    1.97625e+03    1.93226e+03    1.88864e+03      1.84544e+03    1.80272e+03
    1.76060e+03    1.71851e+03    1.67537e+03      1.63123e+03    1.58608e+03
    1.53794e+03    1.49282e+03    1.44476e+03      1.39570e+03    1.34587e+03
    1.29511e+03    1.24352e+03    1.19114e+03      1.13803e+03    1.08424e+03
    1.02983e+03    9.74876e+02    9.19465e+02      8.63688e+02    8.07648e+02
    7.51464e+02    6.95279e+02    6.39239e+02      5.83515e+02    5.28307e+02
    4.73035e+02    4.20347e+02    3.66127e+02      3.17493e+02    2.68807e+02
    2.22477e+02    1.76963e+02    9.65087e+01      6.92460e-11    6.02830e+01
    1.47663e+01    1.44523e+01    8.86730e+00      0.00000e+00
temp     =
    2.55000e+03    2.55000e+03    2.55000e+03      2.55000e+03    2.55000e+03
    2.55000e+03    2.55000e+03    2.55000e+03      2.55000e+03    2.55000e+03
    2.55000e+03    2.55000e+03    2.55000e+03      2.55000e+03    2.55000e+03
    2.55000e+03    2.55000e+03    2.55000e+03      2.55000e+03    2.55000e+03
    2.55000e+03    2.55000e+03    2.55000e+03      2.55000e+03    2.55000e+03
    2.55000e+03    2.55000e+03    2.55000e+03      2.55000e+03    2.55000e+03
    2.55000e+03    2.55000e+03    2.55000e+03      2.55000e+03    2.55000e+03
    2.55000e+03    2.55000e+03    2.55000e+03      2.55000e+03    2.55000e+03
    2.55000e+03    2.55000e+03    2.55000e+03      2.55000e+03    2.55000e+03
    2.55000e+03    2.55000e+03    2.55000e+03      2.55000e+03    2.55000e+03
    2.55000e+03    2.55000e+03    2.55000e+03      2.55000e+03    2.55000e+03
    2.55000e+03    2.55000e+03    2.55000e+03      2.55000e+03    2.55000e+03
    2.55000e+03    2.55000e+03    2.55000e+03      2.55000e+03    2.55000e+03
    2.55000e+03    2.55000e+03    2.55000e+03      2.55000e+03    2.55000e+03
    2.55000e+03    2.55000e+03    2.55000e+03      2.55000e+03    2.55000e+03
    2.55000e+03    2.55000e+03    2.55000e+03      2.55000e+03    2.55000e+03
    2.55000e+03    2.55000e+03    2.55000e+03      2.55000e+03
eoi
     fed  84 iflag=1   &&    30550.000 kg
t=
  1.0090000e+04  1.0090068e+04  1.0090088e+04    1.0090108e+04  1.0090131e+04
  1.0090154e+04  1.0090181e+04  1.0090208e+04    1.0090238e+04  1.0090271e+04
  1.0090306e+04  1.0090340e+04  1.0090375e+04    1.0090409e+04  1.0090444e+04
  1.0090479e+04  1.0090514e+04  1.0090549e+04    1.0090583e+04  1.0090618e+04
  1.0090652e+04  1.0090688e+04  1.0090722e+04    1.0090757e+04  1.0090791e+04
  1.0090826e+04  1.0090860e+04  1.0090896e+04    1.0090930e+04  1.0090965e+04
  1.0090999e+04  1.0091034e+04  1.0091069e+04    1.0091104e+04  1.0091139e+04
  1.0091175e+04  1.0091208e+04  1.0091242e+04    1.0091277e+04  1.0091312e+04
  1.0091347e+04  1.0091381e+04  1.0091416e+04    1.0091450e+04  1.0091485e+04
  1.0091520e+04  1.009155[illegible]e+04  1.0091592e+04    1.0091630e+04  1.0091669e+04
  1.0091710e+04  1.00917[illegible]3e+04  1.0091798e+04    1.0091845e+04  1.0091894e+04
  1.0091945e+04  1.0091999e+04  1.0092056e+04    1.0092115e+04  1.0092179e+04
  1.0092245e+04  1.0092315e+04  1.0092391e+04    1.0092471e+04  1.0092556e+04
  1.0092647e+04  1.0092746e+04  1.0092852e+04    1.0092967e+04  1.0093092e+04
  1.0093229e+04  1.0093380e+04  1.0093547e+04    1.0093733e+04  1.0093944e+04
  1.0094186e+04  1.0094464e+04  1.0094791e+04    1.0095184e+04  1.0095669e+04
  1.0096278e+04  1.0098048e+04  1.0099321e+04    1.0102427e+04
mass=
    1.23270e+03    3.65079e+03    5.04860e+03      6.21666e+03    7.34531e+03
    8.42671e+03    7.45591e+03    1.04273e+04      1.13346e+04    1.21303e+04
    1.27471e+04    1.32546e+04    1.36663e+04      1.39936e+04    1.42464e+04
    1.44337e+04    1.45629e+04    1.46409e+04      1.46739e+04    1.46670e+04
    1.46251e+04    1.45525e+04    1.44529e+04      1.43297e+04    1.41861e+04
    1.40246e+04    1.38479e+04    1.36580e+04      1.34569e+04    1.32464e+04
    1.30281e+04    1.28034e+04    1.25736e+04      1.23397e+04    1.21026e+04
    1.18639e+04    1.16237e+04    1.13829e+04      1.11421e+04    1.09020e+04
    1.06631e+04    1.04257e+04    1.01904e+04      9.95728e+03    9.72679e+03
    9.49953e+03    9.27240e+03    9.03968e+03      8.80146e+03    8.55788e+03
    8.30891e+03    8.05469e+03    7.79536e+03      7.53102e+03    7.26178e+03
```

```
   [illegible]
   5.55657e+03   5.26006e+03   4.96108e+03    4.66013e+03   4.35776e+03
   4.05461e+03   3.75146e+03   3.44909e+03    3.14643e+03   2.85055e+03
   2.55663e+03   2.26803e+03   1.98627e+03    1.71307e+03   1.45036e+03
   1.20040e+03   9.65614e+02   8.20724e+02    3.73625e-10   3.25264e+02
   7.96735e+01   7.61409e+01   4.78446e+01    0.00000e+00
 temp     =
   2.55000e+03   2.55000e+03   2.55000e+03    2.55000e+03   2.55000e+03
   2.55000e+03   2.55000e+03   2.55000e+03    2.55000e+03   2.55000e+03
   2.55000e+03   2.55000e+03   2.55000e+03    2.55000e+03   2.55000e+03
   2.55000e+03   2.55000e+03   2.55000e+03    2.55000e+03   2.55000e+03
   2.55000e+03   2.55000e+03   2.55000e+03    2.55000e+03   2.55000e+03
   2.55000e+03   2.55000e+03   2.55000e+03    2.55000e+03   2.55000e+03
   2.55000e+03   2.55000e+03   2.55000e+03    2.55000e+03   2.55000e+03
   2.55000e+03   2.55000e+03   2.55000e+03    2.55000e+03   2.55000e+03
   2.55000e+03   2.55000e+03   2.55000e+03    2.55000e+03   2.55000e+03
   2.55000e+03   2.55000e+03   2.55000e+03    2.55000e+03   2.55000e+03
   2.55000e+03   2.55000e+03   2.55000e+03    2.55000e+03   2.55000e+03
   2.55000e+03   2.55000e+03   2.55000e+03    2.55000e+03   2.55000e+03
   2.55000e+03   2.55000e+03   2.55000e+03    2.55000e+03   2.55000e+03
   2.55000e+03   2.55000e+03   2.55000e+03    2.55000e+03   2.55000e+03
   2.55000e+03   2.55000e+03   2.55000e+03    2.55000e+03   2.55000e+03
   2.55000e+03   2.55000e+03   2.55000e+03    2.55000e+03   2.55000e+03
   2.55000e+03   2.55000e+03   2.55000e+03    2.55000e+03
eoi
  zro2d  84 iflag=1   ii     7648.000 kg
t=
  1.0090000e+04  1.0090068e+04  1.0090088e+04    1.0090108e+04  1.0090131e+04
  1.0090154e+04  1.0090181e+04  1.0090208e+04    1.0090238e+04  1.0090271e+04
  1.0090306e+04  1.0090340e+04  1.0090375e+04    1.0090409e+04  1.0090444e+04
  1.0090479e+04  1.0090514e+04  1.0090549e+04    1.0090583e+04  1.0090618e+04
  1.0090652e+04  1.0090688e+04  1.0090722e+04    1.0090757e+04  1.0090791e+04
  1.0090826e+04  1.0090860e+04  1.0090896e+04    1.0090930e+04  1.0090965e+04
  1.0090999e+04  1.0091034e+04  1.0091069e+04    1.0091104e+04  1.0091139e+04
  1.0091173e+04  1.0091208e+04  1.0091242e+04    1.0091277e+04  1.0091312e+04
  1.0091347e+04  1.0091381e+04  1.0091416e+04    1.0091450e+04  1.0091485e+04
  1.0091520e+04  1.0091555e+04  1.0091592e+04    1.0091630e+04  1.0091669e+04
  1.0091710e+04  1.0091753e+04  1.0091798e+04    1.0091845e+04  1.0091894e+04
  1.0091945e+04  1.0091999e+04  1.0092056e+04    1.0092115e+04  1.0092179e+04
  1.0092245e+04  1.0092315e+04  1.0092391e+04    1.0092471e+04  1.0092556e+04
  1.0092647e+04  1.0092746e+04  1.0092852e+04    1.0092967e+04  1.0093092e+04
  1.0093229e+04  1.0093380e+04  1.0093547e+04    1.0093733e+04  1.0093944e+04
  1.0094186e+04  1.0094464e+04  1.0094791e+04    1.0095184e+04  1.0095669e+04
  1.0096278e+04  1.0098098e+04  1.0099321e+04    1.0102427e+04
mass=
   3.08599e+02   9.64020e+02   1.26386e+03    1.55630e+03   1.83885e+03
   2.10957e+03   2.36723e+03   2.61041e+03    2.83760e+03   3.03674e+03
   3.19115e+03   3.31621e+03   3.42126e+03    3.50321e+03   3.56650e+03
   3.61338e+03   3.64572e+03   3.66526e+03    3.67351e+03   3.67179e+03
   3.66131e+03   3.64313e+03   3.61819e+03    3.58736e+03   3.55139e+03
   3.51098e+03   3.46673e+03   3.41919e+03    3.36885e+03   3.31616e+03
   3.26150e+03   3.20525e+03   3.14771e+03    3.08917e-03   3.02987e+03
   2.97005e+03   2.90991e+03   2.84963e+03    2.78937e+03   2.72926e+03
   2.66944e+03   2.61002e+03   2.55109e+03    2.49274e+03   2.43504e+03
   2.37815e+03   2.32129e+03   2.26303e+03    2.20340e+03   2.14241e-03
   2.08008e+03   2.01644e+03   1.95152e+03    1.88534e+03   1.81794e+03
   1.74938e+03   1.67970e+03   1.60895e+03    1.53721e+03   1.46455e+03
   1.39105e+03   1.31682e-03   1.24196e+03    1.16664e+03   1.09094e+03
   1.01505e+03   9.39155e+02   8.63458e+02    7.88189e+02   7.13616e+02
   6.40037e+02   5.67788e-02   4.97251e+02    4.28857e+02   3.63094e+02
   3.00513e+02   2.41735e+02   1.30360e+02    9.35347e-11   8.14278e+01
   1.99458e+01   1.95621e+01   1.19776e+01    0.00000e+00
temp     =
   2.55000e+03   2.55000e+03   2.55000e+03    2.55000e+03   2.55000e+03
   2.55000e+03   2.55000e+03   2.55000e+03    2.55000e+03   2.55000e+03
   2.55000e+03   2.55000e+03   2.55000e+03    2.55000e+03   2.55000e+03
   2.55000e+03   2.55000e+03   2.55000e+03    2.55000e+03   2.55000e+03
   2.55000e+03   2.55000e+03   2.55000e+03    2.55000e+03   2.55000e+03
```

```
     2.55000e+03    2.55000e+03    2.55000e+03      2.55000e+03    2.55000e+03
     2.55000e+03    2.55000e+03    2.55000e+03      2.55000e+03    2.55000e+03
     2.55000e+03    2.55000e+03    2.55000e+03      2.55000e+03    2.55000e+03
     2.55000e+03    2.55000e+03    2.55000e+03      2.55000e+03    2.55000e+03
     2.55000e+03    2.55000e+03    2.55000e+03      2.55000e+03    2.55000e+03
     2.55000e+03    2.55000e+03    2.55000e+03      2.55000e+03    2.55000e+03
     2.55000e+03    2.55000e+03    2.55000e+03      2.55000e+03    2.55000e+03
     2.55000e+03    2.55000e+03    2.55000e+03      2.55000e+03    2.55000e+03
     2.55000e+03    2.55000e+03    2.55000e+03      2.55000e+03    2.55000e+03
     2.55000e+03    2.55000e+03    2.55000e+03      2.55000e+03    2.55000e+03
     2.55000e+03    2.55000e+03    2.55000e+03      2.55000e+03    2.55000e+03
     2.55000e+03    2.55000e+03    2.55000e+03      2.55000e+03
eoi
&& dummy sources of h2ov and h2
 h2ov=10 iflag=2
   t=       0.0   10.0   20.0   50.0   100.0
          200.0  300.0  500.0  1000.0  2000.0
&& mass=    0.0    2.0    4.0   10.0    20.0
&&         40.0   60.0  100.0  200.0   400.0
   mass=    0.0    0.0    0.0    0.0     0.0
            0.0    0.0    0.0    0.0     0.0
   temp=  400.0  400.0  400.0  400.0   400.0
          400.0  400.0  400.0  400.0   400.0
 eoi
 h2=10   iflag=2
   t=       0.0   10.0   20.0   50.0   100.0
          200.0  300.0  500.0  1000.0  2000.0
&& mass=    0.0    0.1    0.2    0.3     1.0
&&          2.0    3.0    1.0    0.0     0.0
   mass=    0.0    0.0    0.0    0.0     0.0
            0.0    0.0    0.0    0.0     0.0
   temp=  400.0  400.0  400.0  400.0   400.0
          400.0  400.0  400.0  400.0   400.0
 eoi
&& dch aerosol sources
 && aerosol
 && source=2
 && small=14 iflag=2
 && t= 10090.0  10090.25  10090.5  10090.75  10091.0   10091.5 10092.0
 &&    10092.5  10093.0   10093.5  10094.0   10095.0   10096.0 10097.0
 && mass=  0.0    193.8     307.8    350.4     353.0     314.1   254.2
 &&      202.7    156.2     116.2     88.7      46.4      19.0     0.0
 &&  eoi
 && big=14 iflag=2
 && t= 10090.0  10090.25  10090.5  10090.75  10091.0   10091.5 10092.0
 &&    10092.5  10093.0   10093.5  10094.0   10095.0   10096.0 10097.0
 && mass=  0.0    193.8     307.8    350.4     353.0     314.1   254.2
 &&      202.7    156.2     116.2     88.7      46.4      19.0     0.0
 && eoi

condense

h-burn elev=0.0
       mfcig=0.999  &&  tactiv=10090.0
  flam=5.0 && cfrmng=0.0001 normng=0.0001 mfcig=0.0001 mfoig=0.0001
  && mfsig=0.9999 tactiv=10090.0  &&  for uchb
eoi

struc

&&  roof area
name=conr1  type=roof  shape=slab  nslab=12  chrlen=5.18
  slarea=23.65  tunif=311.
compound= conc   conc   conc    conc   conc      conc
          conc   conc   conc   conc    conc        conc
       x= 0.       3.5e-4   1.e-3    2.e-3    4.e-3       8.e-3  1.6e-2
          3.0e-2   6.0e-2   1.2e-1   2.4e-1   4.8e-1       8.e-1
eoi
```

```
&&

&&  vertical wall surface, open part of cavity
name=conula  type=wall  shape=slab  nslab=12  chrlen=7.0
slarea=125.23  tunif=311.
compound= conc   conc   conc    conc   conc      conc
          conc   conc   conc    conc   conc       conc
       x= 0.       3.5e-4   1.e-3    2.e-3    4.e-3       8.e-3  1.6e-2
          3.6e-2   6.0e-2   1.2e-1   2.4e-1   4.8e-1      8.e-1
eoi

&&  vertical wall surface, constricted annulus
name=conulb  type=wall  shape=slab  nslab=12  chrlen=7.0
slarea=133.4  tunif=311.
compound= conc   conc   conc    conc   conc      conc
          conc   conc   conc    conc   conc       conc
       x= 0.       3.5e-4   1.e-3    2.e-3    4.e-3       8.e-3  1.6e-2
          3.0e-2   6.0e-2   1.2e-1   2.4e-1   4.8e-1      8.e-1
eoi

&& bottom head, insulated hot steel
name=istrfl type=roof shape=sphere nslab=11 chrlen=2.476 tunif=616.
&& bcouter
  touter=616.0 && tsurf=616.0
compound= insul insul insul insul insul   insul insul insul
          fe    fe    fe
       x= 2.476 2.47565 2.475 2.473 2.469   2.461 2.445 2.423 2.40
          2.38  2.32    2.26
eoi

&& vessel side, insulated hot steel
name=istwl type=wall shape=slab nslab=12 chrlen=7.0 tunif=616.
slarea=126.4
&& bcouter
  touter=616.0 && tsurf=616.0
compound= insul insul insul insul insul   insul insul insul insul
          fe    fe    fe
       x= 0.       3.5e-4   1.e-3    2.e-3    4.e-3       8.e-3  1.6e-2
          3.0e-2   5.0e-2   7.0e-2   1.02e-1  1.4e-1 2.16e-1
eoi

 rad-heat   &&  radiant heat transfer: simple gas-struc model
   ensvt  0.8 0.8 0.8 0.8 0.6 0.8   &&  emissivities of strucs, lower cell
   geobl 5.74 5.74 0.2 5.74 0.2 5.74
   && cess     && for sensitivity studies, if desired
 eoi

&& ht-tran off off off off off   && for spurious convection tests

overflow=-1 && to cavity pool

&&     ---- lower cell input ----

low-cell
geometry 59.2
    concrete
       compos=1 conc 5.10e5 temp=311. && 3.567 m basemat
    eoi
    intern
       lay-name=splash  compos=1   fe  100. temp=311.
    eoi

&&          ----- pool layer -----
  pool                          && pool layer specification
    compos=1 h2ol 10.          && composition, material & mass
    temp=311.                   && initial temperature
    physics                     && initiate physics input
      settle
```

```
source=1                        && accumulator water
  h2oi=3  iflag=    1
  t=      10102.5   10125.0       1.0e10
  mass=   3446.1584   0.0000      0.0000
  temp=   324.8       3[illegible].8          0.0000
 eoi
 boil                           && activate pool-boiling model
eoi                             && terminate physics
eoi                             && terminate pool-layer
                    &&
                    &&     ansi power specification
                    &&
                    && dec  -ht  3.2925e06  ttosd=0. dist-pur 0. 1.0 0. 0.
                    && eoi
                    &&
 bc 311.0   0.85e5              && boundary condition temp. and pressure
eoi                             && terminate lou-cell input

&& steam generator doghouse #1
cell=2
control
  nhtm=4 mxslab=12
eoi
geometry 362.5  11.2                    && volume & height
atmos=3  1.010e5  311.0                   && initial pressure & temperature
o2=.2095  n2=.7905  h2ov=0.01   && initial atmos. composition

condense

h-burn elev=27.0
       mfcig=0.999  && tactiv=10090.0
  flam=5.0 && cfrmng=0.0001 normng=0.0001 mfcig=0.0001 mfoig=0.0001
  && mfsig=0.9999 tactiv=10090.0  && for uchb
eoi

struc

&& roof area
name=conr2  type=roof  shape=slab  nslab=11  chrlen=3.5
  slarea=39.05  tunif=311.
compound= conc   conc   conc    conc   conc      conc
          conc   conc   conc   conc    conc
       x= 0.       3.5e-4   1.e-3    2.e-3    4.e-3       8.e-3  1.6e-2
          3.0e-2   6.0e-2   1.2e-1   2.0e-1   2.7e-1
eoi

&& floor area
name=conf2  type=floor  shape=slab  nslab=11  chrlen=3.5
  slarea=23.05  tunif=311.
compound= conc   conc   conc    conc   conc      conc
          conc   conc   conc   conc    conc
       x= 0.       3.5e-4   1.e-3    2.e-3    4.e-3       8.e-3  1.6e-2
          3.0e-2   6.0e-2   1.2e-1   2.0e-1   2.7e-1
eoi

&& vertical wall surface
name=conw2  type=wall  shape=slab  nslab=11  chrlen=5.5
slarea=142.0  tunif=311.
compound= conc   conc   conc    conc   conc      conc
          conc   conc   conc   conc    conc
       x= 0.       3.5e-4   1.e-3    2.e-3    4.e-3       8.e-3  1.6e-2
          3.0e-2   6.0e-2   1.2e-1   2.0e-1   2.7e-1
eoi

&& vertical wall surface (steel)
name=stw2  type=wall  shape=slab  nslab=9  chrlen=5.5
slarea=172.0  tunif=311.
compound= fe   fe   fe    fe   fe      fe
```

```
          fe   fe   fe
       x= 0.       3.5e-4   1.e-3    2.e-3    4.e-3       8.e-3  1.6e-2
          3.0e-2   5.0e-2   6.9e-2
eoi

 rad-heat gasual 3.47   && radiant heat transfer: simple gas-struc model
   emsvt  0.8 0.8 0.8 0.8        && emissivities of strucs and lower cell
   && cess     && for sensitivity studies, if desired
 eoi

&& ht-tran off off off off off   && for spurious convection tests

overflow=-8  && to sump in lower containment

&&  steam generator doghouse #2
cell=5
control
  nhtm=4 mxslab=12
eoi
geometry 362.5  11.2                    &&  volume & height
atmos=3  1.010e5  311.0                      &&  initial pressure & temperature
o2=.2095  n2=.7905  h2ov=0.01   &&  initial atmos. composition

condense

h-burn elev=27.0
       mfcig=0.999  &&  tactiv=10090.0
  flam=5.0 && cf  ...=0.0001 normng=0.0001 mfcig=0.0001 mfoig=0.0001
  && mfsig=0.99xx t...tiv=10090.0  &&  for ucnb
eoi

struc

&&  roof area
name=conr3  type=roof  shape=slab  nslab=11  chrlen=3.5
  slarea=39.05  tunif=311.
compound= conc   conc   conc    conc   conc      conc
          conc   conc   conc    conc   conc
       x= 0.       3.5e-4   1.e-3    2.e-3    4.e-3       8.e-3  1.6e-2
          3.0e-2   6.0e-2   1.2e-1   2.0e-1   2.7e-1
eoi

&&  floor area
name=conf3  type=floor  shape=slab  nslab=11  chrlen=3.5
  slarea=23.05  tunif=311.
compound= conc   conc   conc    conc   conc      conc
          conc   conc   conc    conc   conc
       x= 0.       3.5e-4   1.e-3    2.e-3    4.e-3       8.e-3  1.6e-2
          3.0e-2   6.0e-2   1.2e-1   2.0e-1   2.7e-1
eoi

&&  vertical wall surface
name=conw3  type=wall  shape=slab  nslab=11  chrlen=5.5
slarea=142.0  tunif=311.
compound= conc   conc   conc    conc   conc      conc
          conc   conc   conc    conc   conc
       x= 0.       3.5e-4   1.e-3    2.e-3    4.e-3       8.e-3  1.6e-2
          3.0e-2   6.0e-2   1.2e-1   2.0e-1   2.7e-1
eoi

&&  vertical wall surface (steel)
name=stw3  type=wall  shape=slab  nslab=9  chrlen=5.5
slarea=172.0  tunif=311.
compound= fe   fe   fe    fe   fe      fe
          fe   fe   fe
       x= 0.       3.5e-4   1.e-3    2.e-3    4.e-3       8.e-3  1.6e-2
          3.0e-2   5.0e-2   6.9e-2
eoi
```

```
 rad-heat gasual 3.47   && radiant heat transfer: simple gas-struc model
   ensvt  0.8 0.8 0.8 0.8       && emissivities of strucs and lower cell
   && cess     && for sensitivity studies, if desired
 eoi

 && ht-tran off off off off off   && for spurious convection tests

 overflow=-8  && to sump in lower containment

 && steam generator doghouse #3
 cell=4
 control
   nhtm=4 nxslab=12
 eoi
 geometry 362.5  11.2                  && volume & height
 atmos=3  1.010e5  311.0                  && initial pressure & temperature
 o2=.2095  n2=.7905  h2ov=0.01   && initial atmos. composition

 condense

 h-burn elev=27.0
        mfcig=0.999  && tactiv=10090.0
   flam=5.0 && cfrmng=0.0001 normng=0.0001 mfcig=0.0001 mfoig=0.0001
   && mfsig=0.9999 tactiv=10090.0  &&  for uchb
 eoi

 struc

 && roof area
 name=conr4  type=roof  shape=slab  nslab=11  chrlen=3.5
   slarea=39.05  tunif=311.
 compound= conc   conc   conc    conc   conc      conc
           conc   conc   conc   conc   conc
        x= 0.       3.5e-4   1.e-3    2.e-3    4.e-3       8.e-3  1.6e-2
           3.0e-2   6.0e-2   1.2e-1   2.0e-1   2.7e-1
 eoi

 && floor area
 name=conf4  type=floor  shape=slab  nslab=11  chrlen=3.5
   slarea=23.05  tunif=311.
 compound= conc   conc   conc    conc   conc      conc
           conc   conc   conc   conc   conc
        x= 0.       3.5e-4   1.e-3    2.e-3    4.e-3       8.e-3  1.6e-2
           3.0e-2   6.0e-2   1.2e-1   2.0e-1   2.7e-1
 eoi

 && vertical wall surface
 name=conw4  type=wall  shape=slab  nslab=11  chrlen=5.5
 slarea=142.0  tunif=311.
 compound= conc   conc   conc    conc   conc      conc
           conc   conc   conc   conc   conc
        x= 0.       3.5e-4   1.e-3    2.e-3    4.e-3       8.e-3  1.6e-2
           3.0e-2   6.0e-2   1.2e-1   2.0e-1   2.7e-1
 eoi

 && vertical wall surface (steel)
 name=stw4  type=wall  shape=slab  nslab=9  chrlen=5.5
 slarea=172.0  tunif=311.
 compound= fe   fe   fe    fe   fe      fe
           fe   fe   fe
        x= 0.       3.5e-4   1.e-3    2.e-3    4.e-3       8.e-3  1.6e-2
           3.0e-2   5.0e-2   6.9e-2
 eoi

 rad-heat gasual 3.47   && radiant heat transfer: simple gas-struc model
   ensvt  0.8 0.8 0.8 0.8       && emissivities of strucs and lower cell
   && cess     && for sensitivity studies, if desired
```

```
 eoi

&& ht-tran off off off off off   && for spurious convection tests

overflow=-10 && to sump in lower containment

&&  steam generator doghouse #4
cell=5
control
  nhtm=4 mxslab=12
eoi
geometry 362.5  11.2                    &&  volume & height
atmos=3  1.010e5  311.0                      &&  initial pressure & temperature
o2=.2095  n2=.7905  h2ov=0.01   &&  initial atmos. composition

condense

h-burn elev=27.0
        mfcig=0.999  &&  tactiv=10090.0
  flam=5.0 && cfrmng=0.0001 normng=0.0001 mfcig=0.0001 mfoig=0.0001
  && mfsig=0.9999 tactiv=10090.0  &&  for uchb
eoi

struc

&&  roof area
name=conr5  type=roof  shape=slab  nslab=11  chrlen=3.5
  slarea=39.05  tunif=311.
compound= conc   conc   conc    conc   conc      conc
          conc   conc   conc   conc    conc
       x= 0.       3.5e-4   1.e-3    2.e-3    4.e-3       8.e-3  1.6e-2
          3.0e-2   6.0e-2   1.2e-1   2.0e-1   2.7e-1
eoi

&&  floor area
name=conf5  type=floor  shape=slab  nslab=11  chrlen=3.5
  slarea=23.65  tunif=311.
compound= conc   conc   conc    conc   conc      conc
          conc   conc   conc   conc    conc
       x= 0.       3.5e-4   1.e-3    2.e-3    4.e-3       8.e-3  1.6e-2
          3.0e-2   6.0e-2   1.2e-1   2.0e-1   2.7e-1
eoi

&&  vertical wall surface
name=conw5  type=wall  shape=slab  nslab=11  chrlen=5.5
slarea=142.0  tunif=311.
compound= conc   conc   conc    conc   conc      conc
          conc   conc   conc   conc    conc
       x= 0.       3.5e-4   1.e-3    2.e-3    4.e-3       8.e-3  1.6e-2
          3.0e-2   6.0e-2   1.2e-1   2.0e-1   2.7e-1
eoi

&&  vertical wall surface (steel)
name=stw5  type=wall  shape=slab  nslab=9  chrlen=5.5
slarea=172.0  tunif=311.
compound= fe   fe   fe    fe   fe      fe
          fe   fe   fe
       x= 0.       3.5e-4   1.e-3    2.e-3    4.e-3       8.e-3  1.6e-2
          3.0e-2   5.0e-2   6.9e-2
eoi

 rad-heat gasual 3.47   &&  radiant heat transfer: simple gas-struc model
   emsvt  0.8 0.8 0.8 0.8       &&  emissivities of strucs and lower cell
   && cess     && for sensitivity studies, if desired
 eoi

&& ht-tran off off off off off   && for spurious convection tests
```

```
overflow=-10 && to sump in lower containment

&&  reactor space (upper cavity)
cell=6
control
  nhtm=5 mxslab=12
eoi
geometry 439.0  7.8                    &&  volume & height
atmos=3  1.01122e5  311.0                      &&  initial pressure & temperature
o2=.2095  n2=.7905  h2ov=0.01   &&  initial atmos. composition

condense

h-burn elev=16.0
      &&  tactiv=10090.0
  flam=5.0 && cfrmng=0.0001 mormng=0.0001 mfcig=0.0001 mfoig=0.0001
  && mfsig=0.9999 tactiv=10090.0  &&  for uchb
eoi

struc

&&  roof area
name=conr6  type=roof  shape=slab  nslab=12  chrlen=8.1
  slarea=51.5  tunif=311.
compound= conc   conc   conc    conc   conc      conc conc
          conc   conc   conc   conc    conc
       x= 0.       3.5e-4   1.e-3    2.e-3    4.e-3       8.e-3  1.6e-2
          3.0e-2   6.0e-2   1.2e-1   2.4e-1   4.1e-1  6.3e-1
eoi

&&  floor area
name=conf6  type=floor  shape=slab  nslab=12  chrlen=1.6
  slarea=32.5  tunif=311.
compound= conc   conc   conc    conc   conc      conc  conc
          conc   conc   conc   conc    conc
       x= 0.       3.5e-4   1.e-3    2.e-3    4.e-3       8.e-3  1.6e-2
          3.0e-2   6.0e-2   1.2e-1   2.4e-1   4.1e-1  6.3e-1
eoi

&&  vertical wall area
name=conw6  type=wall  shape=slab  nslab=12  chrlen=9.4
  slarea=240.  tunif=311.
compound= conc   conc   conc    conc   conc      conc  conc
          conc   conc   conc   conc    conc
       x= 0.       3.5e-4   1.e-3    2.e-3    4.e-3       8.e-3  1.6e-2
          3.0e-2   6.0e-2   1.2e-1   2.4e-1   4.1e-1  6.3e-1
eoi

&& vessel side, insulated hot steel
name=istw6 type=wall shape=slab nslab=12 chrlen=4.1 tunif=616.
slarea=57.2
&& bcouter
  touter=616.0 && tsurf=616.0
compound= insul insul insul insul insul   insul insul insul insul
          fe    fe    fe
       x= 0.       3.5e-4   1.e-3    2.e-3    4.e-3       8.e-3  1.6e-2
          3.0e-2   5.0e-2   7.6e-2   1.02e-1  1.54e-1 2.41e-1
eoi

&& vessel top head, insulated hot steel
name=istf6 type=floor shape=slab nslab=12 chrlen=4.9 tunif=616.
slarea=19.0
&& bcouter
  touter=616.0 && tsurf=616.0
compound= insul insul insul insul insul   insul insul insul insul
          fe    fe    fe
       x= 0.       3.5e-4   1.e-3    2.e-3    4.e-3       8.e-3  1.6e-2
          3.0e-2   5.0e-2   7.6e-2   1.02e-1  1.54e-1 2.41e-1
```

```
eoi

 rad-heat gasual 3.95   && radiant heat transfer: simple gas-struc model
   emsvt  0.8 0.8 0.8 0.8 0.8   && emissivities of strucs and lower cell
   && cess     && for sensitivity studies, if desired
 eoi

&& ht-tran off off off off off   && for spurious convection tests

overflow=-1 && to cavity pool

&&  pressurizer doghouse #1
cell=7
control
  nhtm=2 mxslab=12
eoi
geometry 135.0  11.2                    &&  volume & height
atmos=3  1.010e5  311.0                      &&  initial pressure & temperature
o2=.2095  n2=.7905  h2ov=0.01   &&  initial atmos. composition

condense

h-burn elev=27.0
      &&  tactiv=10090.0
  flam=5.0 && cfrmng=0.0001 mormng=0.0001 mfcig=0.0001 mfoig=0.0001
  && mfsig=0.9999 tactiv=10090.0  &&  for uchb
eoi

struc

&&  vertical wall surface
name=con7  type=wall  shape=slab  nslab=11  chrlen=5.5
slarea=64.0  tunif=311.
compound= conc   conc   conc    conc   conc      conc
          conc   conc   conc   conc    conc
       x= 0.       3.5e-4   1.e-3    2.e-3    4.e-3       8.e-3  1.6e-2
          3.0e-2   6.0e-2   1.2e-1   2.0e-1   2.7e-1
eoi

&&  vertical wall surface (steel)
name=stu7  type=wall  shape=slab  nslab=9  chrlen=5.5
slarea=64.0  tunif=311.
compound= fe   fe   fe    fe   fe      fe
          fe   fe   fe
       x= 0.       3.5e-4   1.e-3    2.e-3    4.e-3       8.e-3  1.6e-2
          3.0e-2   5.0e-2   6.9e-2
eoi

 rad-heat gasual 3.47   && radiant heat transfer: simple gas-struc model
   emsvt  0.8 0.8     && emissivities of strucs and lower cell
   && cess     && for sensitivity studies, if desired
 eoi

&& ht-tran off off off off off   && for spurious convection tests

overflow=-9  && to sump in lower containment

&& lower containment #1 ------------------------
cell=8
control  nhtm=3  mxslab=12  jpool=1
  jint= 1 jconc=1 numtbc=1 maxtbc=5
eoi
title
cell #8 (lower containment #1)
geometry   1510.0 14.0
atmos=3 1.01163e5 311.0
n2=0.7905  o2=0.2095 h2ov=0.01 && initial atmosphere composition
```

```
condense

h-burn elev=12.3
      && tactiv=10090.0
  flam=5.0 && cfrmng=0.0001 normng=0.0001 mfcig=0.0001 nfoig=0.0001
  && mfsig=0.9999 iactiv=10090.0  &&  for uchb
eoi

struc

&&  roof area
name=conr8  type=roof  shape=slab  nslab=11  chrle    .7
  slarea=124.  tunif=311.
compound= conc   conc   conc    conc   conc       (   :
          conc   conc   conc    conc   conc
        x= 0.       3.5e-4   1.e-3    2.e-3    4.e          8.e-3  1.6e-2
           3.0e-2   6.0e-2   1.2e-1   2.4e-1   3.6
eoi

&&  vertical wall surface
name=conw8  type=wall  shape=slab  nslab=11  chrlen=14.
slarea=727.  tunif=311.
compound= conc   conc   conc    conc   conc       conc
          conc   conc   conc    conc   conc
        x= 0.       3.5e-4   1.e-3    2.e-3    4.e-3        8.e-3  1.6e-2
           3.0e-2   6.0e-2   1.2e-1   2.4e-1   3.6e-1
eoi

&&  vertical wall surface (steel)
name=stw8  type=wall  shape=slab  nslab=9  chrlen=14.
slarea=784.3  tunif=311.
compound= fe   fe   fe    fe   fe       fe
    *     fe   fe   fe
        x= 0.       3.5e-4   1.e-3    2.e-3    4.e-3        8.e-3  1.6e-2
           3.0e-2   5.0e-2   6.9e-2
eoi

 rad-heat gasgal 3.22   &&  radiant heat transfer: simple gas-struc model
   emsvt  0.8 0.8 0.8 0.8        &&  emissivities of strucs and lower cell
   && cess     && for sensitivity studies, if desired
 eoi

&& ht-tran off off off off off   && for spurious convection tests

overflow=-6  && to sump in lower containment

low-cell
 geometry  124.
    concrete
       compos=1  conc  1.077e6  temp=311. && concrete 3.62 m thick
    eoi
    interm
       lay-name=splash   compos=1  fe  100.  temp=311.
     physics
       ht-coef
       name= pool
         flag= 1
         var-x= time x= 2 1.e+7 1.1e+7 && default ht trans 10090.0 10110.0
         var-y= coef y= 2 5.0e+04  100. && fast quench of debris
       eoi
     eoi
   eoi
 pool compos 1 h2ol=1.0 temp= 311.
   physics
     settle
     boil
   eoi
 eoi
```

```
 bc-sil. 1.65
eoi

&& lower containment #2 ----------------------
cell=9
control  nhtm=3  mxslab=12  nsoatm=5  nspatm=239  naensy=2 jpool=1
  jint= 1 jconc=1 numtbc=1 maxtbc=5
eoi
title
cell #9 (lower containment #2)
geometry   1290.0 14.0
atmos=3 1.01163e5 311.0
n2=0.7905  o2=0.2095 h2ov=0.01 && initial atmosphere composition
source=  5
&&              ------ rpv sources -------
 h2              = 203  iflag=1
t=
  0.00000e+00  6.73400e+03  6.74900e+03  6.76400e+03  6.77900e+03  6.79400e+03
  6.80900e+03  6.82400e+03  6.83900e+03  6.85400e+03  6.86900e+03  6.88400e+03
  6.89900e+03  6.91400e+03  6.92900e+03  6.94400e+03  6.95900e+03  6.97400e+03
  6.98900e+03  7.00400e+03  7.01900e+03  7.03400e+03  7.04900e+03  7.06400e+03
  7.07900e+03  7.09400e+03  7.10900e+03  7.12400e+03  7.13900e+03  7.15400e+03
  7.16900e+03  7.18400e+03  7.19900e+03  7.21400e+03  7.22900e+03  7.24400e+03
  7.25900e+03  7.27400e+03  7.28900e+03  7.30400e+03  7.31900e+03  7.33400e+03
  7.34900e+03  7.36400e+03  7.37900e+03  7.39400e+03  7.40900e+03  7.42400e+03
  7.43900e+03  7.45400e+03  7.46900e+03  7.48400e+03  7.49900e+03  7.51400e+03
  7.52900e+03  7.54400e+03  7.55900e+03  7.57400e+03  7.58900e+03  7.60400e+03
  7.61900e+03  7.63400e+03  7.64900e+03  7.66400e+03  7.67900e+03  7.69400e+03
  7.70900e+03  7.72400e+03  7.73900e+03  7.75400e+03  7.76900e+03  7.78400e+03
  7.79900e+03  7.81400e+03  7.82900e+03  7.84400e+03  7.85900e+03  7.87400e+03
  7.88900e+03  7.90400e+03  7.91900e+03  7.93400e+03  7.94900e+03  7.96400e+03
  7.97900e+03  7.99400e+03  8.00900e+03  8.02400e+03  8.03900e+03  8.05400e+03
  8.06900e+03  8.08400e+03  8.09900e+03  8.11400e+03  8.12900e+03  8.14400e+03
  8.15900e+03  8.17400e+03  8.18900e+03  8.20400e+03  8.21900e+03  8.23400e+03
  8.24900e+03  8.26400e+03  8.27900e+03  8.29400e+03  8.30900e+03  8.32400e+03
  8.33900e+03  8.35400e+03  8.36900e+03  8.38400e+03  8.39900e+03  8.41400e+03
  8.42900e+03  8.44400e+03  8.45900e+03  8.47400e+03  8.48900e+03  8.50400e+03
  8.51900e+03  8.53400e+03  8.54900e+03  8.56400e+03  8.57900e+03  8.59400e+03
  8.60900e+03  8.62400e+03  8.63900e+03  8.65400e+03  8.66900e+03  8.68400e+03
  8.69900e+03  8.71400e+03  8.72900e+03  8.74400e+03  8.75900e+03  8.77400e+03
  8.78900e+03  8.80400e+03  8.81900e+03  8.83400e+03  8.84900e+03  8.86400e+03
  8.87900e+03  8.89400e+03  8.90900e+03  8.92400e+03  8.93900e+03  8.95400e+03
  8.96900e+03  8.98400e+03  8.99900e+03  9.01400e+03  9.02900e+03  9.04400e+03
  9.05900e+03  9.07400e+03  9.08900e+03  9.10400e+03  9.11900e+03  9.13400e+03
  9.14900e+03  9.16400e+03  9.17900e+03  9.19400e+03  9.20900e+03  9.22400e+03
  9.23900e+03  9.25400e+03  9.26900e+03  9.28400e+03  9.29900e+03  9.31400e+03
  9.32900e+03  9.34400e+03  9.35900e+03  9.37400e+03  9.38900e+03  9.40400e+03
  9.41900e+03  9.43400e+03  9.44900e+03  9.46400e+03  9.47900e+03  9.49400e+03
  9.50900e+03  9.52550e+03  9.54365e+03  9.56362e+03  9.58558e+03  9.60974e+03
  9.63631e+03  9.66554e+03  9.69769e+03  9.73306e+03  9.77197e+03  9.81477e+03
  9.86184e+03  9.91363e+03  9.97059e+03  1.00306e+04  1.00906e+04
mass=
  0.00000e+00  0.00000e+00  6.46586e-10  1.95361e-09  3.91460e-09  6.49658e-09
  9.98482e-09  1.20894e-08  1.58053e-08  2.01257e-08  2.44143e-08  2.93924e-08
  3.50880e-08  4.09880e-08  4.78391e-08  5.57648e-08  6.44151e-08  7.46355e-08
  8.67561e-08  1.02599e-07  1.19367e-07  1.39207e-07  1.61221e-07  1.90826e-07
  2.29163e-07  2.77165e-07  3.36703e-07  4.11003e-07  5.02541e-07  6.14533e-07
  7.53180e-07  9.24629e-07  1.13357e-06  1.38931e-06  1.70479e-06  2.09740e-06
  2.58202e-06  3.16654e-06  3.87640e-06  4.75769e-06  5.86152e-06  7.22633e-06
  8.86395e-06  1.07579e-05  1.29934e-05  1.57198e-05  1.90568e-05  2.30674e-05
  2.77688e-05  3.31315e-05  3.90520e-05  4.60057e-05  5.28290e-05  6.06680e-05
  6.99472e-05  8.06680e-05  9.26455e-05  1.05767e-04  1.20049e-04  1.35520e-04
  1.52061e-04  1.69317e-04  1.86731e-04  2.03642e-04  2.19921e-04  2.38989e-04
  2.63256e-04  2.92098e-04  3.23675e-04  3.57049e-04  3.92824e-04  4.32833e-04
  4.77439e-04  5.26900e-04  5.81354e-04  6.40927e-04  7.05575e-04  7.75273e-04
  8.50115e-04  9.29885e-04  1.01443e-03  1.10339e-03  1.19654e-03  1.29455e-03
  1.39984e-03  1.53421e-03  1.70528e-03  1.89639e-03  2.17198e-03  2.59665e-03
  2.98592e-03  3.33757e-03  3.66944e-03  3.96743e-03  4.26463e-03  4.69430e-03
```

```
eq1
```

```
enth=
```

```
h2ov
```

```
+=
```

```
= 259  xelag=1
```

7.16900e+03	7.18400e+03	7.19900e+03	7.21400e+03	7.22900e+03	7.24400e+03
7.25900e+03	7.27400e+03	7.28900e+03	7.30400e+03	7.31900e+03	7.33400e+03
7.34900e+03	7.36400e+03	7.37900e+03	7.39400e+03	7.40900e+03	7.42400e+03
7.43900e+03	7.45400e+03	7.46900e+03	7.48400e+03	7.49900e+03	7.51400e+03
7.52900e+03	7.54400e+03	7.55900e+03	7.57400e+03	7.58900e+03	7.60400e+03
7.61900e+03	7.63400e+03	7.64900e+03	7.66400e+03	7.67900e+03	7.69400e+03
7.70900e+03	7.72400e+03	7.73900e+03	7.75400e+03	7.76900e+03	7.78400e+03
7.79900e+03	7.81400e+03	7.82900e+03	7.84400e+03	7.85900e+03	7.87400e+03
7.88900e+03	7.90400e+03	7.91900e+03	7.93400e+03	7.94900e+03	7.96400e+03
7.97900e+03	7.99400e+03	8.00900e+03	8.02400e+03	8.03900e+03	8.05400e+03
8.06900e+03	8.08400e+03	8.09900e+03	8.11400e+03	8.12900e+03	8.14400e+03
8.15900e+03	8.17400e+03	8.18900e+03	8.20400e+03	8.21900e+03	8.23400e+03
8.24900e+03	8.26400e+03	8.27900e+03	8.29400e+03	8.30900e+03	8.32400e+03
8.33900e+03	8.35400e+03	8.36900e+03	8.38400e+03	8.39900e+03	8.41400e+03
8.42900e+03	8.44400e+03	8.45900e+03	8.47400e+03	8.48900e+03	8.50400e+03
8.51900e+03	8.53400e+03	8.54900e+03	8.56400e+03	8.57900e+03	8.59400e+03
8.60900e+03	8.62400e+03	8.63900e+03	8.65400e+03	8.66900e+03	8.68400e+03
8.69900e+03	8.71400e+03	8.72900e+03	8.74400e+03	8.75900e+03	8.77400e+03
8.78900e+03	8.80400e+03	8.81900e+03	8.83400e+03	8.84900e+03	8.86400e+03
8.87900e+03	8.89400e+03	8.90900e+03	8.92400e+03	8.93900e+03	8.95400e+03
8.96900e+03	8.98400e+03	8.99900e+03	9.01400e+03	9.02900e+03	9.04400e+03
9.05900e+03	9.07400e+03	9.08900e+03	9.10400e+03	9.11900e+03	9.13400e+03
9.14900e+03	9.16400e+03	9.17900e+03	9.19400e+03	9.20900e+03	9.22400e+03
9.23900e+03	9.25400e+03	9.26900e+03	9.28400e+03	9.29900e+03	9.31400e+03
9.32900e+03	9.34400e+03	9.35900e+03	9.37400e+03	9.38900e+03	9.40400e+03
9.41900e+03	9.43400e+03	9.44900e+03	9.46400e+03	9.47900e+03	9.49400e+03
9.50900e+03	9.52550e+03	9.54365e+03	9.56362e+03	9.58556e+03	9.60974e+03
9.63631e+03	9.66554e+03	9.69769e+03	9.73306e+03	9.77197e+03	9.81477e+03
9.86184e+03	9.91363e+03	9.97059e+03	1.00306e+04	1.00906e+04	

mess=

0.00000e+00	0.00000e+00	0.00000e+00	0.00000e+00	0.00000e+00	0.00000e+00
3.01973e+01	3.02207e+01	3.65132e+01	3.07926e+01	3.10078e+01	3.10629e+01
3.10036e+01	3.09561e+01	3.39144e+01	3.38526e+01	3.37897e+01	3.37336e+01
3.36799e+01	3.36351e+01	3.35994e+01	3.35691e+01	3.35409e+01	3.35129e+01
3.34851e+01	3.34579e+01	3.34317e+01	3.34063e+01	3.33816e+01	3.33574e+01
3.33334e+01	3.33099e+01	3.32866e+01	3.32635e+01	6.64815e+01	3.29165e+01
3.27020e+01	3.28631e+01	3.29587e+01	3.29513e+01	3.27001e+01	3.21771e+01
3.14443e+01	3.05638e+01	2.95793e+01	2.85229e+01	2.74164e+01	2.62599e+01
2.50736e+01	2.38896e+01	2.27216e+01	2.15844e+01	2.04834e+01	1.95040e+01
1.85958e+01	1.80219e+01	1.71844e+01	1.63974e+01	1.54557e+01	1.47035e+01
1.40561e+01	1.34625e+01	1.28963e+01	1.23686e+01	1.18613e+01	1.13638e+01
1.09049e+01	1.04771e+01	1.00530e+01	9.64280e+00	9.26113e+00	8.91939e+00
8.59577e+00	8.25487e+00	7.91736e+00	7.61866e+00	7.36665e+00	7.13958e+00
6.90089e+00	6.62044e+00	6.34398e+00	6.11478e+00	5.93474e+00	5.78367e+00
5.64049e+00	5.48839e+00	5.31239e+00	5.17511e+00	4.94785e+00	4.76254e+00
4.63227e+00	4.53496e+00	4.44767e+00	4.36068e+00	4.27338e+00	4.18585e+00
4.09474e+00	3.99106e+00	3.86790e+00	3.71841e+00	3.55096e+00	3.42274e+00
3.35440e+00	3.32022e+00	3.29023e+00	3.25369e+00	3.21574e+00	3.18926e+00
3.17239e+00	3.16277e+00	3.15758e+00	3.15427e+00	3.15039e+00	3.14423e+00
3.13474e+00	3.12015e+00	3.09934e+00	3.07103e+00	3.03499e+00	2.99295e+00
2.94982e+00	2.94623e+00	2.98702e+00	3.03777e+00	3.17202e+00	3.42259e+00
3.55116e+00	3.59907e+00	3.61064e+00	3.58794e+00	3.56674e+00	3.63801e+00
3.65562e+00	3.64855e+00	3.63200e+00	3.61444e+00	3.59103e+00	3.57312e+00
3.56250e+00	3.54348e+00	3.53875e+00	3.52070e+00	3.51534e+00	3.49779e+00
3.46897e+00	3.47974e+00	3.45830e+00	3.42086e+00	3.38022e+00	3.42717e+00
3.42556e+00	3.37199e+00	3.29230e+00	3.19903e+00	3.10041e+00	2.99222e+00
2.88779e+00	2.77911e+00	2.67141e+00	2.55766e+00	2.46402e+00	2.41517e+00
2.40283e+00	2.39973e+00	2.38416e+00	2.36270e 00	2.33558e+00	2.31193e+00
2.29377e+00	2.27543e+00	2.25923e+00	2.23953e+00	2.22230e+00	2.20575e+00
2.18985e+00	2.17493e+00	2.16089e+00	2.14612e+00	2.13370e+00	2.12238e+00
2.11103e+00	2.10019e+00	2.09024e+00	2.08040e+00	2.07203e+00	2.06341e+00
2.05593e+00	2.04868e+00	2.04352e+00	2.04129e+00	2.04428e+00	2.05509e+00
2.07826e+00	2.11654e+00	2.16425e+00	2.22143e+00	2.52761e+00	3.70434e+00
4.86870e+00	5.59489e+00	6.19179e+00	6.72726e+00	6.99801e+00	7.17001e+00
7.46513e+00	9.73817e+00	1.18734e+01	1.20517e+01	1.00432e+01	9.25242e+00
9.67037e+00	9.94477e+00	1.38937e+02	9.75964e+01	1.26096e+02	1.29556e+02
1.33901e+02	5.32354e+01	4.64714e+01	4.47823e+01	4.33873e+01	4.24881e+01
3.80866e+01	[illegible]	3.33933e+01	3.15859e+01	[illegible]	[illegible]

```
  2.91548e+01   2.88653e+01   3.23915e+01   7.07564e+00   3.85881e+00   2.58453e+00
  1.96337e+00   1.64363e+00   1.56454e+00   0.00000e+00   0.00000e+00
enth=
  0.00000e+00   0.00000e+00   0.00000e+00   0.00000e+00   0.00000e+00   0.00000e+00
  2.53000e+06   2.53008e+06   2.53018e+06   2.53032e+06   2.53055e+06   2.53082e+06
  2.53112e+06   2.53142e+06   2.53172e+06   2.53199e+06   2.53223e+06   2.53246e+06
  2.53267e+06   2.53287e+06   2.53304e+06   2.53321e+06   2.53337e+06   2.53352e+06
  2.53366e+06   2.53379e+06   2.53391e+06   2.53403e+06   2.53414e+06   2.53424e+06
  2.53434e+06   2.53443e+06   2.53452e+06   2.53460e+06   2.53467e+06   2.53471e+06
  2.53469e+06   2.53465e+06   2.53463e+06   2.53465e+06   2.53472e+06   2.53482e+06
  2.53489e+06   2.53496e+06   2.53502e+06   2.53507e+06   2.53511e+06   2.53516e+06
  2.53519e+06   2.53523e+06   2.53525e+06   2.53529e+06   2.53529e+06   2.53536e+06
  2.53547e+06   2.53577e+06   2.53608e+06   2.53643e+06   2.53673e+06   2.53701e+06
  2.53732e+06   2.53767e+06   2.53805e+06   2.53845e+06   2.53886e+06   2.53933e+06
  2.53980e+06   2.54026e+06   2.54074e+06   2.54124e+06   2.54174e+06   2.54221e+06
  2.54270e+06   2.54320e+06   2.54369e+06   2.54415e+06   2.54463e+06   2.54509e+06
  2.54556e+06   2.54603e+06   2.54648e+06   2.54691e+06   2.54736e+06   2.54779e+06
  2.54821e+06   2.54865e+06   2.54905e+06   2.54952e+06   2.54994e+06   2.55036e+06
  2.55076e+06   2.55116e+06   2.55156e+06   2.55196e+06   2.55235e+06   2.55273e+06
  2.55311e+06   2.55349e+06   2.55385e+06   2.55418e+06   2.55452e+06   2.55482e+06
  2.55512e+06   2.55542e+06   2.55572e+06   2.55601e+06   2.55629e+06   2.55657e+06
  2.55685e+06   2.55714e+06   2.55741e+06   2.55770e+06   2.55796e+06   2.55824e+06
  2.55851e+06   2.55876e+06   2.55902e+06   2.55926e+06   2.55949e+06   2.55970e+06
  2.55988e+06   2.56006e+06   2.56022e+06   2.56036e+06   2.56053e+06   2.56066e+06
  2.56077e+06   2.56088e+06   2.56097e+06   2.56107e+06   2.56115e+06   2.56124e+06
  2.56132e+06   2.56139e+06   2.56147e+06   2.56154e+06   2.56162e+06   2.56169e+06
  2.56177e+06   2.56184e+06   2.56191e+06   2.56198e+06   2.56205e+06   2.56212e+06
  2.56219e+06   2.56225e+06   2.56231e+06   2.56237e+06   2.56243e+06   2.56248e+06
  2.56252e+06   2.56256e+06   2.56259e+06   2.56263e+06   2.56267e+06   2.56269e+06
  2.56272e+06   2.56275e+06   2.56277e+06   2.56278e+06   2.56279e+06   2.56281e+06
  2.56283e+06   2.56284e+06   2.56286e+06   2.56288e+06   2.56290e+06   2.56292e+06
  2.56294e+06   2.56295e+06   2.56297e+06   2.56299e+06   2.56300e+06   2.56302e+06
  2.56303e+06   2.56306e+06   2.56306e+06   2.56309e+06   2.56311e+06   2.56313e+06
  2.56316e+06   2.56316e+06   2.56319e+06   2.56322e+06   2.56323e+06   2.56325e+06
  2.56328e+06   2.56329e+06   2.56331e+06   2.56334e+06   2.56336e+06   2.56340e+06
  2.56342e+06   2.56345e+06   2.56348e+06   2.56353e+06   2.56359e+06   2.56375e+06
  2.56396e+06   2.56438e+06   2.56488e+06   2.56542e+06   2.56600e+06   2.56665e+06
  2.56732e+06   2.56836e+06   2.56957e+06   2.57104e+06   2.57230e+06   2.57353e+06
  2.57453e+06   2.57567e+06   2.61984e+06   2.64950e+06   2.70726e+06   2.76773e+06
  2.84063e+06   2.84901e+06   2.85513e+06   2.85968e+06   2.86274e+06   2.86474e+06
  2.86602e+06   2.86672e+06   2.86781e+06   2.86866e+06   2.86438e+06   2.86161e+06
  2.85797e+06   2.85273e+06   2.85021e+06   2.87490e+06   2.87662e+06   2.87838e+06
  2.88041e+06   2.88263e+06   2.88502e+06   0.00000e+00   0.00000e+00
eol

 h2ov            = 115  iflag=1
t=
  0.00000e+00   3.37553e+03   3.38475e+03   3.39490e+03   3.40605e+03   3.41833e+03
  3.43183e+03   3.44668e+03   3.46301e+03   3.48098e+03   3.50076e+03   3.52249e+03
  3.54640e+03   3.57271e+03   3.60165e+03   3.63165e+03   3.66165e+03   3.69165e+03
  3.72165e+03   3.75165e+03   3.78165e+03   3.81165e+03   3.84165e+03   3.87165e+03
  3.90165e+03   3.93165e+03   3.96165e+03   3.99165e+03   4.02165e+03   4.05165e+03
  4.08165e+03   4.11165e+03   4.14165e+03   4.17165e+03   4.20165e+03   4.23165e+03
  4.26165e+03   4.29165e+03   4.32165e+03   4.35165e+03   4.38165e+03   4.41165e+03
  4.44165e+03   4.47165e+03   4.50165e+03   4.53165e+03   4.56165e+03   4.59165e+03
  4.62165e+03   4.65165e+03   4.68165e+03   4.71165e+03   4.74165e+03   4.77165e+03
  4.80165e+03   4.83165e+03   4.86165e+03   4.89165e+03   4.92165e+03   4.95165e+03
  4.98165e+03   5.01165e+03   5.04165e+03   5.07165e+03   5.10165e+03   5.13165e+03
  5.16165e+03   5.19165e+03   5.22165e+03   5.25165e+03   5.28165e+03   5.31165e+03
  5.32620e+03   5.33953e+03   5.35327e+03   5.36815e+03   5.38243e+03   5.39647e+03
  5.41045e+03   5.42450e+03   5.43852e+03   5.45253e+03   5.46651e+03   5.48049e+03
  5.49446e+03   5.50843e+03   5.52239e+03   5.53636e+03   5.55031e+03   5.56426e+03
  5.57822e+03   5.59217e+03   5.60612e+03   5.62007e+03   5.63403e+03   5.64798e+03
  5.66194e+03   5.67590e+03   5.68986e+03   5.70383e+03   5.71780e+03   5.73178e+03
  5.74576e+03   5.75974e+03   5.77373e+03   5.78772e+03   5.80172e+03   5.81572e+03
  5.82971e+03   5.84364e+03   5.85745e+03   5.87110e+03   5.88463e+03   5.89871e+03
  5.91273e+03
mass=
```

```
   1.87736e+01  1.86754e+01  1.86509e+01  1.86382e+01  1.86322e+01  1.86268e+01
   1.86221e+01  1.86174e+01  1.96951e+01  2.07355e+01  2.09453e+01  2.09051e+01
   2.08988e+01  2.09020e+01  2.08413e+01  2.05571e+01  2.06324e+01  2.06329e+01
   2.06447e+01  2.06626e+01  2.05203e+01  2.02351e+01  2.21940e+01  2.21914e+01
   2.22123e+01  2.22444e+01  2.22986e+01  2.23655e+01  2.24389e+01  2.25154e+01
   2.25936e+01  2.26728e+01  2.27525e+01  2.28329e+01  2.29135e+01  2.29947e+01
   2.30762e+01  2.27958e+01  2.48395e+01  2.48336e+01  2.48795e+01  2.49550e+01
   2.50443e+01  2.51410e+01  2.52415e+01  2.53443e+01  2.54486e+01  2.55538e+01
   2.56601e+01  2.57670e+01  2.58747e+01  2.59833e+01  2.60925e+01  2.61117e+01
   2.74530e+01  2.79360e+01  2.80332e+01  2.81540e+01  2.82782e+01  2.92032e+01
   3.03137e+01  3.04475e+01  3.05915e+01  3.07426e+01  3.08775e+01  2.96626e+02
   1.71391e+02  1.47998e+02  1.29783e+02  1.52766e+02  1.51468e+02  1.50325e+02
   1.48162e+02  1.49537e+02  1.49481e+02  1.49930e+02  1.49472e+02  1.49931e+02
   1.49560e+02  1.50032e+02  1.49561e+02  1.50063e+02  1.49674e+02  1.49885e+02
   1.49820e+02  1.49767e+02  1.49808e+02  1.49691e+02  1.49792e+02  1.49785e+02
   1.49512e+02  1.49552e+02  1.49515e+02  1.49476e+02  1.49418e+02  1.49366e+02
   1.49311e+02  1.49256e+02  1.49199e+02  1.49141e+02  1.49082e+02  1.49311e+02
   1.50645e+02  1.52463e+02  1.54578e+02  1.51377e+02  1.48528e+02  1.47598e+02
   0.00000e+00
 enth=
   0.00000e+00  1.38531e+06  1.38490e+06  1.38641e+06  1.38807e+06  1.38990e+06
   1.39189e+06  1.39409e+06  1.39652e+06  1.39918e+06  1.40211e+06  1.40532e+06
   1.40884e+06  1.41274e+06  1.41700e+06  1.42166e+06  1.42650e+06  1.43135e+06
   1.43619e+06  1.44103e+06  1.44587e+06  1.45069e+06  1.45549e+06  1.46032e+06
   1.46515e+06  1.46998e+06  1.47480e+06  1.47958e+06  1.48441e+06  1.48924e+06
   1.49407e+06  1.49889e+06  1.50372e+06  1.50857e+06  1.51341e+06  1.51826e+06
   1.52313e+06  1.52800e+06  1.53290e+06  1.53779e+06  1.54270e+06  1.54762e+06
   1.55255e+06  1.55749e+06  1.56236e+06  1.56733e+06  1.57231e+06  1.57730e+06
   1.58231e+06  1.58732e+06  1.59235e+06  1.59740e+06  1.60245e+06  1.60753e+06
   1.61261e+06  1.61771e+06  1.62283e+06  1.62795e+06  1.63310e+06  1.63826e+06
   1.64341e+06  1.64855e+06  1.65375e+06  1.65897e+06  1.66422e+06  1.66947e+06
   1.67468e+06  1.67997e+06  1.68528e+06  1.69061e+06  1.69596e+06  1.70133e+06
   1.70175e+06  1.70167e+06  1.70168e+06  1.70194e+06  1.70210e+06  1.70220e+06
   1.70228e+06  1.70239e+06  1.70248e+06  1.70258e+06  1.70265e+06  1.70275e+06
   1.70283e+06  1.70291e+06  1.70300e+06  1.70308e+06  1.70316e+06  1.70323e+06
   1.70330e+06  1.70337e+06  1.70345e+06  1.70353e+06  1.70360e+06  1.70367e+06
   1.70374e+06  1.70381e+06  1.70388e+06  1.70395e+06  1.70403e+06  1.70411e+06
   1.70417e+06  1.70425e+06  1.70431e+06  1.70440e+06  1.70447e+06  1.70455e+06
   1.70462e+06  1.70468e+06  1.70466e+06  1.70459e+06  1.70457e+06  1.70461e+06
   0.00000e+00
 eoi
 && dummy sources of h2ov and h2
  h2ov=10 iflag=2
    t=       0.0    10.0    20.0    50.0   100.0
           200.0   300.0   500.0  1000.0  2000.0
    mass=    0.0     0.0     0.0     0.0     0.0
             0.0     0.0     0.0     0.0     0.0
    temp= 400.0   400.0   400.0   400.0   400.0
          400.0   400.0   400.0   400.0   400.0
  eoi
  h2=10   iflag=2
    t=       0.0    10.0    20.0    50.0   100.0
           200.0   300.0   500.0  1000.0  2000.0
    mass=    0.0     0.0     0.0     0.0     0.0
             0.0     0.0     0.0     0.0     0.0
    temp= 400.0   400.0   400.0   400.0   400.0
          400.0   400.0   400.0   400.0   400.0
  eoi

 && rcs aerosol source: deleted
  && aerosol
  && source=1
  && rcs= 7 iflag= 1
  && t= 0.0 6190.0 9354.0  9468.0  9588.0  9738.0  10090.0
  && mass= 0.0 0.01227 0.7098 0.3372 0.04443 0.00541 0.0
  && eoi
```

```
condense

h-burn elev=12.3
       && tactiv=10090.0
  flam=5.0 && cfrmng=0.0001 normng=0.0001 mfcig=0.0001 mfoig=0.0001
  && mfsig=0.9999 tactiv=10090.0  &&  for uchb
eoi

struc

&&  roof area
name=conr9  type=roof  shape=slab  nslab=11  chrlen=6.7
  slarea=106.  tunif=311.
compound= conc   conc   conc    conc   conc      conc
          conc   conc   conc    conc   conc
       x= 0.       3.5e-4   1.e-3    2.e-3    4.e-3       8.e-3  1.6e-2
          3.0e-2   6.0e-2   1.2e-1   2.4e-1   3.6e-1
eoi

&&  vertical wall surface
name=conw9  type=wall  shape=slab  nslab=11  chrlen=14.
slarea=623.  tunif=311.
compound= conc   conc   conc    conc   conc      conc
          conc   conc   conc    conc   conc
       x= 0.       3.5e-4   1.e-3    2.e-3    4.e-3       8.e-3  1.6e-2
          3.0e-2   6.0e-2   1.2e-1   2.4e-1   3.6e-1
eoi

&&  vertical wall surface (steel)
name=stw9  type=wall  shape=slab  nslab=9  chrlen=14.
slarea=681.3  tunif=311.
compound= fe   fe   fe    fe   fe      fe
          fe   fe   fe
       x= 0.       3.5e-4   1.e-3    2.e-3    4.e-3       8.e-3  1.6e-2
          3.0e-2   5.0e-2   6.9e-2
eoi

 rad-heat gasuel 3.22   &&  radiant heat transfer: simple gas-struc model
   emsvt  0.6 0.8 0.8 0.8       &&  emissivities of strucs and lower cell
   && cess     && for sensitivity studies, if desired
 eoi

&& ht-tran off off off off off   && for spurious convection tests

overflow=-9  && to sump in lower containment

&& pipes to equalize water levels in lower containment
engineer pipeto8 1 9 8 0.0
         pipe 0.25 1.0 1.0
eoi
engineer pipeto10 1 9 10 0.0
         pipe 0.25 1.0 1.0
eoi

low-cell
 geometry  106.
    concrete
       compos=1  conc  9.209e5  temp=311. && concrete 3.62 m thick
    eoi
    intern
       lay-name=splash   compos=1  fe  100.  temp=311.
     physics
       ht-coef
       name= pool
         flag= 1
         var-x= time x= 2 1.e-7 1.1e+7 && default ht trans 10090.0 10110.0
         var-y= coef y= 2 5.0e+04  100. && fast quench of debris
       eoi
```

```
    eoi
   eoi
 pool compos 1 h2ol=1.0 temp= 311.
   physics
     settle
     boil
   eoi
 eoi
 bc=311. 1.e5
eoi

&& lower containment #3 ----------------------
cell=10
control  nhtn=3  mxslab=12  jpool=1
  jint= 1 jconc=1 numtbc=1 maxtbc=5
eoi
title
cell #10 (lower containment #3)
geometry   1510.0 14.0
atmos=3 1.01163e5 311.0
n2=0.7905  o2=0.2095 h2ov=0.01 && initial atmosphere composition

condense

h-burn elev=12.3
      &&  tactiv=10090.0
  flam=5.0 && cfrmng=0.0001 normng=0.0001 mfcig=0.0001 mfoig=0.0001
  && mfsig=0.9999 tactiv=10090.0  &&  for uchb
eoi

struc

&&  roof area
name=conr10  type=roof  shape=slab  nslab=11  chrlen=6.7
  slarea=124.  tunif=311.
compound= conc   conc   conc    conc   conc      conc
          conc   conc   conc   conc    conc
       x= 0.       3.5e-4   1.e-3    2.e-3    4.e-3       8.e-3  1.6e-2
          3.0e-2   6.0e-2   1.2e-1   2.4e-1   3.6e-1
eoi

&&  vertical wall surface
name=conw10  type=wall  shape=slab  nslab=11  chrlen=14.
slarea=727.  tunif=311.
compound= conc   conc   conc    conc   conc      conc
          conc   conc   conc   conc    conc
       x= 0.       3.5e-4   1.e-3    2.e-3    4.e-3       8.e-3  1.6e-2
          3.0e-2   6.0e-2   1.2e-1   2.4e-1   3.6e-1
eoi

&&  vertical wall surface (steel)
name=stw10  type=wall  shape=slab  nslab=9  chrlen=14.
slarea=784.3  tunif=311.
compound= fe   fe   fe    fe   fe      fe
          fe   fe   fe
       x= 0.       3.5e-4   1.e-3    2.e-3    4.e-3       8.e-3  1.6e-2
          3.0e-2   5.0e-2   6.9e-2
eoi

 rad-heat gasgal 3.22   &&  radiant heat transfer: simple gas-struc model
   emsvt  0.8 0.8 0.8 0.8       &&  emissivities of strucs and lower cell
   && cess     && for sensitivity studies, if desired
 eoi

&& ht-tran off off off off off   && for spurious convection tests

overflow=-10  && to sump in lower containment
```

```
for cell
geometry 124.
  concrete
    compos=1 conc 1.077e6 temp=311. && concrete 3.62 m thick
  eoi
  interm
    ray-name=splash  compos=1 fe 100.  temp=311.
   physics
    ht-coef
    name= pool
      flag= 1
      var-x= time x= 2 1.e+7 1.1e+7 && default ht trans 10090.0 10110.0
      var-y= coef y= 2 5.0e+04  100. && fast quench of debris
    eoi
  eoi
eoi
pool compos 1 h2ol=1.0 temp= 311.
  physics
    settle
    boil
  eoi
eoi
bc=311. 1.e5
eoi

&& lower annulus #1 ----------------------
cell=11
control  nhtn=4  mxslab=12
eoi
title
cell #11 (lower annulus #1)
geometry   864 0 14.0
atmos=3 1.01163e5 311.0
n2=0.7905  o2=0.2095 h2ov=0.01 && initial atmosphere composition

condense

h-turn elev=12.3
     &&  tactiv=10090.0
  flam=5.0 && cfrmng=0.0001 mormng=0.0001 mfcig=0.0001 mfoig=0.0001
  && mfsig=0.9999 tactiv=10090.0  &&  for uchb
eoi

struc

&&  roof area
name=conr11  type=roof  shape=slab  nslab=11  chrlen=3.9
  slarea=215.  tunif=311.
compound= conc   conc   conc    conc   conc      conc
          conc   conc   conc    conc   conc
       x= 0.       3.5e-4   1.e-3    2.e-3    4.e-3       8.e-3  1.6e-2
          3.0e-2   6.0e-2   1.2e-1   2.4e-1   3.6e-1
eoi

&&  floor area
name=conf11  type=floor  shape=slab  nslab=11  chrlen=3.9
  slarea=215.  tunif=311.
compound= conc   conc   conc    conc   conc      conc
          conc   conc   conc    conc   conc
       x= 0.       3.5e-4   1.e-3    2.e-3    4.e-3       8.e-3  1.6e-2
          3.0e-2   6.0e-2   1.2e-1   2.4e-1   3.6e-1
eoi

&&  vertical wall surface
name=conw11  type=wall  shape=slab  nslab=11  chrlen=7.
slarea=627.  tunif=311.
compound= conc   conc   conc    conc   conc      conc
          conc   conc   conc    conc   conc
```

```
        x= 0.        3.5e-4   1.e-3    2.e-3    4.e-3        8.e-3  1.6e-2
           3.0e-2    6.0e-2   1.2e-1   2.4e-1   3.6e-1
eoi

&& vertical wall surface (steel)
name=stwll1  type=wall  shape=slab  nslab=8  chrlen=14.
slar t=595.  tunif=311.
compo nd= fe   fe   fe    fe   fe       fe
          fe   fe
        x= 0.        3.5e-4   1.e-3    2.e-3    4.e-3        8.e-3  1.3e-2
           2.1e-2    3.1e-2
eoi

 rad-heat gasual 1.89   && radiant heat transfer: simple gas-struc model
   emsvt  0.8 0.8 0.8 0.8       && emissivities of strucs and lower cell
   && cess     && for sensitivity studies, if desired
 eoi

&& ht-tran off off off off off   && for spurious convection tests

overflow=-8  && to sump in lower containment

&& lower annulus #2 ----------------------
cell=12
control  nhtm=4  mxslab=12
eoi
title
cell #12 (lower annulus #2)
geometry   846.0 14.0
atmos=3 1.01163e5 311.0
n2=0.7905  o2=0.2095 h2ov=0.01 && initial atmosphere composition

condense

h-burn elev=12.3
      && tactiv=10090.0
  flam=5.0 && cfrmng=0.0001 mormng=0.0001 mfcig=0.0001 mfoig=0.0001
  && mfsig=0.9999 tactiv=10090.0  &&  for uchb
eoi

struc

&&  roof area
name=conr12  type=roof  shape=slab  nslab=11  chrlen=3.9
  slarea=211.  tunif=311.
compound= conc   conc   conc    conc   conc      conc
          conc   conc   conc    conc   conc
        x= 0.        3.5e-4   1.e-3    2.e-3    4.e-3        8.e-3  1.6e-2
           3.0e-2    6.0e-2   1.2e-1   2.4e-1   3.6e-1
eoi

&&  floor area
name=conf12  type=floor     e=slab  nslab=11  chrlen=3.9
  slarea=211.  tunif=311.
compound= conc   conc   conc    conc   conc      conc
          conc   conc   conc    conc   conc
        x= 0.        3.5e-4   1.e-3    2.e-3    4.e-3        8.e-3  1.6e-2
           3.0e-2    6.0e-2   1.2e-1   2.4e-1   3.6e-1
eoi

&&  vertical wall surface
name=conw12  type=wall  shape=slab  nslab=11  chrlen=7.
slarea=613.  tunif=311.
compound= conc   conc   conc    conc   conc      conc
          conc   conc   conc    conc   conc
        x= 0.        3.5e-4   1.e-3    2.e-3    4.e-3        8.e-3  1.6e-2
           3.0e-2    6.0e-2   1.2e-1   2.4e-1   3.6e-1
eoi
```

```
&& vertical wall surface (steel)
name=stul2  type=wall  shape=slab  nslab=8  chrlen=14.
slarea=563.  tunif=311.
compound= fe   fe   fe   fe   fe      fe
          fe   fe
       x= 0.       3.5e-4   1.e-3    2.e-3    4.e-3       8.e-3  1.3e-2
          2.1e-2   3.1e-2
eoi

 rad-heat gasual 1.88   && radiant heat transfer: simple gas-struc model
   emsvt  0.8 0.8 0.8 0.8       && emissivities of strucs and lower cell
   && cess     && for sensitivity studies, if desired
 eoi

&& ht-tran off off off off off   && for spurious convection tests

overflow=-9  && to sump in lower containment

&& lower annulus #3 ----------------------
cell=13
control  nhtm=4  mxslab=12
eoi
title
cell #13 (lower annulus #3)
geometry   952.0 14.0
atmos=3 1.01163e5 311.0
n2=0.7905  o2=0.2095 h2ov=0.01 && initial atmosphere composition

condense

h-burn elev=12.3
      && tactiv=10090.0
  flam=5.0 && cfrmng=0.0001 morming=0.0001 mfcig=0.0001 mfoig=0.0001
  && nfsig=0.9999 tactiv=10090.0  &&  for uchb
eoi

struc

&& roof area
name=conr13  type=roof  shape=slab  nslab=11  chrlen=3.9
  slarea=237.4  tunif=311.
compound= conc   conc   conc    conc   conc      conc
          conc   conc   conc   conc    conc
       x= 0.       3.5e-4   1.e-3    2.e-3    4.e-3       8.e-3  1.6e-2
          3.0e-2   6.0e-2   1.2e-1   2.4e-1   3.6e-1
eoi

&& floor area
name=conf13  type=floor  shape=slab  nslab=11  chrlen=3.9
  slarea=237.4  tunif=311.
compound= conc   conc   conc    conc   conc      conc
          conc   conc   conc   conc    conc
       x= 0.       3.5e-4   1.e-3    2.e-3    4.e-3       8.e-3  1.6e-2
          3.0e-2   6.0e-2   1.2e-1   2.4e-1   3.6e-1
eoi

&& vertical wall surface
name=conw13  type=wall  shape=slab  nslab=11  chrlen=7.
slarea=690.2  tunif=311.
compound= conc   conc   conc    conc   conc      conc
          conc   conc   conc   conc    conc
       x= 0.       3.5e-4   1.e-3    2.e-3    4.e-3       8.e-3  1.6e-2
          3.0e-2   6.0e-2   1.2e-1   2.4e-1   3.6e-1
eoi

&& vertical wall surface (steel)
name=stul3  type=wall  shape=slab  nslab=8  chrlen=14.
```

```
slarea=656.  tunif=311.
compound= fe   fe   fe    fe   fe      fe
          fe   fe
        x= 0.       3.5e-4   1.e-3    2.e-3    4.e-3       8.e-3  1.3e-2
           2.1e-2   3.1e-2
eoi

 rad-heat gasual 1.88   && radiant heat transfer: simple gas-struc model
   emsvt  0.8 0.8 0.8 0.8       && emissivities of strucs and lower cell
   && cess     && for sensitivity studies, if desired
 eoi

&& ht-tran off off off off off   && for spurious convection tests

overflow=-10  && to sump in lower containment

&& lower plenum #1  ---------
cell=14
control nhtn=3  mxslab=12 eoi
title
  cell #14 (lower plenum #1)
geometry  171.25  2.5
atmos=3  1.01089e5  273.5
n2=0.7905  o2=0.2095 h2ov=0.
&&        ------ structure input --------
struc

&& vertical wall surface (steel)
name=stul4a  type=wall  shape=slab  nslab=6  chrlen=2.5
slarea=70.0  tunif=273.5
compound=fe fe fe fe fe   fe
       x= 0.0 0.00035 0.001 0.002 0.004   0.008 0.013
eoi

&& ice condenser support structure (from HECTR deck)
name=stul4b  type=wall  shape=slab  nslab=6  chrlen=0.2
slarea=665.  tunif=273.5
compound=fe fe fe fe fe   fe
       x= 0.0 0.00035 0.001 0.002 0.004   0.006 0.0081
eoi

&& plenum floor
name=conf14  type=floor  shape=slab  nslab=12  chrlen=3.2
slarea=77.5  tunif=273.5
compound= conc conc conc conc conc   conc conc conc conc conc
          conc conc
       x= 0.0 0.00035 0.001 0.002 0.004   0.008 0.016 0.032 0.064 0.13
          0.26 0.5 0.75
eoi

condense

h-burn elev=19.0
        mfcig=0.999  &&  tactiv=10090.0
  && flam=5.0 cfrmng=0.0001 mormng=0.0001 mfcig=0.0001 mfoig=0.0001
  && mfsig=0.9999 tactiv=10090.0  &&  for uchb
eoi

 rad-heat gasual 0.76   &&  radiant heat transfer: simple gas-struc model
   emsvt  0.8 0.8 0.8       &&  emissivities of strucs and lower cell
   && cess     && for sensitivity studies, if desired
 eoi

&& ht-tran off off off off off   && for spurious convection tests

overflow=-8

&& lower plenum #2  ---------
```

```
cell=15
control nhtm=3  mxslab=12 eoi
title
  cell #15 (lower plenum #2)
geometry  171.25  2.5
atmos=3  1.01089e5  273.5
n2=0.7905  o2=0.2095 h2ov=0.01
&&        ------ structure input --------
struc

&& vertical wall surface (steel)
name=stwl5a  type=wall  shape=slab  nslab=6  chrlen=2.5
slarea=70.0  tunif=273.5
compound=fe fe fe fe fe   fe
       x= 0.0 0.00035 0.001 0.002 0.004   0.008 0.013
eoi

&& ice condenser support structure (from HECTR deck)
name=stwl5b  type=wall  shape=slab  nslab=6  chrlen=0.2
slarea=665.  tunif=273.5
compound=fe fe fe fe fe   fe
       x= 0.0 0.00035 0.001 0.002 0.004   0.006 0.0081
eoi

&& plenum floor
name=conf15  type=floor  shape=slab  nslab=12  chrlen=3.2
slarea=77.5  tunif=273.5
compound= conc conc conc conc conc   conc conc conc conc conc
          conc conc
       x= 0.0 0.00035 0.001 0.002 0.004   0.008 0.016 0.032 0.064 0.13
          0.26 0.5 0.75
eoi

condense

h-burn elev=19.0
        mfcig=0.999  &&  tactiv=10090.0
  && flam=5.0 cfrmng=0.0001 normng=0.0001 mfcig=0.0001 mfoig=0.0001
  && mfsig=0.9999 tactiv=10090.0  &&  for uchb
eoi

 rad-heat gasual 0.76   &&  radiant heat transfer: simple gas-struc model
   emsvt  0.8 0.8 0.8       &&  emissivities of strucs and lower cell
   && cess     && for sensitivity studies, if desired
 eoi

&& ht-tran off off off off off   && for spurious convection tests

overflow=-9

&& lower plenum #3  ---------
cell=16
control nhtm=3  mxslab=12 eoi
title
  cell #16 (lower plenum #3)
geometry  171.25  2.5
atmos=3  1.01089e5  273.5
n2=0.7905  o2=0.2095 h2ov=0.01
&&        ------ structure input --------
struc

&& vertical wall surface (steel)
name=stwl6a  type=wall  shape=slab  nslab=6  chrlen=2.5
slarea=70.0  tunif=273.5
compound=fe fe fe fe fe   fe
       x= 0.0 0.00035 0.001 0.002 0.004   0.008 0.013
eoi
```

```
&& ice condenser support structure (from HECTR deck)
name=stu16b  type=wall  shape=slab  nslab=6  chrlen=0.2
slarea=665.  tunif=273.5
compound=fe fe fe fe fe   fe
      x= 0.0 0.00035 0.001 0.002 0.004   0.006 0.0081
eoi

&& plenum floor
name=conf16  type=floor  shape=slab  nslab=12  chrlen=3.2
slarea=77.5  tunif=273.5
compound= conc conc conc conc conc   conc conc conc conc conc
          conc conc
      x= 0.0 0.00035 0.001 0.002 0.004   0.008 0.016 0.032 0.064 0.13
         0.26 0.5 0.75
eoi

condense

h-burn elev=19.0
       mfcig=0.999  &&  tactiv=10090.0
  && flam=5.0 cfrmng=0.0001 mormng=0.0001 mfcig=0.0001 mfoig=0.0001
  && mfsig=0.9999 tactiv=10090.0  &&  for uchb
eoi

 rad-heat gasgal 0.76   &&  radiant heat transfer: simple gas-struc model
   emsvt  0.8 0.8 0.8       &&  emissivities of strucs and lower cell
   && cess     && for sensitivity studies, if desired
 eoi

&& ht-tran off off off off off   && for spurious convection tests

overflow=-9

&& lower plenum #4  ---------
cell=17
control nhtm=3  mxslab=12 eoi
title
  cell #17 (lower plenum #4)
geometry  171.25  2.5
atmos=3  1.01069e5  273.5
n2=0.7905  o2=0.2095 h2ov=0.01
&&        ------ structure input --------
struc

&& vertical wall surface (steel)
name=stu17a  type=wall  shape=slab  nslab=6  chrlen=2.5
slarea=70.0  tunif=273.5
compound=fe fe fe fe fe   fe
      x= 0.0 0.00035 0.001 0.002 0.004   0.008 0.013
eoi

&& ice condenser support structure (from HECTR deck)
name=stu17b  type=wall  shape=slab  nslab=6  chrlen=0.2
slarea=665.  tunif=273.5
compound=fe fe fe fe fe   fe
      x= 0.0 0.00035 0.001 0.002 0.004   0.006 0.0081
eoi

&& plenum floor
name=conf17  type=floor  shape=slab  nslab=12  chrlen=3.2
slarea=77.5  tunif=273.5
compound= conc conc conc conc conc   conc conc conc conc conc
          conc conc
      x= 0.0 0.00035 0.001 0.002 0.004   0.008 0.016 0.032 0.064 0.13
         0.26 0.5 0.75
eoi

condense
```

```
h-burn elev=19.0
        mfcig=0.999  &&  tactiv=10090.0
  && flam=5.0 cfrmng=0.0001 normng=0.0001 mfcig=0.0001 mfoig=0.0001
  && mfsig=0.9999 tactiv=10090.0  &&  for uchb
eoi

 rad-heat gasual 0.76   &&  radiant heat transfer: simple gas-struc model
   emsvt  0.8 0.8 0.8       &&  emissivities of strucs and lower cell
   && cess     && for sensitivity studies, if desired
 eoi

&& ht-tran off off off off off   && for spurious convection tests

overflow=-10

&& ice condenser #1 ----------------------
cell=18
control  nhtm=2  mxslab=12  naensy=1
eoi
title
cell #18 (ice chest cell #1)
geometry   611.0 14.6
atmos=3 1.00992e5 273.5
n2=0.7905  o2=0.2095 h2ov=0.01 && initial atmosphere composition

condense

h-burn elev=27.7
        mfcig=0.999  &&  tactiv=10090.0
  && flam=5.0 cfrmng=0.0001 normng=0.0001 mfcig=0.0001 mfoig=0.0001
  && mfsig=0.9999 tactiv=10090.0  &&  for uchb
eoi

struc

&&  floor area
name=stf18  type=floor  shape=slab  nslab=3  chrlen=3.
  slarea=40.75  tunif=273.5
compound=   fe      fe      fe
       x= 0.        5.5e-4   1.e-3    2.e-3
eoi

&&  vertical wall surface (steel)
name=stw18  type=wall  shape=slab  nslab=6  chrlen=14.6
slarea=514.5  tunif=273.5
compound= fe    fe    fe    fe    fe       fe
       x= 0.        3.5e-4   1.e-3    2.e-3    4.e-3       8.e-3  1.22e-2
eoi

 rad-heat gasual 0.326  &&  radiant heat transfer: simple gas-struc model
   emsvt  0.8 0.8      &&  emissivities of strucs and lower cell
   && cess     && for sensitivity studies, if desired
 eoi

&& ht-tran off off off off off   && for spurious convection tests

overflow=-8  && to sump in lower containment

engineer  icebed1  1 18 8 16.0
  icecond  hitici=14.53  tmsici=2.775e5  citice=264.0  citlex=935.0
  ciarfl=41.75  arhtin=6200.  iclip=14  cihtnl=5.0  cifimx=5.e-5
&& aerosol paramters changed to reduce excessive impaction, diffusion
&& sedimentation collection ---------
  fracsed=0.023  areaimp=140.0  diamimp=0.024  diamdif=0.024
  eoi
eoi
```

```
&& ice condenser #2 ----------------------
cell=19
control  nhtm=2  mxslab=12  naensy=1
eoi
title
cell #19 (ice chest cell #2)
geometry   611.0 14.6
atmos=3 1.00992e5 273.5
n2=0.7905  o2=0.2095 h2ov=0.01 && initial atmosphere composition

condense

h-burn elev=27.7
       mfcig=0.999  &&  tactiv=10090.0
  && flam=5.0 cfrmng=0.0001 mormng=0.0001 mfcig=0.0001 mfoig=0.0001
  && mfsig=0.9999 tactiv=10090.0  &&  for uchb
eoi

struc

&&  floor area
name=stfl9  type=floor  shape=slab  nslab=3  chrlen=3.
  slarea=40.75  tunif=273.5
compound=   fe     fe     fe
      x= 0.       3.5e-4   1.e-3    2.e-3
eoi

&&  vertical wall surface (steel)
name=stwl9  type=wall  shape=slab  nslab=6  chrlen=14.6
slarea=514.5  tunif=273.5
compound= fe   fe   fe   fe   fe      fe
      x= 0.       3.5e-4   1.e-3    2.e-3    4.e-3       8.e-3  1.22e-2
eoi

 rad-heat gasual 0.326  &&  radiant heat transfer: simple gas-struc model
   emsvt  0.8 0.8      &&  emissivities of strucs and lower cell
   && cess     && for sensitivity studies, if desired
 eoi

&& ht-tran off off off off off   && for spurious convection tests

overflow=-9  && to sump in lower containment

engineer  icebed2  1 19 9 16.0
  icecond  hitici=14.53  tmsici=2.775e5  citice=264.0  citlex=335.0
  ciarfl=41.75  arhtin=6200.  iclip=14  cihtmi=5.0  cifinx=5.e-5
&& aerosol paramters changed to reduce excessive impaction, diffusion
&& sedimentation collection ---------
  fracsed=0.023  areaimp=140.0  diamimp=0.024  diamdif=0.024
  eoi
eoi

&& ice condenser #3 ----------------------
cell=20
control  nhtm=2  mxslab=12  naensy=1
eoi
title
cell #20 (ice chest cell #3)
geometry   611.0 14.6
atmos=3 1.00992e5 273.5
n2=0.7905  o2=0.2095 h2ov=0.01 && initial atmosphere composition

condense

h-burn elev=27.7
       mfcig=0.999  &&  tactiv=10090.0
  && flam=5.0 cfrmng=0.0001 mormng=0.0001 mfcig=0.0001 mfoig=0.0001
  && mfsig=0.9999 tactiv=10090.0  &&  for uchb
```

```
eoi

struc

&&  floor area
name=stf20  type=floor  shape=slab  nslab=3  chrlen=3.
  slarea=40.75  tunif=273.5
compound=   fe      fe      fe
       x= 0.        3.5e-4   1.e-3    2.e-3
eoi

&&  vertical wall surface (steel)
name=stw20  type=wall  shape=slab  nslab=6  chrlen=14.6
slarea=514.5  tunif=273.5
compound= fe   fe   fe    fe   fe       fe
       x= 0.        3.5e-4   1.e-3    2.e-3    4.e-3       6.e-3  1.22e-2
eoi

 rad-heat gasgal 0.326  &&  radiant heat transfer: simple gas-struc model
   emsvt  0.8 0.8       &&  emissivities of strucs and lower cell
   && cess     && for sensitivity studies, if desired
 eoi

&& ht-tran off off off off off   && for spurious convection tests

overflow=-9  && to sump in lower containment

engineer  icebed3  1 20 9 16.0
  icecond  hitici=14.53  tmsici=2.775e5  citice=264.0  citlex=335.0
  ciarfl=41.75  arhtin=6200.  iclip=14  cihtmi=5.0  ciflmx=5.e-5
&& aerosol paranters changed to reduce excessive impaction, diffusion
&& sedimentation collection ---------
  fracsed=0.023  areaimp=140.0  dianimp=0.024  diamdif=0.024
  eoi
eoi

&& ice condenser #4 ------------------------
cell=21
control  nhtm=2  mxslab=12  naensy=1
eoi
title
cell #21 (ice chest cell #4)
geometry   611.0 14.6
atmos=3 1.00992e5 273.5
n2=0.7905  o2=0.2095 h2ov=0.01 && initial atmosphere composition

condense

h-burn elev=27.7
       mfcig=0.999  &&  tactiv=10090.0
  && flam=5.0 cfrmng=0.0001 mormng=0.0001 mfcig=0.0001 mfoig=0.0001
  && mfsig=0.9999 tactiv=10090.0  &&  for uchb
eoi

struc

&&  floor area
name=stf21  type=floor  shape=slab  nslab=3  chrlen=3.
  slarea=40.75  tunif=273.5
compound=   fe      fe      fe
       x= 0.        3.5e-4   1.e-3    2.e-3
eoi

&&  vertical wall surface (steel)
name=stw21  type=wall  shape=slab  nslab=6  chrlen=14.6
slarea=514.5  tunif=273.5
compound= fe   fe   fe    fe   fe       fe
       x= 0.        3.5e-4   1.e-3    2.e-3    4.e-3       8.e-3  1.22e-2
```

```
eoi

 rad-heat gaswal 0.326  && radiant heat transfer: simple gas-struc model
   emsvt  0.8 0.8      && emissivities of strucs and lower cell
   && cess     && for sensitivity studies, if desired
 eoi

&& ht-tran off off off off off   && for spurious convection tests

overflow=-10  && to sump in lower containment

engineer  icebed4  1 21 10 16.0
  icecond  hitici=14.53  tmsici=2.775e5  citice=264.0  citlex=335.0
  ciarfl=41.75  arhtin=6200.  iclip=14  cihtmi=5.0  ciflmx=5.e-5
&& aerosol paramters changed to reduce excessive impaction, diffusion
&& sedimentation collection ---------
  fracsed=0.023  areaimp=140.9  diamimp=0.024  diamdif=0.024
  eoi
eoi

&& upper plenum #1 ----------------------
cell=22
control  nhtn=2  mxslab=12
eoi
title
cell #22 (upper plenum #1)
geometry   665.0 5.0
atmos=3 1.00683e5 273.5
n2=0.7905  o2=0.2095 h2ov=0.01 && initial atmosphere composition

condense

h-burn elev=37.6
        &&  tactiv=10090.0
  && flam=5.0 cfrmng=0.0001 mornng=0.0001 mfcig=0.0001 mfoig=0.0001
  && mfsig=0.9999 tactiv=10090.0  &&  for uchb
eoi

struc

&&  floor area
name=stf22  type=floor  shape=slab  nslab=6  chrlen=3.5
  slarea=133.  tunif=273.5
compound=   fe      fe      fe      fe      fe          fe
       x= 0.       3.5e-4   1.e-3    2.e-3    4.e-3       8.e-3  1.3e-2
eoi

&&  vertical wall surface
name=stw22  type=wall  shape=slab  nslab=6  chrlen=5.
  slarea=500.  tunif=273.5
compound=   fe      fe      fe      fe      fe          fe
       x= 0.       3.5e-4   1.e-3    2.e-3    4.e-3       8.e-3  1.3e-2
eoi

 red-heat gaswal 3.78   && radiant heat transfer: simple gas-struc model
   emsvt  0.8 0.8       && emissivities of strucs and lower cell
   && cess     && for sensitivity studies, if desired
 eoi

&& ht-tran off off off off off   && for spurious convection tests

overflow=-9  && to sump in lower containment

&& upper plenum #2 ----------------------
cell=23
control  nhtn=2  mxslab=12
eoi
title
```

```
cell #23 (upper plenum #2)
geometry   665.0 5.0
atmos=3 1.00883e5 273.5
n2=0.7905  o2=0.2095 h2ov=0.01 && initial atmosphere composition

condense

h-burn elev=37.6
       &&  tactiv=10090.0
  && flam=5.0 cfrmng=0.0001 mormng=0.0001 mfcig=0.0001 mfoig=0.0001
  && mfsig=0.9999 tactiv=10090.0  &&  for uchb
eoi

struc

&&  floor area
name=stf23  type=floor  shape=slab  nslab=6  chrlen=3.5
  slarea=133.  tunif=273.5
compound=   fe      fe      fe      fe      fe         fe
       x= 0.       3.5e-4   1.e-3    2.e-3    4.e-3       8.e-3  1.3e-2
eoi

&&  vertical wall surface
name=stw23  type=wall  shape=slab  nslab=6  chrlen=5.
  slarea=500.  tunif=273.5
compound=   fe      fe      fe      fe      fe         fe
       x= 0.       3.5e-4   1.e-3    2.e-3    4.e-3       8.e-3  1.3e-2
eoi

 rad-heat gasmal 3.75   &&  radiant heat transfer: simple gas-struc model
   emsvt  0.8 0.8       &&  emissivities of strucs and lower cell
   && cess     && for sensitivity studies, if desired
 eoi

&& ht-tran off off off off off   && for spurious convection tests

overflow=-9  && to sump in lower containment

&& upper dome region #1  -----------------
cell=24
control  nhtm=5  nxslab=12
eoi
title
cell #24 (upper dome region #1)
geometry  6387.0 21.0
atmos=3 1.00810e5 303.0
n2=0.7905  o2=0.2095 h2ov=0.01 && initial atmosphere composition

condense

h-burn elev=44.2
      &&  tactiv=10090.0
  flam=5.0 && cfrmng=0.0001 mormng=0.0001 mfcig=0.0001 mfoig=0.0001
  && mfsig=0.9999 tactiv=10090.0  &&  for uchb
eoi

struc

&&  upper dome
name=str24  type=roof  shape=slab  nslab=6  chrlen=17.5
  slarea=881.  tunif=303.
compound=   fe      fe      fe      fe      fe         fe
       x= 0.       3.5e-4   1.e-3    2.e-3    4.e-3       8.e-3  1.27e-2
eoi

&&  vertical walls (steel)
name=stw24  type=wall  shape=slab  nslab=6  chrlen=8.0
  slarea=910.  tunif=303.
```

```
compound=  fe     fe     fe     fe     fe     fe
      x= 0.      3.5e-4   1.e-3    2.e-3    4.e-3      8.e-3  1.3e-2
eoi

&& floor area (steel)
name=stf24  type=floor  shape=slab  nslab=6  chrlen=3.7
  slarea=90.0  tunif=303.
compound=  fe     fe     fe     fe     fe     fe
      x= 0.      3.5e-4   1.e-3    2.e-3    4.e-3      8.e-3  1.3e-2
eoi

&& vertical walls (concrete)
name=conw24  type=wall  shape=slab  nslab=12  chrlen=5.5
  slarea=217.5  tunif=303.
compound= conc   conc   conc   conc   conc     conc  conc
          conc   conc   conc   conc   conc
      x= 0.      3.5e-4   1.e-3    2.e-3    4.e-3      8.e-3  1.6e-2
         3.0e-2   6.0e-2   1.2e-1   2.4e-1   4.8e-1     9.1e-1
eoi

&& floor area (concrete)
name=conf24  type=floor  shape=slab  nslab=12  chrlen=10.0
  slarea=107.  tunif=303.
compound= conc   conc   conc   conc   conc     conc  conc
          conc   conc   conc   conc   conc
      x= 0.      3.5e-4   1.e-3    2.e-3    4.e-3      8.e-3  1.6e-2
         3.0e-2   6.0e-2   1.2e-1   2.4e-1   4.8e-1     9.1e-1
eoi

 rad-heat gasmal 10.4   && radiant heat transfer: simple gas-struc model
   emsvt  0.8 0.8 0.8 0.8 0.8    && emissivities of strucs and lower cell
   && cess     && for sensitivity studies, if desired
 eoi

&& ht-tran off off off off off   && for spurious convection tests

overflow=-9  && to sump in lower containment

&& upper dome region #2  ----------
cell=25
control  nhtm=5  mxslab=12
eoi
title
cell #25 (upper dome region #2)
geometry  6367.0 21.0
atmos=3 1.00810e5 303.0
n2=0.7905  o2=0.2095 h2ov=0.01 && initial atmosphere composition

condense

h-burn elev=44.2
     && tactiv=10090.0
  flam=5.0 && cfrmng=0.0001 mormng=0.0001 mfcig=0.0001 mfoig=0.0001
  && mfsig=0.9999 tactiv=10090.0  &&  for uchb
eoi

struc

&& upper dome
name=str25  type=roof  shape=slab  nslab=6  chrlen=17.5
  slarea=881.  tunif=303.
compound=  fe     fe     fe     fe     fe     fe
      x= 0       3.5e-4   1.e-3    2.e-3    4.e-3      8.e-3  1.27e-2
eoi

&& vertical walls (steel)
name=stw25  type=wall  shape=slab  nslab=6  chrlen=8.0
  slarea=919.  tunif=303.
```

```
compound=   fe      fe      fe      fe      fe      fe
       x= 0.        3.5e-4   1.e-3    2.e-3    4.e-3       8.e-3  1.3e-2
eoi

&&  floor area (steel)
name=stf25  type=floor  shape=slab  nslab=6  chrlen=3.7
  slarea=90.0  tunif=303.
compound=   fe      fe      fe      fe      fe      fe
       x= 0.        3.5e-4   1.e-3    2.e-3    4.e-3       8.e-3  1.3e-2
eoi

&&  vertical walls (concrete)
name=conw25  type=wall  shape=slab  nslab=12  chrlen=5.5
  slarea=217.5  tunif=303.
compound= conc    conc    conc    conc    conc      conc  conc
          conc    conc    conc    conc    conc
       x= 0.        3.5e-4   1.e-3    2.e-3    4.e-3       8.e-3  1.6e-2
          3.0e-2   6.0e-2   1.2e-1   2.4e-1   4.8e-1      9.1e-1
eoi

&&  floor area (concrete)
name=conf25  type=floor  shape=slab  nslab=12  chrlen=10.0
  slarea=107.  tunif=303.
compound= conc    conc    conc    conc    conc      conc  conc
          conc    conc    conc    conc    conc
       x= 0.        3.5e-4   1.e-3    2.e-3    4.e-3       8.e-3  1.6e-2
          3.0e-2   6.0e-2   1.2e-1   2.4e-1   4.8e-1      9.1e-1
eoi

 rad-heat gasval 10.4   &&  radiant heat transfer: simple gas-struc model
   emsvt  0.8 0.8 0.8 0.8 0.8    &&  emissivities of strucs and lower cell
   && cess     && for sensitivity studies, if desired
 eoi

&& ht-tran off off off off off   && for spurious convection tests

overflow=-9  && to sump in lower containment

&& lower dome region  ------------------
cell=26
control  nhtm=2  mxslab=12
eoi
title
cell #26 (lower dome region and refueling space)
geometry  5852.0 16.2
atmos=3 1.00969e5 303.0
n2=0.7905  o2=0.2095 h2ov=0.01 && initial atmosphere composition

condense

h-burn elev=26.0
      &&  tactiv=10090.0
  flam=5.0 && cfrmng=0.0001 mormng=0.0001 mfcig=0.0001 mfoig=0.0001
  && mfsig=0.9999 tactiv=10090.0  &&  for uchb
eoi

struc

&&  vertical walls (concrete)
name=conw26  type=wall  shape=slab  nslab=12  chrlen=14.
  slarea=1834.  tunif=303.
compound= conc    conc    conc    conc    conc      conc  conc
          conc    conc    conc    conc    conc
       x= 0.        3.5e-4   1.e-3    2.e-3    4.e-3       8.e-3  1.6e-2
          3.0e-2   6.0e-2   1.2e-1   2.4e-1   4.8e-1      9.1e-1
eoi

&&  floor area (concrete)
```

```
name=conf26  type=floor  shape=slab  nslab=12  chrlen=10.0
  slarea=403.  tunif=303.
compound= conc   conc   conc    conc   conc      conc  conc
          conc   conc   conc    conc   conc
       x= 0.       3.5e-4   1.e-3    2.e-3    4.e-3       8.e-3  1.6e-2
          3.0e-2   6.0e-2   1.2e-1   2.4e-1   4.8e-1      9.1e-1
eoi

 rad-heat gasual 9.21   && radiant heat transfer: simple gas-struc model
   emsvt  0.8 0.8       && emissivities of strucs and lower cell
   && cess     && for sensitivity studies, if desired
 eoi

&& ht-tran off off off off off   && for spurious convection tests

&& primary system cell generates blowdown steam and h2 sources
&& scaled from 20-cell surry deck for sequoyah fully pressurized case
cell=27
control  && nhtm=1  mxslab=8
eoi
title
     ----  primary system: used to generate blowdown sources-------
geometry  701.83 5.0 && volume increased to hold sat'd steam mass
atmos=2  0.0  618.6
  h2ov= 36380.1 h2= 279.2  && multiply surry value with 1.272
&& ---------heat sink structures----------
 && struc
 && name=wall1           type=wall           shape=slab
 && nslab=8              iouter=30           chrlen=10.0
 && slarea=1.0           tunif=600.0
 && compound=fe   fe   fe  fe  fe  fe  fe  fe
 && x=0.0 3.e-4 8.4e-4 1.812e-3 2.906e-3 5.5e-3 1.0e-2 1.7e-2 3.e-2
 && eoi
 && rad-heat
 &&  geobl  1.0
 &&  emsvt= 0.8
 &&  && cess
 && eoi
condense

cell=28
control  && nhtm=1  mxslab=10
eoi
title
  cell #28 (environment cell)
geometry  1.e20  1.0e20
atmos=2  1.0e+5  303.0
n2=0.7905 o2=0.2095

 && struc
 && name=stf28  type=floor  shape=slab  nslab=2 chrlen=1.0
 && slarea=1.0 tunif=303.0
 && compound=fe fe
 &&        x=0.0 0.00637 0.01271
 && eoi

eof
&& time-dependent size for rcs aerosol source
aertim= 1
name=rcs flag=1
  var-x= time
  x=7
   8190.   9264.   9354.   9468.   9588.   9738.   10090.
  var-y= amean
  y=7
   5.2e-6  5.2e-6   1.0e-6  1.7e-6  1.2e-6  1.7e-6  2.3e-6
eoi
          rcs    1.0e-6   0.693
```

END JOB

RUN SEQUENCE NUMBER 7

LASER PRINTER QUEUE ua7_users

JOB IDENTIFICATION am4ua5 JOBCOM= e00019899 900717151258

PROCESSED BY ONODE Tue Jul 17 15:22:01 1990

USER TITLE

NUMBER OF PAGES 46